Capillary Electrophoresis Methods for Chiral Drug Analysis and Cyclodextrin-Guest Complexation Mechanisms

Dissertation

To Fulfill the Requirements for the Degree of

„Doctor rerum naturalium" (Dr. rer. nat.)

Submitted to the Council of the Faculty of Biological Sciences

of the Friedrich Schiller University Jena

by Pharmacist, MSc Sulaiman Krait

born on 17.04.1983 in Damascus, Syria

My Family

Abbreviations

α-CD	α-Cyclodextrin
Amb	Ambrisentan
ATP	Analytical target profile
BGE	Background electrolyte
CD(s)	Cyclodextrin(s)
CE	Capillary electrophoresis
CM-α-CD	Carboxymethyl-α-CD sodium salt
CM- β -CD	Carboxymethyl-β -CD sodium salt
CM-γ-CD	Carboxymethyl-γ-CD sodium salt
COSY	Correlation spectroscopy
CPP	Critical process parameter
CQA	Critical quality attribute
CZE	Capillary zone electrophoresis
DAD	Diode array detector
DCV	Daclatasvir
D-MDT	Dexmedetomidine
DM-β-CD	Heptakis(2,6-di-O-methyl)-β-cyclodextrin
DoE	Design of experiments
DS	Degree of substitution
DXM	Dextromethorphan
EMA	European medicines agency
EMO	Enantiomeric migration order
EOF	Electroosmotic flow
ESI	Electrospray ionization
FDA	Food and Drug Administration
γ-CD	γ-Cyclodextrin
HDI	Hydrodynamic injection
HE-β-CD	Hydroxyethyl-β-cyclodextrin
HPLC	High performance liquid chromatography
HP-α-CD	Hydroxypropyl-α-cyclodextrin
HP-γ-CD	Hydroxypropyl-γ-cyclodextrin
HS-β-CD	Heptakis(6-O-sulfo)-β- cyclodextrin

HSQCED	Heteronuclear single quantum coherence edited to result in CH_2 signals at opposite phase of CH and CH_3 signals
ICH	International Council for Harmonization of Technical Requirements for Pharmaceuticals for Human Use
ID	Inner diameter
IStd	Internal standard
L-MDT	Levomedetomidine
LOD	Limit of detection
LOQ	Limit of quantitation
LVM	Levomethorphan
µAU	Micro-absorbance unit
MD	Molecular dynamics
MDT	Medetomidine
MS	Mass spectrometry
M-α-CD	Methyl-α-cyclodextrin
M-β-CD	Methyl-β-cyclodextrin
M-γ-CD	Methyl-γ-cyclodextrin
NMR	Nuclear magnetic resonance
NOE	Nuclear Overhauser effect
Ph. Eur.	European pharmacopoeia
QbD	Quality by design
OFAT	One-factor-at-a-time or
ROESY	Rotating frame nuclear Overhauser effect spectroscopy
R_s	Resolution
RSD	Relative standard deviation
SBE-β-CD	Sulfobutylether β-cyclodextrin
S-α-CD	Sulfated α-cyclodextrin
S-β-CD	Sulfated β-cyclodextrin
S-γ-CD	Sulfated γ-cyclodextrin
TMA-β-CD	2-Hydroxy-3-*N,N,N* trimethylamine propyl-β-cyclodextrin chloride
TM-β-CD	Heptakis(2,3,6-tri-O-methyl)-β- cyclodextrin
TOCSY	Total correlated spectroscopy
UV	Ultraviolet
ε	Dielectric constant

Contents

1. Introduction

1.1. Stereochemistry and its significance to drugs

1.1.1. Basic definitions

Stereoisomers are compounds that have the same constitution (same molecular formula, same atomic bonding) but differ in the spatial orientation of the atoms or groups of atoms within the molecule. This is due to the presence of one or more stereogenic centers in the compound, i.e. an atom where the interchange of two ligands or substituents creates a new stereoisomer. When a pair of stereoisomers are non-superimposable mirror images of each other they are called enantiomer. Enantiomers possess identical physico-chemical properties, outside chiral environments, except that they rotate the plane of polarized light in opposite directions and by equal amounts. An equimolar mixture of enantiomers is called a racemate or a racemic mixture [1; 2]. Dextromethorphan (DXM) is an example of a drug compound that has an enantiomer (Fig.1).
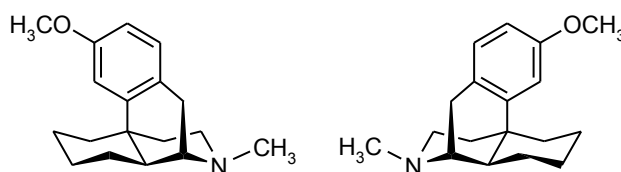
Figure 1 Dextromethorphan (left) and its enantiomer levomethorphan (right)

When the stereoisomers are not enantiomers of each other are termed diastereoisomers [1; 2]. An example of compounds having diastereoisomers is the antiviral drug dolutegravir which has two stereogenic centers having a (4*R*,12a*S*) configuration. Fig. 2 shows dolutegravir and its (4*R*, 12a*R*) Diastereomer.
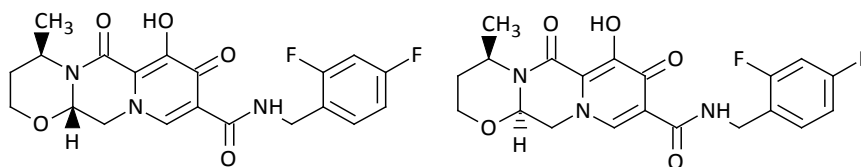
Figure 2 Dolutegravir (left) and its (4*R*, 12a*R*) Diastereomer (right)

1.1.2. Stereoselectivity and physiological activity

The significance of drug stereochemistry in pharmacology was recognized since 1926 [3]. Due to the different spatial arrangement of the chiral drugs, they may not interact in the same way with receptors and/or enzymes. In other words, they interact in a stereoselective way with the targets, which is shown

simplified in Fig. 3. This may lead to different pharmacological responses that range from inactivity to different undesirable effects, which may include toxicity or teratogenicity. Many publications addressed the significance of stereochemistry in drug research and development [4–9].
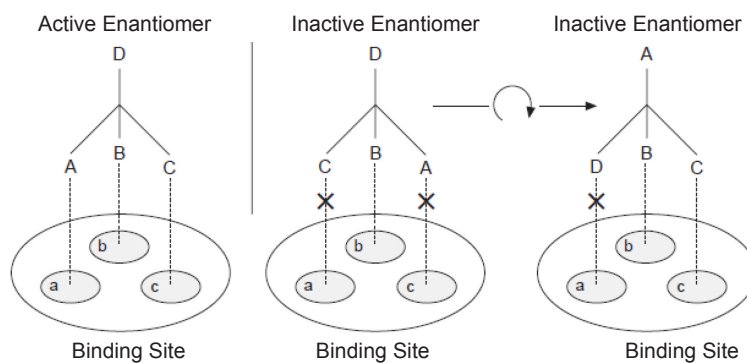
Figure 3 The active enantiomer has a 3-dimensional structure that allows drug domain A to interact with binding site domain a, B to interact with b, and C to interact with c. In contrast, the inactive enantiomer cannot be aligned to bind the same 3 sites simultaneously. The difference in 3-dimensional structure allows the active enantiomer to bind and have a biological effect, whereas the inactive enantiomer cannot (reproduced with permission from [9]).

Medetomidine (MDT), studied in manuscripts 3 and 4, is a good example of enantiomers with different potency. Dexmedetomidine (D-MDT) is used as a sedative in anesthesia management in surgery and in intensive care medicine [10; 11]. D-MDT displayed much higher activity in animal experiments, compared to its enantiomer levomedetomidine [12; 13].

DXM (Fig. 1), which is studied in manuscript 2, is an example of the undesirable effects of the enantiomer since it is widely used as an antitussive in over-the-counter cough and cold medicines [14]. DXM has an *ent*-morphinan structure, while its enantiomer levomethorphan (LVM, Fig. 1) has a morphinan structure and is an opioid analgesic drug with strong respiratory depression. The compound was never clinically developed and is classified as a controlled substance worldwide [15].

1.1.3. Chiral drugs in market and chiral switches

As of 2008, a review of the new chiral drug development in Japan reported an increasing trend in the pharmaceutical development of single isomers rather than racemates [16]. Parallel to this, the annual distribution of FDA-approved drugs from 1992 to 2008 indicated a clear trend that the racemate drugs are decreasing from 1992 (about 21%) to 2008 (5%), without any new racemic drug introduction in 2001 and 2003. The chiral drugs increased from 30–40% in the 1990s to around 60% or above since 2000 [5].

The concept of "chiral switches" was introduced in the late nineties [17; 18], which means replacement of an already approved racemate by a single enantiomer [19], but the term was redefined to include drugs that were essentially developed as racemates but not necessarily approved and marketed as racemates prior to the switch [20]. Chiral switch is not to be mixed up with the sequence of operations that alternate between equilibrium and non-equilibrium conditions to switch the absolute configuration of a chiral center [21]. Dexmedetomidine (D-MDT), which is studied in manuscripts 3 and 4, represents an example of a chiral switch where the racemate MDT was available for veterinary use in the United States in 1996, while D-MDT was approved in 2006 for use in dogs and cats [22], but D-MDT was already approved by the US-FDA in 1999 for human use [23].

Chiral switching has potential advantages that include improving therapeutic index through increased potency and selectivity and decreased side-effects; improving the onset and duration of effect; and a decreasing propensity for drug-drug interactions, mediated largely by exploitation of stereoselectivity in pharmacokinetic properties [19].

The chiral switches are thoroughly reviewed in the literature [24–26]. However, patenting of single enantiomers of already approved racemate is controversial. The main contra arguments are that it is mainly meant to extend patent franchise and protect against generic competition with the racemate, in addition to the enormous expenditure with no evidence of superiority of the single enantiomer over the racemate at comparable doses in some cases [27; 26].

1.1.4. Regulatory guidelines for the enantiomeric purity of drugs

The United States food and drug administration (FDA) issued a guideline on the Development of New Stereoisomeric Drugs in 1992 [28] and the European medicines agency (EMA) issued a similar one in 1993 [1]. However, both guidelines did not specify a limit for the enantiomeric purity of single isomeric substances [29; 30]. Although the guideline of International Council for Harmonisation of Technical Requirements for Pharmaceuticals for Human Use (ICH) regarding specifications for test procedures and acceptance criteria for new drug substances and products (Q6A) excluded the chiral impurities from the thresholds defined in the guidelines Q3A and Q3B, but there is general consent that enantiomeric impurities should be considered in the same manner as other impurities [31–33]. DXM (Fig. 1) represents a good example for the development of regulations regarding enantiomeric purity since it was only covered by test of specific rotation in the pharmacopoeias. In 2013, severe adverse effects including cyanosis, respiratory distress, and seizures in addition to 60 fatalities were reported by the World Health organization due to consumption of dextromethorphan cough syrups contaminated with the respiratory suppressant enantiomeric impurity LVM [34; 35]. This led to introducing chromatographic tests for the enantiomeric purity of DXM in the United States Pharmacopeia [36] and the International Pharmacopoeia [37].

1.2.   Capillary Electrophoresis

1.2.1.   Basic principles and instrumentation

Capillary electrophoresis (CE) is a physical analytical technique based on the migration of charged analytes in an electrolyte solution inside a capillary under the influence of a direct-current electric field [38; 36]. The separation takes place usually in a narrow bore fused silica capillary with an inner diameter (ID) of 25-100 micrometers, but it was later extended to include microfluidic or nanofluidic channels (primarily on plastic or glass chips) [39].

A basic CE system (Fig. 4) is composed of silica capillary whose both open ends are immersed in two containers filled with an ionic solution known as the Background electrolyte (BGE). The same solution is also filled into the capillary. An electrode is immersed in each container (a cathode and an anode), and both are attached to a high voltage power supply that supplies a direct current having an adjustable voltage (usually from 0.5 up to 30 kilovolts), with the possibility of automatic polarity switching.
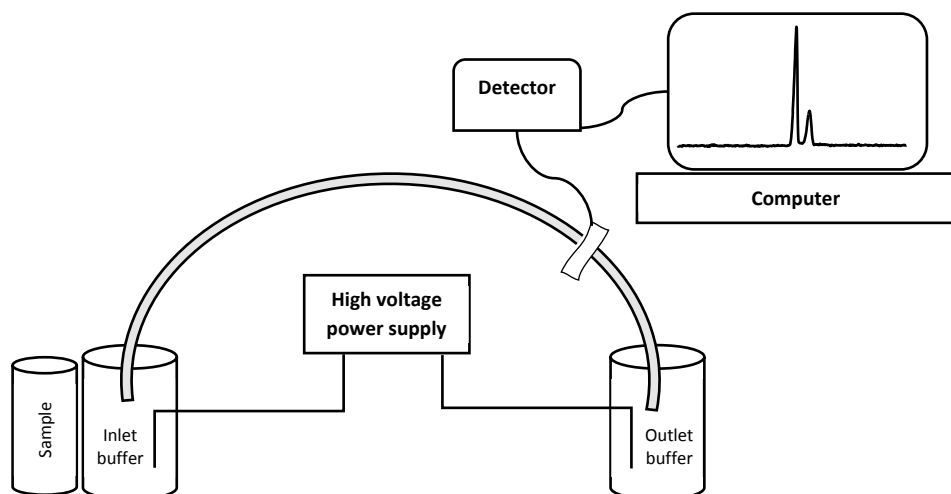
Figure 4 Schematic configuration of a basic CE system with on capillary detection

The most common CE separations involve aqueous buffers as BGEs, although other solvents are also (less frequently) applied in non-aqueous Capillary electrophoresis (NACE), where polar organic solvents (e.g. Methanol, acetonitrile, formamide, N-methylformamide) are used to prepare the BGEs [40].

CE silica capillaries are coated with a polymer (e.g. polyimide) to ensure flexibility, therefore a contactless detector is installed on the so-called detection window which is UV-Vis transparent part of the capillary usually situated near the outlet end in the capillary. The prevalent contactless (on capillary) detection principle is UV Absorption which is a default part of the commercial CE systems either as an adjustable single wavelength detector or a photo diode array detector (DAD). Contactless conductivity detection (CCD) and laser induced fluorescence (LIF) are also examples of on capillary detection with

the latter being very sensitive but only capable of measuring fluorescent samples which may require prior sample labeling. A sensitive and selective direct mass spectrometric (CE-MS) detection is also possible by coupling the open end of the capillary through an interface to the detector [41].

Different approaches are deployed for introduction of sample solution into the capillary. These include hydrodynamic injection (HDI) by applying pressure or vacuum, electrokinetic injection (EKI), and gravity (siphoning) [42]. HDI and EKI are predominantly applied for sample injection.

Joule heating is inherent to CE because of the electric current established across the capillary filled with an electrolyte solution. It is necessary to maintain the temperature of the capillary stable in order to ensure a good peak shape and a reproducible separation. Thermostatic mechanisms for CE capillaries depend on air or liquid cooling by using perfluorinated compounds [43].

CE systems are usually connected to a computer that controls the device and acquires the detector signals. In early systems the signals were recorded with an integrator. Most instruments for routine use have an integrated autosampler.

1.2.1.1.   Driving forces in capillary electromigration

The mobility of an analyte under an electric field is determined by two phenomena, electrophoresis and electroosmosis [44; 38].

Electrophoresis is the force that drives charged particles in solution under the action of an electric field. The electrophoretic mobility of a solute (μ_{ep}) depends on its own characteristics (charge, molecular size and shape) and those of the buffer where the migration takes place (type and ionic strength of the electrolyte, pH, viscosity and additives) [42]. The electrophoretic velocity (v_{ep}) of a solute, assuming a spherical shape, is given by the equation:

$$v_{ep} = \mu_{ep} \times E = \left(\frac{q}{6\pi\eta r}\right) \times \left(\frac{V}{L}\right) \qquad (1)$$

Where: q = the effective charge of the solute, η = viscosity of the electrolyte solution, r = Stoke's radius of the solute, V = applied voltage, L = total length of the capillary, $E = V/L$ electric field strength.

If two analytes have different mobilities, in a CE system, they will be separated as they migrate in different velocities.

Electroosmosis has a fundamental role in CE operation. When an electric field is applied to a conductive solution in a capillary that has fixed charges on its interior wall, a plug-like flow of solvent is generated inside the capillary, called electro-osmotic flow (EOF). In a bare (uncoated) fused silica capillary, the inner surface contains ionizable silanol groups (SiOH) that have pk_a values from 4 to 6. At pH values higher than 4, silanol groups ionize, and thus the inner capillary surface has a negative charge [45]. As hydrated cations accumulate near the surface, a so-called double layer (Fig. 5) is built. The EOF results from the effect of the applied electric field on the solution double layer at the wall and drives

the solutes towards the cathode in this case. The EOF velocity depends on the electro-osmotic mobility (μ_{eo}) which in turn depends on the charge density on the capillary internal wall and the buffer characteristics (conductivity and viscosity) [46]. The electro-osmotic velocity (v_{eo}) is given by the equation:

$$v_{eo} = \mu_{eo} \times E = \left(\frac{\varepsilon\zeta}{\eta}\right) \times \left(\frac{V}{L}\right) \qquad (2)$$

Where: ε = buffer solution's dielectric constant, ζ = zeta potential of the capillary surface.

The predominant factor that controls the zeta potential in a bare silica capillary is the pH of the BGE, therefore the EOF becomes faster with the higher pH values and reaches the maximum when the silanol groups are fully ionized above ca. pH 9 [42].
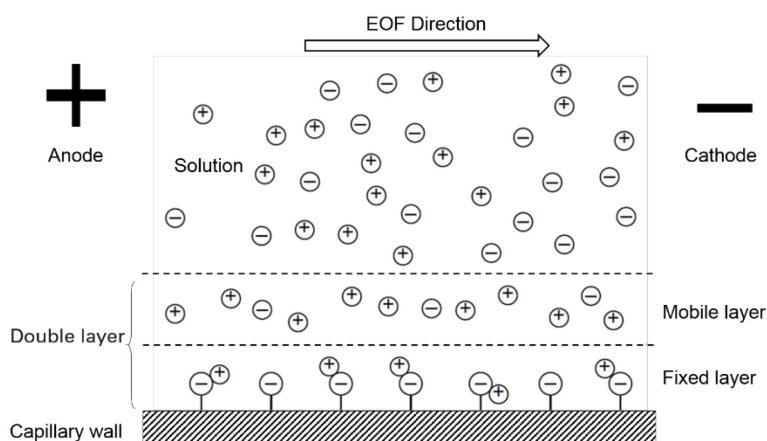
Figure 5 Electro osmotic flow (EOF) in a bare fused silica capillary

The overall velocity of the solute (v) is the sum of both driving forces:

$$v = v_{eo} + v_{ep} = E \times (\mu_{eo} + \mu_{eo}) \qquad (3)$$

Dividing equation (3) by the strength of the electric field E results in the effective mobility (μ_{eff}):

$$\mu_{eff} = \mu_{eo} + \mu_{eo} \qquad (4)$$

The electrophoretic mobility and the EOF may act synergistically driving the analyte in the same direction or against each other in different directions. Cations migrate to the cathode in an uncoated silica capillary since their own mobility is in the EOF direction, while Anions that tend to migrate oppositely due to their charge are ruled by the EOF value that can drive them to the cathode when it is faster than their own electrophoretic velocities. Hence, both cations and anions can be separated in one run with a suitable EOF. The EOF can be suppressed, modified, or even reversed by derivatizing the capillary wall or coating it using different strategies [47].

1.2.2.   Examples of capillary electrophoresis modes

1.2.2.1.   Capillary zone electrophoresis (CZE)

Very often, capillary electrophoresis refers to CZE, which is the simplest form of CE. In this mode, the analytes are separated in a capillary containing only buffer without any anticonvective medium [38; 36], and separation occurs because solutes migrate at different velocities and in discrete zones. CZE can be performed in the presence or absence of EOF and its high flexibility allows analyzing compounds with low and high molecular weights [48].

1.2.2.2.   Micellar electrokinetic chromatography (MEKC)

MEKC is a hybrid of electrophoresis and chromatography where samples are separated by differential partitioning between two phases. The main advantage is that it can simultaneously separate neutral solutes as well as charged ones [42]. Surfactants are added to the BGE to enable the separation of neutral species at a concentration above its critical micelle concentration (CMC), which leads to the formation of micelles (aggregates of surfactant molecules) that are often spherical with the hydrophobic tails oriented towards the center, and the charged heads forming the surface adjacent to the buffer. Sodium dodecyl sulfate (SDS) is predominantly used as the surfactant in MEKC. The micelles act as a pseudo stationary phase, where the analytes will distribute between them and the bulk aqueous phase depending on their partition coefficient. The hydrophilic neutral analytes having no affinity for the micelle remain in the aqueous phase and migrate with the EOF, while hydrophobic neutral species will migrate in the micellar phase depending on their hydrophobicity, which in turn affects the mobility of their "carrier" micelles. The migration behavior of charged analytes is more complex since it combines the hydrophobic partitioning, electrophoretic mobility and electrostatic interaction with the micelles [50; 48].

1.2.2.3.   Capillary gel electrophoresis (CGE)

The separation takes place inside a capillary filled with a gel that acts as a molecular sieve in this mode. The sieving effect occurs as solutes of various sizes migrate through the gel filled capillary toward the detector, as smaller molecules migrate faster through the network of the gel and thus can be separated from larger ones. This technique is applied in biochemistry for the separation of analytes having no differences in mass-to-charge ratio (e.g. nucleic acids and proteins or their complexes) [48; 42; 49].

1.2.3.   Capillary electrophoresis for chiral analysis

1.2.3.1.   Theory of chiral separation in CE

Chiral separation in CE can be achieved indirectly, i.e. via derivatizing the samples with a single enantiomer reagent which binds covalently to the enantiomers in the sample and forms diastereomers

that can be separated in an achiral environment. Nevertheless, the prevalent method is the direct separation by adding a suitable chiral selector to the BGE which enables the enantioresolution, via the formation of transient diastereomeric complexes with the enantiomers in a thermodynamic equilibrium [51; 52].

When using a single selector, and assuming the 1:1 stoichiometry of the analyte–selector complexes, the equilibria between the S and R enantiomers of the analyte and the chiral selector, C, are given by:

$$S + C \to SC \qquad K_S = \frac{[SC]}{[S][C]}$$

$$R + C \to RC \qquad K_R = \frac{[RC]}{[R][C]} \qquad (5)$$
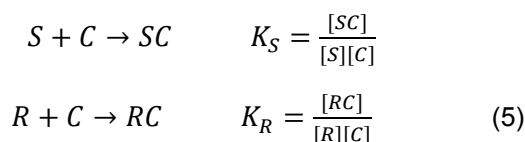
The solute enantiomers may exist in a complexed and a noncomplexed form in the presence of a chiral selector and the effective mobility (μ_{eff}) of each enantiomer can be given as:

$$\mu_{eff} = \frac{\mu_f + \mu_C.K.[C]}{1 + K.[C]} \qquad (6)$$

where μ_C is the mobility of the analyte–selector complex, μ_f the mobility of the free analyte, K the complexation constant of the corresponding enantiomer, and [C] the molar concentration of the chiral selector [53; 54].

In order that an enantioseparation takes place, a difference in the effective mobilities of the enantiomers, μ_{eff}^S and μ_{eff}^R is required:

$$\Delta\mu_{eff} = \mu_{eff}^S - \mu_{eff}^R = \frac{\mu_f^S + \mu_C^S.K_S.[C]}{1 + K_S.[C]} - \frac{\mu_f^R + \mu_C^R.K_R.[C]}{1 + K_R.[C]} \qquad (7)$$

As seen in equation (7), the enantioseparations in CE are governed by the difference of complex mobilities and/or the difference of complexation constants. These two enantioselective principles are called the chromatographic and the electrophoretic mechanisms.

The **chromatographic** (or thermodynamic) mechanism, which also governs enantioresolution in HPLC, is based on the different affinities of the selector toward the solute enantiomers, which can be expressed as complexation constants ($K_S \neq K_R$) [52].

The **electrophoretic** enantioselective mechanism results from differences in the mobilities of the enantiomer-selector complexes, for example as a result of differences in their hydrodynamic radii or the so-called complexation-induced pK_a shift [55; 56].

The separation in chiral CE can be due to both mechanisms, but the chromatographic mechanism is typically the dominant one since the enantiomer–selector complexes have similar charge densities and their hydrodynamic radii do not differ significantly [52]. Nevertheless, it is also possible to obtain an enantioseparation when both enantiomers have similar affinities to the selector ($K_R = K_S$) [56].

1.2.3.2.   Cyclodextrins as chiral CE additives

Many additives can be used as chiral selectors in CE separations. These include cyclodextrins, macrocyclic antibiotics, crown ethers, polysaccharides and proteins among others [57; 58]. Nevertheless, cyclodextrins are the most used chiral selectors in CE due to their stability, UV-transparency, availability, the large number of derivatives, and the affordability of most of them [59–61].

Cyclodextrins (CDs) are cyclic oligosaccharides, which consist of α1,4-linked d-glucopyranose units. The three native CDs are α-CD which consists of six glucose units, β-CD seven and γ-CD eight. The three-dimensional structure of CDs is like hollow toroids with a lipophilic cavity and a hydrophilic outside [59]. The narrow rim contains the primary 6-hydroxyl groups, while the wider rim features the secondary 2- and 3-hydroxyl groups (Fig. 6). A large number of CD derivatives can be prepared by chemical derivatization of the hydroxyl groups and many of them are commercially available [62; 58]. CDs are also applied as chiral selectors in GC [63], and HPLC [64].
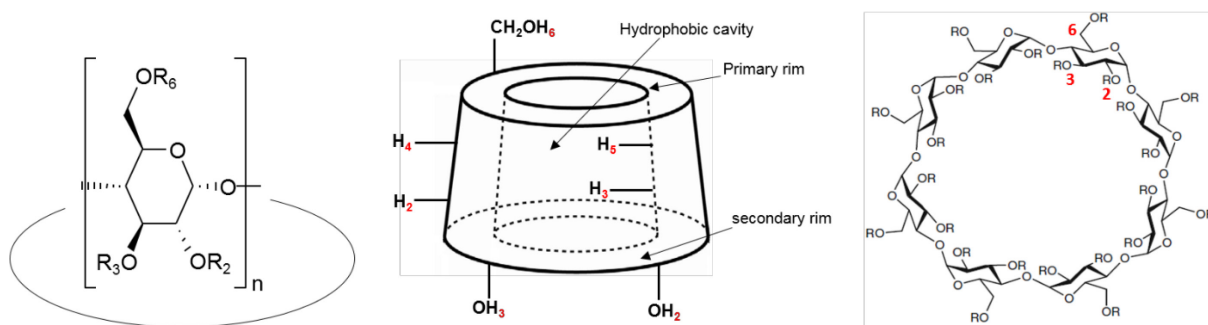
Figure 6 The general formula of CDs where: α-CD (n=6), β-CD (n=7) and γ-CD (n=8) **(left)**, the three-dimensional toroidal shape of the CDs with the spatial positions of OH groups (2,3,6) and hydrogens (2,3,4,5) **(middle)**, and the structure of γ-CD showing the substitution sites on the hydroxyl groups **(right)**

The native α-, β-, and γ-cyclodextrins have many neutral derivatives (methyl, ethyl, hydroxyalkyl, etc.) or ionizable ones (aminomethyl, carboxymethyl, sulfobutyl ether, etc.) groups. The structures of the most frequently use CDs in this work are summarized in Table 1.

Table 1 Structures of selected CDs deployed in the current work (In randomly substituted CDs not all OH groups are derivatized)

CD	n	R$_2$	R$_3$	R$_6$
α-CD	6	H	H	H
M-α-CD	6	CH$_3$	CH$_3$	CH$_3$
HP-α-CD	6	CH$_2$-CHOH-CH$_3$	CH$_2$-CHOH-CH$_3$	CH$_2$-CHOH-CH$_3$
CM-α-CD	6	CH$_2$-COOH	CH$_2$-COOH	CH$_2$-COOH
S-α-CD	6	SO$_3$H	SO$_3$H	SO$_3$H
β-CD	7	H	H	H
M-β-CD	7	CH$_3$	CH$_3$	CH$_3$
DM-β-CD	7	CH$_3$	CH$_3$	CH$_3$
TM-β-CD	7	CH$_3$	CH$_3$	CH$_3$
HE-β-CD	7	CH$_2$-CH$_2$-OH	CH$_2$-CH$_2$-OH	CH$_2$-CH$_2$-OH
HP-β-CD	7	CH$_2$-CHOH-CH$_3$	CH$_2$-CHOH-CH$_3$	CH$_2$-CHOH-CH$_3$
CM-β-CD	7	CH$_2$-COOH	CH$_2$-COOH	CH$_2$-COOH
SBE-β-CD	7	(CH$_2$)$_4$-SO$_3$H	(CH$_2$)$_4$-SO$_3$H	(CH$_2$)$_4$-SO$_3$H
S-β-CD	7	SO$_3$H	SO$_3$H	SO$_3$H
HS-β-CD	7	H	H	SO$_3$H
γ-CD	8	H	H	H
M-γ-CD	8	CH$_3$	CH$_3$	CH$_3$
HP-γ-CD	8	CH$_2$-CHOH-CH$_3$	CH$_2$-CHOH-CH$_3$	CH$_2$-CHOH-CH$_3$
CM-γ-CD	8	CH$_2$-COOH	CH$_2$-COOH	CH$_2$-COOH
S-γ-CD	8	SO$_3$H	SO$_3$H	SO$_3$H

M-α-CD, methyl-α-CD; **HP-α-CD**, hydroxypropyl-α-CD; **CM-α-CD**, carboxymethyl-α-CD; **S-α-CD**, sulfated α-CD; **CM-β-CD**, carboxymethyl-β-CD; **M-β-CD**, methyl-β-CD; **DM-β-CD**, heptakis(2,6-di-O-methyl)-β-CD; **S-β-CD**, sulfated β-CD; **HP-γ-CD**, hydroxypropyl-γ-CD; **CM-γ-CD**, carboxymethyl-γ-CD; **M-γ-CD**, methyl-γ-CD; **S-γ-CD**, sulfated γ-CD; **HS-β-CD**, heptakis(6-di-O-sulfo)-β-CD; **HP-β-CD**, hydroxypropyl-β-CD; **SBE-β-CD**, sulfobutylether-β-CD, **TM-β-CD**, heptakis(2,3,6-tri-O-methyl)-β-CD

1.2.3.3.   Chiral CE in pharmaceutical analysis

A key feature of CE is the overall simplicity of the instrumentation. Moreover, CE has many established benefits such as the small sample volume (usually a few nanoliters), high separation efficiency, low cost, eco-friendliness due to the reduced use of organic solvents, and high flexibility in method development

[65; 66]. Consequently, it has been increasingly used for the analysis of pharmaceuticals [67–70; 49; 71] including of peptides/proteins, chiral pharmaceuticals, and other small-molecule drugs.

As an effective method for stereoisomer separations, chiral CE is widely applied for analytical enantioseparations of drug compounds in pharmaceuticals and biological media [62; 72–77].

Although CE and other electromigration techniques are well-established in the analysis of biomolecules, such as DNA and proteins, they are still not widely used as routine methods for the enantiomeric purity of drugs in the official compendia compared to HPLC [78].

1.3.   Experimental design in development of analytical separation methods

The classic development and optimization of analytical separation methods depended in the past on screening the effect of each factor affecting the separation alone (one-factor-at-a-time or OFAT). This approach is time consuming due to the large number of experiments and it doesn't take the factors interaction into account. Quality by design (QbD) approach has largely replaced OFAT as a strategy for the development of analytical separation methods in the recent years. QbD is described as the definition of a systematic approach for the setting up of analytical methods [79]. It employs multivariate design of experiments (DoE) and risk assessment tools for the identification of the critical process parameters (CPPs), which are the experimental factors that influence the critical quality attributes (CQAs) of the method [79–83]. This leads to understanding of the quantitative effects of the CPPs on the analytical process [84]. Risk analysis is also an essential part of the analytical pharmaceutical development which incurs the product and the process [85; 86]. The steps of an analytical separation method development using QbD are described concisely here, with specific concentration on CE and chiral CE methods.

1.3.1.   Determination of the analytical target profile and scouting experiments

The first step in QbD-assisted method development is defining the analytical target profile (ATP), which is a set of criteria that define what will be measured and the performance criteria of the method, but without necessarily specifying the method itself [87]. The aim of an analytical separation technique is to obtain an assay that allows the successful separation and quantification of the analytes in a short analysis time, with accepted reproducibility and ruggedness [81]. The CQAs are quality criteria for the results generated by analytical method and can be defined considering the ATP. The analytical run time and the resolution (enantioresolution in chiral CE) are mainly identified as CQAs in CE methods, but they may also include the theoretical plate count, signal to noise ratio, and/or signal intensity [80; 83]. Initial scouting experiments are performed afterwards in order to provide an idea of the method that can be further optimized. This includes in case of chiral CE screening different chiral selectors to identify a suitable one (or a combination).

1.3.2. Identification of the CPPs

Many factors affect the CQAs of separation methods such as the column (length, type, dimensions, particle size), and the mobile phase composition in HPLC. Initial risk assessment of the factors leads to fixing some of them and identifying others as CPPs for further optimization by DoE. The CPPs include may include quantitative as well as qualitative factors.

The CPPs in CE methods are selected from many factors that affect the method which can be categorized as instrumental parameters and factors related to the electrolyte solution.

Instrumental parameters include the applied voltage which can be increased to shorten the run time, but this would increase the capillary temperature through Joule heating and may cause peak broadening due to viscosity gradients in the buffer inside the capillary. The capillary temperature is another instrumental factor which affects the migration velocity mainly through decreasing the BGE viscosity, but care should be taken for the stability of the samples. The dimensions of the capillary (length and internal diameter) are also important factors, where a longer capillary increases the separation times but enhances the resolutions and yields lower field intensity with lower current thereby. A larger internal diameter enhances the sensitivity of the detection but increases the current for a given field intensity and BGE composition.

Electrolyte solution factors include the buffer type, which should be appropriately chosen for in the pH range of interest, and the buffer concentration to ensure proper capacity and minimize current generation. Buffer pH is an important factor since it affects the charge of the analyte or additives and can also change the EOF. Organic solvents (methanol, acetonitrile, etc.) may be added to aqueous BGEs to increase the solubility of the solute or other additives and/or to affect the degree of ionization of the sample components. In addition, the type and concentration of the chiral selector(s) in chiral CE, affects the enantioresolution, the BGE viscosity, and the generated current in case of charged selectors.

1.3.3. Knowledge space and initial screening of factors

After identifying the CPPs and the CQAs in light of the ATP and the initial scouting experiments, the knowledge space is determined by DoE. In order to perform a reasonable number of analytical runs, the effect of the CPPs as factors (within predefined ranges) on the CQAs as responses is usually determined by screening designs (e.g. fractional factorial designs) [79; 81]. The resulting statistical model leads to an initial estimation of the relative effects of the factors on each CQA, which can be estimated by graphical tools. Subsequently, some factors are fixed considering the results and the others are considered CQAs and further optimized.

1.3.4. Design space definition by response surface methodology

The design space for analytical methods can be defined as a zone of theoretical robustness where no drastic changes in the levels of the CQAs of the method should be observed [79]. The design space is

determined by response surface methodology (RSM) which comprises the prediction and optimization of the responses by using response-surface designs (e.g. central composite designs or full factorial designs) [88; 89].

1.3.5. Working point and robustness testing

The definition of the design space allows selecting a working point that meets the required CQAs within an accepted risk of failure. Subsequently, the robustness [90] of the working point is verified in order to ensure its suitability for use before further validation [84].

1.4. Cyclodextrin-selectand complexation

Complexation of guest molecules often occurs via their inclusion into the CD cavity either from the narrower or the wider side of the torus, displacing solvent molecules from the cavity. The driving forces are Van der Waals and hydrophobic interactions, hydrogen bonding with the hydroxyl groups on the rims, and steric factors. In the case of charged CD derivatives, ionic interactions also play a role [91–93]. While most selector-selectand complexes were shown to be of the inclusion type, several studies demonstrated the formation of external complexes which led to effective CE enantioseparations [94–96].

Structural information on the complexes can be obtained by NMR and X-ray analyses. Nuclear Overhauser effect-based NMR methods, in particular rotating frame nuclear Overhauser effect spectroscopy (ROESY), allow the determination of correlation of spatially close nuclei and proved to be a valuable tool to elucidate the structure of selector-selectand complexes [97–100]. Furthermore, as NMR is a solution technique, experiments can be carried out under conditions comparable to those used in CE with regard to BGE composition, pH and temperature.

CE can be applied to study the complexation between high- and low-molecular weight compounds [101–104].

1.4.1. Stoichiometry of CD complexes

The stoichiometry of CD complexes has been determined by many techniques [105–107], including NMR spectroscopy [97; 98; 100]. The most commonly reported stoichiometry for CD complexes is 1:1 (solute:CD) [105; 107; 106] although higher order aggregates have also been published. The composition 1:2 is the second most abundant [107]. In contrast, stoichiometries of 1:3, 2:1 and 2:2 have been rarely reported. Furthermore, ternary CD complexes including additional background electrolyte components such as SDS in addition to the analytical solute with a ratio of 1:1:1 were described [108; 109].

2. Scopes and objectives

The regulatory requirements for the chiral purity of pharmaceuticals have become more important over time. Although chiral HPLC is widely used for this purpose as it is mainly the method of choice in compendial monographs for the enantiomeric purity determination, but chiral capillary electrophoresis is also a strong and flexible tool thereof, with an increasing number of examples published over the years.

In the recent years QbD methodology largely replaced the trial and error approach which involves optimizing one experimental factor each time. QbD has become a standard approach followed foe method development in analytical separation techniques including CE.

Regarding chiral CE, cyclodextrins are the most widely applied selectors due to their versatility, stability, UV-transparency, and the commercial availability of many derivatives. The underlying mechanisms of chiral recognition using CDs can be studied with CE itself by calculating the thermodynamic parameters that govern the separation. NMR spectroscopy is also an important tool for elucidating the structures of the CD complexes with the analytes. Additionally, molecular dynamics (MD) simulations help to understand the complexation mechanisms.

Considering all this, the aim of the work was:

- Development and validation of CE assays for the enantiomeric purity of the drugs Amb, DXM and D-MDT at the 0.1% level, with acceptable accuracy and precision.

- Following a QbD methodology for method development, optimization and validation.

- Elucidation of the chiral separation mechanisms for DXM and D-MDT.

- Explaining the role of a dual selector system in peak shape improvement in the case of DXM.

- Using CE, NMR, and molecular dynamics to understand the role of CD cavity size and CD substitution pattern in the reversal of enantiomeric migration order.

- Clarifying an unusual complexation behavior of γ-CD and daclatasvir which is observed in CE, by using NMR and mass spectroscopy in addition to CE methods.

3. Manuscripts

3.1. Manuscript 1

Quality by Design-Guided Development of a Capillary Electrophoresis Method for the Chiral Purity Determination of Ambrisentan

Personal Contribution (85 %): study design and concept development, experimental work, data analysis and interpretation, preparation of manuscript draft.

Gerhard K. E. Scriba (10 %): supervision or research, finalizing manuscript.

Michal Douša (5 %): supplying ambrisentan and the *R*-enantiomer.

Overview:

The manuscript describes the development of a chiral CE method for the determination of the chiral purity of the drug ambrisentan utilizing experimental design methodologies. Method development, optimization and robustness testing were supported by chemometrics. The method was validated and allowed the detection of 0.1 % of the enantiomeric impurity.

ORIGINAL

Quality by Design-Guided Development of a Capillary Electrophoresis Method for the Chiral Purity Determination of Ambrisentan

Sulaiman Krait[1] · Michal Douša[2] · Gerhard K. E. Scriba[1]

Abstract A quality by design approach utilizing experimental design methodologies was applied to develop a CE method to evaluate the enantiomeric purity of (*S*)-ambrisentan, a selective endothelin receptor antagonist used for the treatment of pulmonary arterial hypertension. Initial method scouting was performed by screening native cyclodextrins (CDs) as well as neutral CD derivatives and a positively charged derivative at pH 5 and pH 9, identifying γ-CD as suitable selector at pH 5. Upon defining the critical quality attributes and the critical process parameters, i.e., chiral resolution and run time, method development was performed by application of a screening design for the identification of the significant variables and, subsequently, by a response surface methodology for obtaining the design space. A Plackett–Burman design was employed for robustness testing. The final working point conditions used a background electrolyte composed of a 50-mM sodium acetate buffer, pH 4.0, containing 30 mM γ-CD in a 75-μm ID fused-silica capillary with an effective length of 40 cm at an applied voltage of 25 kV and a capillary temperature of 25 °C. The method was validated according to the ICH Q2(R1) guideline and allowed the determination of a relative concentration of the (*R*)-enantiomer of 0.1 %.

✉ Gerhard K. E. Scriba
   gerhard.scriba@uni-jena.de

1 Department of Pharmaceutical Chemistry, Friedrich Schiller University Jena, Philosophenweg 14, 07743 Jena, Germany

2 Zentiva, a.s., U Kabelovny 130, 10237 Praha 10, Czech Republic

Introduction

Pulmonary arterial hypertension (PAH) is a rare disease that can be idiopathic or heritable in nature, or associated with other pathophysiological conditions such as scleroderma or congenital heart disease [1]. It is characterized by narrowing of the small pulmonary arteries and increased vascular resistance eventually leading to right ventricular failure [2]. The exact pathophysiological processes leading to PAH are still unknown although it is recognized that PAH has a multifactorial pathobiology involving various biochemical pathways and cell types [3]. Endothelin-1, a 21-amino acid peptide, that plays a key role in the pathobiology of PAH exerts vasoconstrictor and mitogenic effects via binding to the endothelin A and B receptors in the pulmonary vascular smooth muscle cells [4].

(*S*)-Ambrisentan [(*S*)-2-[(4,6-dimethylpyrimidin-2-yl)oxy]-3-methoxy-3,3-diphenylpropanoic acid, Fig. 1] is a diphenylpropanoic acid derivative which acts as a selective endothelin receptor antagonist with a bioavailability and half-life which allow once-daily dosing [5]. It was approved by US Food and Drug Administration (FDA) in 2007 [6] and by the European Medicines Agency (EMA) in 2008 [7]. Several HPLC methods for the determination of (*S*)-ambrisentan and its related substances in bulk drug or dosage forms [8–12] as well as LC–MS methods for the analysis of the drug in plasma [12–15] have been reported. Because (*S*)-ambrisentan is an enantiomerically pure drug possessing (*S*)-configuration, LC methods have been developed for the analysis of the chiral purity of the drug [16, 17].
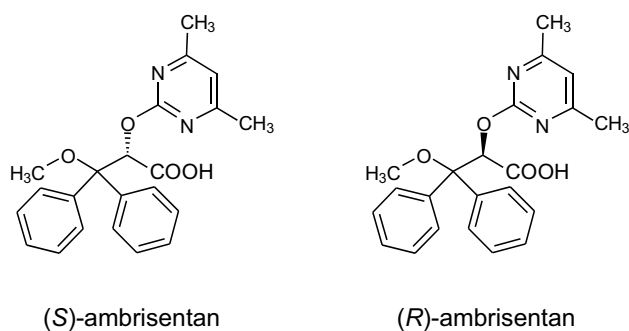
Fig. 1 Structures of (*S*)-ambrisentan and (*R*)-ambrisentan

CE has long been recognized as a suitable technique for enantioseparations including the analysis of the chiral purity of drugs due to the high separation efficiency and low consumption of sample and chemicals [18–21]. Therefore, the aim of the present study was the development of a CE method for the determination of the chiral purity of (*S*)-ambrisentan. Quality by design (QbD) was employed as a risk-based approach in analytical method development [22–24]. Using predefined critical quality attributes, a screening phase followed by response surface methodology allowed the definition of a design space in combination with Monte Carlo simulations.

Materials and Methods

Chemicals

(*S*)-Ambrisentan (purity 99.7 %) and (*R*)-ambrisentan (purity 99.6 %) were a gift from Zentiva (Praha, Czech Republic). A commercial sample was from TCI Europe (Zwijndrecht, Belgium). β-cyclodextrin (β-CD) was from Wacker Chemie AG (Burghausen, Germany). Hydroxyethyl-β-cyclodextrin (HE-β-CD, degree of substitution (DS) ~4.9), γ-cyclodextrin (γ-CD), and metformin hydrochloride were from Sigma-Aldrich (Steinheim, Germany). α-Cyclodextrin (α-CD), hydroxypropyl-α-cyclodextrin (HP-α-CD, DS ~4.5), methyl-β-cyclodextrin (M-β-CD, DS ~12), hydroxypropyl-β-cyclodextrin (HP-β-CD, DS ~4.5), hydroxypropyl-γ-cyclodextrin (HP-γ-CD, DS ~4.5) and (2-hydroxy-3-*N,N,N*-trimethylamino)propyl-β-cyclodextrin chloride (TMA-β-CD, DS 2.5–4.5) were from Cyclolab Ltd. (Budapest, Hungary). Boric acid, sodium tetraborate decahydrate, glacial acetic acid and sodium hydroxide were from Merck (Darmstadt, Germany). Water was purified by a GenPure system (Thermo Fischer, Waltham, USA).

Sample Solutions

A stock solution of (*S*)-ambrisentan at a concentration of 1.4 mg L^{-1} was prepared in water/methanol/0.1 M sodium hydroxide (6:2:2, v/v/v), while a stock solution of (*R*)-ambrisentan at a concentration of 0.5 mg mL^{-1} was prepared in water/methanol/0.1 M sodium hydroxide (8:1:1, v/v/v). Dilution of the stock solutions to the appropriate concentrations was performed in such a way that the sample solutions were obtained in the solvent system water/methanol/0.1 M sodium hydroxide (8:1:1, v/v/v). Sample solutions were stored at –20 °C for a maximum of 14 days. Prior to use, the solutions were filtered (0.22 μm) and sonicated for 5 min.

Instrumentation

CE experiments were performed using a Beckman P/ACE MDQ capillary electrophoresis system (Beckman Coulter, Krefeld, Germany) equipped with a UV–Vis diode array detector. The 32 Karat software (version 8.0) was used for system control, data acquisition and processing. 40/50.2-cm fused-silica capillaries with an ID of either 50 or 75 μm and an OD of 363 μm were from BGB Analytik (Schloßböckelheim, Germany). A new capillary was successively rinsed at a pressure of 20 psi (138 kPa) with 0.1 M sodium hydroxide for 10 min, water for 15 min, and acetic acid 1 % (v/v) for 20 min. At the beginning and end of each day, the capillary was rinsed with 0.1 M sodium hydroxide for 5 min, water for 10 min and acetic acid 1 % (v/v) for 20 min. Between analyses, the capillary was flushed with water for 1 min, acetic acid 1 % (v/v) for 1 min and the background electrolyte (BGE) for 3 min. The BGE consisted of 30 mM γ-CD in 50 mM acetic acid, adjusted to pH 4.0 by the addition of 0.1 M sodium hydroxide. The BGE was filtered (0.22 μm) and sonicated for 10 min prior to its use. The applied voltage was 25 kV, and the capillary temperature was set at 25 °C. Hydrodynamic sample injection was performed at a pressure of 0.7 psi (4.8 kPa) for 5 s. UV detection was carried out at the cathodic end at 200 nm.

Software

MODDE 10.1 (Umetrics, Umea, Sweden) was used for the experimental design and statistical analysis of the screening, response surface methodology and robustness testing. The data obtained from the respective designs were fitted to a model using the quadratic polynomial equation [25]:

$$y = \beta_0 + \sum_{i=1}^{f} \beta_i x_i + \sum_{1 \le i \le j}^{f} \beta_{ij} x_i x_j + \sum_{i=1}^{f} \beta_{ii} x_i^2 ,$$

where *y* is the predicted response (resolution or migration time), β_0 is the intercept, β_i are the coefficients to be optimized (voltage, temperature, buffer pH and concentration, and/or CD concentration), β_{ij} are the interaction

coefficients, and β_{ii} are the quadratic coefficients, with the interaction effect terms restricted to two-factor interactions. Microsoft Excel 2007 was used for the statistical analysis of the validation data.

Results and Discussion

Quality by design for analytical methods requires to define the analytical target profile and, subsequently, to develop and validate the method considering the critical quality attributes and critical process parameters [22–24]. Thus, the analytical target profile was defined as a method allowing the precise determination of the (R)-enantiomer at a relative concentration of 0.1 % within an analysis time of less than 10 min.

Method Scouting

(S)-Ambrisentan is a weak acid with a pK$_a$ of about 4.0 [26]. Therefore, a 100-mM sodium acetate buffer, pH 5.0, and a 25-mM sodium tetraborate buffer, pH 9.0, were initially evaluated. At these pH values, (S)-ambrisentan will be negatively charged. Native CDs as well as the neutral CD derivatives M-β-CD, HE-β-CD, HP-α-CD, HP-β-CD and HP-γ-CD and the positively charged CD derivative TMA-β-CD were studied as chiral selectors at concentrations of about 25 mM in a 50-μm ID capillary with an effective length of 40 cm at a capillary temperature of 20 °C and an applied voltage of 20 kV. A sample solution containing 40 μg mL^{-1} (S)-ambrisentan and 20 μg mL^{-1} (R)-ambrisentan was used. Neutral CDs were evaluated under normal polarity of the applied voltage, while the polarity was reversed in the presence of TMA-β-CD. At pH 9.0, no separation of (S)-ambrisentan and its (R)-enantiomer could be achieved with any of the CDs. In contrast, partial separation was observed at pH 5.0 in the presence of β-CD and HP-γ-CD with the (R)-enantiomer migrating first and using M-β-CD with (S)-ambrisentan migrating first. Only in the presence of γ-CD as chiral selector at pH 5.0, a baseline separation was achieved with the (R)-enantiomer migrating before (S)-ambrisentan. Because migration of an impurity before the major compound is preferable for CE impurity assays, γ-CD was chosen as chiral selector for further method development.

Critical Quality Attributes and Critical Process Parameters

Method development in the light of the QbD approach was performed using experimental design methodologies. Resolution (R_S) between (S)-ambrisentan and the (R)-enantiomer and the migration time of (S)-ambrisentan as the second migrating enantiomer as measure for analysis time were defined as critical quality attributes. The target values were set as baseline resolution, i.e., $R_S \geq 1.5$, and migration time of (S)-ambrisentan ≤10 min. Risk assessment of experimental factors affecting these attributes was based on the initial scouting experiments as well as general experience in chiral CE methods. Consequently, the instrumental parameters, separation voltage and capillary temperature, as well as parameters related to the BGE, i.e., pH, electrolyte concentration and CD concentration, were considered as critical process parameters.

Determination of the Knowledge Space

A fractional factorial Res V+ design was used to generate a three-level screening matrix for evaluating the effect of the critical process parameters using the following factor ranges: voltage 15–25 kV, capillary temperature 15–25 °C, pH of the BGE 3.8–5.5, acetate concentration 50–200 mM and γ-CD concentration 10–50 mM. Peak resolution and migration time were the responses. The experiments were performed using a sample solution containing 500 μg mL^{-1} (S)-ambrisentan and 5 μg mL^{-1} of the (R)-enantiomer, i.e., at a relative concentration of the enantiomeric impurity of 1 %. The design matrix as well as the data of the responses are summarized in Table S1 (see supplementary material). The data were subsequently fitted by multiple linear regression, and the models were adjusted by deleting non-significant interacting factors and adding detected square values to increase the Q^2 values, which estimate the precision of the prediction, to enhance the validity of the model. Final Q^2 values were 0.975 and 0.985 for the peak resolution and migration time models, respectively. Statistical analysis of the regression coefficients of R_S and migration time are shown in Fig. 2. The main factors affecting R_S (Fig. 2a) were pH and BGE concentration with pH showing a negative correlation (R_S increased with decreasing pH), while BGE concentration displayed a positive effect (R_S increased with concentration). Smaller effects were seen for temperature and applied voltage where increasing R_S values were observed for decreasing values of the variables. CD concentration had no significant effect on peak resolution within this experimental model. On the other hand, migration time of (S)-ambrisentan as a measure of run time (Fig. 2b) was mainly affected by the applied voltage and capillary temperature as well as BGE concentration. Thus, migration times decreased with increasing voltage and temperature, while migration times increased with increasing BGE concentrations. The pH of the BGE and γ-CD concentration were also significant but with minor effects as compared to voltage, temperature and BGE concentration.

Response Surface Methodology and Design Space

In light of the screening results of the critical process parameters, pH exerted a major effect on peak resolution and a minor effect on the run time. Thus, to obtain a high R_S value, the pH of the BGE was fixed at pH 4.0 so that it was not directly set at the edge of the screening range. Also, because the CD concentration was insignificant for peak resolution and had only a minor effect on the run time, it was set at 30 mM, i.e., the medium value of the screening range. The remaining parameters, voltage, temperature and electrolyte concentration, were further investigated by response surface methodology. A three-level central composite face-centered design of the variables, voltage (15–25 kV), capillary temperature (15–25 °C)

and acetate concentration (50–200 mM), was employed as summarized in Table S2 (see supplementary material). A sample solution containing 500 µg mL^{-1} (S)-ambrisentan and 5 µg mL^{-1} of the (R)-enantiomer was used. The data of the responses R_S and migration time were fitted by multiple linear regression and the validity of the models was enhanced by deleting non-significant interacting and square factors. Q^2 values were 0.747 and 0.864 for the peak resolution and migration time models, respectively. The regression coefficients are shown in (Fig. 3).

Figure 4a shows the sweet plots at three levels of acetate concentration of 50, 125, and 200 mM to illustrate the area represented by voltage and capillary temperature where the target values of the critical quality attributes $R_S \geq 1.5$

Fig. 2 Regression coefficients plot of the screening design of the responses **a** resolution and **b** migration time of (S)-ambrisentan. *V* applied voltage, *Temp* capillary temperature, *Buf* acetate buffer concentration in the BGE, *CD* γ-CD concentration in the BGE, *pH* pH of the BGE; $x \times x$ represent the quadratic terms for the respective parameter and $x \times y$ the interaction terms between two parameters
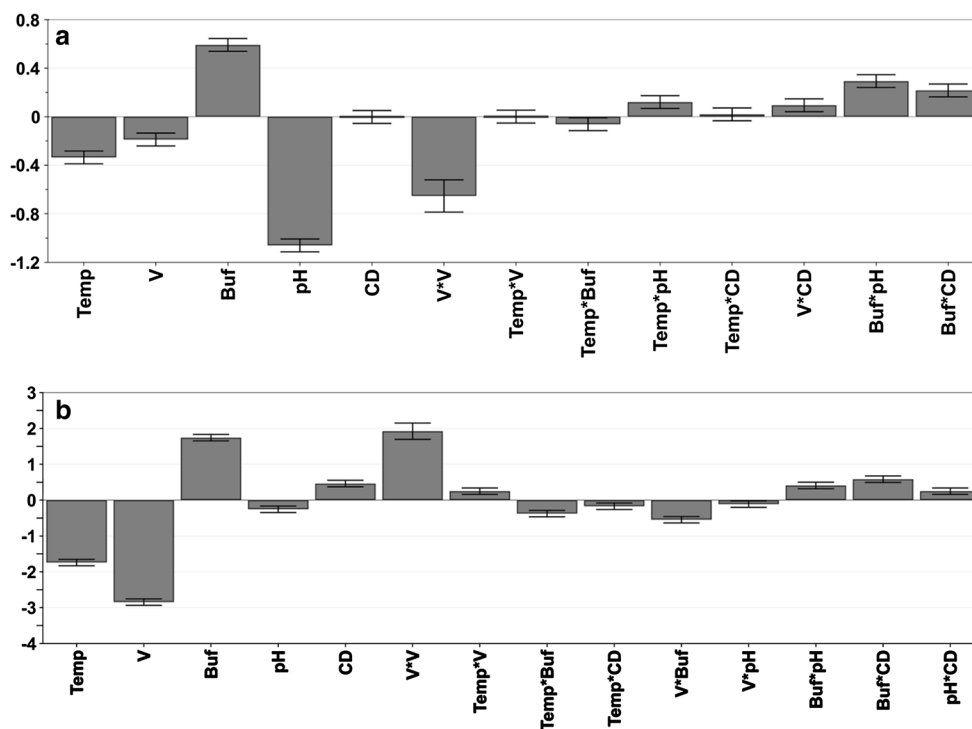
Fig. 3 Regression coefficients plot of the response surface design of the responses **a** resolution and **b** migration time of (S)-ambrisentan. *V* applied voltage, *Temp* capillary temperature, *Buf* acetate buffer concentration in the BGE, $x \times x$ represent the quadratic terms for the respective parameter and $x \times y$ the interaction terms
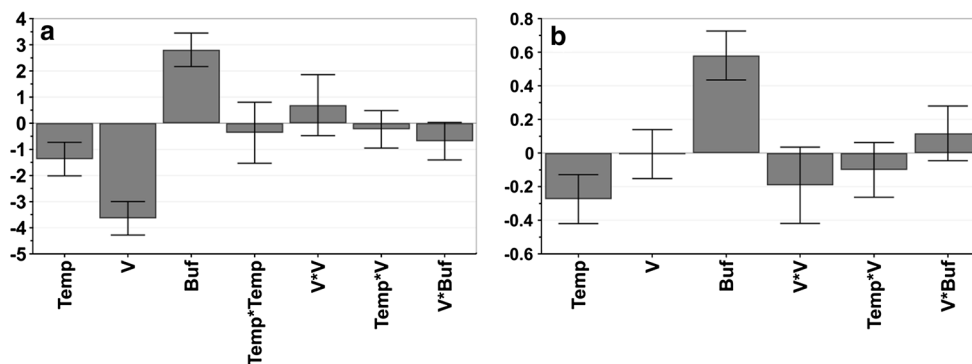
and migration time of (S)-ambrisentan ≤10 min were met. The largest area was obtained at a buffer concentration of 50 mM. Subsequent Monte Carlo simulations at the three buffer concentrations for the determination of the design space are shown in Fig. 4b. The green areas mark the conditions where failure of obtaining a peak resolution ≥1.5 within a run time ≤10 min is less than 1 %. As in the case of the sweet plots, the area is larger at the lowest buffer concentration. Subsequently, the following analysis conditions were chosen as working point: 50 mM sodium acetate buffer, pH 4.0, containing 30 mM γ-CD as chiral selector, a capillary temperature of 25 °C and an applied voltage of 25 kV. The pH of the final BGE was equal to the approximate pK_a of (S)-ambrisentan which illustrates the well-known fact that a chiral separation by CE can often be achieved at a pH of the BGE close to the pK_a of the analyte. An electropherogram

obtained for the separation of the enantiomers under these experimental conditions is shown in Fig. 5.

Robustness Testing

To ensure the detection of a relative concentration of 0.1 % of the (R)-enantiomer, the sample concentration was increased to 700 µg mL^{-1} for (S)-ambrisentan and 7 µg mL^{-1} for (R)-ambrisentan, and the ID of the capillary was increased to 75 µm. Prior to method validation, the robustness of the method was verified by deliberately changing the critical process parameters within the following ranges: voltage 25 ± 1 kV, temperature 25 ± 1 °C, buffer pH 4.0 ± 0.1, buffer concentration 50 ± 2 mM and γ-CD concentration 30 ± 2.5 mM. A Plackett–Burman design was applied for the robustness test. The matrix as
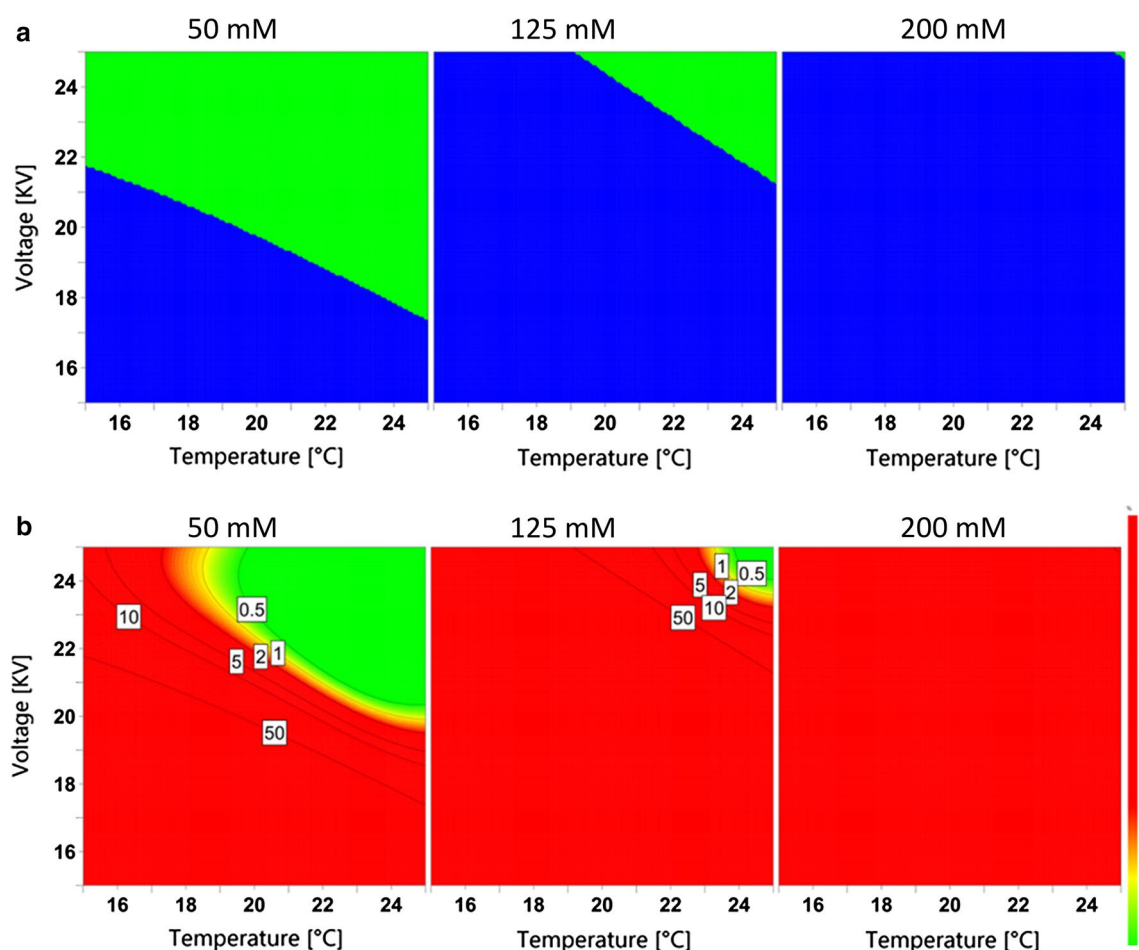
Fig. 4 Sweet spot plots (**a**) and design space plots for risk of failure (**b**) at three levels of acetate buffer concentration of 50, 125, and 200 mM with the area represented by applied voltage and capillary temperature. **a** *Green areas* represent areas where both criteria, $R_S \geq 1.5$ and migration time ≤10 min, are met, while the *blue zones* indicate where only the R_S criterion is met. **b** *Green areas* represent areas with a risk of failure of less than 1 % to meet the criteria $R_S \geq 1.5$ and migration time ≤10 min
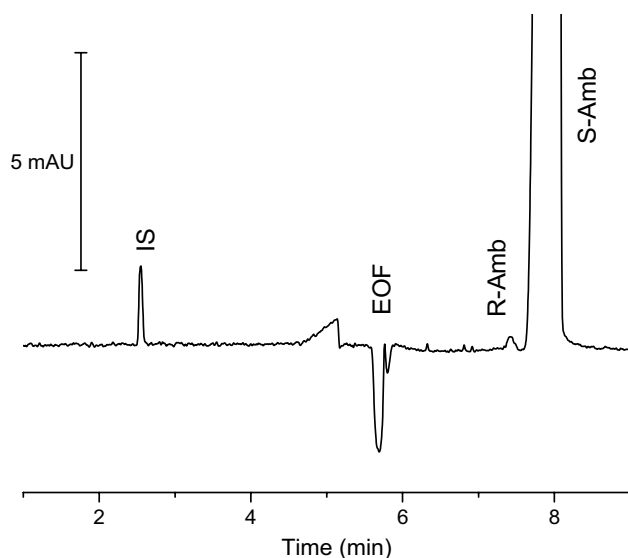
Fig. 5 Electropherograms of a sample containing 700 µg mL^{-1} (*S*)-ambrisentan and 0.7 µg mL^{-1} of the (*R*)-enantiomer corresponding to a relative concentration of 0.1 %. Experimental conditions, 40/50.2 cm, 75 µm ID fused-silica capillary, 50 mM sodium acetate buffer, pH 4.0, containing 30 mM γ-CD, 25 kV, 25 °C. *S-Amb* (*S*)-ambrisentan, *R-Amb* (*R*)-ambrisentan, *IS* internal standard metformin hydrochloride, concentration 15 µg mL^{-1}

well as the resulting data for the critical quality attributes R_S and migration time are summarized in Table S3 (see supplementary material). Statistical analysis revealed no correlation with standard deviations including zero. Furthermore, the data were within the acceptance criteria, i.e., $R_S > 1.5$ and analysis time <10 min. Thus, the method was robust and was subsequently validated.

Method Validation

The optimized method was validated according to the ICH guideline Q2(R1) [27]. Metformin hydrochloride at a concentration of 15 µg mL^{-1} was selected as internal standard. Metformin is a basic compound and, therefore, migrates before the EOF so that the total analysis time is not affected.

The specificity of the method was demonstrated by the resolution between the peaks of (*S*)-ambrisentan and its (*R*)-enantiomer. A sample containing only (*S*)-ambrisentan at a concentration of 700 µg mL^{-1} showed no interfering peaks at the migration times of the (*R*)-stereoisomer or the internal standard (data not shown). The limit of detection (LOD) and the limit of quantitation (LOQ) for (*R*)-ambrisentan were calculated based on signal-to-noise (S/N) ratios of 3 and 10, respectively, and were found to be 0.2 and 0.7 µg mL^{-1}. An electropherogram of a sample containing 0.7 µg mL^{-1} of the (*R*)-enantiomer in the presence of 700 µg mL^{-1} (*S*)-ambrisentan, corresponding to a relative concentration of the enantiomeric impurity of 0.1 %, is shown in Fig. 5.

The linearity of the method was evaluated by analyzing five sample concentrations in triplicate between 0.7 and 7.0 µg mL^{-1} of (*R*)-ambrisentan in the presence of 700 µg mL^{-1} (*S*)-ambrisentan (relative concentrations of 0.1–1 %). Linear regression of the ratios of the corrected peak areas of (*R*)-ambrisentan and the internal standard yielded the equation $y = (0.09085 \pm 0.0017)x + (0.04714 \pm 0.00761)$ with a coefficient of determination $r^2 = 0.9955$. Accuracy and precision data are listed in Table 1. Repeatability was estimated using nine determinations covering

Table 1 Accuracy and precision data

	(*R*)-enantiomer concentration (µg mL^{-1})	Relative concentration (%)	Internal standard method (%)	Peak normalization method (%)
Accuracy[a]	0.14	0.2	97.5 ± 6.9	94.2 ± 3.9
	3.85	0.55	101.8 ± 7.0	104.2 ± 2.2
	6.3	0.9	99.4 ± 2.9	98.7 ± 0.3
Content repeatability[b]			4.9	4.8
Content intermediate precision[c]			6.6	6.6
Resolution repeatability			3.4	
Resolution intermediate precision			6.4	
Migration time repeatability			1.0	
Migration time intermediate precision			5.9	

[a] Accuracy is expressed as mean recovery ± confidence interval % (n = 3, $\alpha/2 = 0.025$)

[b] Repeatability is evaluated on 9 runs = 3 samples × 3 concentrations and expressed as RSD

[c] Intermediate precision is evaluated upon 3 consecutive days on 9 runs (3 samples @ 3 concentrations) and expressed as RSD

the specified range for the procedure (three concentrations, three replicates each) [27], while data for intermediate precision were obtained at the three specified concentration levels by injecting triplicates of the samples on three consecutive days. Overall, acceptable figures of merit with RSD values below 10 % were obtained. This also applied to peak resolution and migration time of (S)-ambrisentan. In addition, intermediate precision was also estimated using the normalization approach, i.e., calculating the amount of (R)-ambrisentan from the peak area of the enantiomeric impurity relative to the sum of the peak areas of (S)-ambrisentan plus its (R)-enantiomer (Table 1). Comparable RSD values of repeatability and precision were observed, but accuracy was lower in this case illustrating the well-known fact that the use of an internal standard in CE improves the accuracy of a method. Nonetheless, either using an internal standard method or using peak normalization is suitable for the determination of the stereoisomeric purity of (S)-ambrisentan.

With regard to analysis time and LOQ, the CE method was comparable to published chiral HPLC methods utilizing either a cellulose-based stationary phase in the reversed-phase mode [16] or an amylose-based stationary phase in the normal phase mode [17].

Method Application

The method was subsequently applied to the analysis of a sample obtained from a chemical supplier. The concentration of the (R)-enantiomer was 0.15 ± 0.01 %, calculated using the internal standard and 0.17 ± 0.01 % when using peak area normalization. Similar contents of (R)-ambrisentan have been analyzed by HPLC [16]. Thus, the CE method can be used for the determination of the enantiomeric purity of (S)-ambrisentan.

Conclusions

A QbD approach was successfully applied in the development and optimization of a capillary electrophoresis method for the determination of the chiral purity of (S)-ambrisentan. Method scouting followed by screening of the critical process parameters led to the selection of initial experimental conditions which were further optimized by response surface methodology. This led to the determination of the design space from which the experimental conditions of the working point were derived. The final validated method proved to be robust and simple and allowed the determination of a relative concentration 0.1 % of the enantiomeric impurity with RSD values below 10 % and within an analysis time of less than 10 min. These performance parameters are comparable to

the reported HPLC methods [16, 17]. The practical applicability of the assay was demonstrated for a commercial sample, in which 0.15 ± 0.01 % of the (R)-enantiomer were found. In conclusion, the method proved to be suitable for the determination of the chiral purity of (S)-ambrisentan and represents another example of the applicability of CE for the determination of the stereoisomeric purity of drugs.

Compliance with Ethical Standards

Ethical Approval This article does not contain any studies with human participants or animals performed by any of the authors.

Conflict of Interest The authors declare no conflict of interest.

References

1. McLaughlin VV, Davis M, Cornwell W (2011) Pulmonary arterial hypertension. CurrProblCardiol 36:461–517. doi:10.1016/j.cpcardiol.2011.08.002
2. Raiesdana A, Loscalzo J (2006) Pulmonary arterial hypertension. Ann Med 38:95–110. doi:10.1080/07853890600622143
3. Galiè N, Hoeper MM, Humbert M, Torbicki A, Vachiery JL, Barbera JA, Beghetti M, Corris P, Gaine S, Gibbs JS, Gomez-Sanchez MA, Jondeau G, Klepetko W, Opitz C, Peacock A, Rubin L, Zellweger M, Simonneau G (2009) Guidelines for the diagnosis and treatment of pulmonary hypertension: the task force for the diagnosis and treatment of pulmonary hypertension of the European Society of Cardiology (ESC) and the European Respiratory Society (ERS), endorsed by the International Society of Heart and Lung Transplantation (ISHLT). Eur Heart J 30:2493–2537. doi:10.1093/eurheartj/ehp297
4. Galiè N (2004) The endothelin system in pulmonary arterial hypertension. Cardiovasc Res 61:227–237. doi:10.1016/j.cardiores.2003.11.026
5. Galie N, Olschewski H, Oudiz RJ, Torres F, Frost A, Ghofrani HA, Badesch DB, McGoon MD, McLaughlin VV, Roecker EB, Gerber MJ, Dufton C, Wiens BL, Rubin LJ (2008) Ambrisentan for the treatment of pulmonary arterial hypertension: results of the ambrisentan in pulmonary arterial hypertension, randomized, double-blind, placebo-controlled, multicenter, efficacy (ARIES) study 1 and 2. Circulation 117:3010–3019. doi:10.1161/CIRCULATIONAHA.107.742510
6. Center for Drug Evaluation and Research (2007) Letaris FDA approval letter. http://www.accessdata.fda.gov/drugsatfda_docs/appletter/2007/022081s000LTR.pdf. Accessed 30 Apr 2016
7. European Medicines Agency Volibris' Summary of product characteristics (2013). http://www.ema.europa.eu/docs/en_GB/document_library/EPAR_-_Product_Information/human/000839/WC500053065.pdf. Accessed 30 Apr 2016
8. Satheeshkumar N, Naveenkumar G (2014) A stability-indicating reversed-phase high-performance liquid chromatography method for ambrisentan: an endothelin receptor antagonist. J Chromatogr Sci 52(8):894–898. doi:10.1093/chromsci/bmt138

9. Ramisetti NR, Kuntamukkala R (2014) LC–MS/MS characterization of forced degradation products of ambrisentan: development and validation of a stability-indicating RP-HPLC method. New J Chem 38:3050–3061. doi:10.1039/c4nJ00075g

10. Nazeerunnisa M, Garikapati L, Bethanabhatla SS (2015) Development and validation of a stability-indicating HPLC method for determination of ambrisentan in bulk drugs. Malays J Anal Sci 19:595–602

11. Patel JK, Patel NK (2014) Stability-indicating RP-HPLC method for the determination of ambrisentan and tadalafil in pharmaceutical dosage form. Sci Pharm 82:749–763. doi:10.3797/scipharm.1403-22

12. Narayana MBV, Chandrasekhar KB, Rao BM (2014) A validated specific stability-indicating RP-HPLC assay method for ambrisentan and its related substances. J Chromatogr Sci 52(8):818–825 10.1093/chromsci/bmt121

13. Spence R, Mandagere A, Dufton C, Venitz J (2008) Pharmacokinetics and safety of ambrisentan in combination with sildenafil in healthy volunteers. J Clin Pharmacol 48:1451–1459. doi:10.1177/0091270008324180

14. Lukram OK, Sharma R (2014) High-performance liquid chromatography tandem mass spectrometry method for quantification of endothelin receptor antagonist drug, ambrisentan, in human plasma and its application in a pharmacokinetic study. Biomed Chromatogr 28:1147–1155. doi:10.1002/bmc.3136

15. Nirogi R, Kandikere V, Komarneni P, Aleti R, Padala N, Kalaikadhiban I (2012) LC–ESI–MS/MS method for quantification of ambrisentan in plasma and application to rat pharmacokinetic study. Biomed Chromatogr 26:1150–1156. doi:10.1002/bmc.2670

16. Dousa M, Gibala P (2012) Rapid determination of ambrisentan enantiomers by enantioselective liquid chromatography using cellulose-based chiral stationary phase in reverse phase mode. J Sep Sci 35:798–803. doi:10.1002/jssc.201101062

17. Kaja RK, SurendhraNath KV, Babuji K, Satyanarayana PVV, Kumar KS (2009) A validated LC method for the enantiomeric separation of ambrisentan in bulk drug and pharmaceutical dosage forms. Anal Chem Indian J 8:155–160

18. Jac P, Scriba GKE (2013) Recent advances in electrodriven enantioseparations. J Sep Sci 36:52–74. doi:10.1002/jssc.201200836

19. Sanchez-Hernandez L, Guijarro-Diez M, Marina ML, Crego AL (2014) New approaches in sensitive chiral CE. Electrophoresis 35:12–27. doi:10.1002/elps.201300355

20. El Deeb S, Wätzig H, El-Hady DA, Albishri HM, Sänger-van de Griend C, Scriba GKE (2014) Recent advances in capillary electrophoretic migration techniques for pharmaceutical analysis. Electrophoresis 35:170–189. doi:10.1002/elps.201300411

21. El Deeb S, Wätzig H, El-Hady DA, Sänger-van de Griend C, Scriba GKE (2016) Recent advances in capillary electrophoretic migration techniques for pharmaceutical analysis (2013–2015). Electrophoresis 37:1591–1608. doi:10.1002/elps.201600058

22. Orlandini S, Gotti R, Furlanetto S (2014) Multivariate optimization of capillary electrophoresis methods: a critical review. J Pharm Biomed Anal 87:290–307. doi:10.1016/j.jpba.2013.04.014

23. Orlandini S, Pinzauti S, Furlanetto S (2013) Application of quality by design to the development of analytical separation methods. Anal Bioanal Chem 405:443–450. doi:10.1007/s00216-012-6302-2

24. Rozet E, Lebrun P, Debrus B, Boualnger B, Hubert P (2013) Design spaces for analytical methods. Trends Anal Chem 42:157–167. doi:10.1016/j.trac.2012.09.007

25. Hanrahan G, Gomez FA (2009) Chemometric methods in capillary electrophoresis. Wiley, Hoboken

26. Center for Drug Evaluation and Research (2007) Chemistry Reviews Letaris™, http://www.accessdata.fda.gov/drugsatfda_docs/nda/2007/022081s000_ChemR.pdf. Accessed 30 April 2016

27. ICH Harmonised Tripartite Guideline (2005) Validation of analytical procedures: text and methodology Q2 (R1). http://www.ich.org/fileadmin/Public_Web_Site/ICH_Products/Guidelines/Quality/Q2_R1/Step4/Q2_R1__Guideline.pdf. Accessed 15 Mar 2016

3.2.   Manuscript 2

Development of a Capillary Electrophoresis Method for the Determination of the Chiral Purity of Dextromethorphan by a Dual Selector System using Quality by Design Methodology

Personal Contribution (85 %): study design and concept development, experimental work, data analysis and interpretation, preparation of manuscript draft.

Gerhard K. E. Scriba (10 %): supervision or research, finalizing manuscript

Matthias Heuermann (5 %): supplying levomethorphan.

Overview:

Dextromethorphan is a centrally acting antitussive drug, while its enantiomer levomethorphan is an illicit drug with opioid analgesic effects. The present study involves the development of a CE-based limit test for levomethorphan. The analytical target profile was defined as a method that should be able to determine levomethorphan with acceptable precision and accuracy at the 0.1 % level. From initial scouting experiments, a dual selector system consisting of sulfated β-cyclodextrin and methyl-α-cyclodextrin was identified. Design of experiments methodology was used in method development, optimization and validation. The method was validated according to ICH guideline Q2(R1) and applied to the analysis of a capsule formulation. Furthermore, the apparent binding constants between the enantiomers and the cyclodextrins as well as complex mobilities were determined to understand the migration behavior of the analytes.

RESEARCH ARTICLE

Development of a capillary electrophoresis method for the determination of the chiral purity of dextromethorphan by a dual selector system using quality by design methodology

Sulaiman Krait[1] | Matthias Heuermann[2] | Gerhard K. E. Scriba[1] (iD)

[1]Department of Pharmaceutical Chemistry, Friedrich Schiller University, Jena, Germany

[2]Centre For Health (LZG.NRW), Bochum, Germany

Correspondence
Prof. Gerhard K. E. Scriba, Department of Pharmaceutical Chemistry, Friedrich Schiller University, Philosophenweg 14, 07743 Jena, Germany.
Email: gerhard.scriba@uni-jena.de

Dextromethorphan is a centrally acting antitussive drug, while its enantiomer levomethorphan is an illicit drug with opioid analgesic effects. As capillary electrophoresis has been proven as an ideal technique for enantiomer analysis, the present study was conducted in order to develop a capillary electrophoresis-based limit test for levomethorphan. The analytical target profile was defined as a method that should be able to determine levomethorphan with acceptable precision and accuracy at the 0.1 % level. From initial scouting experiments, a dual selector system consisting of sulfated β-cyclodextrin and methyl-α-cyclodextrin was identified. The critical process parameters were evaluated in a fractional factorial resolution IV design followed by a central composite face-centered design and Monte Carlo simulations for defining the design space of the method. The selected working conditions consisted of a 30/40.2 cm, 50 μm id fused-silica capillary, 30 mM sodium phosphate buffer, pH 6.5, 16 mg/mL sulfated β-cyclodextrin, and 14 mg/mL methyl-α-cyclodextrin at 20°C and 20 kV. The method was validated according to ICH guideline Q2(R1) and applied to the analysis of a capsule formulation. Furthermore, the apparent binding constants between the enantiomers and the cyclodextrins as well as complex mobilities were determined to understand the migration behavior of the analytes.

KEYWORDS

capillary electrophoresis, design of experiments, dextromethorphan, dual selector system, enantiomeric purity

1 | INTRODUCTION

Dextromethorphan   ((9S,13S,14S)-3-methoxy-17-methylmorphinan,   (+)-3-methoxy-N-methylmorphinan,   DXM; Fig. 1) is an N-methyl-D-aspartate receptor antagonist and σ1 receptor agonist. The compound is widely used as an antitussive in over-the-counter cough and cold medicines and in combination with quinidine for the treatment of pseudobulbar affect [1,2]. DXM has an *ent*-morphinan structure. The enantiomer levomethorphan ((9R,13R,14R)-3-methoxy-17-methylmorphinan,   (−)-3-methoxy-N-methylmorphinan, LVM; Fig. 1) displays morphinan structure and is an opioid analgesic drug with strong respiratory depression. The compound was never clinically developed and is classified as a controlled substance worldwide (www.incb.org/documents/Narcotic-Drugs/Yellow_List/55th_Edition/YL_-55th_edition_2016.pdf). Severe adverse effects including cyanosis, respiratory distress, and seizures as well as about 60 deaths have been reported by the World Health Organization in different countries after consumption

Conflict of interest: The authors declare no conflict of interest.

Dextromethorphan   Levomethorphan
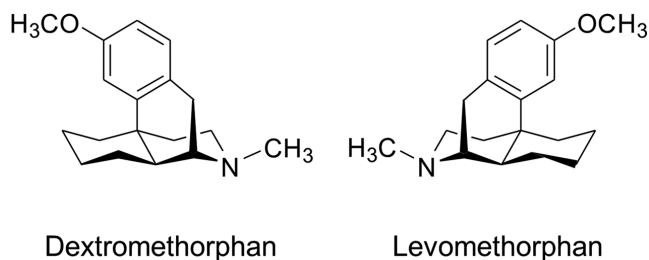
F I G U R E 1   Structures of dextromethorphan and levomethorphan

of DXM-containing medicines contaminated with LVM (www.who.int/medicines/publications/drugalerts/App_Drug_Alert_No_129_Paraguay_Dextro.pdf, www.int./medicines/publications/drugalerts/Final_Alert_126_Information_on_Dextromethorphan.pdf). As a consequence, chromatographic tests for the enantiomeric purity of DXM were included in the United States Pharmacopeia [3] and the International Pharmacopoeia [4], using vancomycin and cellulose *tris*(4-methylbenzoate), respectively, as chiral selectors on the stationary phase. The limit of LVM is 0.1% in both pharmacopeias. Furthermore, liquid chromatographic enantioseparations of the compounds have been reported using chiral stationary phases based on β-cyclodextrin (β-CD) [5], phenylcarbamate β-CD [6], or vancomycin [5,7]. Cellulose *tris*(3,5-dimethylphenylcarbamate) proved to be a suitable selector for the separation of DXM and LVM by SFC [7]. Finally, the indirect separation of the methorphan enantiomers by GC was accomplished after derivatization with (–)-menthyl chloroformate on a (5–phenyl)-methylpolysiloxane stationary phase [8].

Within the last decades, CE has been increasingly used as a high resolution technique for the analysis of pharmaceutical drugs [9–12] including enantioseparations [13–17]. Aumatell et al. reported the enantioseparation of methorphan by CD-modified MEKC using a BGE composed of 50 mM SDS in a 50 mM sodium borate buffer, pH 9.05, containing 60 mM β-CD as chiral selector and 20% v/v 1-propanol [18]. Lurie and Cox achieved the separation of DXM and LVM in a dynamically coated capillary using hydroxypropyl-β-CD as chiral selector in CElixir buffer, pH 2.5, containing 15% v/v methanol [19]. Hydroxypropyl-β-CD was also used as chiral selector in 150 mM sodium phosphate buffer, pH 4.4, containing 20% v/v methanol and a fused-silica capillary for the analysis of plasma samples in opiate-overdose-related deaths [20,21]. However, none of these methods were suitable for the analysis of the enantiomeric purity of DXM due to low resolution [19–21] or long analysis times of about 1 h [18]. Therefore, the aim of the present study was the development of a CE method for the determination of the enantiomeric purity of DXM at the 0.1% level of LVM with acceptable accuracy and precision implementing quality by design (QbD) principles.

QbD has been applied increasingly in analytical chemistry and includes the use of multivariate design of experiments and risk-assessment tools for identifying the critical process parameters (CPPs), that is, the experimental factors that influence the critical quality attributes (CQAs) of the method. Consequently, an in-depth understanding of the analytical process is provided [22–26].

2 | MATERIALS AND METHODS

2.1 | Chemicals and reagents

Dextromethorphan hydrobromide monohydrate was from Fagron (Barsbüttel, Germany). Levomethorphan was from Cerilliant (Round Rock, USA). Dextromethorphan capsules from ratiopharm (Ulm, Germany) were obtained from a local community pharmacy. β-CD and methyl-α-cyclodextrin (M-α-CD, batch M1, degree of substitution (DS) ~11) were from Wacker Chemie (Burghausen, Germany). Hydroxyethyl-β-CD (DS ~4.9), γ-CD, sulfated α-CD sodium salt, sulfated β-CD sodium salt (S-β-CD, batch S1: DS ~12–15, batch S2: DS ~7–11), Tris, riboflavin 5′-phosphate sodium salt hydrate, and procainamide hydrochloride were from Sigma–Aldrich (Steinheim, Germany). α-CD, M-α-CD (batch M2, DS ~11), hydroxypropyl-α-CD (DS ~4.5), carboxymethyl-α-CD sodium salt (CM-α-CD, DS ~3.5), methyl-β-CD (DS ~12), hydroxypropyl-β-CD (DS ~4.5), carboxymethyl-β-CD sodium salt (CM-β-CD, DS ~3.5), succinyl-β-CD (DS~3.5), heptakis(2,6-di-*O*-methyl)-β-CD (DS ~14), carboxymethyl-γ-CD sodium salt (DS ~3.5), and hydroxypropyl-γ-CD (DS ~4.5) were from Cyclolab (Budapest, Hungary), while sulfobutyl-β-CD sodium salt (DS ~6.6) was from CyDex Pharmaceuticals (San Diego, USA). Boric acid, orthophosphoric acid (85%), glacial acetic acid, sodium hydroxide, triethanolamine, DMSO, 2-[4-(2-hydroxyethyl)-1-piperazinyl]-ethanesulfonic acid, and piperazine-1,4-bis(2-ethanesulfonic acid) were from Merck (Darmstadt, Germany). Water was purified by a GenPure system from Thermo Fischer (Waltham, USA). Ethanol (96%) was from Carl Roth (Karlsruhe, Germany). Methanol (HPLC grade) was from Fisher Scientific (Loughborough, UK). All chemicals were obtained at the highest purity commercially available.

2.2 | Instrumentation

All experiments were carried out using a Beckman P/ACE MDQ CE system (Beckman Coulter, Krefeld, Germany) equipped with a UV-Vis diode array detector and controlled by 32 KARAT software (version 8.0) for system control, data acquisition, and processing. Hydrodynamic sample injection was performed at a pressure of 0.7 psi (4.8 kPa) for 5 s. UV

detection was carried out at the cathodic end of the capillary at 200 nm unless otherwise specified. pH measurements were performed with a WTW Multi-3410 IDS multiparameter digital pH meter equipped with a SenTix SP-T 900 electrode (Xylem Analytics Germany Sales, Weilheim, Germany) calibrated with buffer solutions at pH 4.00, 7.00, and 9.00 from Carl Roth.

Fifty micrometer id fused-silica capillaries were from BGB Analytik (Schloßböckelheim, Germany). A new capillary was successively rinsed at a pressure of 20 psi (138 kPa) with 1 M sodium hydroxide for 10 min, followed by water for 15 min. For the CD screening with BGEs with pH ≤ 6.0, the capillary was rinsed successively with 0.1 M phosphoric acid for 5 min and water for 10 min at the beginning of the day, while in the case of BGEs with pH > 6.0, the capillary was rinsed with 0.1 M sodium hydroxide for 5 min and water for 10 min. Between runs, the capillary was flushed with water for 1 min and the BGE for 3 min.

Viscosity measurements of buffers containing M-α-CD were performed in quadruplicate according to Allmendinger et al. [27] using the CE instrument as viscosimeter and 0.1% m/v riboflavin-5′-phosphate as the boundary marker.

2.3 | Buffer and sample solutions

The BGEs were prepared by dissolving the CDs in water followed by addition of the corresponding amount of the acid component and diluting with water to about 90% of the required volume. The pH was subsequently adjusted by the required base and made up to the final volume by water. Tris/phosphate buffer was prepared by dissolving Tris and the CD in water and adjusting the pH using phosphoric acid. All BGEs were filtered through (0.22 μm) polypropylene syringe filters (BGB Analytik) and sonicated for 10 min before use.

Stock solutions of DXM hydrobromide equivalent to 2.0 mg/mL of DXM and of LVM at a concentration of 1.0 mg/mL were prepared in 0.01 M HCl. Sample solutions were prepared by dilution in 0.01 M HCl. For preparation of sample solutions of DXM hydrobromide capsules, the content of ten capsules was homogenized in a mortar. An accurately weighed amount equivalent to 20 mg of DXM was suspended in 5.0 mL 96% v/v ethanol and sonicated for 20 min to yield a solution containing 4.0 mg/mL of DXM. The suspension was centrifuged at 5000 rpm for 15 min and 375 μL of the supernatant were transferred to a 1.5 mL Eppendorf vial and evaporated to dryness using an Eppendorf Concentrator plus (Eppendorf Deutschland, Wesseling-Berzdorf, Germany). The residue was reconstituted in 970 μL 0.01 M HCl and 30 μL of procainamide hydrochloride stock solution (1.0 mg/mL) were added as internal standard.

2.4 | Software and data analysis

MODDE 11.0 (Umetrics, Umeå, Sweden) was used for the experimental design and statistical analysis of the screening, response surface methodology, and robustness testing. The data obtained from the respective designs were fitted to a model using the quadratic polynomial equation [22]:

$$y = \beta_0 + \sum_{i=1}^{f} \beta_i x_i + \sum_{1 \leq i \leq j}^{f} \beta_{ij} x_i x_j + \sum_{i=1}^{f} \beta_{ii} x_i^2, \quad (1)$$

where y is the predicted response (resolution or migration time), β_0 is the intercept, β_i is the coefficient to be optimized (voltage, temperature, buffer pH, and concentration and/or CD concentration), β_{ij} the interaction coefficients, and β_{ii} the quadratic coefficients, with the interaction effect terms restricted to two-factor interactions.

Microsoft Excel 2007 was used for the statistical analysis of the validation data. CEval version 0.6 g [28] was used for calculating CD–enantiomer binding constants and complex mobilities.

3 | RESULTS AND DISCUSSION

Starting point of analytical QbD is the selection of the analytical technique and definition of the analytical target profile (ATP). Subsequently, the CPPs are identified and the design space of the method is established, which refers to the experimental conditions meeting the ATP [23–25]. Design of experiments procedures are employed in the process [22,26]. Thus, the ATP was defined that the developed CE method should allow the determination of LVM in DXM in the range of at least 0.1% up to 1.0% relative to the parent drug with a precision and accuracy of ≤15% at the 0.1% level and ≤10% above the 0.1% level in an analysis time of ≤10 min.

3.1 | Initial method scouting

Because DXM is a weak base with an estimated pK_a value of about 9.2 [29], the initial selector screening was performed in a 100 mM sodium phosphate BGE, pH 2.5, using a 40/50.2 cm, 50 μm id fused-silica capillary at a temperature of 20°C and an applied voltage of 20 kV. The sample solution contained 90 μg/mL of DXM and 10 μg/mL of LVM. Native α-CD, β-CD, and γ-CD as well as neutral and charged derivatives were studied at a concentration of approximately 20 mM, or in the case of sulfated or sulfobutyl CD derivatives at 10 mM based on the average molecular weight of the CDs. Native and neutral CDs were evaluated under normal polarity of the applied voltage, while negatively charged CDs were also studied under reversed polarity conditions when the analytes could not be detected at

TABLE 1 Results of the CD screening in 100 mM sodium phosphate buffer, pH 2.5

CD	α	Migration order	Polarity of voltage	Comments
α-CD (20 mM)	1.02	LVM > DXM	(+)	Partial separation
M-α-CD (20 mM)	1.02	DXM > LVM	(+)	Partial separation
HP-α-CD (20 mM)	1.04	DXM > LVM	(+)	Baseline separation
HP-γ-CD (20 mM)	1.02	DXM > LVM	(+)	Partial separation
CM-α-CD (20 mM)	1.05	DXM > LVM	(+)	Baseline separation
CM-β-CD (20 mM)	1.02	DXM > LVM	(+)	Partial separation
CM-γ-CD (20 mM)	1.04	DXM > LVM	(+)	Baseline separation
S-β-CD (10 mM)	1.49	LVM > DXM	(-)	Baseline separation

Only CDs yielding at least partial enantioseparation are listed.
CM-α-CD, carboxymethyl-α-CD; CM-β-CD, carboxymethyl-β-CD; CM-γ-CD, carboxymethyl-γ-CD;
HP-α-CD, hydroxypropyl-α-CD; HP-γ-CD, hydroxypropyl-γ-CD; S-β-CD, sulfated-β-CD.

normal polarity of the applied voltage. CDs leading to at least a partial enantioseparation under these conditions are summarized in Table 1. Good resolution was noted when using CM-α-CD or S-β-CD but this was associated with high baseline noise and peak fronting in the case of S-β-CD. Subsequently, 100 mM triethanolamine-phosphoric acid buffer, pH 2.5, 100 mM sodium acetate buffer, pH 5.0, and sodium citrate buffer, pH 6.0, were studied as alternative BGEs. However, none of these conditions substantially improved the separation of DXM and LVM, their peak shape or baseline noise. Therefore, screening was further performed in sodium phosphate buffer, pH 7.0, and sodium borate buffer, pH 8.5, under normal polarity of the applied voltage. In the presence of 10 mM S-β-CD, high resolution was observed with R_S values of about 21 and 24, respectively. DXM migrated before LVM. However, substantial peak tailing occurred. Because lower baseline noise was found for the phosphate-based buffer, different buffer co-ions of phosphate including triethanolamine and lithium were studied but even worsened the peak shape. In 2-[4-(2-hydroxyethyl)-1-piperazinyl]-ethanesulfonic acid buffer, pH 7.0, piperazine-1,4-bis(2-ethanesulfonic acid) buffer, pH 7.0, or Tris-phosphoric acid buffer, pH 8.0, no peaks could be detected within 30 min. Addition of organic solvents up to a concentration of 20% v/v did not improve peak shape or baseline noise. Therefore, sodium phosphate buffer, pH 7.0, in combination with S-β-CD was selected for further evaluation.

Dual CD systems have been applied to drug CE enantioseparations [30,31] and were also employed to improve the peak shape of basic compounds [32]. Consequently, neutral and charged CDs were tested in combination with S-β-CD in 50 mM sodium phosphate buffer pH 7.0. Improvement of peak shape associated with a decrease of resolution was observed for CM-α-CD and M-α-CD as co-selectors. Thus, M-α-CD was chosen for further method development because, as a neutral compound, the CD will not increase the electric current of the BGE. Figure 2 illustrates the effect of the
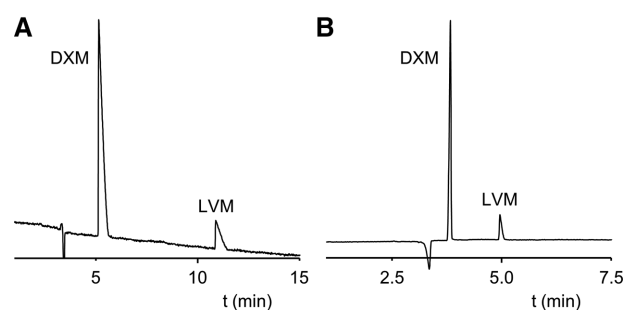
FIGURE 2 Electropherograms of the separation of DXM and LVM using (A) 20 mg/mL S-β-CD and (B) 20 mg/mL S-β-CD and 10 mg/mL M-α-CD in 50 mM sodium phosphate buffer, pH 7.0. Other experimental conditions: 30/40.2 cm, 50 μm id fused-silica capillary; 20°C; 16 kV; detection at 200 nm.

combination of S-β-CD and M-α-CD on the resolution and peak shape of the separation of the methorphan enantiomers.

3.2 | Knowledge space and identification of critical process parameters

The CQAs of the method were defined as target values of a resolution of at least 5 and an analysis time of ≤ 10 min so that the migration time of the second migrating LVM should not exceed 8 min. Based on the scouting experiments, the experimental parameters BGE pH and concentration, the concentrations of the selectors S-β-CD and M-α-CD, as well as separation voltage and temperature were studied in further detail using a fractional factorial resolution IV design in the ranges of voltage 10–20 kV, capillary temperature 15–25°C, pH 6.4–8.0, phosphate buffer concentration 30–100 mM, S-β-CD concentration 10–24 mg/mL, and M-α-CD concentration 6–20 mg/mL. Due to the relatively high resolution value achieved in the scouting, the capillary was shortened so that the experiments were performed in a 30/40.2 cm, 50 μm id fused-silica capillary. The sample consisted of 1500 μg/mL
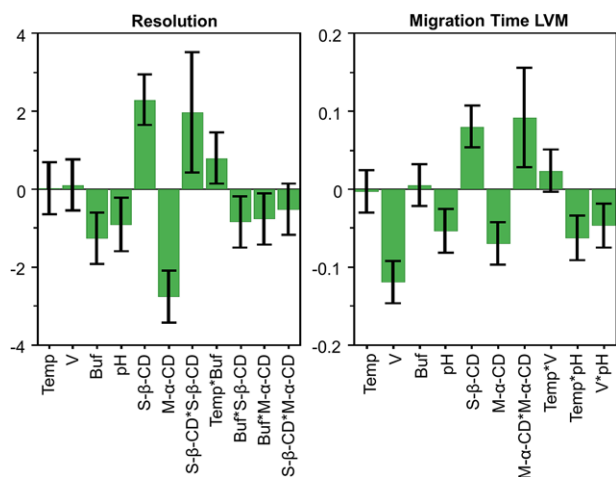
FIGURE 3 Coefficient plot (scaled and centered) of the screening design showing the relative effect of the factors on the responses; *x* × *y* represents the interaction terms between two parameters. Note: V, applied voltage; Temp, capillary temperature; pH, pH of buffer solution; Buf, buffer concentration; S-β-CD, S-β-CD concentration; M-α-CD, M-α-CD concentration.

FIGURE 4 Probability plot of the design space. Notes: Threshold of responses (min/target/max): migration time of LVM (−/−/8 min), number of theoretical plates of LVM peak (3000/−/−), height of LVM peak (3000 μAU/−/−) and tailing factor of the DXM peak (0.5/1/3). The design space (green zone) is identified as the zone where the risk of failure is ≤ 1%. For the color version of the figure, the reader is referred to the online version of the article.

DXM and 15 μg/mL LVM, that is, a relative concentration of LVM of 1.0%. The design matrix as well as the respective values of the responses, peak resolution, and migration time of LVM are summarized in Supporting Information Table S1. Three experiments were carried out at the center of the design for estimating the repeatability. The coefficient plots of the variables as well as their interaction terms are shown in Fig. 3. Temperature and voltage did not significantly affect peak resolution, while migration time of LVM was not influenced by temperature and buffer concentration. pH affected both, resolution and migration time. S-β-CD increased resolution and run time, while M-α-CD decreased both responses. To better understand the combination terms, a sweet plot was constructed at low buffer concentration (30 mM) and a temperature of 20°C as shown in Supporting Information Figure S1. Although both CQAs were met for a large variety of experimental settings, the plot indicated that low electrolyte pH was favorable. Consequently, BGE concentration and pH were fixed at 30 mM and pH 6.5, respectively, and temperature was set at 20°C. The concentration of the CDs and separation voltage were considered CPPs and further optimized.

3.3 | Method optimization and determination of the design space

The three CPPs voltage (10–20 kV), S-β-CD (10–30 mg/mL), and M-α-CD (5–15 mg/mL) were optimized in the indicated ranges using a central composite face-centered design. Capillary dimensions and sample concentration were identical to the screening design. The design matrix can be found in Supporting Information Table S2 containing three repetitions

at the center of the design for estimation of repeatability. Peak resolution in all experiments was above the initial threshold of 5 (see Supporting Information Table S2). Therefore, peak resolution was not considered a CQA so that optimization efforts concentrated on analysis time and the peak performance criteria as responses, that is, the tailing factor of the DXM peak (calculated according to the United States Pharmacopeia by the instrument software) as well as the number of theoretical plates and the peak height of the LVM peak.

Setting the migration time of LVM as measure of the analysis time at ≤ 8 min, the number of theoretical plates and the peak height of the LVM peak at ≥3000 and ≥3000 μAU, respectively, as well as the tailing factor of the DXM peak in the range of 0.5 to 3 with the target value of 1, the design space of the method was derived by Monte Carlo simulations as shown in Fig. 4. The level of probability of failure was selected at ≤ 1%. Because faster analysis was achieved at higher values of the applied voltage, 20 kV were selected to ensure fast analysis. The other working point conditions included a sodium phosphate buffer concentration of 30 mM, a pH of 6.5, a concentration of S-β-CD of 16 mg/mL, and a concentration of M-α-CD of 14 mg/mL. Procainamide hydrochloride was chosen as an internal standard and was added to the sample to achieve a final concentration of 30 μg/mL. An electropherogram of standards under the optimized experimental conditions is shown in Fig. 5A.

3.4 | Method validation and application

3.4.1 | Method robustness

Method robustness was estimated using a Plackett-Burman design with a variation of the experimental conditions around the center point of the optimized working conditions, that is,
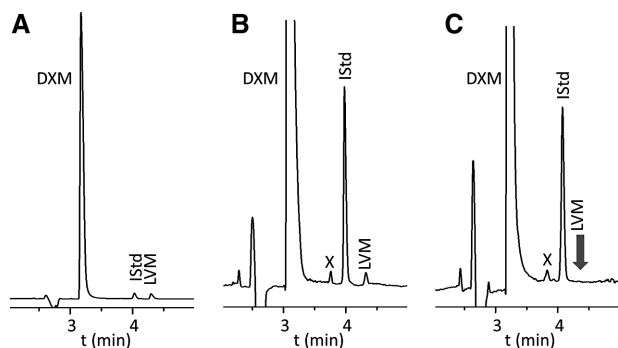
FIGURE 5 Electropherograms of a solution of 1.5 mg/mL DXM spiked with (A) 15 μg/mL LVM (1.0% relative concentration) and (B) 1 μg/mL LVM (0.067%); (C) electropherogram of DXM hydrochloride capsules equivalent to a DXM concentration of 1.5 mg/mL. Notes: X, unknown impurity; IStd, internal standard procainamide hydrochloride at a concentration of 30 μg/mL. Experimental conditions: 30/40.2 cm, 50 μm id fused-silica capillary; 30 mM sodium phosphate buffer, pH 6.5, containing 16 mg/mL S-β-CD and 14 mg/mL M-α-CD; 20°C; 20 kV; detection at 200 nm; hydrodynamic injection at 0.7 psi for 5 s.

voltage 20 ± 1 kV, temperature 20 ± 1°C, buffer concentration 30 ± 1 mM, and pH 6.5 ± 0.1, S-β-CD concentration 16 ± 1 mg/mL and M-α-CD concentration 14 ± 1 mg/mL. In addition, two different batches of S-β-CD and M-α-CD were included. The design matrix is summarized in Supporting Information Table S3. Effects of the variations of the parameters within the indicated ranges did not significantly affect the number of theoretical plates of the LVM peak or the tailing factor of the DXM peak. The coefficient plots for migration time of LVM and height of the LVM peak are shown in Supporting Information Figure S2. Except for buffer concentration on migration time and S-β-CD concentration on peak height, all variables were significant including variation of the CD batch. However, under all experimental conditions evaluated, the responses always met the predefined requirements (Supporting Information Table S3). Thus, migration time of LVM never exceeded 6 min (threshold ≤ 8 min) and peak height was higher than 4500 μAU (threshold ≥ 3000 μAU). Therefore, the method can be considered robust. Nonetheless, care should be taken in the preparation of the BGE and instrumental parameters such as capillary temperature and voltage should be controlled carefully.

3.4.2 | Method validation and application

The optimized method was validated according to the Q2 (R1) guideline (www.ich.org/fileadmin/Public_Web_Site/ICH_Products/Guidelines/Quality/Q2_R1/Step4/Q2_R1_Guideline.pdf) in the range of 1.0–10 μg/mL LVM in the presence of DXM at a concentration of 1.5 mg/mL. Procainamide hydrochloride at a concentration of 30 μg/mL served as internal standard. The data are summarized in Table 2. LOD and LOQ values were estimated based on an

S/N of 3 and 10, respectively. RSD values of repeatability and intermediate precision of content and migration time were well below 10% indicating sufficient precision of the method. Accuracy was estimated by spiking DXM at a concentration of 1.5 mg/mL with known amounts of LVM. Values ranged between 88.9 ± 3.6% at the 0.1% level and 99.2 ± 0.9% at the 0.9% level so that the method can be considered accurate as well. Absence of a peak at the migration time of LVM in samples of pure DXM assured selectivity of the method with regard to LVM. A representative electropherogram of a DXM sample spiked with LVM at the LOQ (0.07% level) is shown in Fig. 5B. A small amount of an unknown impurity was in the drug substance. The amount of the compound was estimated at about 0.07% based on peak normalization.

The method was subsequently applied to a capsule dosage form upon extraction of the analytes with ethanol. The electropherogram is shown in Fig. 5C. LVM could not be detected. A small amount of the unknown impurity, which was found in the DXM standard, was also detected in the formulation at an estimated level of 0.06%. Accuracy was also estimated for the analysis of the capsules by spiking the content with known amounts of LVM (Table 2). Values between 93.0 ± 2.8% (0.1% level) and 105.5 ± 2.9% (0.9% level) indicated satisfactory accuracy of the method in the case of capsule formulations as well.

3.5 | Determination of apparent binding constants and mobilities

To understand the migration behavior of the analytes in the applied dual selector system, a mechanistic study determining the complexation constants and mobilities of the diastereomeric CD–analyte complexes was performed in an attempt to explain the effect of M-α-CD on peak tailing in the S-β-CD-mediated enantioseparation of methorphan. The data were obtained as best fit parameters of the dependence of the effective mobility on the CD concentration assuming the formation of 1:1 CD–analyte complexes according to Eq. (2) [33]:

$$\mu_{\text{eff}} = \frac{\mu_f + \mu_c \cdot K \cdot [\text{CD}]}{1 + K \cdot [\text{CD}]}, \tag{2}$$

where μ_{eff} is the effective mobility, μ_c the mobility of the CD–analyte complex, μ_f the mobility of the free analyte, K the complexation constant, and [CD] the molar concentration of the CDs. CEVal was used for data fitting because this software allows correction of the migration times in case of strongly tailing peaks according to the Haarhoff−van der Linde function [28,34]. In case of S-β-CD, observed mobilities of the analytes were corrected for the EOF using DMSO as EOF marker, while in the case of M-α-CD, observed mobilities were corrected for the increasing viscosity of the buffers due to the increasing concentrations of the CDs.

T A B L E 2   Assay validation data

Parameter	Level	Levomethorphan
Range (µg/mL)		1.0–15 µg/mL (0.1–1.0%)
Coefficient of determination R^2		0.9989
LOD (µg/mL; S/N = 3)		0.3 µg/mL (0.02%)
LOQ (µg/mL; S/N = 10)		1.0 µg/mL (0.07%)
Migration time repeatability (RSD)		1.2%
Migration time intermediate precision (RSD)		5.8%
Content repeatability[a] (RSD)		5.3%
Content intermediate precision[b] (RSD)		5.7%
Accuracy drug substance[c]	1.5 µg/mL (0.1%)	88.9 ± 3.6%
	7.5 µg/mL (0.5%)	96.1 ± 2.0%
	13.5 µg/mL (0.9%)	99.2 ± 0.9%
Accuracy capsules[c]	1.5 µg/mL (0.1%)	93.0 ± 2.8%
	7.5 µg/mL (0.5%)	101.9 ± 7.0%
	13.5 µg/mL (0.9%)	105.5 ± 2.9%

[a]Nine runs of three samples at three concentrations on one day.
[b]Nine runs of three samples at three concentrations on three consecutive days.
[c]Expressed as mean recovery ± confidence interval % ($\alpha/2$ = 0.025). DXM samples or capsules were spiked with the indicate amount of LVM.

T A B L E 3   Apparent complexation constants, K, and mobilities of the free analytes, μ_f, and of the CD–analyte complexes, μ_c

	S-β-CD		M-α-CD	
	DXM	LVM	DXM	LVM
μ_f (10^{-9} m^2 s^{-1} V^{-1})	14.8 (13.7, 15.8)		24.1 (23.6, 24.5)	
μ_c (10^{-9} m^2 s^{-1} V^{-1})	–38.0 (–42.2, –34.4)	–43.2 (–45.5, –41.2)	9.97 (9.42, 10.48)	9.91 (9.38, 10.40)
K (M^{-1})	260 (211, 319)	606 (516, 716)	354 (292, 429)	399 (330, 484)

The numbers in brackets represent the 95% confidence intervals.

In the case of S-β-CD, the mobilities were determined in the range of 0–12 mg/mL in 30 mM sodium phosphate buffer, pH 6.5. Because of the strong EOF at pH 6.5, an enantiosepa-ration could not be observed in the presence of M-α-CD as selector. Therefore, the data for M-α-CD were determined in 100 mM sodium phosphate buffer, pH 2.1, using a CD concentration of 0–50 mg/mL. DXM with a pK_a of 9.2 [29] is essentially fully protonated at both pH values so that the following discussion assumes that the complexation between the M-α-CD and the analyte enantiomers is not significantly altered at pH 6.5 versus pH 2.1. This assumption also applies to the mobility of the free analytes, μ_f, and the mobility of the complexes μ_c, which are independent of the EOF. The data are summarized in Table 3. It should be noted that the data are apparent constants and mobilities rather than ther-modynamic values because the ionic strength of the buffers was not determined and concentrations were used instead of activity. Moreover, S-β-CD is a randomly substituted CD so that the actual charge of the compound is not known either.

LVM is complexed much stronger by S-β-CD compared to DXM. Moreover, the mobility of the S-β-CD–LVM complex greatly exceeded the mobility of the S-β-CD–DXM complex. This explains the enantiomer migration order, that is, migra-tion after the EOF and DXM > LVM, and also the increasing peak deformation, especially of the LVM peak due to mis-match of the mobilities of the CD–analyte complexes and the buffer ions. In the case of M-α-CD, LVM is also bound stronger than DXM, but complex mobilities are not signif-icantly different from each other for both enantiomers. Due to competing effects between both CDs, this results in slow-ing down the overall mobility of LVM more effectively as compared to DXM resulting in a reduced peak resolution. However, the reduced mobility of the analytes also reduced the extent of the mobility mismatch between analytes and buffer ions, yielding lower peak deterioration and, conse-quently, sharper and higher peaks. Improvement of peak shape by combination of S-β-CD and neutral CD derivatives in the case of basic drugs has been observed previously [32]. How-ever, in these cases, the analytes migrated before the EOF and

addition of the neutral CD enhanced enantioresolution as reported for most dual CD systems [30,31].

4 | CONCLUDING REMARKS

Using a QbD approach, a CE method was developed for the determination of the stereochemical impurity LVM in DXM drug substance and pharmaceutical formulations at the 0.1% level. A dual CD system consisting of the charged derivative S-β-CD and the neutral derivative M-α-CD was derived from screening experiments followed by a fractional factorial resolution IV design for investigation of the knowledge space. Setting BGE concentration and pH at low values and temperature of 20°C, the concentration of the CDs as well as separation voltage were further optimized using response surface methodology to obtain the design space by Monte Carlo simulation. Selection of the working conditions was followed by a Placket–Burman design for robustness testing before validation of the method in the range of 0.07–1.0% LVM relative to a sample concentration of 1.5 mg/mL DXM.

RSD values of repeatability and intermediate precision of migration time and content were well below 10%. Accuracy was ≤15% at the 0.1% level and ≤10% above this level. The method proved to be suitable for the analysis of a capsule formulation of DXM. Summarizing, the present method represents the first CE method for the assessment of the enantiomeric purity of DXM at the 0.1% level as set in drug monographs of pharmacopeias employing HPLC assays.

In an attempt to understand the improvement of the peak shape by addition of M-α-CD to the S-β-CD-containing BGE, apparent complexation constants and mobilities of the diastereomeric CD–enantiomer complexes were determined. The stronger tailing of the LVM peak compared to the DXM peak especially at higher S-β-CD concentrations could be explained by the high mobility of the CD–LVM complex. Both enantiomers displayed essentially identical complex mobilities in the case of M-α-CD, which were also considerably lower than the mobilities of the corresponding S-β-CD complexes. This reduced the overall mobility of LVM and DXM, thereby improving the peak shape. A concomitant decrease of the enantioresolution was observed but proved negligible for the development of the assay due to the high resolution obtained in the presence of S-β-CD

ORCID

Gerhard K. E. Scriba 🆔
http://orcid.org/0000-0003-2950-060X

REFERENCES

1. Lauterbach, E. C., Shillcutt, S. D., Phillips, D. E., in: V. R. Preedy (Ed.), Neuropathology of Drug Addictions and Substance Misuse, Elsevier, Amsterdam 2016, pp. 707–717.

2. Patatanian, E., Casselman, J., Dextromethorphan/quinidine for the treatment of pseudobulbar affect. *Consult. Pharm.* 2014, *29*, 264–269.

3. Monograph Dextromethorphan Hydrobromide, The United States Pharmacopeia, 40th ed., The United States Pharmacopeial Convention, Rockville, MD 2017.

4. Monograph Dextromethorphan Hydrobromide, The International Pharmacopoeia, 6th ed., World Health Organization, Geneva 2016.

5. Pihlainen, K., Kostiainen, R., Effect of the eluent on enantiomer separation of controlled drugs by liquid chromatography-ultraviolet absorbance detection-electrospray ionization tandem mass spectrometry using vancomycin and native β-cyclodextrin chiral stationary phases. *J. Chromatogr. A* 2004, *1033*, 91–99.

6. Kikura-Hanajiri, R., Kawamura, M., Miyajima, A., Sunouchi, M., Goda, Y., Chiral analyses of dextromethorphan/levomethorphan and their metabolites in rat and human samples using LC-MS/MS. *Anal. Bioanal. Chem.* 2011, *400*, 165–174.

7. Li, L., Direct enantiomer determination of methorphan by HPLC-MS and SFC-MS. *Forensic Chem.* 2016, *2*, 82–85.

8. Koo, C., Cox, M., Klass, G., Johnston, M., Stereochemical analysis of methorphan using (-)-menthyl chloroformate. *J. Forensic Sci.* 2012, *57*, 1549–1555.

9. Deeb, S. E., Wätzig, H., El-Hady, D. A., Albishri, H. M., Sänger-van de Griend, C., Scriba, G. K. E., Recent advances in capillary electrophoretic migration techniques for pharmaceutical analysis. *Electrophoresis* 2014, *35*, 170–189.

10. El Deeb, S., Wätzig, H., Abd El-Hady, D., Sänger-van de Griend, C., Scriba, G. K. E., Recent advances in capillary electrophoretic migration techniques for pharmaceutical analysis (2013-2015). *Electrophoresis* 2016, *37*, 1591–1608.

11. Suntornsuk, L., Recent advances of capillary electrophoresis in pharmaceutical analysis. *Anal. Bioanal. Chem.* 2010, *398*, 29–52.

12. Zhu, Q., Scriba, G. K. E., Analysis of small molecule drugs, excipients and counter ions in pharmaceuticals by capillary electromigration methods - recent developments. *J. Pharm. Biomed. Anal.* 2018, *147*, 425–438.

13. Jáč, P., Scriba, G. K. E., Recent advances in electrodriven enantioseparations. *J. Sep. Sci.* 2013, *36*, 52–74.

14. Scriba, G. K. E., Fundamental aspects of chiral electromigration techniques and application in pharmaceutical and biomedical analysis. *J. Pharm. Biomed. Anal.* 2011, *55*, 688–701.

15. Lu, H., Chen, G., Recent advances of enantioseparations in capillary electrophoresis and capillary electrochromatography. *Anal. Methods* 2011, *3*, 488–508.

16. Preinerstorfer, B., Lämmerhofer, M., Lindner, W., Advances in enantioselective separations using electromigration capillary techniques. *Electrophoresis* 2009, *30*, 100–132.

17. Sánchez-Hernández, L., Guijarro-Diez, M., Marina, M. L., Crego, A. L., New approaches in sensitive chiral CE. *Electrophoresis* 2014, *35*, 12–27.

18. Aumatell, A., Wells, R. J., Chiral differentiation of the optical isomers of racemethorphan and racemorphan in urine by capillary zone electrophoresis. *J. Chromatogr. Sci.* 1993, *31*, 502–508.

19. Lurie, I. S., Cox, K. A., Rapid chiral separation of dextro- and levo-methorphan using capillary electrophoresis with dynamically coated capillaries. *Microgram J.* 2005, *3*, 138–141.

20. Bertaso, A., Musile, G., Gottardo, R., Seri, C., Tagliaro, F., Chiral analysis of methorphan in opiate-overdose related deaths by using capillary electrophoresis. *J. Chromatogr. B* 2015, *1000*, 130–135.

21. Bortolotti, F., Bertaso, A., Gottardo, R., Musile, G., Tagliaro, F., Dextromethorphan/levomethorphan issues in a case of opiate overdose. *Drug Test. Anal.* 2013, *5*, 781–784.

22. Hanrahan, G., Gomez, F. A., Chemometric Methods in Capillary Electrophoresis, Wiley, Oxford 2010.

23. Hubert, C., Houari, S., Rozet, E., Lebrun, P., Hubert, P., Towards a full integration of optimization and validation phases: an analytical-quality-by-design approach. *J. Chromatogr. A* 2015, *1395*, 88–98.

24. Orlandini, S., Pinzauti, S., Furlanetto, S., Application of quality by design to the development of analytical separation methods. *Anal. Bioanal. Chem.* 2013, *405*, 443–450.

25. Rozet, E., Lebrun, P., Hubert, P., Debrus, B., Boulanger, B., Design spaces for analytical methods. *Trends Anal. Chem.* 2013, *42*, 157–167.

26. Orlandini, S., Gotti, R., Furlanetto, S., Multivariate optimization of capillary electrophoresis methods: a critical review. *J. Pharm. Biomed. Anal.* 2014, *87*, 290–307.

27. Allmendinger, A., Dieu, L.-H., Fischer, S., Mueller, R., Mahler, H.-C., Huwyler, J., High-throughput viscosity measurement using capillary electrophoresis instrumentation and its application to protein formulation. *J. Pharm. Biomed. Anal.* 2014, *99*, 51–58.

28. Dubský, P., Ördögová, M., Malý, M., Riesová, M., CEval: all-in-one software for data processing and statistical evaluations in affinity capillary electrophoresis. *J. Chromatogr. A* 2016, *1445*, 158–165.

29. Kumar, A., Mann, H. J., Remmel, R. P., Simultaneous analysis of cytochrome P450 probes—dextromethrophan, furbiprofen and midazolam and their major metabolites by HPLC-mass-spectrometry/fluorescence after single step extraction from plasma. *J. Chromatogr. B* 2007, *853*, 287–293.

30. Fillet, M., Chankvetadze, B., Crommen, J., Blaschke, G., Designed combination of chiral selectors for adjustment of enantioseparation selectivity in capillary electrophoresis. *Electrophoresis* 1999, *20*, 2691–2697.

31. Fillet, M., Hubert, P., Crommen, J., Enantiomeric separations of drugs using mixtures of charged and neutral cyclodextrins. *J. Chromatogr. A* 2000, *875*, 123–134.

32. Grard, S., Morin, P., Dreux, M., Ribet, J.-P., Enhancement of second-migrating enantiomer peak symmetry of basic drugs using dual-cyclodextrin system in capillary electrophoresis. *Electrophoresis* 2000, *21*, 3028–3034.

33. Wren, S. A. C., Theory of chiral separation in capillary electrophoresis. *J. Chromatogr.* 1993, *636*, 57–62.

34. Erny, G. L., Bergström, E. T., Goodall, D. M., Grieb, S., Predicting peak shape in capillary zone electrophoresis: a generic approach to parametrizing peaks using the Haarhoff−van der Linde (HVL) function. *Anal. Chem.* 2001, *73*, 4862–4872.

SUPPORTING INFORMATION

Additional Supporting Information may be found online in the supporting information tab for this article.

3.3.   Manuscript 3

Quality by design-assisted development of a capillary electrophoresis method for the chiral purity determination of dexmedetomidine.

Personal Contribution (85 %): study design and concept development, experimental work, data analysis and interpretation, preparation of manuscript draft.

Gerhard K. E. Scriba (15 %): supervision or research, finalizing manuscript

Overview:

The manuscript describes the first chiral CE assay for the determination of the stereochemical purity of dexmedetomidine. Design of experiments methodology was used in method development, optimization and validation. The assay proved to be precise and accurate meeting the analytical target profile and could be applied to the analysis of drug substance.

Sulaiman Krait
Gerhard K. E. Scriba iD

Friedrich Schiller University,
Department of Medicinal/
Pharmaceutical Chemistry, Jena,
Germany

Research Article

Quality by design-assisted development of a capillary electrophoresis method for the chiral purity determination of dexmedetomidine

Dexmedetomidine is a selective α_2-adrenergic agonist used for patient sedation, while its enantiomer levomedetomidine has no sedative effects. As CE has been shown to be a powerful technique for enantiomer analysis, the aim of the study was the quality by design-based development of a CE-based limit test for the enantiomeric impurity levomedetomidine. The analytical target profile was defined that the method should be able to determine levomedetomidine with acceptable precision and accuracy at the 0.1% level. From initial scouting experiments, sulfated β-cyclodextrin was selected as chiral selector. The critical process parameters were identified in a fractional factorial resolution V+ design, while a central composite face centered design and Monte Carlo simulations were used for defining the design space of the method. The selected working conditions were a 21.3/31.5 cm, 50 μm id fused-silica capillary, a 50 mM sodium phosphate buffer, pH 6.5, containing 40 mg/mL sulfated β-cyclodextrin, a capillary temperature of 17°C and an applied voltage of 10 kV. Validation according to the ICH guideline Q2(R1) demonstrated repeatability and intermediate precision of content and migration time between 9.3 and 4.2% with accuracy in the range of 92.0 and 98.9%.

Additional supporting information may be found in the online version of this article at the publisher's web-site

1 Introduction

Dexmedetomidine [(*S*)-4-[1-(2,3- dimethylphenyl)ethyl]-1*H*-imidazole, D-MDT, Fig. 1], is a selective centrally acting α_2-adrenergic agonist used as a sedative in anesthesia management in surgery and in intensive care medicine [1, 2]. The advantage of D-MDT over other sedatives is the absence of respiratory depression [2]. In animal experiments, the compound displayed much higher activity as compared to its enantiomer levomedeto-

midine (L-MDT, Fig. 1) [3, 4]. D-MDT was approved by the US Food and Drug Administration in 1999 [www.accessdata.fda.gov/drugsatfda_docs/label/2013/02103 8s021lbl.pdf], and by the European Medicines Agency in 2011 [www.ema.europa.eu/docs/en_GB/document_library/EPAR _-_Public_assessment_report/human/002268/WC50011563 2.pdf] for use in humans and is also approved in the USA and Europe for veterinary use [www.fda.gov/ohrms/ dockets/98fr/2007-141-267-fois002.pdf, www.ema.europa. eu/docs/en_GB/document_library/EPAR_-_Summary_for_ the_public/veterinary/000070/WC500062498.pdf].

D-MDT is typically prepared by synthesis of racemic MDT via various synthetic routes and subsequent resolution of the enantiomers via fractionated crystallization using enantiomerically pure acids such as (*R*)-(−)-mandelic acid, (−)-camphor-10-sulfonic acid, (2*R*,3*R*)-(+)-tartaric acid or derivatives thereof [5]. Consequently, the enantiomeric purity of D-MDT must be evaluated during quality control. The HPLC enantioseparation of MDT has been reported using an

---

Correspondence: Professor Gerhard K. E. Scriba, Friedrich Schiller University, Department of Medicinal/Pharmaceutical Chemistry, Philosophenweg 14, 07743 Jena, Germany
Fax: +49-3641-949802
E-mail: gerhard.scriba@uni-jena.de

Abbreviations: ATP, analytical target profile; **CPP**, critical process parameter; **CQA**, critical quality attribute; **D-MDT**, dexmedetomidine; **DoE**, design of experiments; **DS**, degree of substitution; **ICH**, International Council on Harmonization; **L-MDT**, levomedetomidine; **MDT**, medetomidine; **QbD**, quality by design; **S-β-CD**, sulfated β-cyclodextrin

Color Online: See the article online to view Fig. 3 in color.
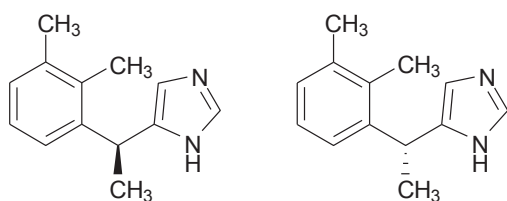
Figure 1. Structures of dexmedetomidine and levomedetomidine.

α_1-acid glycoprotein column and a mobile phase composed of a phosphate buffer, pH 7.0 and acetonitrile [6, 7]. 0.5% of L-MDT could be detected in D-MDT [7]. Furthermore, the United States Pharmacopeia contains a monograph for D-MDT hydrochloride, limiting L-MDT to 1.0% by a chiral HPLC method, which also employs an α_1-acid glycoprotein chiral stationary phase and a mobile phase consisting of phosphate buffer, pH 7.0 and acetonitrile [8]. Despite the fact that enantiomeric impurities and their limits are excluded from the requirements for impurities in drug substances such as stated in the International Council of Harmonization (ICH) guideline Q3A(R2) Impurities in New Drug Substances [www.ich.org/fileadmin/Public_Web_Site/ICH_Products/Guidelines/Quality/Q3A_R2/Step4/Q3A_R2__Guideline.pdf], there is general consent that enantiomeric impurities should be considered in the same manner as other impurities. Consequently, analytical methods should be able to quantify enantiomeric impurities at the 0.1% level or below.

Capillary electrophoresis (CE) has been increasingly used for the analysis of pharmaceuticals [9–12] including enantioseparations [13–16] due to the high resolution and experimental flexibility of the technique. Therefore, the aim of the present study was the development of a CE method for the determination of the enantiomeric purity of D-MDT allowing the quantitation of L-MDT at the 0.1% level with acceptable accuracy and precision. In the process, quality by design (QbD) principles were implemented. QbD has been increasingly applied in analytical chemistry in recent years [17–21]. This approach employs multivariate design of experiments (DoE) and risk-assessment tools for the identification of the critical process parameters (CPPs), which are the experimental factors that influence the critical quality attributes (CQAs) of the method. This methodology results in the understanding of quantitative effects of the CQAs on the analytical process.

2 Materials and methods

2.1 Chemicals and reagents

D-MDT hydrochloride was from TCI Europe (Zwijndrecht, Belgium). Racemic MDT hydrochloride was from Carbosynth (Compton, UK). β-cyclodextrin (β-CD) and methyl-

α-CD (M-α-CD, DS ~11) were from Wacker Chemie AG (Burghausen, Germany). γ-CD, sulfated α-CD sodium salt, sulfated β-CD sodium salt (S-β-CD, batch S1: DS ~12–15, batch S2: DS ~7–11), L-Trp were from Sigma-Aldrich (Steinheim, Germany). α-CD, methyl-α-CD (DS ~11), hydroxypropyl-α-CD (DS ~4.5), carboxymethyl-α-CD sodium salt (CM-α-CD, DS ~3.5), methyl-β-CD (DS ~12), hydroxypropyl-β-CD (DS ~4.5), carboxymethyl-β-CD sodium salt (CM-β-CD, DS ~3.5), succinyl-β-CD (DS ~3.5), *heptakis*(2,6-di-*O*-methyl)-β-CD (DS ~14, 50% purity), *heptakis*(2,6-di-*O*-methyl)-β-CD (95% purity), carboxymethyl-γ-CD sodium salt (DS ~3.5), *heptakis*(6-*O*-sulfo)-β-CD and hydroxypropyl-γ-CD (DS ~4.5) were from Cyclolab Ltd. (Budapest, Hungary), while sulfobutyl-β-CD sodium salt (DS ~6.6) was from CyDex Pharmaceuticals (San Diego, USA). Orthophosphoric acid (85%), citric acid monohydrate, glacial acetic acid, sodium hydroxide, and triethanolamine were from VWR (Darmstadt, Germany). Water was purified by a GenPure system from Thermo Fischer (Waltham, USA). All chemicals were obtained at the highest purity commercially available.

2.2 Instrumentation

All measurements were carried out on a Beckman P/ACE MDQ capillary electrophoresis system (Beckman Coulter, Krefeld, Germany) equipped with a UV-Vis diode array detector and controlled by the 32 KARAT software (version 8.0) for system control, data acquisition and processing. Hydrodynamic sample injection was performed at a pressure of 0.7 psi (4.8 kPa) for 5 s for the CD scouting, while a pressure of 0.7 psi (4.8 kPa) for 7 s was used during screening and optimization phases, robustness testing, method validation and sample analysis. UV detection was carried out at the cathodic end of the capillary at 200 nm unless otherwise specified. pH measurements were carried out using a WTW Multi-3410 IDS digital pH meter equipped with a SenTix SP-T 900 electrode (Xylem Analytics Germany GmbH, Weilheim, Germany) calibrated with buffer solutions at pH 4.00, 7.00, and 9.00 from Carl Roth (Karlsruhe, Germany).

Fused-silica capillaries with 50 μm id were from BGB Analytik (Schloßböckelheim, Germany). A new capillary was successively rinsed at a pressure of 20 psi (138 kPa) with 1 M sodium hydroxide for 10 min, followed by water for 15 min. For the CD screening with a background electrolytes (BGE) at pH $\leq$ 6.0, the capillary was rinsed successively with 0.1 M phosphoric acid for 5 min and water for 10 min at the beginning of the day. When using a BGE with pH > 6.0, the capillary was rinsed with 0.1 M sodium hydroxide for 5 min and water for 10 min. Between runs, the capillary was flushed with water for 1 min and the BGE for 3 min.

2.3 Background electrolyte and sample solutions

The BGEs were prepared by dissolving the respective CD in water followed by addition of the corresponding amount of

the acid component and diluting with water to about 90% of the required volume. The pH was subsequently adjusted and the water was added to the final volume. All BGEs were filtered through polypropylene syringe filters (0.22 μm, BGB Analytik, Schloßböckelheim, Germany) and sonicated for 10 min prior to use.

Stock solutions of D-MDT hydrochloride equivalent to 4.0 mg/mL of D-MDT and racemic MDT hydrochloride equivalent to 4.0 mg/mL of MDT were prepared in 0.01 M hydrochloric acid. Sample solutions were prepared by dilution of the stock solutions with 0.01 M HCl. Samples containing L-MDT were obtained by mixing appropriate volumes of solutions of racemic MDT with solutions of D-MDT.

2.4 Software and data analysis

MODDE 11.0 (Umetrics, Umeå, Sweden) was used for the experimental design and statistical analysis of the screening, response surface methodology and robustness testing. The data obtained from the respective designs were fitted to a model using the quadratic polynomial equation [21]:

$$y = \beta_0 + \sum_{i=1}^{f} \beta_i x_i + \sum_{1 \leq i \leq j}^{f} \beta_{ij} x_i x_j + \sum_{i=1}^{f} \beta_{ii} x_i^2$$

where y are the predicted response (separation selectivity α, migration time or current), β_0 the intercept, β_i the coefficients, which were optimized (voltage, temperature, buffer pH and concentration and CD concentration), β_{ij} the interaction coefficients (restricted to two-factor interactions) and β_{ii} the quadratic coefficients. Statistical analysis of the validation data was performed using Microsoft Excel 2013.

3 Results and discussion

The first step in developing an analytical method following the QbD methodology is the choice of the technique and the definition of the analytical target profile (ATP). Subsequently, the CPPs are identified in initial experiments followed by the establishment of the design space of the method. The latter refers to experimental conditions where the ATP is fulfilled [18–21]. In the process, DoE methodology is employed.

With regard to the stereoselective D-MDT assay, the ATP was defined that the CE method should allow the determination of L-MDT in the presence of D-MDT in the range of at least 0.1% up to 1.5% relative to the concentration to the parent drug with precision and accuracy of ≤10% in an analysis time of ≤10 min.

3.1 Initial method scouting

CDs as the most widely used chiral selectors in CE [13,16,22] were evaluated as chiral selectors for the assay. MDT is a weak base with a pK_a value of about 7.08 [23]. Thus, the selector

screening was performed in a 50 mM sodium phosphate buffer, pH 2.5, using a 40/50.2 cm, 50 μm id fused-silica capillary at 20°C and an applied voltage of 20 kV. The sample solution contained 100 μg/mL of D-MDT and 50 μg/mL of L-MDT. Native α-CD, β-CD and γ-CD as well as neutral and charged derivatives were studied at concentrations of about 5 and 20 mM. Uncharged CDs were evaluated under normal polarity of the applied voltage, while negatively charged CDs were also studied at reversed polarity. The best resolution was observed in the presence of sulfated α-CD and sulfated β-CD (S-β-CD) with α-values >1.2. Because the highest α-value was found for S-β-CD and the price of this CD is relatively low, S-β-CD was selected for further evaluation.

Using a sample containing 0.7 mg/mL of D-MDT and 7 μg/mL of L-MDT (i.e. 1% relative concentration), several phosphate-based buffers, pH 2.5, in combination with sodium or triethanolamine as counter ions and S-β-CD concentrations, 50 mM sodium citrate buffer, pH 2.5, and 50 mM sodium acetate buffer, pH 4.8, containing S-β-CD were studied. In addition, short end injection was evaluated. However, under all conditions severe peak tailing was observed for D-MDT due to the high sample concentration. Subsequently, 50 mM sodium phosphate buffer, pH 7.0, at normal polarity of the applied voltage was investigated. These conditions led to improved peak shape. Moreover, under these conditions, L-MDT migrated before D-MDT, which is favorable when a minor impurity has to be determined in the presence of a large excess of a drug. Using triethanolamine as counter ion resulted in higher background noise. Therefore, sodium phosphate buffer, pH 7.0, in combination with S-β-CD as selector was chosen for method development. Shortening of the capillary to an effective length of 21.3 cm resulted in reduced analysis time. Figure 2 shows a comparison of the enantioseparation in 50 mM sodium phosphate buffer, pH 2.5, (short end injection) and in 50 mM sodium phosphate buffer, pH 7.0.
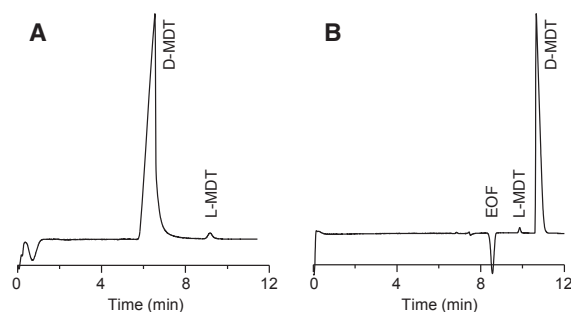
Figure 2. Electropherograms of the S-β-CD-mediated separation of D-MDT and L-MDT at (A) pH 2.5 and (B) pH 7.0. Experimental conditions: (A) 10.2/50.2 cm, 50 μm id fused-silica capillary (short end injection); 50 mM sodium phosphate buffer, pH 2.5; 30 mg/mL S-β-CD; 20°C; −20 kV and (B) 21.3/31.5 cm, 50 μm id fused-silica capillary; 50 mM sodium phosphate buffer, pH 7.0; 50 mg/mL S-β-CD; 20°C; 6 kV; UV detection at 200 nm. Sample concentration: 700 μg/mL D-MDT and 7 μg/mL L-MDT.

3.2 Knowledge space and identification of critical process parameters

The CQAs of the method were defined to comprise peak resolution expressed as separation selectivity α of at least 1.05, a current <100 μA and a migration time of D-MDT of ≤10 min so that the analysis time would not exceed 12 min. Considering the scouting experiments, BGE pH and concentration, concentration of the S-β-CD, as well as separation voltage and temperature were studied in detail using a fractional factorial resolution V+ design. The ranges were BGE pH 6.3 to 8.5, phosphate buffer concentration 50 to 100 mM, S-β-CD concentration 30 to 50 mg/mL, voltage 6 to 10 kV and capillary temperature 15 to 25°C. The sample consisted of 1.0 mg/mL D-MDT and 10 μg/mL L-MDT (i.e., relative concentration of 1.0%).

The design matrix as well as the respective values of the CQAs as responses, i.e. α-value, current and migration time of D-MDT are summarized in Supporting Information Table 1. The coefficient plots of the variables as well as their interaction terms are shown in Supporting Information Fig. 1. Significant effects were detected for all parameters and for most interaction terms. Increasing the pH of the BGE negatively affected separation selectivity in addition to increasing the current. Thus, low pH seems favorable, although this leads to increased migration times. Similarly, increasing phosphate buffer concentration results in lower α-values and increased currents but with a smaller effect on migration times. Voltage and temperature affected migration time and current more significantly than separation selectivity α. Increasing S-β-CD concentrations increased all responses. Consequently, the concentration and pH of the phosphate buffer were fixed at 50 mM and pH 6.5, respectively, to achieve high separation selectivity and short migration times as well as low current. The concentration of S-β-CD, the capillary temperature and the separation voltage were considered CPPs and further optimized.

3.3 Method optimization and design space

The CPPs voltage (6–10 kV), S-β-CD concentration (30–50 mg/mL) and capillary temperature (15–25°C) were further optimized in the indicated ranges using a central composite face centered design and keeping the responses as above. The design matrix is summarized in Supporting Information Table 2.

Setting the CQA limits at α > 1.05, current < 100 μA and migration time ≤10 min, the design space was obtained by Monte Carlo simulations setting the level of probability of failure at ≤1%. Figure 3 shows the plots for concentrations of S-β-CD of 30, 40 and 50 mg/mL. Because the larger space was found at a selector concentration of 40 mg/mL, this concentration was chosen for S-β-CD. Moreover, voltage was set at 10 kV in order to achieve a short analysis time. Temperature was set at 17°C so that the final experimental conditions included a 21.3/31.5 cm, 50 μm id fused-silica

capillary, a BGE composed of a 50 mM sodium phosphate buffer, pH 6.5, containing 40 mg/mL S-β-CD, a capillary temperature of 17°C and an applied voltage of 10 kV. These conditions resulted in currents of approximately 75 μA. L-Trp was selected as internal standard to compensate for injection errors. An electropherogram of standards under the optimized experimental conditions is shown in Fig. 4A.

3.4 Method robustness

In order to achieve the desired limit of 0.1% L-MDT in D-MDT the sample concentration was set at 2.0 mg/mL of D-MDT and 20 μg/mL of L-MDT (0.1% relative concentration) containing 60 μg/mL L-Trp as internal standard. Method robustness was estimated using a Plackett-Burman design by varying the experimental conditions around the center point of the working conditions, i.e. buffer concentration 50 ± 2.5 mM and pH 6.5 ± 0.1, S-β-CD concentration 40 ± 2 mg/mL, voltage 10 ± 1 kV and temperature 17 ± 1°C. In addition, two batches of S-β-CD were included. The design matrix is summarized in Supporting Information Table 3. In addition to the three optimized responses, the quantitative robustness was assessed using the ratio of the corrected peak areas of L-MDT and the internal standard as a measure. The regression analysis of the model indicated that the responses α-value, current and the ratio of corrected peak areas were not significantly affected by the small variations of the experimental parameters (data not shown). This included the different batches of S-β-CD tested. In contrast, in the case of migration time, a significant although minor effect of all variables on this response was detected (Supporting Information Fig. 2). However, none of the conditions led to a migration time above 8.2 min, which is well below the threshold of ≤10 min set in the ATP. Therefore, the method can be considered robust. Nonetheless, the BGE should be prepared carefully and the instrumental parameters voltage and capillary temperature should be strictly controlled.

3.5 Method validation and application

The optimized method was validated according to the Q2 (R1) guideline (www.ich.org/fileadmin/Public_Web_Site/ICH_Products/Guidelines/Quality/Q2_R1/Step4/Q2_R1__Guideline.pdf) in the range of 2.0 - 30 μg/mL L-MDT in the presence of D-MDT at a concentration of 2.0 mg/mL (relative concentration of L-MDT 0.1 to 1.5%). L-Trp at a concentration of 60 μg/mL served as internal standard. The data are summarized in Table 1. LOD and LOQ values were estimated at 0.6 μg/mL (0.03%) and 2.0 μg/mL (0.1%), respectively, based on a signal-to-noise ratio of 3 and 10. Repeatability and intermediate precision of content and migration time were well below 10%, which indicated sufficient precision of the method. Accuracy was estimated by spiking a solution containing 2.0 mg/mL D-MDT with L-MDT to yield concentration levels of 4, 16 and 28 μg/mL
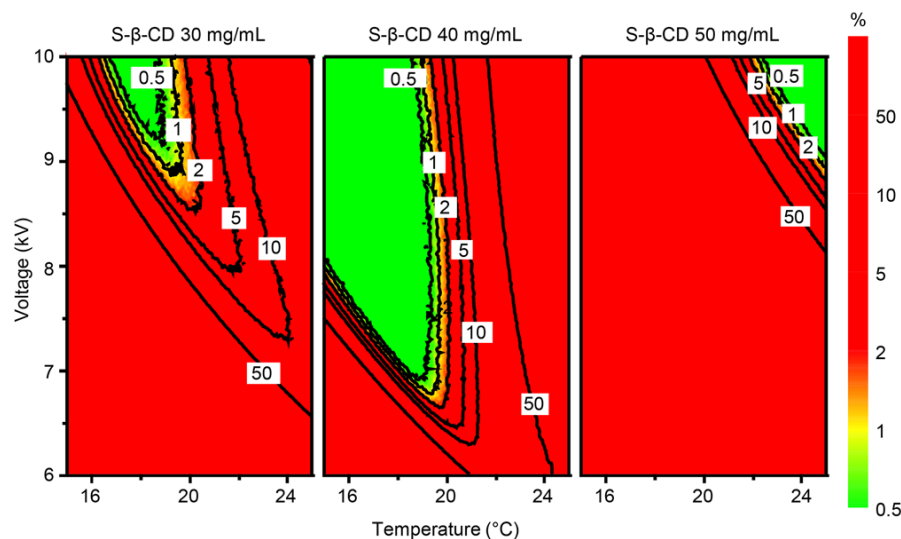
Figure 3. Probability plot of the design space obtained by Monte Carlo simulations. The design space (green zone) defines combinations of parameters where the risk of failure is ≤ 1%, to meet the three criteria, α-value> 1.05, Current ≤ 100 μA, and migration time of D-MDT ≤10 min. For the color version of the figure, the reader is referred to the online version of the article.
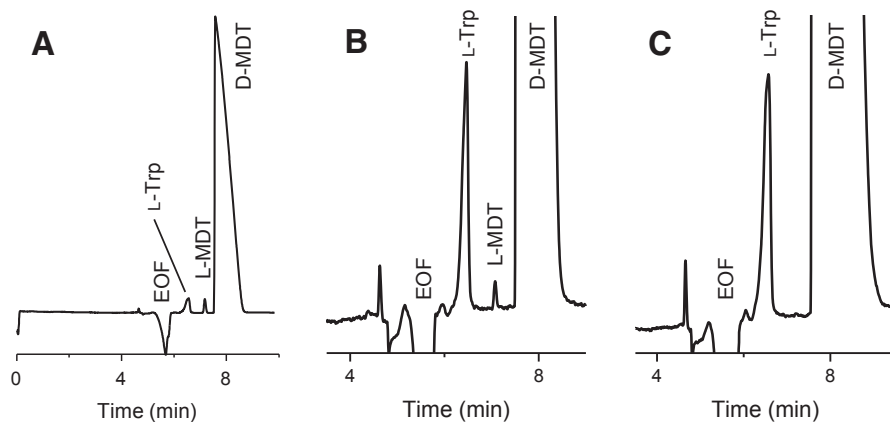
Figure 4. Electropherograms of a solution of 2 mg/mL D-MDT spiked with (A) 20 μg/mL L-MDT (1.0% relative concentration) and (B) 2 μg/mL L-MDT (0.1% relative concentration). (C) Analysis of a commercial D-MDT hydrochloride sample at a concentration equivalent to 2 mg/mL D-MDT. Experimental conditions: 21.3/31.5 cm, 50 μm id fused-silica capillary; 50 mM sodium phosphate buffer, pH 6.5; 40 mg/mL S-β-CD; 17°C; 10 kV; UV detection at 200 nm.

and ranged between 92.0 ± 6.4% and 98.9 ± 1.7%. Thus, the method can be considered accurate. Because no peak at the migration time of L-MDT was detected in samples of D-MDT the method can also be considered selective. A representative electropherogram of D-MDT spiked with L-MDT at the LOQ (0.1% level) is shown in Fig. 4B.

The method was subsequently applied to a sample of D-MDT hydrochloride substance obtained from a commercial source. The electropherogram is shown in Fig. 4C. L-MDT was below the LOD.

4 Concluding remarks

A CE method was developed for the determination of the stereochemical purity of D-MDT drug substance using a systematic QbD approach. S-β-CD was chosen as chiral selector from screening experiments. Separation after the EOF in a BGE pH 6.5 resulted in the desired migration order so

that the minor impurity L-MDT migrated before the large peak of D-MDT. A fractional factorial resolution V+ design was used for the investigation of the knowledge space and the identification of the CQAs. Because separation selectivity and migration time decreased with increasing pH and concentration of the BGE, these parameters were set at low values while S-β-CD concentration as well as the instrumental parameters separation voltage and capillary temperature were further optimized using response surface methodology. The design space was derived by Monte Carlo simulations followed by selection of the working conditions. The method was robust as assessed by a Plackett-Burman design. Subsequent validation in the range of a relative L-MDT concentration of 0.1 to 1.5% indicated repeatability and intermediate precision <10% with an accuracy of >90%. Analysis time was <10 min. In summary, the present method is the first CE method for the determination of the enantiomeric purity of D-MDT at the 0.1% level.

L-MDT could not be detected in a commercial batch of D-MDT. Therefore, the limit of L-MDT of 1.0% stated in the

Table 1. Assay validation data

Parameter	Level	L-MDT
Range		2.0–30 μg/mL (0.1–1.5%)
Coefficient of determination R^2		0.9897
LOD (S/N = 3)		0.6 μg/mL (0.03%)
LOQ (S/N = 10)		2.0 μg/mL (0.1%)
Migration time repeatability (RSD)		4.2%
Migration time intermediate precision (RSD)		9.3%
Content repeatability[a] (RSD)		4.7%
Content intermediate precision[b] (RSD)		5.4%
Accuracy[c]	4 μg/mL (0.2%)	92.0 ± 6.4%
	16 μg/mL (0.8%)	96.8 ± 3.0%
	28 μg/mL (1.4%)	98.9 ± 1.7%

a) nine runs, three samples at three concentrations on one day.
b) nine runs, mean of three samples at three concentrations on three consecutive days.
c) Expressed as mean recovery ± confidence interval% (α/2 = 0.025). D-MDT samples were spiked with the racemic MDT solution to yield the indicated amount of L-MDT.

monograph of D-MDT hydrochloride of United States Pharmacopeia [8] could be questioned. It may be speculated that the high limit of L-MDT is due to the chromatographic assay in the monograph, which utilizes an α_1-acid glycoprotein chiral stationary phase. However, this would have to be investigated by direct comparison of the chromatographic method with the CE-based method, which was out of the scope of the present study.

5 References

[1] Jones, C. R., *Int. Anesthesiol. Clin.* 2013, *51*, 81–96.

[2] Cormack, J. R., Orme, R. M., Costello, T. G., *J. Clin. Neurosci.* 2005, *12*, 375–378.

[3] Savola, J.-M., Virtanen, R., *Eur. J. Pharmacol.* 1991, *195*, 193–199.

[4] Vickery, R. G., Sheridan, B. C., Segal, I. S., Maze, M., *Anesth. Analg.* 1988, *67*, 611–615.

[5] Bobošíková, M., Mathia, F., Végh, D., Marchalín, S., Halinkovičová, M. *Acta Chim. Slov.* 2013, *6*, 240–244.

[6] Kivikoski, J. H., Rissanen, K. T., Parhi, S. S.L., *Tetrahedron: Asymmetry* 1993, *4*, 45–58.

[7] Örn, G., Lahtonen, K., Jalonen, H., *J. Chromatogr. A* 1990, *506*, 627–635.

[8] *The United States Pharmacopeia*, 41st Edition, The United States Pharmacopeial Convention, Rockville, MD 2018.

[9] Zhu, Q., Scriba, G. K. E., *J. Pharm. Biomed. Anal.* 2017, *147*, 425–438.

[10] El Deeb, S., Wätzig, H., Abd El-Hady, D., Sänger-van de Griend, C. E., Scriba, G. K. E., *Electrophoresis* 2016, *37*, 1591–1608.

[11] Deeb, S. E., Wätzig, H., El-Hady, D. A., Albishri, H. M., Sänger-van de Griend, C. E., Scriba, G. K. E., *Electrophoresis* 2014, *35*, 170–189.

[12] Altria, K., Marsh, A., Sänger-van de Griend, C. E., *Electrophoresis* 2006, *27*, 2263–2282.

[13] Sánchez-Hernández, L., Guijarro-Diez, M., Marina, M. L., Crego, A. L., *Electrophoresis* 2014, *35*, 12–27.

[14] Preinerstorfer, B., Lämmerhofer, M., Lindner, W., *Electrophoresis* 2009, *30*, 100–132.

[15] Lu, H., Chen, G., *Anal. Methods* 2011, *3*, 488–508.

[16] Jáč, P., Scriba, G. K. E., *J. Sep. Sci.* 2013, *36*, 52–74.

[17] Orlandini, S., Gotti, R., Furlanetto, S., *J. Pharm. Biomed. Anal.* 2014, *87*, 290–307.

[18] Rozet, E., Lebrun, P., Hubert, P., Debrus, B., Boulanger, B., *Trends Anal. Chem.* 2013, *42*, 157–167.

[19] Orlandini, S., Pinzauti, S., Furlanetto, S., *Anal. Bioanal. Chem.* 2013, *405*, 443–450.

[20] Hubert, C., Houari, S., Rozet, E., Lebrun, P., Hubert, P., *J. Chromatogr. A* 2015, *1395*, 88–98.

[21] Hanrahan, G., Gomez, F. A., *Chemometric Methods in Capillary Electrophoresis*, Wiley, Oxford 2010.

[22] Zhu, Q., Scriba, G. K. E., *Chromatographia* 2016, *79*, 1403–1435.

[23] Wiczling, P., Nasal, A., Kubik, L. Kaliszan, R., *Eur. J. Pharm. Sci.* 2012, *47*, 1–5.

3.4.   Manuscript 4

Investigation of the complexation between cyclodextrins and medetomidine enantiomers by capillary electrophoresis, NMR spectroscopy and molecular modeling

Krait. S, Salgado. A, Chankvetadze. B, Gago. F, Scriba. G.K.E., Journal of Chromatography A 2018; 1567: 198-210. https://doi.org/10.1016/j.chroma.2018.06.010

Personal Contribution (50%): study design and concept development, capillary electrophoresis experiments, calculation of complexation constants, data analysis and interpretation, writing the manuscript draft (except the NMR and molecular modelling).

Antonio Salgado (25%): conducting the NMR experiments, data analysis and interpretation, writing the manuscript draft (NMR part).

Federico Gago (10%): performing the molecular dynamics simulations, data analysis and interpretation.

Bezhan Chankvetadze (5 %): cooperation in study design and discussion.

Gerhard K. E. Scriba (10%): study design and concept development, supervision or research, finalizing manuscript

Overview:

The manuscript describes the first detailed study on the complexation of the enantiomers of medetomidine by CDs. In CE experiments reversal of the enantiomeric migration order depending on the applied CD was noted. Specifically, reversal or the migration order was observed for the pairs β-CD and γ-CD as well as for randomly substituted sulfated β-CD and single isomer HS-β-CD. In order to understand this migration behavior, complexation constants and complex mobilities were determined by CE. The structures of the analyte-CD complexes were derived from ROESY NMR experiments, which agreed with the CE data. Finally, molecular modeling and molecular dynamics simulations were applied to understand and confirm structures of the complexes as well as the complexation behavior by the CDs.

Investigation of the complexation between cyclodextrins and medetomidine enantiomers by capillary electrophoresis, NMR spectroscopy and molecular modeling☆

Sulaiman Krait [a,1], Antonio Salgado [b,1], Bezhan Chankvetadze [c], Federico Gago [d], Gerhard K.E. Scriba [a,*]

[a] Friedrich-Schiller-University Jena, Department of Pharmaceutical/Medicinal Chemistry, Philosophenweg 14, 07743 Jena, Germany
[b] University of Alcalá, NMR Spectroscopy Centre (CERMN), CAI Químicas, Faculty of Pharmacy, 28805 Alcalá de Henares, Madrid, Spain
[c] Tbilisi State University, Institute of Physical and Analytical Chemistry, School of Exact and Natural Sciences, 0179 Tbilisi, Georgia
[d] University of Alcalá, Department of Biomedical Sciences (Unidad Asociada IQM-CSIC) and Instituto de Investigación Química Ándrés M. del Río (IQAR), 28805 Alcalá de Henares, Madrid, Spain

A B S T R A C T

The migration order of the enantiomers of medetomidine in the presence of cyclodextrins studied by capillary electrophoresis in phosphate buffer, pH 2.5, depended on the cavity size and the substitution pattern of the cyclodextrins. Opposite migration order was observed in the presence of β-cyclodextrin (β-CD) and γ-cyclodextrin (γ-CD) as well as randomly sulfated β-CD (S-β-CD) and *heptakis*(6-O-sulfo)-β-CD (HS-β-CD). This could be rationalized by the fact that dexmedetomidine formed more stable complexes with β-CD and S-β-CD, while levomedetomidine interacted stronger with γ-CD and HS-β-CD. The structure of the complexes was derived from rotating frame nuclear Overhauser (ROESY) experiments for β-CD, γ-CD and HS-β-CD. In the case of the native CDs, the phenyl ring of medetomidine entered the cavity through the wider secondary rim of the CDs, whereas the protonated imidazole ring was positioned inside the CD cavity interacting with the sulfate groups of HS-β-CD. Furthermore, molecular dynamics calculations also suggested opposite affinities of the medetomidine enantiomers toward β-CD and γ-CD.

© 2018 Elsevier B.V. All rights reserved.

1. Introduction

Cyclodextrins (CDs) are cyclic oligosaccharides, which consist of α1,4-linked D-glucopyranose units. α-CD contains six glucose units, β-CD seven and γ-CD eight. CDs can be topologically described as hollow toroids with a lipophilic cavity and a hydrophilic outside. The wider rim contains the secondary 2- and 3-hydroxyl groups, while the narrower rim features the primary 6-hydroxyl groups. The hydroxyl groups can be chemically modified resulting in a large number of derivatives, many of which are commercially available. Due to their ability to form complexes with a large variety of compounds, CDs have found numerous pharmaceutical, chemical, (bio)technological, food, cosmetic or textile applications [1–3]. With regard to separation sciences, CDs have been applied as chiral selectors in GC [4], HPLC [5] and especially CE [6–9].

Complexation of guest molecules often occurs via their inclusion into the CD cavity either from the narrower or the wider side of the torus, displacing solvent molecules from the cavity. Van der Waals and hydrophobic interactions as well as hydrogen bonding with the hydroxyl groups on the rims and steric factors are considered the driving forces. In the case of charged CD derivatives, ionic interactions also play a role [10–12]. While most selector-selectand complexes were shown to be of the inclusion type, several studies demonstrated that so-called external complexes can also be formed leading to effective CE enantioseparations [13–15]. Due to the fact that the selector-selectand complexes are mobile, two enantioselective principles govern enantioseparations in CE [16,17]. The chromatographic enantioselective principle (also referred to as the thermodynamic mechanism) is based on the different affinities of the selector toward the solute enantiomers, which can be expressed as complexation constants. The electrophoretic enantioselective principle is due to differences in the mobilities of the enantiomer-selector complexes, for example as a result of differences in the hydrodynamic radii of the complexes or the so-called complexation-induced pK_a shift [18]. Consequently, the enantiomer migration order in CE does not necessarily correlate

---

Manuscript 4   43

_____

S. Krait et al. / J. Chromatogr. A 1567 (2018) 198–210   199

with the binding strength between the selector and the enantiomers as it is the case in HPLC where the selector is immobile (except for the rarely used technique of a chiral mobile phase additive).

Structural information on the complexes can be obtained by spectroscopic techniques such as NMR and X-ray analyses. Nuclear Overhauser effect-based NMR methods, in particular rotating frame nuclear Overhauser effect spectroscopy (ROESY), allow the determination of correlation of spatially close nuclei and proved to be a valuable tool to elucidate the structure of selector-selectand complexes [19–22]. Furthermore, as NMR is a solution technique, experiments can be carried out under conditions comparable to those used in CE with regard to the composition of the electrolyte solution, pH and temperature.

Molecular dynamics (MD) simulations also yield 3-dimensional illustrative structures of the CD-solute complexes [23–27]. In addition, MD approaches allow the calculation of binding energies, which cannot be experimentally determined at present. Furthermore, MD simulations can provide information on the interactions between selectors and solutes as well as on the different steps involved in the chiral recognition process. These may include the approach of solutes and selector, displacement of solvent molecules in the CD cavity or the establishment of specific van der Waals and electrostatic interactions in the complex, including direct and water-bridged hydrogen bonds.

Medetomidine (4-[1-(2,3-dimethylphenyl)ethyl]-1H-imidazole) is an α_2-adrenoreceptor agonist, which is used as an analgesic and anesthetic drug in veterinary medicine [28]. The pharmacological activity has been attributed mainly to the dextrorotary (S)-enantiomer dexmedetomidine [29], which has been developed for human use as a sedative in anesthesia management in surgery and in intensive care medicine [30]. In the process of the development of a CE-based assay for the determination of the stereochemical purity of dexmedetomidine using CDs as chiral selectors [31], different enantiomer migration orders depending on the CD were observed. The aim of the present study was the investigation of the complexation of the medetomidine enantiomers by CDs and a detailed characterization of selected CD complexes by CE, NMR spectroscopy and MD simulations.

2. Experimental

2.1. Chemicals and reagents

Dexmedetomidine hydrochloride was from TCI Europe (Zwijndrecht, Belgium). Racemic medetomidine hydrochloride was from Carbosynth (Compton, UK). β-CD and methyl-α-CD (degree of substitution (DS) ∼11) were from Wacker Chemie AG (Burghausen, Germany). γ-CD, hydroxyethyl-β-CD (DS ∼4.9), sulfated α-CD sodium salt (DS ∼12), sulfated β-CD sodium salt (S-β-CD, DS ∼12-15) and riboflavin 5′-phosphate sodium salt hydrate were from Sigma-Aldrich (Steinheim, Germany). α-CD, hydroxypropyl-α-CD (DS ∼4.5), carboxymethyl-α-CD sodium salt (DS ∼3.5), methyl-β-CD (M-β-CD, DS ∼12), hydroxypropyl-β-CD (DS ∼4.5), carboxymethyl-β-CD sodium salt (DS ∼3.5), succinyl-β-CD (DS ∼3.5), heptakis(2,3,6-tri-O-methyl)-β-CD (TM-β-CD), heptakis(2,6-di-O-methyl)-β-CD (DM-β-CD, 95% isomeric purity), heptakis(6-O-sulfo)-β-CD (HS-β-CD), carboxymethyl-γ-CD sodium salt (DS ∼3.5) and hydroxypropyl-γ-CD (DS ∼4.5) were from Cyclolab Ltd. (Budapest, Hungary), while sulfobutyl-β-CD sodium salt (DS ∼6.6) was from CyDex Pharmaceuticals (San Diego, CA, USA). Methyl-γ-CD (DS ∼13-16) and sulfated γ-CD sodium salt (DS ∼13-16) were from Cyclodextrin-Shop (Tilburg, The Netherlands). Orthophosphoric acid (85%) and sodium hydroxide were from VWR (Darmstadt, Germany). Water was purified by a GenPure system

from Thermo Fischer (Waltham, MA, USA). All chemicals were obtained at the highest purity commercially available. Deuterium oxide (D$_2$O, 99% atom D) and deuterated phosphoric acid (D$_3$PO$_4$, 85% w/w in D$_2$O, 98 atom D) were from Sigma-Aldrich (Saint-Louis, MO, USA). Sodium deuteroxide (NaOD, 40% w/w in D$_2$O, 99.5% atom D) was from Deutero GmbH (Kastellaun, Germany).

2.2. CE experiments

CE measurements were performed on a Beckman P/ACE MDQ capillary electrophoresis system (Beckman Coulter, Krefeld, Germany) equipped with a UV–vis diode array detector and controlled by 32 the KARAT software (version 8.0) for system control, data acquisition and processing. Hydrodynamic sample injection was performed at a pressure of 0.7 psi (4.8 kPa) for 5 s. Separations were carried out in 40/50.2 cm, 50 μm I.D. fused-silica capillaries (BGB Analytik, Schloßböckelheim, Germany) at 20 °C. A new capillary was successively rinsed at a pressure of 20 psi (138 kPa) with 1 M sodium hydroxide for 10 min, followed by water for 15 min. At the beginning of each day the capillary was flushed with 0.1 M orthophosphoric acid for 10 min followed by water for 10 min. Between analyses, the capillary was flushed with 0.1 M orthophosphoric acid for 1 min, water for 2 min, and the background electrolyte for 2 min. Background electrolytes for CD screening and determination of the complexation constants in the case of γ-CD, S-β-CD and HS-β-CD consisted of 50 mM sodium phosphate buffer, pH 2.5 obtained by addition of the appropriate amount of orthophosphoric acid to water and adjustment of the pH using 0.1 M sodium hydroxide solution. In the case of β-CD as selector, urea was added for solubilization of the CD. Thus, screening was performed in 50 mM sodium phosphate buffer containing 2 M urea, while complexation parameters were determined in 150 mM sodium phosphate buffer, pH 2.0, containing 2 M urea. Both buffers were also prepared from orthophosphoric acid and 0.1 M sodium hydroxide solution. The following concentrations of the CDs for the determination of the complexation parameters: β-CD (0, 10, 20, 30, 40 mM), γ-CD (0, 10, 20, 30, 40, 50 mM), S-β-CD (0, 8, 16, 20, 24, 28, 32 mM) and HS-β-CD (0, 15, 20, 25, 30, 40, 50 mM).

CEval [32] was used for the calculation of the complexation constants and complex mobilities. Viscosity measurements of buffers was performed in quadruplicate according to Allmendinger et al. [33] using the CE instrument as viscosimeter and 0.1% (m/v) riboflavin-5′-phosphate as boundary-marker.

2.3. NMR experiments

A Varian INNOVA 500 NMR system (Varian, Palo Alto, CA, USA), fitted with an inverse 5 mm HCX ^{1}H/^{13}C/^{15}N/^{31}P probe head, gradient module and variable temperature unit was used for all NMR experiments. The spectrometer resonance frequency for ^{1}H was 499.61 MHz. The ^{1}H 90° hard pulse width was optimized for each sample. The ^{1}H spectral width was set to 8012.8 Hz. All NMR signals were assigned based on COSY, TOCSY and HSQC data, where appropriate. The signal of residual HDO (4.65 ppm) was used as internal standard. For the 1D ROESY experiments, all excitation windows were selected manually depending on the comparative isolation of the spin system to study, with which the duration and potency of the soft (selective) excitation pulses were automatically adjusted with the VnmrJ software (version 3.2 revision A, Agilent Technologies, Santa Clara, CA, USA). The number of transients in each 1D ROESY experiment was set to 512. The duration of the low power pulse for mixing was 400 ms in every case. All NMR experiments were run at 25 °C. All NMR spectra were processed with the Mestre NOVA software (version 12.0.0, Mestrelab Research S. L., Santiago de Compostela, Spain).

CD	n	R₂	R₃	R₆
α-CD	6	H	H	H
M-α-CD	6	CH₃	CH₃	CH₃
HP-α-CD	6	CH₂-CHOH-CH₃	CH₂-CHOH-CH₃	CH₂-CHOH-CH₃
CM-α-CD	6	CH₂-COOH	CH₂-COOH	CH₂-COOH
S-α-CD	6	SO₃Na	SO₃Na	SO₃Na
β-CD	7	H	H	H
M-β-CD	7	CH₃	CH₃	CH₃
DM-β-CD	7	CH₃	H	CH₃
TM-β-CD	7	CH₃	CH₃	CH₃
HE-β-CD	7	CH₂-CH₂-OH	CH₂-CH₂-OH	CH₂-CH₂-OH
HP-β-CD	7	CH₂-CHOH-CH₃	CH₂-CHOH-CH₃	CH₂-CHOH-CH₃
CM-β-CD	7	CH₂-COOH	CH₂-COOH	CH₂-COOH
SBE-β-CD	7	(CH₂)₄-SO₃Na	(CH₂)₄-SO₃Na	(CH₂)₄-SO₃Na
Suc-β-CD	7	CO-CH₂-CH₂-COOH	CO-CH₂-CH₂-COOH	CO-CH₂-CH₂-COOH
S-β-CD	7	SO₃Na	SO₃Na	SO₃Na
HS-β-CD	7	H	H	SO₃Na
γ-CD	8	H	H	H
M-γ-CD	8	CH₃	CH₃	CH₃
HP-γ-CD	8	CH₂-CHOH-CH₃	CH₂-CHOH-CH₃	CH₂-CHOH-CH₃
CM-γ-CD	8	CH₂-COOH	CH₂-COOH	CH₂-COOH
S-γ-CD	8	SO₃Na	SO₃Na	SO₃Na

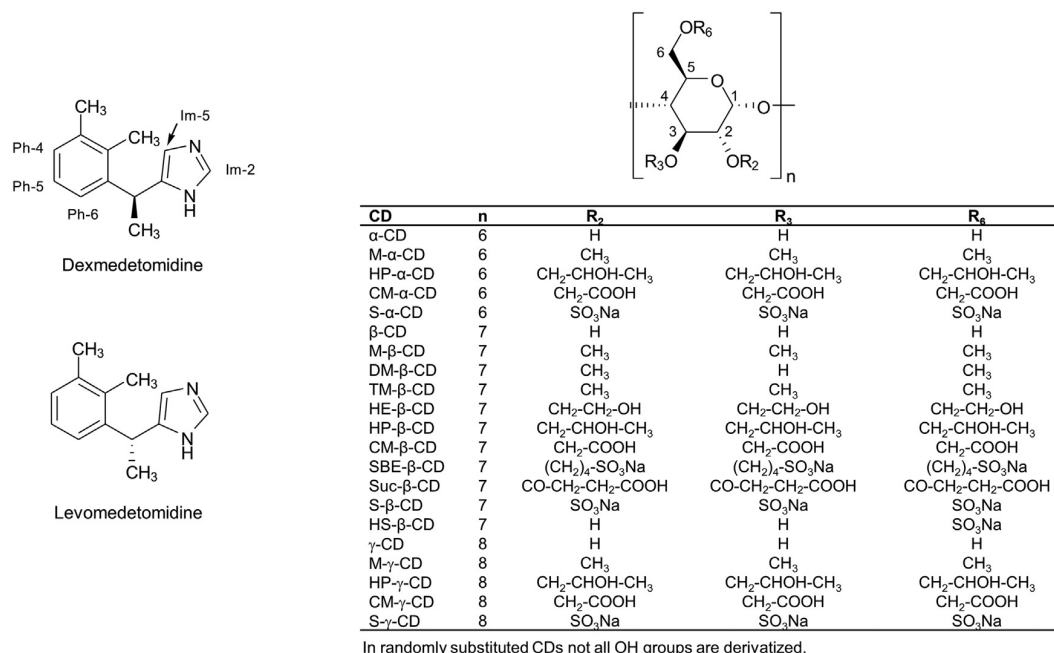In randomly substituted CDs not all OH groups are derivatized.

Fig. 1. Structure of medetomidine enantiomers and CDs.

The concentration of the analytes in the NMR samples was about 30-fold higher than that in the CE experiments so that reproducible NMR spectra were obtained. Samples were prepared by weighing amounts of medetomidine spiked with dexmedetomidine with β-CD, γ-CD or HS-β-CD and dissolving in 0.7 mL 50 mM D_3PO_4 in D_2O, adjusted to an apparent pH 2.5 with sodium deuteroxide in D_2O (40% w/v). In the case of β-CD the samples also contained 2 mM urea. All samples were vortexed for 1 min and filtered through 0.45 μm polypropylene filters prior to data acquisition.

2.4. Molecular modeling and MD simulations

The 3D structures of β-CD, γ-CD and dexmedetomidine were retrieved from Cambridge Structural Database (CSD) [34] entries AGAZOX [35], KOHBUE [36] and UQODEL [37], respectively. HS-β-CD was built using CSD entry MEZWIZ (heptakis(6-O-triisopropylsilyl)-β-CD) [38] as a template and replacing the triisopropylsilyloxy groups with sulfate substituents in all glucopyranose units with the aid of the builder module implemented in the molecular graphics program PyMOL [39]. Geometry optimization of all molecules and point charge derivation were achieved by means of the AM1-BCC method [40], as implemented in the *sqm* program [41] contained in the AMBER Tools [42] distribution. The standard parm10 and ff14SB force field parameter sets in AMBER 14 [43] were used for all atoms. PyMOL was also employed for visualization of MD trajectories and 3D figure generation.

The three pairs of complexes between the two medetomidine enantiomers (*S* and *R*) and the three CDs were modelled upon manually docking each analyte into the CD cavity in orientations that qualitatively agreed with the 1D ROESY NMR results. Each complex was then immersed in a box of TIP3P water molecules that extended 12 Å away from any solute atom. In order to achieve electroneutrality in the simulated systems, the positive charge of medetomidine in the complexes with β-CD and γ-CD was neutralized by substituting one chloride ion for a water molecule located close to the most positive electrostatic potential region. The excess of negative charges in the inclusion complexes with the sulfated CDs was neutralized by addition of sodium counterions in the respective

electrostatically favored regions. Upon reorientation of all solute hydrogens and water molecules, each complex was relaxed by performing 500 steps of steepest-descent followed by 5000 steps of conjugate-gradient energy minimization. The resulting geometry-optimized coordinates were used as input for unrestrained MD simulations at 300 K and a constant pressure of 1 atm running the AMBER *pmemd.cuda* [44] code in parallel on 4 GeForce Nvidia GTX980 graphics processing units (GPUs). The application of SHAKE to all bonds allowed an integration time step of 2 fs to be used. A cut-off distance of 9 Å was used for the nonbonded interactions and the list of nonbonded pairs was updated every 25 steps. Periodic boundary conditions were applied and electrostatic interactions were represented using the smooth particle mesh Ewald method [45] with a grid spacing of 1 Å. The coupling constants for the temperature and pressure baths were 1.0 and 0.2 ps, respectively. The water molecules and the counterion were first equilibrated around the positionally restrained solute for an initial heating period lasting 120 ps. Thereafter each inclusion complex was allowed to evolve freely for a 100-ns period during which coordinates collected every ns were subjected to a simulated annealing procedure [46] that consisted in cooling down the system from 300 to 273 K over a 1-ns period. The geometry of each "frozen" snapshot was further regularized by carrying out an energy minimization until the root-mean-square of the Cartesian elements of the gradient was less than 0.01 kcal mol^1 Å^1. The resulting set of 100 representative structures for each complex was analyzed with the *cpptraj* module in AMBER [47] to measure relevant distances and angles. Solvent-corrected binding energies, as well as their decomposition into van der Waals, Coulombic, apolar and desolvation contributions were obtained by use of our in-house MM-ISMSA program [48].

3. Results and discussion

3.1. CD-mediated CE enantioseparation of medetomidine

The structure of the medetomidine enantiomers and the CDs, which were used in the present study, are summarized in Fig. 1. The CDs included CDs differing in the cavity size, i.e., α-CD, β-CD and γ-

Table 1
Enantioseparation of medetomidine using CDs as chiral selectors in 50 mM sodium phosphate buffer, pH 2.5.

CD[a]	α	Migration order[b]	Polarity of voltage	Comments
α-CD	1.000	–	+	no separation
M-α-CD	1.009	L-MDT > D-MDT	+	partial separation
HP-α-CD	1.009	D-MDT > L-MDT	+	partial separation
CM-α-CD	1.033	L-MDT > D-MDT	+	baseline separation
S-α-CD	1.243	L-MDT > D-MDT	+	baseline separation
β-CD	1.009	L-MDT > D-MDT	+	partial separation
M-β-CD	1.009	L-MDT > D-MDT	+	partial separation
DM-β-CD (95 %)	1.000	–	+	no separation
TM-β-CD	1.005	L-MDT > D-MDT	+	partial separation
HE-β-CD	1.008	L-MDT > D-MDT	+	partial separation
HP-β-CD	1.000	–	+	no separation
CM-β-CD	1.061	L-MDT > D-MDT	+	baseline separation
Suc-β-CD	1.000	–	+	no separation
SBE-β-CD	1.000	–	–	no separation
S-β-CD	1.579	L-MDT > D-MDT	–	baseline separation
HS-β-CD	1.031	D-MDT > L-MDT	–	baseline separation
γ-CD	1.022	D-MDT > L-MDT	+	baseline separation
M-γ-CD	1.016	L-MDT > D-MDT	+	partial separation
HP-γ-CD	1.015	D-MDT > L-MDT	+	partial separation
CM-γ-CD	1.028	L-MDT > D-MDT	+	baseline separation
S-γ-CD	1.072	L-MDT > D-MDT	–	baseline separation

[a] M-α-CD, methyl-α-CD; HP-α-CD, hydroxypropyl-α-CD; CM-α-CD, carboxymethyl-α-CD; S-α-CD, sulfated α-CD; M-β-CD, methyl-β-CD; DM-β-CD, *heptakis*(2,6-di-*O*-methyl)-β-CD (95%); TM-β-CD, *heptakis*(2,3,6-tri-*O*-methyl)-β-CD; HE-β-CD, hydroxyethyl-β-CD; HP-β-CD, hydroxypropyl-β-CD; CM-β-CD, carboxymethyl-β-CD; Suc-β-CD, succinyl-β-CD; SBE-β-CD, sulfobutylether-β-CD; S-β-CD, sulfated β-CD; HS-β-CD, *heptakis*(6-*O*-sulfo)-β-CD; M-γ-CD, methyl-γ-CD; HP-γ-CD, hydroxypropyl-γ-CD; CM-γ-CD; carboxymethyl-γ-CD; S-γ-CD, sulfated γ-CD. The CD concentration was 20 mM except for S-α-CD, where it was 5 mM. The concentration of the randomly substituted CDs was calculated using their average molecular weight.
[b] Migration order as observed at the cathodic end of the capillary.
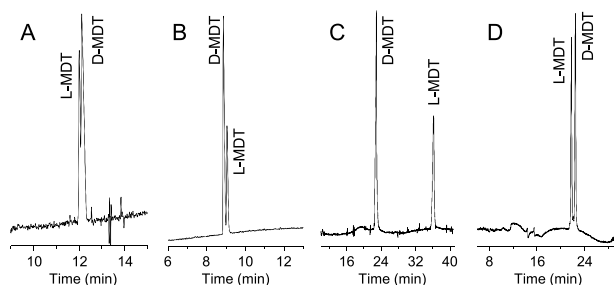

Fig. 2. Electropherograms of the separation of the medetomidine enantiomers using (A) β-CD, (B) γ-CD, (C) S-β-CD and (D) HS-β-CD. Experimental conditions: 40/50.2 cm, 50 µm I.D. fused silica capillary; 50 mM sodium phosphate buffer, pH 2.5; 20 °C; detection at 200 nm. Other conditions: (A) 20 mM β-CD, 2 M urea, 20 kV; (B) 20 mM γ-CD, 20 kV; (C) 20 mM S-β-CD, –20 kV; (D) 20 mM HS-β-CD, –20 kV. The sample consisted of 100 µg/mL dexmedetomidine and 50 µg/mL medetomidine. D-MDT, dexmedetomidine; L-MDT, levomedetomidine.

CD as well as different uncharged and charged substituents. Except for the native CDs, HS-β-CD and TM-β-CD, all other CDs were randomly substituted so that they consisted of a number of compounds differing in the substitution pattern. The results of the separation of the enantiomers of medetomidine in 50 mM phosphate buffer, pH 2.5, are summarized in Table 1. In the presence of most CDs at least a partial separation could be observed using concentrations of 20 mM. For those CDs where no separation was observed under standard conditions, CD concentrations were decreased to 5 mM as well as increased to 50 or 80 mM. However, none of these conditions resulted in enantioresolutions, except for sulfated α-CD, where enantioseparation was only observed at a concentration of 5 mM. The enantiomer migration order shown in Table 1 as determined at the cathodic end of the capillary depended on the type of CD. Interestingly, opposite migration order was observed in the presence of β-CD and γ-CD (Fig. 2A and B), indicating an effect of the size of the cavity on analyte complexation. This applied only to the native CDs, while in the case of all substituted CDs, whether uncharged or charged, the enantiomer migration order is independent of the cavity size. Opposite enantiomer migration order

using the native CDs, i.e. as a function of the cavity size, has been observed for a number of analytes including dipeptides, ketoprofen, or aminogluthetimide, as summarized in [49].

In the case of sulfated β-CDs, the enantiomer migration order also depended on the substitution pattern. Thus, the levo-enantiomer migrated before dexmedetomidine in the presence of the single isomer HS-β-CD, while opposite enantiomer migration order was observed with randomly substituted S-β-CD (Fig. 2C and D). It should be noted that the migration order in Table 1 is listed for detection at the cathode so that it is opposite to the migration order shown in the figures, which were obtained under reversed polarity of the applied voltage, i.e. with detection at the anodic end of the capillary. The migration behavior can be explained by the fact that S-β-CD is in fact a mixture of CDs with different substitution patterns as stated above resulting in different effective mobilities of the enantiomers as compared to HS-β-CD. Moreover, higher enantioresolution was observed in the presence of the randomly substituted S-β-CD compared to the single isomer HS-β-CD, which is also an often observed phenomenon [50]. Another interesting observation refers to the methylated β-CDs. Randomly substituted M-β-CD as well as the trisubstituted TM-β-CD partially resolved the medetomidine enantiomers under the experimental conditions applied for the screening, while in the presence of the 2,6-disubstituted DM-β-CD no enantioseparation was observed. Thus, it may be speculated that the enantioseparation observed in the case of randomly substituted M-β-CD is accomplished by CDs with a substitution pattern differing from the 2,6-disubstitution.

3.2. Determination of apparent complexation constants and complex mobilities

In order to understand the opposite migration behavior of the enantiomers in the presence of β-CD and γ-CD as well as S-β-CD and HS-β-CD, the apparent complexation constants and the mobilities of the diastereomeric CD-solute complexes were determined. The data were obtained as best fit parameters of the effective mobility as a function of CD concentration assuming the formation of 1:1 complexes between the selectors and the solutes according to Eq. (1) [51]:

Table 2

Apparent complexation constants, K, and mobilities of the free analytes, μ_f, and of the CD-analyte complexes, μ_c. The numbers in brackets represent the confidence interval ($\alpha/2 = 0.025$).

	β-CD[1]		γ-CD[2]		S-β-CD[2]		HS-β-CD[2]	
	D-MDT	L-MDT	D-MDT	L-MDT	D-MDT	L-MDT	D-MDT	L-MDT
μ_f ($10^{-9} \cdot m^2 \cdot s^{-1} \cdot V^{-1}$)	19.54		23.70		25.03		25.35	
	(19.34, 19.74)		(23.33, 24.07)		(24.77, 25.29)		(25.13, 25.58)	
μ_c ($10^{-9} \cdot m^2 \cdot s^{-1} \cdot V^{-1}$)	6.57	6.70	7.89	8.28	−15.20	−12.77	−16.92	−16.55
	(4.98, 7.80)	(5.04, 7.99)	(4.6, 10.14)	(5.56, 10.23)	(−15.67, −14.74)	(−13.24, −12.30)	(−17.51, −16.34)	(−17.13, −15.98)
K (M^{-1})	48.2	46.9	42.3	48.5	557	533	204	221
	(38.3, 59.8)	(36.9, 58.7)	(29.5, 58.3)	(34.9, 65.6)	(504, 620)	(480, 596)	(188, 221)	(204, 241)

[1] 150 mM sodium phosphate buffer, pH 2.0, containing 2 M urea.
[2] 50 mM sodium phosphate buffer, pH 2.5.

$$\mu_{eff} = \frac{\mu_f + \mu_c \bullet K \bullet [CD]}{1 + K \bullet [CD]} \qquad (1)$$

where μ_{eff} is the effective mobility, μ_c the mobility of the CD-analyte complex, μ_f the mobility of the free analyte, K the complexation constant and [CD] the molar concentration of the CDs. The observed mobilities were corrected for the increasing viscosity in the buffers due to the increasing CD concentrations. The EOF was assumed to be negligible at pH 2.5 and was not considered because it could not be observed within 60 min. β-CD was investigated in the concentration range of 0–40 mM, while γ-CD and HS-β-CD were studied in the range of 0–50 mM and S-β-CD in the range of 0–32 mM. In the case of the randomly substituted S-β-CD, the average molecular weight corresponding to a DS of 13.5 sulfate groups was used for the calculations. Due to the relatively poor enantioseparation in the case of β-CD in 50 mM sodium phosphate buffer, pH 2.5, the concentration of the phosphate buffer was increased to 150 mM and the pH lowered to pH 2.0 in order to obtain sharp peak allowing the determination of the mobilities of the enantiomers. The data are summarized in Table 2. These are apparent constants and mobilities rather than thermodynamic data because the ionic strength of the buffers was not determined and molar concentrations were used instead of activities. In the case of randomly substituted S-β-CD, the data are not only apparent but also averaged over all CD isomers.

In the case of β-CD and γ-CD, the opposite enantiomer migration order can be explained by opposite affinities of the analyte enantiomers toward the respective CDs. Dexmedetomidine bound stronger to β-CD compared to the levo-enantiomer, while the opposite was found for γ-CD (Table 2). As expected, the stronger bound enantiomer migrates second. The small difference between the complexation constants of the enantiomers with β-CD could explain the lower resolution observed for this CD versus γ-CD. Interestingly, in both cases, the mobility of the levomedetomidine-CD complex exceeds the mobility of the diastereomeric complex containing dexmedetomidine (Table 2). This counteracts the enantioseparation by γ-CD but no significant deterioration of the resolution was observed with increasing CD concentrations. This can be attributed to the relatively small and insignificant differences between the complex mobilities and the somewhat larger difference between the complexation constants of γ-CD so that the increasing mobility of the complex with increasing CD concentrations does not significantly affect the overall enantioseparation. Thus, in the case of β-CD as well as γ-CD the enantioseparation is governed by the complexation constants. Recent studies of the reversal of the enantiomer migration order based on opposite affinities of CDs toward the analyte enantiomers include clen-

penterol [27], phenylalanine derivatives [52] or ketoprofen [53]. Further examples have been summarized in [49].

Opposite recognition of the medetomidine enantiomers was also found for S-β-CD and HS-β-CD. Dexmedetomidine is complexed stronger than its enantiomer by S-β-CD, while levomedetomidine is complexed stronger than dexmedetomidine by HS-β-CD (Table 2). The limiting mobility of the stronger dexmedetomidine–S-β-CD complex also significantly exceeded the mobility of the complex between the CD and levomedetomidine resulting in the large resolution between the enantiomers (Fig. 2C). However, higher complex mobility was observed for the weaker bound dexmedetomidine in the case of HS-β-CD (Table 2), which results in the deterioration of the enantioseparation at higher HS-β-CD concentrations. Thus, in contrast to β-CD and γ-CD, the separation of the medetomidine enantiomers with the negatively charged S-β-CD and HS-β-CD is governed by both, the complexation constants and the complex mobilities. For S-β-CD, both enantioselective principles in CE cooperate leading to a large enantioresolution while they counteract each other in the case of HS-β-CD resulting in a loss of enantioseparation at higher CD concentrations. A detailed discussion of the effect of complex mobility on the enantiomer migration order in CE including several examples can be found in [49,54].

3.3. NMR studies

The ^1H NMR resonances of the medetomidine-CD complexes as well as the chemical shifts of β-CD, γ-CD and HS-β-CD are summarized in Table 3. The signals were assigned based on COSY, TOCSY and HSQC data, where appropriate. S-β-CD and the respective complex were not studied because unequivocal signal assignment of a randomly substituted CD is not possible. Because these CDs are a mixture of many isomers differing in the substitution pattern as well as the position of the substituents, overlap of signals occurs so that meaningful conclusions from irradiation experiments cannot be drawn. 1D ROESY experiments were preferred over 2D ROESY because of easier interpretation of intramolecular nuclear Overhauser effects (NOEs). Moreover, enantiomeric bias, i.e. the stronger NOE response of one enantiomer over the other enantiomer, can be derived directly from the comparison of the 1D ROESY spectrum with the ^1H NMR spectrum. Racemic drug was used for ROESY experiments, while non-racemic mixtures (racemic medetomidine spiked with dexmedetomidine) were applied in a second experiment in order to assign the signals of the respective enantiomer in case of signal splitting.

Table 3

^{1}H NMR chemical shifts of medetomidine-CD complexes. In case of signal splitting upon complexation, the resonance of dexmedetomidine is indicated by (+), while the shift of the levomedetomidine protons are characterized by (−). For assignment of the medetomidine protons see also Fig. 1.

Position	Medetomidine		
	β-CD complex	γ-CD complex	HS-β-CD complex
aliphatic CH	4.48	4.46	4.49
aliphatic CH$_3$	1.55 (−)	1.48	1.51 (−)
	1.55 (+)		1.51 (+)
Im H-2	8.48	8.47 (+)	8.47 (+)
		8.49 (−)	8.48 (−)
Im H-5	7.02 (+)	7.13 (+)	7.14 (+)
	7.04 (−)	7.14 (−)	7.15 (−)
Ph H-4	7.07	6.87 (−)	7.03
		6.90 (+)	
Ph H-5	7.08s	6.94 (−)	7.04
		6.96 (+)	
Ph H-6	6.96 (−)	6.75 (−)	6.84 (−)
	6.99 (+)	6.78 (+)	6.87 (+)
Ph 2-Me	2.17	2.11	2.15 (+)
			2.16 (−)
Ph 3-Me	2.17	2.05 (−)	2.18
		2.08 (+)	
	β-CD	**γ-CD**	**HS-β-CD**
H-1	4.92	4.96	4.96
H-2	3.52	3.54	3.52
H-3	3.71	3.72	3.78
H-4	3.43	3.45	3.57
H-5	3.65	3.61	3.82
H-6	3.74	3.70	4.10
			4.15

3.3.1. β-CD complex

The ^{1}H NMR spectrum of the mixture of racemic medetomidine spiked with dexmedetomidine and β-CD is shown in Fig. 3A for β-CD and Fig. 3B for medetomidine. All signals appeared sharp and well resolved, although some overlapping was found, in particular for the aromatic protons of medetomidine (6.94–7.14 ppm) and some β-CD hydrogens (H-3, H-5 and both H-6, between 3.60 and 3.80 ppm). In some cases, splitting of signals was observed for some medetomidine resonances upon complexation with β-CD (Table 3). However, the splitting was too small to attempt selective irradiation experiments for each enantiomer.

The 1D ROESY experiments showed intermolecular NOE interactions between almost all medetomidine hydrogens with the internal H-3 and H-5 protons of β-CD (Fig. 3A). Selective irradiation at Ph H-4,5 (7.09 ppm) and at 2,3-Me (2.17 ppm) resulted in NOEs with H-3 and H-5 of β-CD (3.71 and 3.65 ppm, respectively). A weak effect was also observed for H-6 (3.74 ppm). In contrast, excitation of Ph H-6 of medetomidine (6.98 ppm) and the aliphatic CH and CH$_3$ protons (4.48 and 1.55 ppm, respectively) resulted primarily in a NOE with H-3 of β-CD. In our hands, no intermolecular NOEs were observed upon irradiation of the imidazole hydrogens. These results indicated that the phenyl ring of medetomidine is inserted into the β-CD cavity through the larger, secondary rim, while the (protonated) imidazole moiety remained outside the cavity and is exposed to the solvent.

Irradiation at the hydrogens of β-CD corroborated these findings, even though some signal overlapping occurred (Fig. 3B). Irradiation at 3.73 ppm (H-3 and H-6 of β-CD) gave NOEs with all medetomidine hydrogens, including those of the imidazole moiety. A schematic representation of the tentative medetomidine–β-CD complex is shown in Fig. 4A.

It is noteworthy, that a slight enantiomeric bias was observed in the NOEs with the aromatic Ph H-6 and Im H-5, as dexmedetomidine seemed to give a slightly larger NOE response than the R-(−)-enantiomer when compared to the parent ^{1}H NMR spectrum (Fig. S1, supplementary material). This is consistent with the CE

experiments, where a stronger complexation of dexmedetomidine by β-CD compared to the levo-enantiomer was found (Table 2).

3.3.2. γ-CD Complex

The ^{1}H NMR spectrum of a sample containing racemic medetomidine spiked with dexmedetomidine in the presence of γ-CD is shown in Fig. 5A for γ-CD and in Fig. 5B for medetomidine. All signals looked sharp, well resolved and easily identifiable, although resonances of H-3 and H-6 of γ-CD were close (3.71 ppm). All signals of medetomidine split upon complexation, with the exception of aliphatic CH and CH$_3$ protons (1.48 and 4.46 ppm, respectively; Table 3). The NOE interaction pattern was quite similar to that observed for the medetomidine–β-CD complex, as all the observed intermolecular NOEs involved the internal hydrogen atoms of γ-CD (Fig. 5A). Selective irradiation at medetomidine imidazole H-5 (7.14 ppm) seemed to give a NOE exclusively with γ-CD H-3 (3.73 ppm), while excitation at medetomidine phenyl and aliphatic protons resulted in NOEs with both, H-3 and H-5 of γ-CD. This would again suggest the formation of an insertion complex, in which the phenyl ring of the drug is accommodated inside the γ-CD cavity and the imidazolium moiety was situated closer to the larger CD rim and exposed to the solvent. Additional ROESY experiments, in which the γ-CD protons were selectively irradiated, were consistent with this conclusion (Fig. 5B). A tentative schematic complex structure is shown in Fig. 4B.

Enantiomeric bias was also found. Thus, irradiation at γ-CD H5 (3.61 ppm) resulted in a stronger NOE response for the phenyl proton H-6 of levomedetomidine (Fig. S2, supplementary material) indicating that this enantiomer is complexed stronger by γ-CD as compared to dexmedetomidine. This is opposite to the observation made in the case of β-CD, yet consistent with the CE data as a larger complexation constant was derived between γ-CD and levomedetomidine compared to dexmedetomidine (Table 2). Due to the very high plate numbers, CE allows to observe very tiny differences in the recognition pattern while even quite powerful spectroscopic techniques do not allow to find a structural rationale for such differences.

3.3.3. HS-β-CD complex

The ^{1}H NMR spectrum of the mixture of a sample containing racemic medetomidine spiked with dexmedetomidine and HS-β-CD is shown in Fig. 6A for HS-β-CD and in Fig. 6B for medetomidine. Like in the previous cases, all signals appeared sharp and were well resolved, although some overlapping occurred (medetomidine Ph H-4 and Ph H-5 at 7.04 ppm). Most of the medetomidine signals split upon complexation (Table 3).

Irradiation at medetomidine Im H-5 (7.15 ppm) resulted in a NOE with HS-β-CD H-3 (3.78 ppm). Irradiation at the aliphatic CH (4.49 ppm) of medetomidine also resulted in a NOE with HS-β-CD H-3. However, when the aliphatic methyl group (1.51 ppm) was selectively excited only comparatively small NOE responses with HS-β-CD H-5 (3.82 ppm) and H-6 (4.10 and 4.15 ppm) were found. Irradiation at medetomidine phenyl H-4 and H-5 resulted in NOEs with HS-β-CD H-3 and H-5, perhaps more intensely with H-5. Irradiation at phenyl H-6 (6.86 ppm) gave a NOE with HS-β-CD H-3 and H-5 and, to a minor extent, with both H-6 protons of HS-β-CD. Irradiation at the aromatic methyl groups of medetomidine (2.17 ppm) showed a NOE with HS-β-CD H-5 and H-3 as well as a small effect with both H-6 atoms (Fig. 6A).

Selective irradiation at HS-β-CD H-5 resulted in NOE interactions with the aliphatic and phenyl protons as well as a small effect with the imidazole H-5, but not with imidazole H-2. Selective irradiation at HS-β-CD H-3 gave essentially an identical interaction pattern. Yet, irradiation at the HS-β-CD H-6 protons (centred at 4.13 ppm) was particularly relevant (Fig. 6B) because NOE interactions with all medetomidine hydrogens except the aliphatic CH
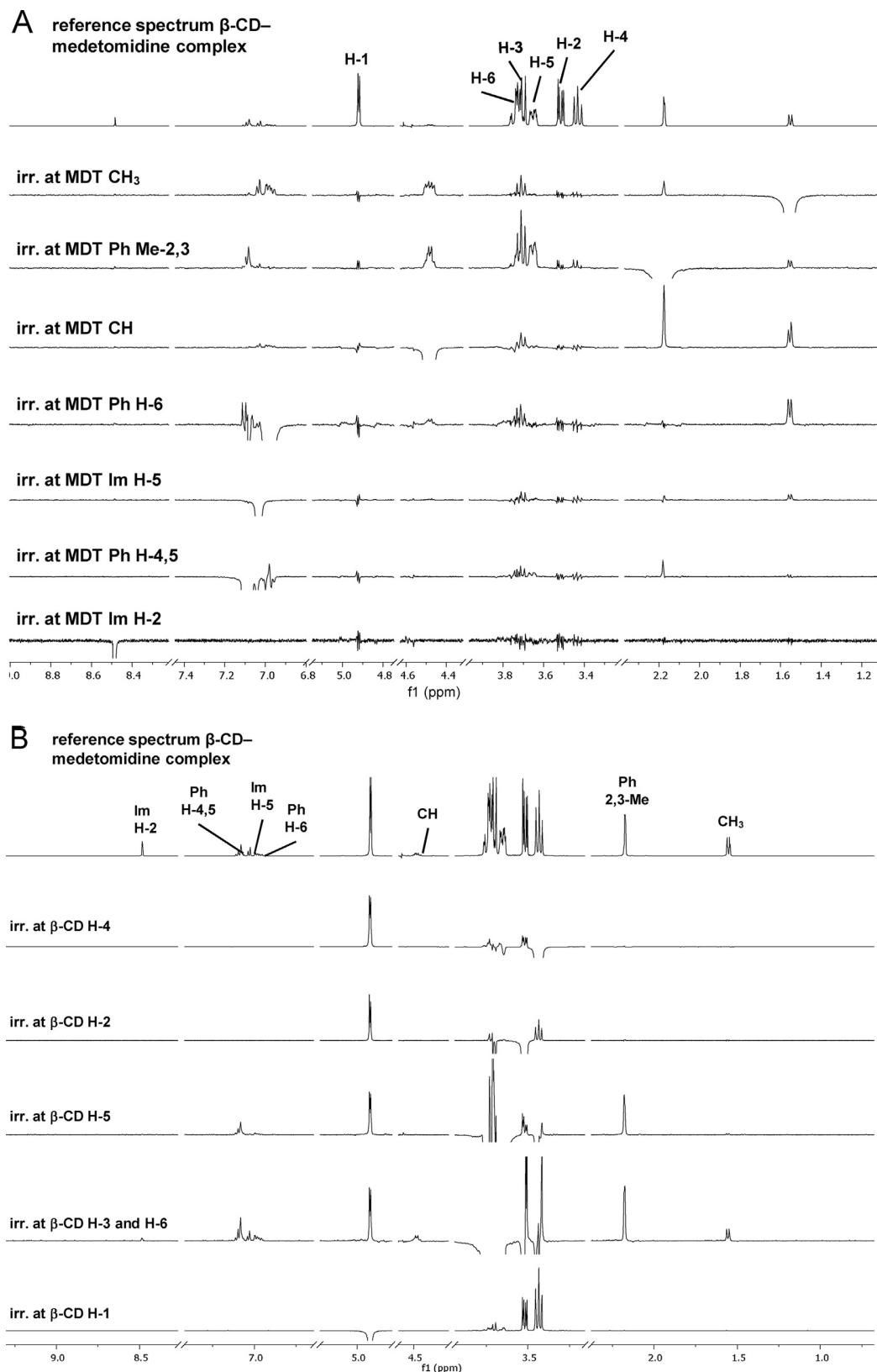
Fig. 3. ^{1}H NMR reference spectra and 1D ROESY spectra of the complex between β-CD and medetomidine upon irradiation of medetomidine protons (A) and upon irradiation of β-CD protons (B). The sample contained 3.8 mg racemic medetomidine spiked with dexmedetomidine and 25 mg β-CD in 0.7 mL 50 mM D_3PO_4 in D_2O, adjusted to an apparent pH 2.5 with sodium deuteroxide in D_2O.
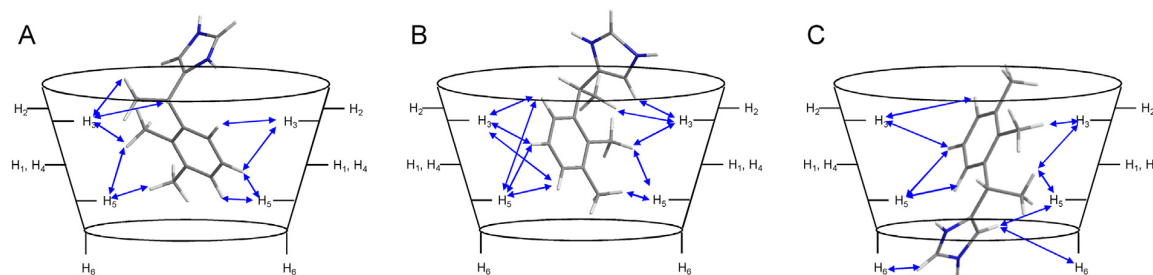
Fig. 4. Schematic representation of the structures of the medetomidine-CD complexes derived from the NMR ROESY data. (A) complex with β-CD, (B) complex with γ-CD and (C) complex with HS-β-CD.

were found. This implies proximity of medetomidine to the primary rim of HS-β-CD. Interestingly, albeit those NOEs were not very strong, NOE responses of the imidazole protons were slightly larger than those of the phenyl hydrogens of medetomidine. This supports a structure of the HS-β-CD complex different from the structures of the respective β-CD and γ-CD complexes. With HS-β-CD, the protonated imidazolium moiety seems to be positioned "upside down" in the cavity close to the primary ring interacting probably through water-mediated hydrogen bonds with the negatively charged sulfate groups. The phenyl ring would therefore find itself inside the CD cavity as shown schematically in Fig. 4C.

Irradiation at the HS-β-CD H-6 protons also evidenced an enantiomeric bias as a larger response was noted for the protons of levomedetomidine (Fig. S3, supplementary material). This suggests a tighter complexation of the levo-enantiomer with HS-β-CD compared to dexmedetomidine, which is consistent with the complexation data derived by CE (Table 2).

3.4. Molecular modeling and MD simulations

As in the NMR spectroscopy study, randomly substituted S-β-CD was not included because of the fact that the CD is a mixture of positional and substitution isomers. Molecular modeling would only be possible for the individual CD isomers but this would not allow to deduce meaningful data of the overall complexation process between S-β-CD and medetomidine.

The structures of the CD complexes between the respective CDs and the medetomidine enantiomers as derived by molecular modeling are summarized in Fig. 7. In both β-CD inclusion complexes (Fig. 7A), each medetomidine enantiomer is bound with the imidazolium moiety pointing towards the rim formed by the 2- and 3-hydroxyl groups and essentially exposed to the solvent so that long-lived direct hydrogen bonds were not observed. On the contrary, the xylene group is buried in the hydrophobic environment provided by C5 and C6 glucopyranose atoms thus explaining the intermolecular NOEs arising from the proximity of phenyl H-5 and H-6 protons of the drug with the H-5 and H6 protons of the glucopyranose units of β-CD. Essentially the same orientation is observed in the γ-CD-medetomidine complexes (Fig. 7B). The hydrophobic xylene group is found within the cavity, whose bottom is defined by the C5 and C6 atoms of the glucopyranose subunits. As a consequence, the shortest inter-proton distances are also observed between the H-5 and H-6 protons of several glucose units in γ-CD and the phenyl H-5 and H-6 hydrogens of medetomidine, which is in good agreement with the reported NOEs. The imidazolium ring rotates freely compared to the phenyl ring and its protonated nitrogens engage in hydrogen bonding interactions with surrounding water molecules as well as with 2- and 3-hydroxyl groups of the CD. The Im-5 proton faces H-3 and H-5 of γ-CD in good agreement with the observed NOEs.

In contrast, in the HS-β-CD complexes the imidazolium appears to be buried inside the cavity and surrounded by the sulfate groups attached to the O6 atom of each glucose unit (Fig. 7C). This favorable electrostatic interaction is quite strong but direct hydrogen bonds are permanently in competition with similar interactions with solvent water molecules. In this orientation, Ph-5 and Ph-6 protons of medetomidine face protons on H-3 and H-5 of the CD, hence the observed NOEs.

The total binding energies of the CD complexes with the medetomidine enantiomers derived from 100 representative structures in the MD simulations are shown as a box-and-whisker plot in Fig. 8. Despite the expected heterogeneities in the respective populations, the proposed binding modes were conclusive and led to stable MD trajectories for all the inclusion complexes studied. As reported earlier for several clenpenterol CD complexes [26], some of the intermolecular hydrogen bonds were mediated by bridging water molecules. Compared to the CE data (Table 2), opposite binding strengths between the CDs and the medetomidine enantiomers were also suggested by MD simulations (Fig. 8). In accordance with CE, dexmedetomidine formed a stronger complex with β-CD, while preferred binding of levomedetomidine by γ-CD could also be derived from the respective binding energies.

In the case of the HS-β-CD complexes, similar distribution of the binding energies of 100 simulations were found for both medetomidine enantiomers (Fig. 8). This may reflect incomplete sampling for these highly charged complexes and/or entrapment into some local minima. We also noted that repulsion between the sulfate groups largely prevents direct simultaneous binding of any two sulfates to the charged imidazolium group of the drug enantiomers. It may be speculated that an incomplete sulfate substitution pattern may actually give rise to enhanced binding energies. In addition, distinct water-mediated hydrogen-bonding patterns (data not shown) may underlie the observed migration differences in the electric field.

4. Conclusions

The present study investigated the complexation of the enantiomers of medetomidine by various CDs. Specifically, the opposite migration order observed in the presence of β-CD and γ-CD as well as for S-β-CD and HS-β-CD was studied in detail by CE, NMR spectroscopy and molecular modeling. S-β-CD was not included in NMR and molecular modeling because this randomly substituted CD is a mixture of positional and substitution isomers so that meaningful data could not be obtained by these techniques. CE and NMR data were in good agreement. Thus, dexmedetomidine was bound stronger by β-CD than levomedetomidine, which was also reflected in an enantioselective NOE of the resonance of the imidazole H-5 and H-6 of the phenyl moiety of the drug in ROESY experiments. In contrast, levomedetomidine was complexed stronger by γ-CD and HS-β-CD and a stronger NOE was observed for the phenyl H-6 in
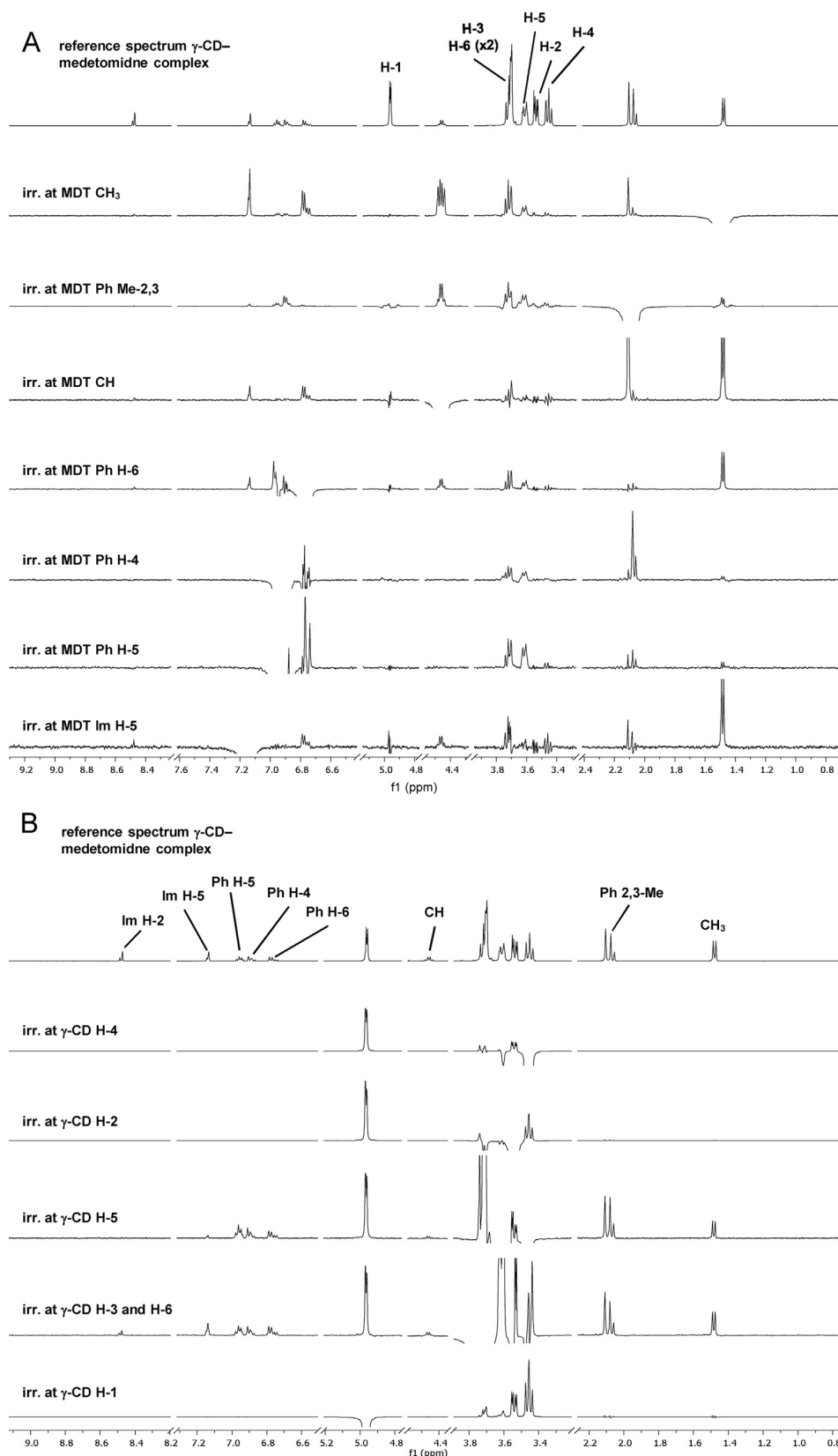
Fig. 5. ^{1}H NMR reference spectra and 1D ROESY spectra of the complex between γ-CD and medetomidine upon irradiation of medetomidine protons (A) and upon irradiation of γ-CD protons (B). The sample contained 4.2 mg racemic medetomidine spiked with dexmedetomidine and 23.3 mg γ-CD in 0.7 mL 50 mM D_3PO_4 in D_2O, adjusted to an apparent pH 2.5 with sodium deuteroxide in D_2O.
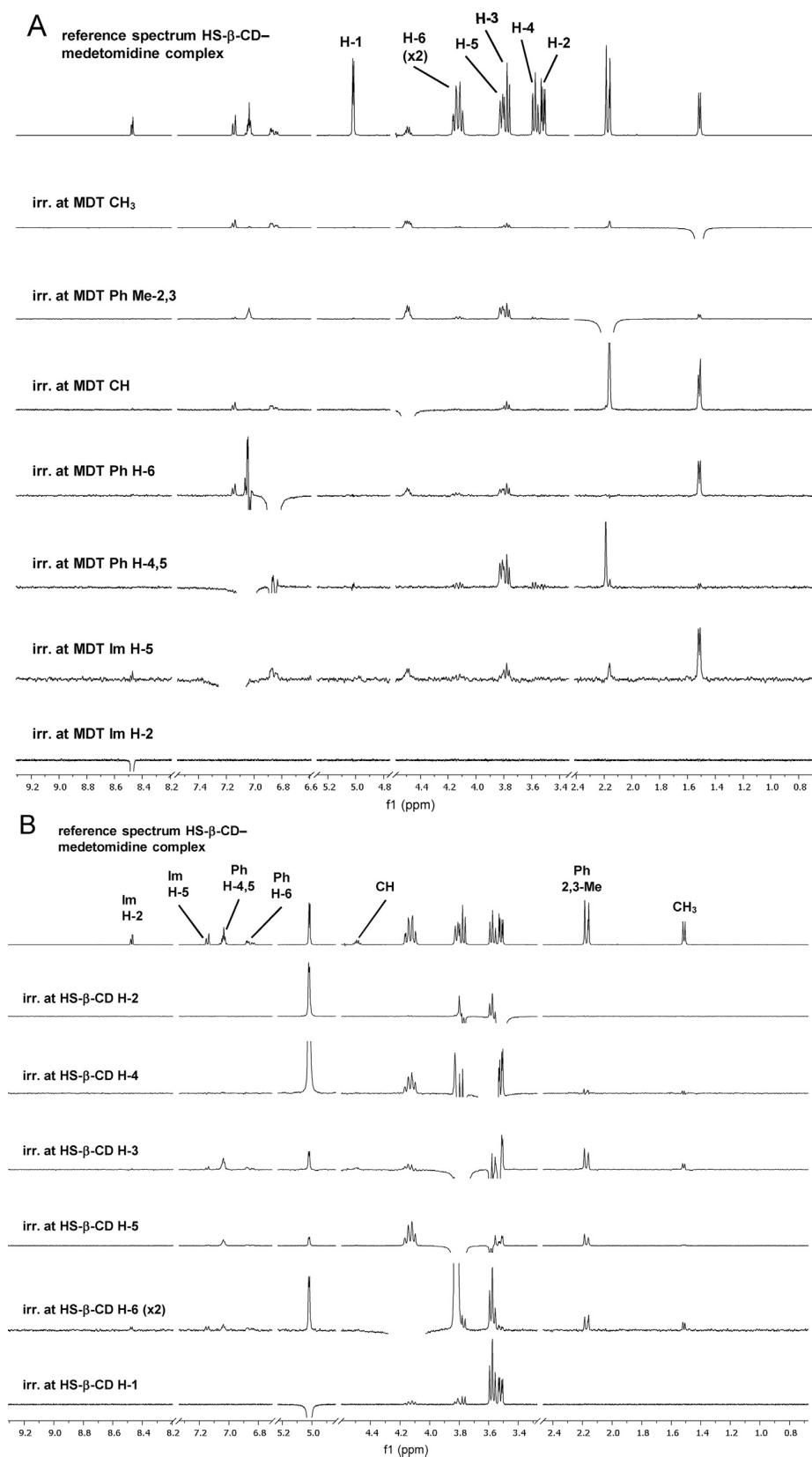
Fig. 6. ^{1}H NMR reference spectra and 1D ROESY spectra of the complex between HS-β-CD and medetomidine upon irradiation of medetomidine protons (A) and upon irradiation of HS-β-CD protons (B). The sample contained 3.6 mg racemic medetomidine spiked with dexmedetomidine and 22.1 mg HS-β-CD in 0.7 mL 50 mM D_3PO_4 in D_2O, adjusted to an apparent pH 2.5 with sodium deuteroxide in D_2O.
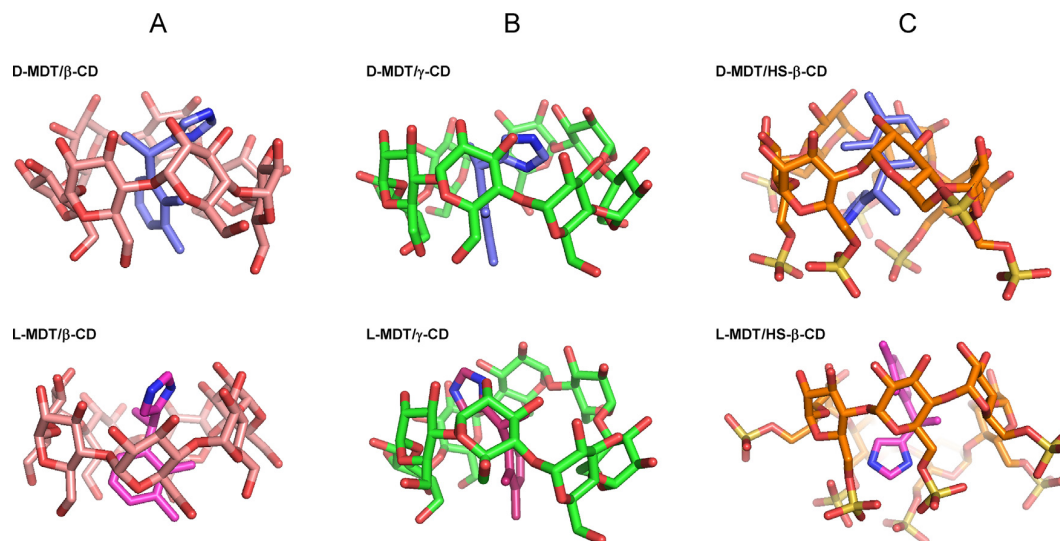
Fig. 7. Molecular modeling structures of the medetomidine enantiomers with (A) β-CD, (B) γ-CD and (C) HS-β-CD. The complexes with dexmedetomidine (D-MDT) are presented in the top layer, while the complexes with levomedetomidine (L-MDT) are shown in the bottom layer.
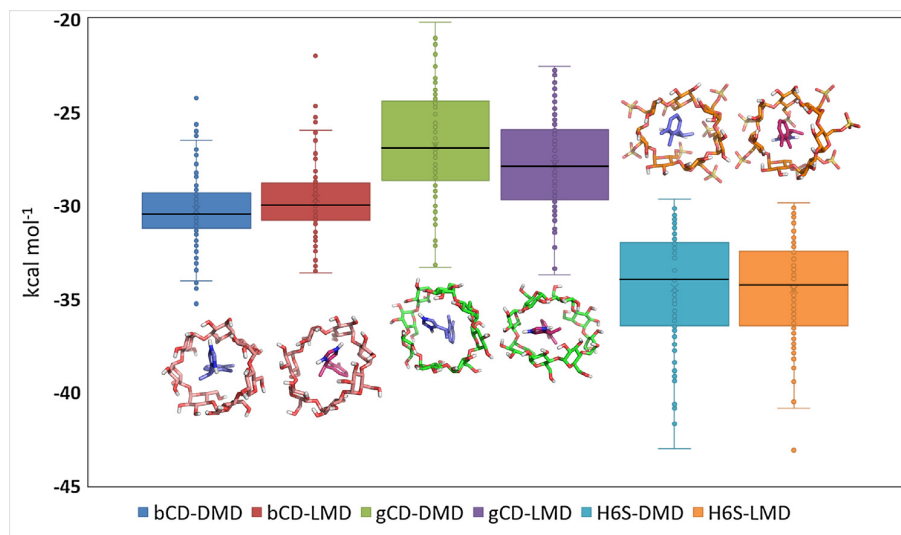
Fig. 8. Box-and-whisker plot of the complexes between the CDs and the medetomidine enantiomers displaying the distribution of the binding energies into quartiles. The line inside each box represent the mean for the 100 calculated values whereas the vertical whiskers indicate the variability outside the upper and lower quartiles. Points outside those whiskers were considered outliers. DMD, dexmedetomidine, LMD, levomedetomidine.

the presence of both CDs as well as the imidazole protons when complexed with HS-β-CD.

Molecular modeling supported the structures derived from NMR experiments. In the case of β-CD and γ-CD, the phenyl moiety of medetomidine entered the cavity from the wider secondary rim of the CDs, while the protonated imidazole ring was exposed to the bulk solvent. In the complex with HS-β-CD, the protonated imidazolium moiety appears to be positioned inside the CD cavity interacting with the sulfate groups in position 6 of the glucose molecules. Compared to CE and NMR data, enantioselective recognition of the medetomidine enantiomers by the CDs was also suggested by MD simulations and reflected the observed reversal of the enantiomer migration order in the case of β-CD and γ-CD.

Acknowledgements

Conflict of Interest

The authors have declared no conflict of interest.

Appendix A. Supplementary data

Supplementary material related to this article can be found, in the online version, at doi:https://doi.org/10.1016/j.chroma.2018.06.010.

References

[1] E. Bilensoy, Cyclodextrins in pharmaceutics, cosmetics and biomedicine, in: Current and Future Industrial Applications, Wiley, Hoboken, 2011.

[2] H. Dodziuk, Cyclodextrins and Their Complexes: Chemistry, Analytical Methods, Applications, Wiley, Weinheim, 2006.

[3] G. Crini, Review: a history of cyclodextrins, Chem. Rev. 114 (2014) 10940–10975, http://dx.doi.org/10.1021/cr500081p.

[4] V. Schurig, Use of derivatized cyclodextrins as chiral selectors for the separation of enantiomers by gas chromatography, Ann. Pharm. Franc. 68 (2010) 82–98, http://dx.doi.org/10.1016/j.pharma.2009.11.004.

[5] Y. Xiao, S.-C. Ng, T.T. Tan, Y. Wang, Recent development of cyclodextrin chiral stationary phases and their applications in chromatography, J. Chromatogr. A 1269 (2012) 52–68, http://dx.doi.org/10.1016/j.chroma.2012.08.049.

[6] P. Rezanka, K. Navratilova, M. Rezanka, V. Kral, D. Sykora, Application of cyclodextrins in chiral capillary electrophoresis, Electrophoresis 35 (2014) 2701–2721, http://dx.doi.org/10.1002/elps.201400145.

[7] L. Escuder-Gilabert, Y. Martin-Biosca, M.J. Medina-Hernandez, S. Sagrado, Cyclodextrins in capillary electrophoresis: recent developments and new trends, J. Chromatogr. A 1357 (2014) 2–23, http://dx.doi.org/10.1016/j.chroma.2014.05.074.

[8] J.M. Saz, M.L. Marina, Recent advances on the use of cyclodextrins in the chiral analysis of drugs by capillary electrophoresis, J. Chromatogr. A 2016 (1467) 79–94, http://dx.doi.org/10.1016/j.chroma.2016.08.029.

[9] Q. Zhu, G.K.E. Scriba, Advances in the use of cyclodextrins as chiral selectors in capillary electrokinetic chromatography: fundamentals and applications, Chromatographia 79 (2016) 1403–1435, http://dx.doi.org/10.1007/s10337-016-3167-0.

[10] G.K.E. Scriba, Chiral recognition in separation sciences - an update, J. Chromatogr. A 1467 (2016) 56–78, http://dx.doi.org/10.1016/j.chroma.2016.05.061.

[11] G.K.E. Scriba, Chiral recognition mechanisms in analytical separation sciences, Chromatographia 75 (2012) 815–838, http://dx.doi.org/10.1007/s10337-012-2261-1.

[12] M. Lämmerhofer, Chiral recognition by enantioselective liquid chromatography: mechanisms and modern chiral stationary phases, J. Chromatogr. A 1217 (2010) 814–856, http://dx.doi.org/10.1016/j.chroma.2009.10.022.

[13] B. Chankvetadze, N. Burjanadze, D.M. Maynard, K. Bergander, D. Bergenthal, G. Blaschke, Comparative enantioseparations with native β-cyclodextrin and heptakis-(2-O-methyl-3,6-di-O-sulfo)-β-cyclodextrin in capillary electrophoresis, Electrophoresis 23 (2002) 3027–3034, http://dx.doi.org/10.1002/1522-2683(200209)23:17<3027::AID-ELPS3027>3.0.CO;2-V.

[14] L. Chankvetadze, A.-C. Servais, M. Fillet, A. Salgado, J. Crommen, B. Chankvetadze, Comparative enantioseparation of talinolol in aqueous and non-aqueous capillary electrophoresis and study of related selector-selectand interactions by nuclear magnetic resonance spectroscopy, J. Chromatogr. A 1267 (2012) 206–216, http://dx.doi.org/10.1016/j.chroma.2012.08.063.

[15] A. Gogolashvili, E. Tatunashvili, L. Chankvetadze, T. Sohajda, J. Szemann, A. Salgado, B. Chankvetadze, Separation of enilconazole enantiomers in capillary electrophoresis with cyclodextrin-type chiral selectors and investigation of structure of selector-selectand complexes by using nuclear magnetic resonance spectroscopy, Electrophoresis 38 (2017) 1851–1859, http://dx.doi.org/10.1002/elps.201700078.

[16] B. Chankvetadze, Separation selectivity in chiral capillary electrophoresis with charged selectors, J. Chromatogr. A 792 (1997) 269–295, http://dx.doi.org/10.1016/S0021-9673(97)00752-8.

[17] B. Chankvetadze, W. Lindner, G.K.E. Scriba, Enantiomer separations in capillary electrophoresis in the case of equal binding constants of the enantiomers with a chiral selector: commentary on the feasibility of the concept, Anal. Chem. 76 (2004) 4256–4260, http://dx.doi.org/10.1021/ac0355202.

[18] M. Hammitzsch-Wiedemann, G.K.E. Scriba, Mathematical approach by a selectivity model for rationalization of pH- and selector concentration-dependent reversal of the enantiomer migration order in capillary electrophoresis, Anal. Chem. 81 (2009) 8765–8773, http://dx.doi.org/10.1021/ac901160p.

[19] B. Chankvetadze, Combined approach using capillary electrophoresis and NMR spectroscopy for an understanding of enantioselective recognition mechanisms by cyclodextrins, Chem. Soc. Rev. 33 (2004) 337–347, http://dx.doi.org/10.1039/B111412N.

[20] H. Dodziuk, W. Kozinsky, A. Ejchart, NMR studies of chiral recognition by cyclodextrins, Chirality 16 (2004) 90–105, http://dx.doi.org/10.1002/chir.10304.

[21] P. Mura, Analytical techniques for characterization of cyclodextrin complexes in aqueous solution: a review, J. Pharm. Biomed. Anal. 101 (2014) 238–250, http://dx.doi.org/10.1016/j.jpba.2014.02.022.

[22] A. Salgado, B. Chankvetadze, Applications of nuclear magnetic resonance spectroscopy for the understanding of enantiomer separation mechanisms in capillary electrophoresis, J. Chromatogr. A 1467 (2016) 95–144, http://dx.doi.org/10.1016/j.chroma.2016.08.060.

[23] Q. Zhao, W. Zhang, R. Wang, Y. Wang, D. Ouyang, Research advances in molecular modeling in cyclodextrins, Curr. Pharm. Des. 23 (2017) 522–531, http://dx.doi.org/10.2174/1381612822666161208142617.

[24] A.A. Elbashir, Combined approach using capillary electrophoresis and molecular modeling for an understanding of enantioselective recognition

[25] mechanisms, J. Appl. Sol. Chem. Model. 1 (2012) 121–126, http://dx.doi.org/10.1007/128.2013.439.

[25] E.A. Castro, D.A.J. Barbiric, Molecular modeling and cyclodextrins: a relationship strengthened by complexes, Curr. Org. Chem. 10 (2006) 715–729, http://dx.doi.org/10.2174/138527206776818928.

[26] K.B. Lipkowitz, Atomistic modeling of enantioselective binding, Acc. Chem. Res. 33 (2000) 555–562, http://dx.doi.org/10.1021/ar980115w.

[27] A. Salgado, E. Tatunashvili, A. Gogolashvili, B. Chankvetadze, F. Gago, Structural rationale for the chiral separation and migration order reversal of clenpenterol enantiomers in capillary electrophoresis using two different β-cyclodextrins, Phys. Chem. Chem. Phys. 19 (2017) 27935–27939, http://dx.doi.org/10.1039/c7cp04761d.

[28] L.K. Cullen, Medetomidine sedation in dogs and cats: a review of its pharmacology, antagonism and dose, Br. Vet. J. 152 (1996) 519–535, http://dx.doi.org/10.1016/s0007-1935(96)8005-4.

[29] J.-M. Savola, R. Virtanen, Central α₂-adrenoceptors are highly stereoselective for dexmedetomidine, the dextro enantiomer of medetomidine, Eur. J. Pharmacol. 195 (1991) 193–199, http://dx.doi.org/10.1016/0014-2999(91)90535-X.

[30] N. Bhana, K.L. Goa, K.J. McClellan, Dexmedetomidine, Drugs 59 (2000) 263–268, http://dx.doi.org/10.2165/00003495-200059020-00012.

[31] S. Krait, G.K.E. Scriba, Quality by design-assisted development of a capillary electrophoresis method for the chiral purity determination of dexmedetomidine, Electrophoresis 39 (2018), http://dx.doi.org/10.1002/elps.201800100.

[32] P. Dubský, M. Ördögová, M. Malý, M. Riesová, Ceval: all-in-one software for data processing and statistical evaluations in affinity capillary electrophoresis, J. Chromatogr. A 1445 (2016) 158–165, http://dx.doi.org/10.1016/j.chroma.2016.04.004.

[33] A. Allmendinger, L.-H. Dieu, S. Fischer, R. Mueller, H.-C. Mahler, J. Huwyler, High-throughput viscosity measurement using capillary electrophoresis instrumentation and its application to protein formulation, J. Pharm. Biomed. Anal. 99 (2014) 51–58, http://dx.doi.org/10.1016/j.jpba.2014.07.005.

[34] I.R. Thomas, I.J. Bruno, J.C. Cole, C.F. Macrae, E. Pidcock, P.A. Wood, WebCSD: the online portal to the Cambridge structural database, J. Appl. Crystallogr. 43 (2010) 362–366, http://dx.doi.org/10.1107/S0021889810000452.

[35] J.M. Alexander, J.L. Clark, T.J. Brett, J. Stezowski, Chiral discrimination in cyclodextrin complexes of amino acid derivatives: beta-cyclodextrin/N-acetyl-L-phenylalanine and N-acetyl-D-phenylalanine complexes, Proc. Natl. Acad. Sci. U. S. A. 99 (2002) 5115–5120, http://dx.doi.org/10.1073/pnas.072647599.

[36] J. Ding, T. Steiner, V. Zabel, B.E. Hingerty, S.A. Mason, W. Saenger, Topography of cyclodextrin inclusion complexes. 28. Neutron diffraction study of the hydrogen bonding in partially deuterated g-cyclodextrin.dntdot.15.cntdot.7D2O at T = 110 K, J. Am. Chem. Soc. 113 (1991) 8081–8089, http://dx.doi.org/10.1021/ja00021a039.

[37] P.B. Pansuriva, G.E.M. Maguire, H.B. Friedrich, Physicochemical characterization and decomposition kinetics of (S)-4-[1-(2,3-dimethylphenyl)ethyl]-3H-imidazole HCl/S-enantiomer of medetomidine HCl, J. Therm. Anal. Calorim. 124 (2015) 269–278, http://dx.doi.org/10.1007/s10973-015-5086-y.

[38] T. Kida, T. Iwamoto, H. Asahara, T. Hinoue, M. Akashi, Chiral recognition and kinetic resolution of aromatic amines via supramolecular chiral nanocapsules in nonpolar solvents, J. Am. Chem. Soc. 135 (2013) 3371–3374, http://dx.doi.org/10.1021/ja312367k.

[39] W.L. DeLano, The PyMOL Molecular Graphics System, Schrödinger, LLC, New York, 2013.

[40] A. Jakalian, B.L. Bush, D.B. Jack, C.I. Bayly, Fast, efficient generation of high-quality atomic charges. AM1-BCC model: I. Method, J. Comput. Chem. 21 (2000) 132–146, http://dx.doi.org/10.1002/(SICI)1096-987X(20000130)21:2<132::AID-JCC5>3.0.CO;2-P.

[41] R.C. Walker, M.F. Crowley, D.A. Case, The implementation of a fast and accurate QM/MM potential method in AMBER, J. Comput. Chem. 29 (2008) 1019–1031, http://dx.doi.org/10.1002/jcc.20857.

[42] D.A. Case, T.E. Cheatham 3rd, T. Darden, H. Gohlke, R. Luo, K.M. Merz Jr, A. Onufriev, C. Simmerling, B. Wang, R.J. Woods, The AMBER biomolecular simulation programs, J. Comput. Chem. 26 (2005) 1668–1688, http://dx.doi.org/10.1002/jcc.20290.

[43] J.T.B.D.A. Case, R.M. Betz, D.S. Cerutti, T.E. Cheatham III, T.A. Darden, R.E. Duke, T.J. Giese, H. Gohlke, A.W. Goetz, N. Homeyer, S. Izadi, P. Janowski, J. Kaus, A. Kovalenko, T.S. Lee, S. LeGrand, P. Li, T. Luchko, R. Luo, B. Madej, K.M. Merz, G. Monard, P. Needham, H. Nguyen, H.T. Nguyen, I. Omelyan, A. Onufriev, D.R. Roe, A. Roitberg, R. Salomon-Ferrer, C.L. Simmerling, W. Smith, J. Swails, R.C. Walker, J. Wang, R.M. Wolf, X. Wu, D.M. York, P.A. Kollman, AMBER 2015, University of California, San Francisco, 2015.

[44] R. Salomon-Ferrer, A.W. Götz, D. Poole, S. Le Grand, R.C. Walker, Routine microsecond molecular dynamics simulations with AMBER on GPUs. 2. Explicit solvent particle mesh Ewald, J. Chem. Theory Comput. 9 (2013) 3878–3888, http://dx.doi.org/10.1021/ct400314y.

[45] T. Darden, D. York, L. Pedersen, Particle mesh Ewald: Anan N·log(N) method for Ewald sums in large systems, J. Chem. Phys. 98 (1993) 10089–10092, http://dx.doi.org/10.1063/1.464397.

[46] T.A. Brunger, P.D. Admans, Molecular dynamics applied to X-ray structure refinement, Acc. Chem. Res. 35 (2002) 404–412, http://dx.doi.org/10.1021/ar010034r.

_____

[47] D.R. Roe, T.E. Cheatham 3rd, PTRAJ and CPPTRAJ: software for processing and analysis of molecular dynamics trajectory data, J. Chem. Theory Comput. 9 (2013) 3084–3095, http://dx.doi.org/10.1021/ct400341p.

[48] J. Klett, A. Núnez-Salgado, H.G. Dos Santos, Á. Cortés-Cabrera, A. Perona, R. Gil-Redondo, D. Abia, F. Gago, A. Morreale, MM-ISMSA: an ultrafast and accurate scoring function for protein-protein docking, J. Chem. Theory Comput. 8 (2012) 3395–3408, http://dx.doi.org/10.1021/ct300497z.

[49] B. Chankvetadze, Enantiomer migration order in chiral capillary electrophoresis, Electrophoresis 23 (2002) 4022–4035, http://dx.doi.org/10.1002/elps.200290016.

[50] P. Dubsky, L. Müllerova, M. Dvorak, B. Gas, Generalized model of electromigration with 1:1 (analyte:selector) complexation stoichiometry: part I. Theory, J. Chromatogr. A 1384 (2015) 142–146, http://dx.doi.org/10.1016/j.chroma.2015.01.029.

[51] S.A.C. Wren, Theory of chiral separation in capillary electrophoresis, J. Chromatogr. 636 (1993) 57–62.

[52] A. Aranyi, A. Péter, I. Ilisz, F. Fülöp, G.K.E. Scriba, Cyclodextrin-mediated enantioseparation of phenylalanine amide derivatives and amino alcohols by capillary electrophoresis – role of complexation constants and complex mobilities, Electrophoresis 35 (2014) 2848–2854, http://dx.doi.org/10.1002/elps.201400142.

[53] S. Samakashvili, A. Salgado, G.K.E. Scriba, B. Chankvetadze, Comparative enantioseparation of Ketoprofen with trimethylated α-, β- and γ-cyclodextrins in capillary electrophoresis and study of related selector-selectand interactions using nuclear magnetic resonance spectroscopy, Chirality 25 (2013) 79–88, http://dx.doi.org/10.1002/chir.22111.

[54] G.K.E. Scriba, Fundamental aspects of chiral electromigration techniques and application in pharmaceutical and biomedical analysis, J. Pharm. Biomed. Anal. 55 (2011) 688–701, http://dx.doi.org/10.1016/j.jpba.2010.11.018.

3.5.   Manuscript 5

Unusual Complexation Behavior between Daclatasvir and γ-Cyclodextrin.

A Multiplatform Study

Sulaiman Krait, Antonio Salgado, Claudio Villani, Lukas Naumann, Christian Neusüß, Bezhan Chankvetadze, and Gerhard K. E. Scriba.

Personal Contribution (40 %): study design, capillary electrophoresis (except CE-MS) and HPLC experiments, data analysis and interpretation, writing the manuscript draft (except the NMR, MS and CE-MS parts).

Antonio Salgado (30 %): conducting the NMR experiments, data analysis and interpretation, writing the manuscript draft (NMR part).

Claudio Villani (5 %): calculation of the free energy barriers by computer simulation.

Lukas Naumann (10 %): CE-MS and MS experiments.

Christian Neusüß (5 %): Supervision of CE-MS and MS experiments and writing their relevant part of the manuscript.

Bezhan Chankvetadze (5 %): cooperation in study design, and data interpretation.

Gerhard K. E. Scriba (5 %): study design and concept development, supervision or research, finalizing the manuscript.

Overview:

The manuscript describes a phenomenon hitherto unknown for cyclodextrins as hosts in CE which is the simultaneous formation of complexes with different stoichiometries between γ-cyclodextrin and the antiviral drug daclatasvir. In addition, the complexes displayed unexpected electrophoretic migration behavior as the complex migrated faster than the non-complexed analyte. Finally, the 2:1 complex was extremely stable so that it was detectable using cyclodextrin-free background electrolytes.

Various techniques were applied in the study including capillary electrophoresis, HPLC, NMR spectroscopy and mass spectrometry to understand the phenomenon. Solution structure of daclatasvir and some analogs, structure of the complexes formed between daclatasvir as well as analogs with γ-cyclodextrin were derived.

The complexes of a daclatasvir diastereomer and two related substances were also elucidated.

Unusual Complexation Behavior between Daclatasvir and γ-Cyclodextrin. A Multiplatform Study

Sulaiman Krait [a†], Antonio Salgado [b†], Claudio Villani [c], Lukas Naumann [d], Christian Neusüß [d], Bezhan Chankvetadze [e], and Gerhard K.E. Scriba *[a]

During a screening of cyclodextrins (CDs) as chiral selectors for the separation of daclatasvir (DCV) and its enantiomer by capillary electrophoresis (CE), an unprecedented phenomenon for CDs was observed, that is two peaks with a plateau in between using γ-CD as chiral selector. The same result was encountered when enantiopure DCV was injected or when analyzing a sample containing enantiopure DCV and γ-CD in a CD-free background electrolyte. Peak coalescence was observed at 45 °C and at a pH above 3.5. Two peaks with a plateau were also observed for DCV stereoisomers as well as a structural analog. However, only a single peak was detected if one or both amino acid moieties of DCV were lacking. Nuclear magnetic resonance (NMR) experiments including Nuclear Overhauser effect-based methods showed that in solution DCV adopted a folded conformation in which the isopropyl side chain of the valine residues pointed toward the aromatic rings of DCV. Moreover, NMR unequivocally demonstrated the simultaneous formation of DCV-γ-CD inclusion complexes with 1:1 and 2:1 stoichiometry, which was corroborated by mass spectrometry. In both complexes, DCV also adopted a folded structure. The RSSR-diastereomer of DCV as well as an analog lacking one of the amino acid moieties also formed 1:1 and 2:1 complexes with γ-CD although a plateau was only observed in the case of the RSSR-diastereomer. As shown by CE-MS, both DCV–γ-CD complexes surprisingly comigrated as the first peak, while the second migrating peak represents non-complexed DCV.

Introduction

Daclatasvir (DCV, dimethyl N,N'-([1,1'-biphenyl]-4,4'-diylbis{1H-imidazole-4,2-diyl-[(2S)-pyrrolidine-2,1-diyl][(2S)-3-methyl-1-oxobutane-1,2-diyl]})dicarbamate, Figure 1) is an inhibitor of the hepatitis C nonstructural protein 5A replication complex.[1] The drug is used in combination with sofosbuvir for the treatment of infections with hepatitis C virus genotypes 1 − 4.[2,3] DCV is a biphenyl with two identical halves each containing two stereogenic centers each. The compound possesses S,S,S,S configuration. Due to the four stereogenic centres, there are also other diastereomers including meso forms of the compound beside the *R,R,R,R*-configured enantiomer (RRRR-DCV). Capillary electrophoresis (CE) is considered an effective method for stereoisomer separations, especially enantioseparations,

due to the high-resolution ability as well as the flexibility of the technique.[4-6]

Other advantages include low consumption of chemicals and analytes and the availability of several operation modes. Furthermore, CE can be applied to study the complexation between high- and low-molecular weight compounds.[7-10] In CE, the chiral selector is added to the background electrolyte (BGE). Enantioseparations are based on the formation of transient diastereomeric complexes between the chiral selector and the analyte enantiomers, which differ in their binding thermodynamics.[11,12] Moreover, the diastereomeric complexes may differ in their electrophoretic mobility, so that enantioseparations can be also based on this phenomenon, even in the case of equal complexation constants.[12,13] With regard to chiral selectors, cyclodextrins (CDs) are by far the most often applied selectors for enantioseparations in CE.[14-16] When screening different CDs in sodium phosphate buffer, pH 2.5, as BGE for their ability to separate DCV and its enantiomer it was noted, that some CDs such as methyl-β-CD (M-β-CD) or hydroxypropyl-β-CD yielded an enantioseparation, while in the case of other CDs such as γ-CD or sulphated β-CD two peaks with a plateau be-tween them were observed. This indicates a slow dynamic equilibrium with regard to the CE timescale. Moreover, the same behaviour, i.e. two peaks with a plateau in between, was also encountered when enantiopure DCV was analysed in a γ-CD containing BGE at pH 2.5.

[a.] Department of Medicinal/Pharmaceutical Chemistry, Friedrich Schiller University Jena, Philosophenweg 14, 07743 Jena, Germany. E-mail: gerhard.scriba@uni-jena.de

[b.] NMR Spectroscopy Centre (CERMN), CAI Químicas, Faculty of Pharmacy, University of Alcalá, 28805 Alcalá de Henares, Madrid, Spain.

[c.] Department of Chemistry and Technology of Drugs, Sapienza University of Rome, Piazzale Aldo Moro 5, 00185 Rome, Italy

[d.] Aalen University, Department of Chemistry, Beethovenstrasse 1, 73430 Aalen, Germany

[e.] Tbilisi State University, Institute of Physical and Analytical Chemistry, School of Exact and Natural Sciences, 0179 Tbilisi, Georgia

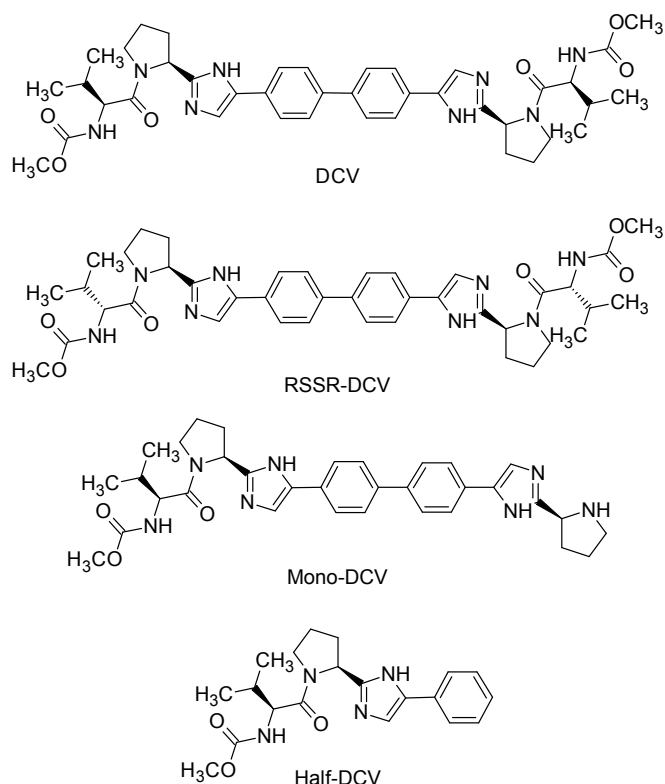† These authors contributed equally to the work.

Figure 1. Structures of DCV, RSSR-DCV, mono-DCV and half-DCV. For the structures of further compounds see Figure S1.

To the best of our knowledge, such a phenomenon has not yet been de-scribed for CDs as chiral selectors. Therefore, the present study was conducted in order to obtain some insight into the complexation between DCV and γ-CD.

Materials and methods

Chemicals

DCV dihydrochloride and mono des(*N*-carboxymethyl)valine DCV (mono-DCV, *N*-[(1*S*)-2-methyl-1-[[(2*S*)-2-[5-[4'-[2-[(2*S*)-2-pyrrolidinyl]-1H-imidazol-5-yl][1,1'-biphenyl]-4-yl]-1H-imidazol-2-yl]-1-pyrrolidinyl]carbonyl]propyl]carbamic acid methyl ester) were a gift from Mylan Laboratories Ltd. (Hyderabad, India), while RRRR-DCV dihydrochloride, the RSSR-diastereomer dihydrochloride (RSSR-DCV), the RSSS-diastereomer dihydrochloride (RSSS-DCV) and the mono isoleucine analog of DCV (Ile-DCV, *N*-[(1*S*,2*S*)-1-[[(2*S*)-2-[5-[4'-[2-[(2*S*)-1-[(2*S*)-2-[(methoxycarbonyl)amino]-3-methyl-1-oxobutyl]-2-pyrrolidinyl]-1*H*-imidazol-5-yl][1,1'-biphenyl]-4-yl]-1*H*-imidazol-2-yl]-1-pyrrolidinyl]carbonyl]-2-methylbutyl]carbamic acid methyl ester) were kindly supplied by Laurus Labs Ltd. (Hyderabad, India). *tert*-Butyl-(2*S*)-2-[5-[4-[4-[2-[(2*S*)-1-[(2-methylpropan-2-yl)oxycarbonyl]pyrrolidin-2-yl]-1*H*-imidazol-5-yl]phenyl]phenyl]-1*H*-imidazol-2-yl]pyrrolidine-1-carboxylate (BOC-bis-pyrrolidinyl-imidazolyl biphenyl, BOC-BPIB) and 4,4'-bis(2-((*S*)-pyrrolidin-2-yl)-1H-imidazol-5-yl)-1,1'-biphenyl tetrahydrochloride (bis-pyrrolidinyl-imidazolyl biphenyl, BPIB) were from abcr GmbH (Karlsruhe, Germany). *N*-[(1*S*)-2-methyl-1-[[(2*S*)-2-(5-phenyl-1*H*-imidazol-2-yl)-1-pyrrolidinyl]carbonyl]propyl]-carbamic acid methyl ester (half-DCV) was synthesized as described in the supporting information.

Capillary electrophoresis

CE experiments were performed on a Beckman P/ACE MDQ capillary electrophoresis system (Beckman Coulter, Krefeld, Germany) equipped with a UV-Vis diode array detector and controlled by the 32 KARAT software (version 8.0) for system control, data acquisition and processing. Polymicro® fused-silica capillaries 40/50.2 cm, 50 μm i.d. were from CM Scientific (Silsden, UK). A new capillary was rinsed at a pressure of 20 psi (138 kPa) with 1 M sodium hydroxide for 20 min, followed by water for 10 min. Before each run, the capillary was flushed with water for 2 min followed by the background electrolyte (BGE) for 2 min. If not stated otherwise, experiments were carried out at 20 °C and an applied voltage of 25 kV. The detection wavelength was 305 nm, except for half-DCV, which was detected at 250 nm. Samples were injected hydrodynamically at a pressure of 0.7 psi (4.8 kPa) for 5 s. The background electrolytes BGEs containing γ-CD were prepared by dilution the appropriate amount of the acid component to approx. 80 % of the final volume. γ-CD was added, and the pH was adjusted with the base component before making up to the final volume. Selector-free electrolyte solutions were prepared accordingly.

Capillary electrophoresis-mass spectrometry

CE-MS experiments were carried out on an Agilent G1600X CE System coupled with an Agilent 6510 QTOF (Agilent, Santa Clara, CA, U.S.A.) using a fused-silica capillary (60 cm effective length, 50 μm i.d.) and a separation voltage 30 kV. Injections were performed for 9 s at a pressure of 5 kPa. A new capillary was rinsed according to the CE-UV experiments. The BGE consisted of 100 mM ammonium formate adjusted to pH 2.6 by addition of 2 % ammonia solution. Experiments in the presence of γ-CD were carried out at a concentration of 50 mM of the CD. The MS instrument settings were the same as for the direct infusion experiment. A tri-axial sheath flow CE-MS sprayer was used for coupling CE with MS. Therefore, a methanol/water/formic acid (50/49/1, v/v) sheath liquid was used for grounding and the separation capillary had a protrusion of 0.05 mm.

NMR spectroscopy

NMR spectra were recorded with a Varian NMR System (Varian Inc, Palo Alto, CA, USA), fitted with a CHX ^{1}H/^{13}C/^{15}N-^{31}P probe head, gradient module and variable temperature unit. The spectrometer resonance frequency for ^{1}H was 499.61 MHz. The 90º hard pulse for proton was optimized for each sample. The signal due to residual HDO (4.65 ppm) was used as internal standard. ^{1}H signals were assigned upon COSY, HSQC and 1D TOCSY results when appropriate. For the 1D TOCSY experiments, the spinlock (mixing) time was set to 80 ms. The structures of supramolecular aggregates and the conformation of DCV in solution, either in the complexed or in the free form, relied upon 1D and 2D ROESY results at various mixing times

_____

(200, 300 and 400 ms). All NMR data were processed with the MestReNova software (v. 14.1.0, Mestrelab Research, S.L., Santiago de Compostela, Spain). Samples were prepared by weighing about 12 to 13 mg γ-CD and/or 2 to 3 mg of the compound and dissolution in 0.6 to 0.8 mL of 50 mM D_3PO_3 in D_2O adjusted to an apparent pH 2.5 or 4.0 by NaOD.

Results and Discussion

Unusual electrophoretic migration, dependence on solute structure and variables

Screening of CDs as chiral selectors for the CE separation of DCV and its enantiomer was carried out in 50 mM sodium phosphate buffer, pH 2.5, containing the CDs at concentrations of 5 mM and 20 mM. The results are summarized in Table S1. Partial enantioseparations were observed using carboxymethyl-α-CD and 2-hydroxypropyl-β-CD, while baseline separations could be found for M-β-CD, carboxymethyl-γ-CD and sulfated γ-CD. Surprisingly, two peaks with a plateau in between were observed in the presence of sulfated β-CD and γ-CD. Figure 2 shows representative electropherograms of the analysis of a non-racemic mixture of DCV and its enantiomer in the presence of M-β-CD (Figure 2A) and γ-CD (Figure 2B) as examples of baseline separations and the plateau phenomenon, respectively. Moreover, two peaks with a plateau in between were also observed when enantiopure DCV or the enantiomer RRRR-DCV were analyzed in the presence of γ-CD (Figure 2C and 2D, respectively). In contrast, a single peak was detected for DCV or RRRR-DCV when M-β-CD was added to the BGE (data not shown). Therefore, the plateau phenomenon indicates an equilibrium, which is slow on the CE time scale and apparently not related to an enantiodifferentiation. Typically, complexation equilibria between analytes and CDs in CE enantioseparations are very fast on the CE timescale so that separate peaks are not detected for the free and complexed analyte. Consequently, further experiments were conducted in order to investigate the slow equilibrium phenomenon.

The plateau was observed in the γ-CD concentration range up to 100 mM and could be detected at CD concentrations as low as 0.1 mM (Figure S2A). In addition, the area of the first migrating peak slightly increased with the γ-CD concentration.
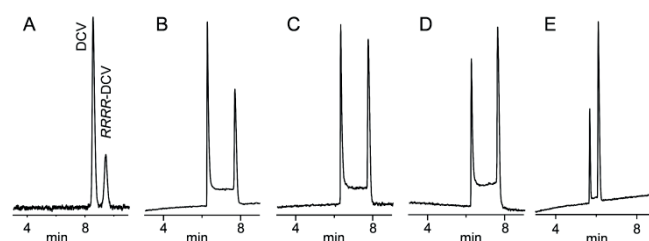

Figure 2. Electropherograms (A) a nonracemic mixture of DCV and RRRR-DCV in the presence of 7 mg/mL M-β-CD in the BGE, (B) a nonracemic mixture of DCV and RRRR-DCV in the presence of 20 mM γ-CD in the BGE, (C) DCV in the presence of 20 mM γ-CD in the BGE, (D) RRRR-DCV in the presence of 20 mM γ-CD in the BGE and (E) sample containing DCV and γ-CD analyzed in a CD-free BGE.

Similar data were observed as a function of the phosphate buffer concentration (20 to 200 mM) (Figure S2B). The effects of the capillary temperature between 15°C and 45 °C (Figure S3A) showed a dynamic behavior indicating in-capillary equilibria with two well separated peaks at slow exchange regimes at lower temperatures and progressive coalescence at higher temperatures. The plateau area between the resolved peaks became more pronounced under fast exchange regimes between 20 and 35 °C, eventually leading to complete coalescence at 45°C. Computer simulation of the exchange-broadened peaks (Figure S4) [17-20] gave the rate constants for the in-capillary process leading from the first to the second migrating species spanning between $0{,}7 \cdot 10^{-3}$ s^{-1} at 15°C and $1.38 \cdot 10^{-3}$ s^{-1} at 40°C. The averaged value of the free energy barriers was calculated as $\Delta G^{\ddagger}$ = 20.97 kcal/mol. This value indicates a significantly slower process than those reported for other CD complexations. Linear regression of the Eyring plot (ln (k/T) vs 1/T) yielded activation enthalpy $\Delta H^{\ddagger}$ = 20.80 kcal/mol and entropy $\Delta S^{\ddagger}$ = -0.6 cal/mol·K, indicating the process is enthalpy controlled, with only a minor entropic contribution. Upon increasing the pH of the BGE from 2.5 to 4.5 peak coalescence around pH 4 was observed (Figure S3B). DCV possesses two basic imidazole nitrogen atoms with pK_a values of 5.6 and 4.9. [21] Thus, protonation of both imidazole nitrogen atoms appears to be a prerequisite for the observation of the slow equilibrium leading to the plateau in the CE experiments.

In addition, two diastereoisomers of DCV, a structural analog containing Ile instead of Val as one of the amino acid moieties, mono-DCV, which lacks one MOC-Val moiety, two synthetic precursors, BPIB (lacking both MOC-Vals side chains) and the BOC-protected derivative BOC-BPIB, as well as the "monomeric" half-DCV were analyzed by CE (Figures 1 and S1). In analogy to DCV, two peaks with a plateau in between were also observed for the R,S,S,R- and R,S,S,S-configured diastereomers as well as Ile-DCV (Figure S5). In contrast, only a single peak was observed for mono-DCV, half-DCV or the pyrrolidine derivatives BPIB and BOC-BPIB (Figure S5). Therefore, a structural prerequisite for the appearance of the plateau seems to be a "symmetrical" structure containing two MOC-amino acid moieties, which may, however, differ to some extent. The stereochemistry at the chiral centers did not play an important role as this behavior was seen with all available stereoisomers of DCV.

In order to exclude the very unlikely enantiomerization of DCV in the presence of γ-CD under the CE conditions, a sample containing DCV and γ-CD (kept at room temperature for 30 min) was analyzed by HPLC on a Lux i-Cellulose-5 column. This system effectively separates the enantiomers of DCV (Figure S6A). Only a single peak at the retention time of DCV was detected for the γ-CD-containing DCV sample (Figure S6B) so that enantiomerization in the presence of γ-CD could be excluded. Surprisingly, when this sample was analyzed by CE using a CD-free phosphate buffer-based BGE, pH 2.5, two peaks with a plateau in between were also observed (Figure 2E). The plateau was independent of parameters for the preparation of the γ-CD-containing DCV sample solution. A temperature study revealed coalescence of the peaks also at about 45 °C. Computer

_____

simulations (Figure S7) yielded rate constants for the conversion of the first into the second migrating species spanning one order of magnitude from $0.57 \cdot 10^{-3}$ s^{-1} at 20°C to $5.7 \cdot 10^{-3}$ s^{-1} at 35°C. The averaged value of the free energy barriers was calculated as $\Delta G^{\ddagger} = 21.33$ kcal/mol, a value that is of the same order of magnitude of that obtained for the γ-CD containing BGE system.

With regard to the observation of a plateau between two peaks in CE, the "complete" DCV structure, i.e. a symmetrical biphenyl-imidazole-pyrrolidine molecule with two MOC-Val side chains seems to be required. The appearance of the plateau is independent of the stereochemistry of DCV as well as minor modifications in the amino acid moiety. Furthermore, the molecule must be fully protonated as peak coalescence was observed at about pH 4. The phenomenon is not generally observed for all CDs because a "true" enantioseparation and, consequently, no plateau could be obtained in the screening experiments (Table S1). The cavity size of the CD does not appear to be a prerequisite, because the plateau was found for γ-CD containing 8 glucopyranose units and sulfated β-CD, which is formed by 7 glucopyranose units, while it was not found in the case of sulfated γ-CD and M-β-CD.

Structure of dynamic supramolecular complexes

The structures of the complexes of γ-CD with DCV, the RSSR diastereomer, mono-DCV as well as half-DCV were further studied in deuterated sodium phosphate buffer by ^{1}H-NMR experiments because nuclear Overhauser effect (NOE) based NMR methods, in particular rotating frame nuclear Overhauser effect spectroscopy (ROESY) techniques, allow the analysis of spatially close nuclei also in CD-based complexes. [22-25] Signals were assigned based on COSY, TOCSY and HSQCED data.

DCV. The ^{1}H-NMR spectrum of DCV recorded in deuterated phosphate buffer is shown in Figure 3 and the resonances are reported in Table S2. Surprisingly, two sets of signals were observed for most resonances. Based on the well resolved signals for the two pyrrolidine H-2 protons, two conformers were identified. The major one showed a triplet at 5.14 ppm (J = 7.6 Hz), while the minor one featured a double doublet at 5.61 ppm (J_1 = 7.6 Hz and J_2 = 1.5 Hz). Assuming an envelope-type conformation of the pyrrolidine ring, the H-2 in the pyrrolidine ring in the major conformer had axial configuration and equatorial configuration in the minor one. The molar ratio of the conformers was 1.0:0.14 as concluded from the respective integrals of the H-2 protons as well as the signals of the methoxy groups at 3.53 and 3.23 ppm. This ratio did not change significantly when heating the probe to 60 °C (data not shown). Moreover, in a 2D ROESY experiment, NOEs between the methyl groups of the valine side chain with the aromatic protons of the phenyl and imidazole rings were observed (Figure S8) indicating that DCV existed in a folded structure in solution where the valine side chains were close to the aromatic rings of the molecule, while the MOC moieties pointed away from it. Such a folded structure has been also reported in modelling studies[26] and when DCV is complexed to the nonstructural protein 5A replication complex. [27] Moreover, a

NOE interaction between the methyl protons of the isopropyl side chain and the pyrrolidine H-2 proton was observed for the minor conformer, so that the methyl groups appear to be located closer to the pyrrolidine ring in the folded structure of this conformer as compared to the major conformer.

DCV and γ-CD. The 1H-NMR spectrum of a sample containing DCV and γ-CD is shown in Figure 3C in comparison to the spectra of γ-CD (Figure 3A) and DCV (Figure 3B). Details of signal assignment are summarized in Table S3. Unlike most reported cases in the literature where usually only a single set of signals for the analyte and another one for the CD are observed, [22-25] three sets of 1H resonances were seen for DCV and two sets of signals for γ-CD. As to the γ-CD resonances, the more intense set if signals coincided with the resonances of pure γ-CD, while the less intense signals were shifted upfield. Considerable shifts were also seen for the signals related to DCV, particularly in the aromatic region (insert Figure 3C). The "minor" set of DCV resonances encountered minor downfield shifts, while the two other sets of "major" signals were shifted upfield com-pared to DCV in the absence of γ-CD. By comparing the integrals of signals, the two "major" DCV sets seemed to be equimolar (same integral values), while the "minor" DCV signals integrated for less, so that a 1.0:1.0:0.24 ratio (mol/mol/mol) was determined at 25°C. The integrals of the aromatic protons of the two "major" DCV species and the integral of the anomeric H-1 signal of the "minor" γ-CD yielded a molar ratio of 1:1:1.

A 2D ROESY experiment (Figure S9) yielded evidence for the presence of two structurally different complexes. All observed intermolecular NOE responses involved the inner hydrogens of γ-CD (H-3 and H-5) and the aromatic pro-tons of DCV. A NOE between the inner protons of the "major" γ-CD and the "minor" DCV species indicated the presence of a 1:1 inclusion complex, which is often reported for CDs. [22-24] However, a second supramolecular structure was identified based on the NOEs between the inner protons of the "minor" γ-CD and the aromatic protons of both "major" DCV species. This indicated the formation of a 2:1 complex (DCV:γ-CD) in which two DCV molecules are inserted into the CD cavity. A 1D ROESY experiment further corroborated this assumption because selective irradiation at the resonance at 7.25 ppm representing the phenyl protons H-2 and H-6 of one of the "major" DCV species resulted in a NOE with the same protons of the other "major" DCV at 7.17 ppm (Figure S10). Likewise, irradiation at the resonance of 7.17 ppm showed a NOE response for the signals at 7.25 ppm (data not shown). Therefore, the aromatic rings of the two DCV molecules in the 2:1 complex appear to be in close vicinity. The complex stoichiometry also explains the upfield shift of the protons of the "minor" γ-CD due to the anisotropic ring current effect generated by the aromatic moieties of the DCV molecules, which are spatially closer in the 2:1 complex than in the 1:1 complex. Further evidence of the two coexisting complexes was provided by a DOSY experiment, because the diffusion coefficient of H-1 of the "minor" species involved in the 2:1 complex was smaller than that of H-1 of its "major" counterpart (representing the 1:1 complex as well as non-complexed γ-CD).
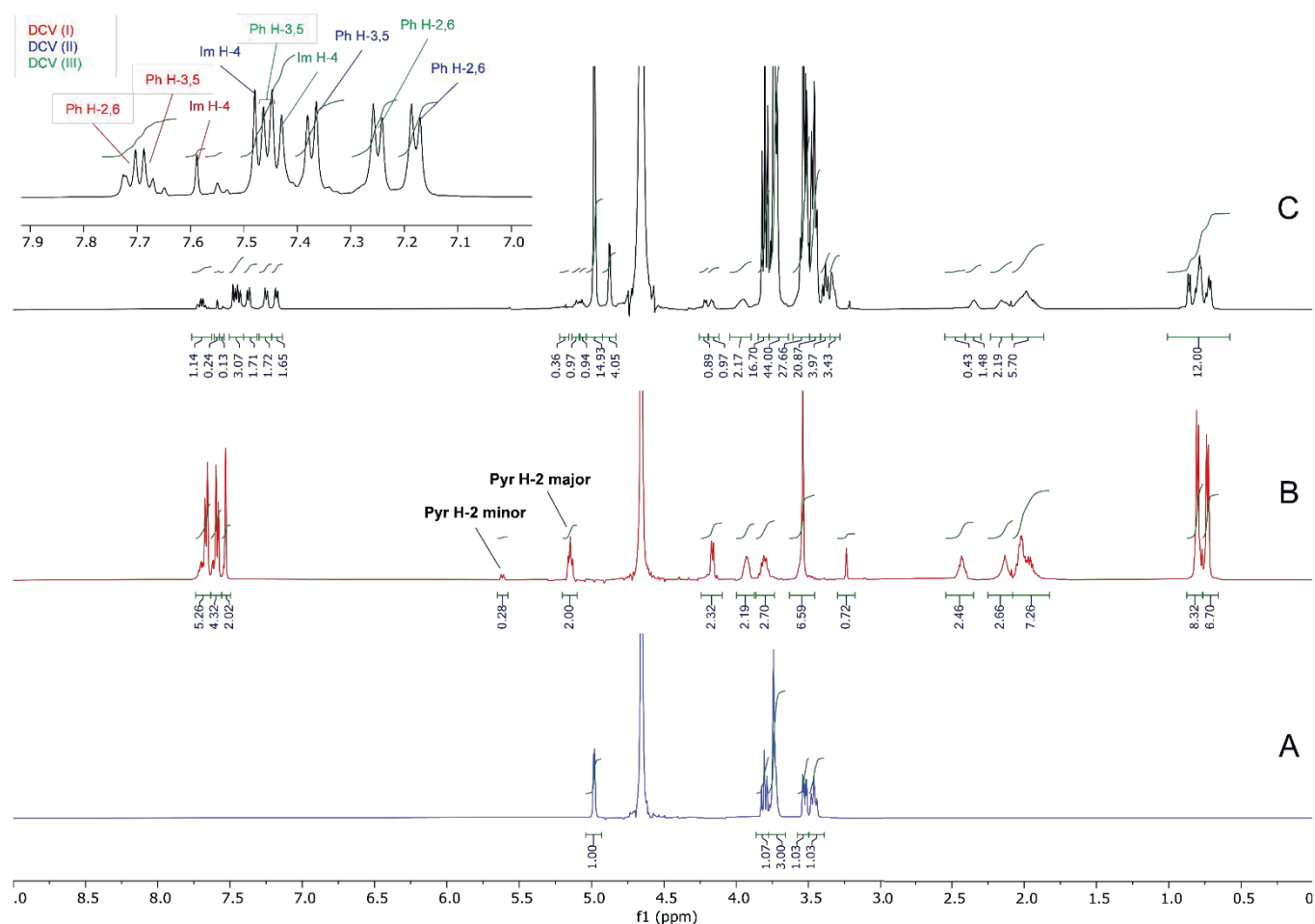
Figure 3. 1H-NMR spectra of (A) γ-CD, (B) DCV and (C) DCV plus γ-CD in 50 mM deuterated phosphate buffer in D₂O, apparent pH 2.5. The insert shows the expanded region of the aromatic protons. For signal assignments see Tables S2 and S3 (supplementary electronic material). Experimental conditions: (A) 3.6 mg DCV·2HCl in 0.7 mL 50 mM D₃PO₄ in D₂O (6.4 mM), pH 2.5, 25 °C; (B) 13.0 mg γ-CD in 0.7 mL 50 mM D₃PO₄ in D₂O (14.3 mM), pH 2.5, 25 °C; (C) 3.0 mg DCV·2HCl and 13.0 mg γ-CD in 0.7 mL 50 mM D₃PO₄ in D₂O (5.3 mM, 14.3 mM), pH 2.5, 25 °C.

Intramolecular NOEs were also observed for the DCV molecules. Cross peaks between the methyl groups of the valine side chains (0.70 - 0.80 ppm) and the aromatic hydrogens (7.35 - 7.50 ppm) indicated that DCV adopts the same folded structure in the complexes as it had been observed for the solution structure in the absence of γ-CD. This applies to both, the 1:1 and the 2:1 complexes. Information on the conformation of the pyrrolidine ring in the complexes from coupling constants of the pyrrolidine H-2 signal could not be derived because of significant signal overlapping. A schematic illustration of the tentative structures of both complexes is shown in (Figure 4). The ratio of the 1:1 versus the 2:1 complex was about 0.24:1.0 based, for example, on the integrals of the imidazole H-5 of the minor DCV at 7.59 ppm and the doublet of the phenyl H-2,6 protons at 7.18 ppm. Measuring the spectra at 40 °C, 60 °C and 80 °C resulted in ratio between the complexes of about 0.39:1.0, 0.9:1.0 and 2.3:1.0, respectively. Thus, the 2:1 complex is more abundant at lower temperatures, while the 1:1 complex is the major species at 80 °C with inversion of the ratio above 60 °C. Therefore, the peak coalescence at about 40 °C observed in the CE experiments is not based on the equilibrium between the complexes.
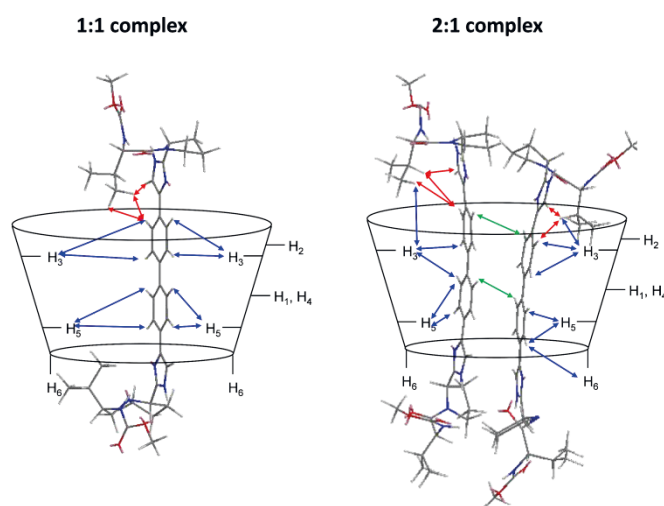
Figure 4. Schematic representation of the 1:1 and 2:1 complexes formed between DCV and γ-CD. The intermolecular NOEs derived from ROESY experiments are indicated by arrows; red: intramolecular NOEs, blue: intermolecular NOEs between DCV and γ-CD, green: intermolecular NOEs between DCV molecules in the 2:1 complex.

Upon cooling the sample to 25 °C, the 1:1 versus 2:1 complex ratio returned to the original value of 0.24:1.0. Because pH-dependent peak coalescence was observed in CE at pH 4.0, NMR experiments were also performed at this apparent pH. The ^{1}H-NMR spectra of DCV in the absence and presence of γ-CD at pH 4.0 (Figure S11) were essentially identical to the spectrum recorded at pH 2.5 (Figure 4). COSY, TOCSY as well as 1D and 2D ROESY data also clearly demonstrated the presence 1:1 and 2:1 complexes at pH 4.0 (data not shown). The molar ratio was about 0.23:1.0, i.e. identical to pH 2.5. Moreover, NOE interactions did not differ significantly to those at pH 2.5 so that identical structures of the complexes can be concluded at both pH values. This clearly indicated that the plateau observed in CE is not due to an equilibrium between the two complexes.

The presence of both complexes in solution was confirmed by direct infusion ESI-TOF-MS of a solution containing DCV and γ-CD in ammonium formate buffer, pH 2.6. Control experiments employed the linear oligosaccharide maltoheptaose as well as α-CD, in order to avoid misinterpretation as supramolecular associates may be formed in the gas phase, which do not exist in solution. [28,29] α-CD did not yield an enantioseparation or a plateau with DCV in the screening experiments.

In the presence of γ-CD, the resulting mass spectrum (Figure S12) shows two intensive signals at m/z 739.4 and m/z 370.2 corresponding to singly and doubly charged DCV. The low-intensity signal at m/z 1017.4 is consistent with the doubly charged 1:1 DCV-γ-CD complex, while the signals at m/z 1387.1 and m/z 925.7 are in accordance with the doubly and triply charged 2:1 complex between DCV and γ-CD. Calculated and observed masses were in good agreement (Table S4). Only the DCV signals at m/z 739.4 and m/z 370.2 could be detected in the presence of α-CD or maltoheptaose (data now shown). Therefore, the signals representing the 1:1 and 2:1 DCV-γ-CD complexes are not artefacts created in the ion source and confirm the NMR results on the concomitant formation of complexes with 1:1 and 2:1 stoichiometry between DCV and γ-CD in solution.

The most commonly reported stoichiometry for CD complexes is 1:1 (solute:CD) [30-32] although higher order aggregates have also been published. The composition 1:2 is the second most abundant.[31] In contrast, stoichiometries of 1:3, 2:1 and 2:2 have been rarely reported. Furthermore, ternary CD complexes including additional background electrolyte components such as SDS in addition to the analytical solute with a ratio of 1:1:1 were described.[33,34] Unless NMR has been employed, the nature of the complexes (inclusion or "external" complex) cannot be concluded. With regard to 2:1 complexes involving CDs, several reports demonstrated their formation. [35-38] In most cases the stoichiometry of the complexes was derived from Job's plots, while the orientation and stacking of both solutes within the CD cavity was derived from molecular modeling. [35-37] There are also reports of 2:1 complexes, in which one solute molecule was included in the CD cavity, while the second one was coordinated externally. [39,40] Neither these studies nor the abovementioned publications on 2:1 aggregates provided evidence for the presence of two complexes with different stoichiometries in solution. To the best of our knowledge only one publication reported the simultaneous presence complexes with different stoichiometry (1:1 and 2:1) between dimetindene and carboxymethyl-β-CD, [41] but the structures could not be unequivocally resolved in that study. In contrast, the presence of the two complexes between DCV and γ-CD including their stoichiometry was unequivocally demonstrated based on NMR and MS data.

In addition, the structures of the complexes of the diastereomeric RSSR-DCV as well as mono-DCV and half-DCV with γ-CD were determined by ^{1}H-NMR spectroscopy. A detailed discussion can be found in the Supporting Information. Table 1 compares the CE behaviour as well as complex stoichiometries, their ratios and structures of the guest molecules of DCV and the three analogues studied in more detail. Although the number of analytes is limited, a biphenyl structure appears to be required for the formation of a 2:1 complex. The stereochemistry of the amino acid moiety does not affect the simultaneous formation of two complexes but might change the ratio between them.

Migration order

In order to confirm the role of interaction between DCV and γ-CD, the CE capillary was used as a microreactor. Individual plugs of DCV and γ-CD were injected in a capillary containing CD-free BGE, pH 2.5, which were separated by a short plug of buffer to prevent contact between the plugs due to diffusion. The results are shown in Figure 5. When DCV was injected as the first plug so that die not migrate through the γ-CD plug only a single peak was detected at the migration time of DCV (Figure 5A), while two peaks with a plateau was found when DCV was injected as the second plug so that it had to migrate through the γ-CD plug on the way to the detector (Figure 5B).

Table 1. CE behavior, stoichiometry and structure of γ-CD complexes with DCV and analogs

Compound	CE	Complex stoichiometry	Complex ratio	Structure of guest molecule(s) in complex(es)
DCV	Plateau	1:1 and 2:1	~ 0.24:1	Folded conformation of MOC-Val residues
RSSR-DCV	Plateau	1:1 and 2:1	~ 1:1	Extended conformation of MOC-Val residues in complexes
Mono-DCV	–	1:1 and 2:1 [a]	~ 0.4:1	Folded conformation of MOC-Val residue in complexes
Half-DCV	–	1:1	–	Folded conformation of MOC-Val residue in complex

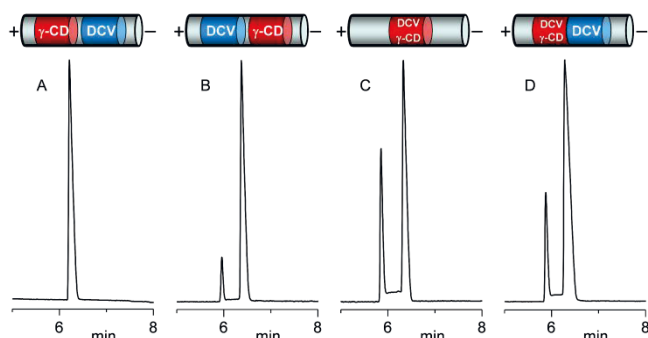[a] no unequivocal proof of a 2:1 complex by NOEs but presence likely

Figure 5. Plug-plug CE experiments. The order of the injected plugs is schematically shown above the electropherograms. Injection sequence: (A) DCV > γ-CD, (B) γ-CD > DCV, (C) DCV + γ-CD, (D) DCV > DCV + γ-CD. The BGE consisted of 50 mM sodium phosphate buffer, pH 2.5. The direction of migration is toward the cathode.

Injecting a mixture of DCV and γ-CD also resulted in two peaks with a plateau (Figure 5C). Moreover, the area of the second migrating peak increased significantly when a DCV-plug was injected before a plug of a mixed DCV plus γ-CD sample (Figure 5D), indicating that the first migrating peak represents the unresolved mixture of the 1:1 and 2:1 DCV-γ-CD complexes, while the second peak is due to free DCV.

This was confirmed by CE-MS experiments (Figure 6). When analyzing pure DCV in a CD-free BGE, only a single peak with m/z 739.4 at the migration time of DCV is observed (Figure 6A). Mass traces corresponding to complexes with γ-CD could not be detected above baseline noise. In contrast, two peaks with the plateau were detected in the analysis of a sample containing DCV and γ-CD using a CD-free BGE (Figure 6B).
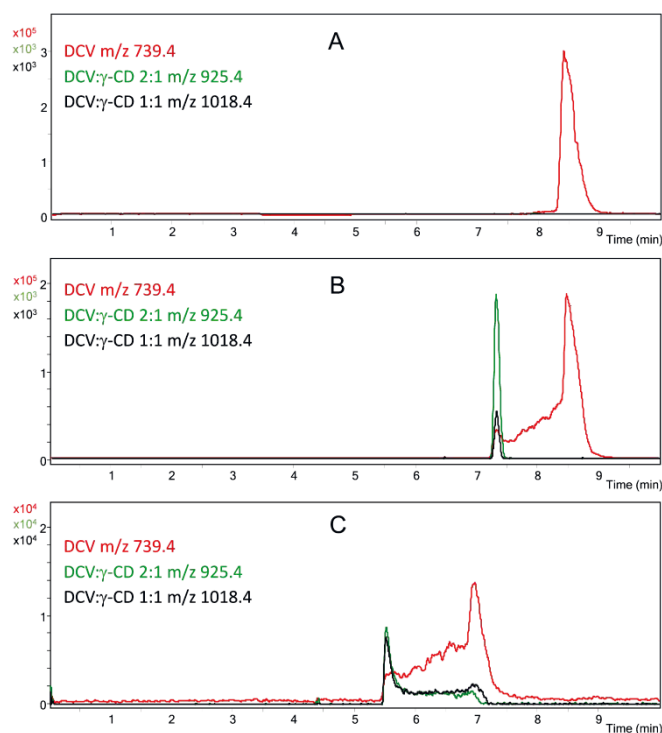

Figure 6. CE-MS experiments of (A) pure DCV and (B) a sample containing DCV and γ-CD using 50 mM ammonium formate buffer pH 2.6 as BGE. (C) CE-MS analysis of DCV using 50 mM ammonium formate buffer pH 2.6, containing 50 mM γ-CD as BGE.

The trace of m/z 739.4 proved that DCV is present in the peaks as well as the plateau, while the mass traces m/z 925.4 and m/z 1018.4 representing the 2:1 and 1:1 complex, respectively, were only detected in the first migrating peak. When γ-CD is present in the BGE (Figure 6C), the mass traces of the 1:1 and 2:1 complexes at m/z 925.4 and m/z 1018.4 as well as free DCV (m/z 739.4) were detected, while in the second migrating peak free DCV dominated. In contrast to the analysis of the DCV plus γ-CD sample analyzed in a CD-free BGE (Figure 6B), the plateau is also formed by the complexes in addition to non-complexed DCV. This difference can be explained by the presence of γ-CD in the BGE. Free DCV resulting from the dissociation of the complexes can be complexed again if the CD is present in the BGE, while this is not possible in the absence of γ-CD in the BGE because in the latter case γ-CD and DCV are electrophoretically separated. The CE-MS data show that both complexes exhibit the same mobility so that they are not separated independent of the presence or absence of γ-CD in the BGE. This is also unexpected considering the theoretical difference in the mass-to-charge ratios of both complexes. Taking into account the low abundance of the ion representing the 1:1 complex in the experiments obtained in the absence of γ-CD in the BGE (Figure 6B) it could be hypothesized that the 2:1 complex possesses a higher stability, which results in the fact that the complex can still be observed in a CD-free BGE injecting a sample containing DCV and γ-CD. Upon dissociation of one DCV molecule, the resulting 1:1 complex is considerably less stable and quickly liberates DCV, which cannot form a complex again because γ-CD and DCV are electrophoretically separated. In contrast, when γ-CD is present in the BGE, the complexes can be reestablished upon dissociation into γ-CD and DCV so that the plateau between the peaks is composed of all three species, i.e. both complexes as well as free DCV (Figure 6C).

The faster migration of the complexes compared to free DCV as demonstrated by the plug-plug as well as CE-MS data is unexpected, because non-complexed DCV should have a higher charge density (charge-to-mass ratio) than the complex based on the molecular weight of the species and, consequently, migrate first. It has been described for CE enantioseparations of peptides that the enantiomer migration order can be based on a complexation-induced pKa shift translating into a faster mobility of the stronger complex between one of the enantiomers and a CD. [42,43] However, at pH 2.5, a pH about 2 - 3 orders of magnitude below the pKa value of DCV, the compound would be fully protonated in the free as well as the complexed form. Therefore, the reason for a higher mobility of the complex due to a pKa shift upon complexation of DCV can be excluded. A speculative explanation could be based on differences in the solvation shell of the molecules/complexes assuming a larger shell in the case of free DCV. It is known that small inorganic ions such as Li+ migrate slower than larger ions in CE[44] because of a much larger solvation shell.[45]

Furthermore, the CE capillary was used as a microreactor for the analysis of the equilibrium between DCV and γ-CD applying the so-called nonequilibrium capillary electrophoresis of

equilibrium mixtures (NECEEM).[46,47] Applying a sample containing 6 mM γ-CD and 0.1 mM DCV (n = 3) gave the equilibrium dissociation rate constant K_D = 1.32·10-2 M (RSD = 4.4 %) the complex formation rate constant k_{on} = 9.36·10^{-2} M^{-1}·s^{-1} (RSD = 9.5 %) and the complex dissociation constant k_{off} = 1.23·10^{-3} s^{-1} (RSD = 7.1 %). The approximate proportions of free DCV, the complex and the decay (plateau) in this equilibrium mixture were about 69 %, 17 % and 14 % (mol/mol/mol), respectively.

Conclusions

Two peaks with a plateau in between were observed in CE when DCV was analyzed in a γ-CD-containing BGE and also when a sample composed of DCV and γ-CD using a CD-free BGE. This is an unprecedented phenomenon for CDs in CE. Equilibria between peptides and ligands are slow on the CE timescale so that two peaks with a plateau can be observed, where the peaks represent the complex and the free ligand, respectively, while the plateau is formed by the dissociating ligand.[10,47] In contrast, equilibria involving CDs are typically very fast on the CE timescale so that only a single peak is observed when enantiopure (or achiral) compounds are analyzed in the presence of CDs in the BGE. The process was dependent on the pH of the BGE and the temperature, peak coalescence was observed above pH 3.5 and at about 45 °C, respectively.

Furthermore, the simultaneous presence of 1:1 and 2:1 complexes formed between either DCV, RSSR-DCV or mono-DCV and γ-CD was demonstrated by NMR and MS experiments. According to NMR data, DCV or the analogs are included in the cavity of the CD. In the case of the 2:1 complexes the solutes appear to be stacked. The equilibrium between the complexes with different stoichiometry were not the reason for the formation of the plateau as unequivocally shown by CE-MS. Surprisingly, the complexes displayed identical mobility so that they were not separated in CE. In addition, they migrated faster than non-complexed DCV which implies a higher charge-density than DCV probably due to differences in the solvation shells.

Although the number of investigated compounds is limited, the plateau phenomenon was only observed for "complete" derivatives with a symmetrically substituted biphenyl-imidazole-pyrrolidine structure containing MOC-amino acid moieties at both pyrrolidine "ends". Mono-DCV did not display two peaks with a plateau although 1:1 and 2:1 complexes are most likely present in solution. No indication for a 2:1 complex could be found for half-DCV. Thus, it may be hypothesized that upon accommodation of two stacked DCV molecules in the cavity of γ-CD, the molecules are "locked" because of the amino acid residues at both ends. This results in a highly stable 2:1 complex that dissociates only slowly so that it can still be detected in CD-free BGE. The stereochemistry of the chiral centers does not seem to play a role. However, if one of the MOC-Val moieties is missing (mono-DCV) the compounds are not locked, so that the equilibrium of complex formation is fast and only a single peak is observed in CE.

References

1   M. Belema, V. N. Nguyen, C. I. Bachand, D. H. Deon, J. T. Goodrich, C. A. James, R. Lavoie, O. D. Lopez, A. Martel, J. L. Romine, E. H. Ruediger, L. B. Snyder, D. R. St. Laurent, F. Yang, J. Zhu, H. S. Wong, D. R. Langley, S. P. Adams, G. H. Cantor, A. Chimalakonda, A. Fura, B. M. Johnson, J. O. Knipe, D. D. Parker, K. S. Santone, R. A. Fridell, J. A. Lemm, D. R. O'Boyle, R. J. Colonno, M. Gao, N. A. Meanwell, L. G. Hamann, *J. Med. Chem*. 2014, **57**, 2013-2032.
2   Anonymous, *J. Hepatol*. 2018, **69**, 461-511.
3   Anonymous, *Clin. Infect. Dis*. 2018, **67**, 1477-1492.
4   B. Chankvetadze, *J. Chromatogr. A* 2018, **1567**, 2-25.
5   P. Ját, G. K. E. Scriba, *J. Sep. Sci*. 2013, **36**, 52-74.
6   E. Sánchez-López, M. Castro-Puyana, M. L. Marina, A. L. Crego, *Anal. Sep. Sci*. 2015, **2**, 731-774.
7   C. Zhang, A. G. Woolfork, K. Suh, S. Overbude, C. Bi, M. Elzoeiry, D. S. Hage, *J. Pharm. Biomed. Anal*. 2020, **177**, 112882.
8   H. Nevidalova, L. Michalcova, Z. Glatz, *Electrophoresis* 2019, **40**, 625-642.
9   F. Yu, Q. Zhao, D. Zhang, Z. Yuan, H. Wang, *Anal. Chem*. 2019, **91**, 372-387.
10 V. A. Galievsky, A. S. Stasheuski, S. N. Krylov, *Anal. Chem*. 2015, **87**, 157-171.
11 G. K. E. Scriba, *J. Pharm. Biomed. Anal*. 2011, **55**, 688-701.
12 B. Chankvetadze, *J. Chromatogr. A* 1997, **792**, 269-295.
13 B. Chankvetadze, W. Lindner, G. K. E. Scriba, *Anal. Chem*. 2004, **76**, 4256-4260.
14 Q. Zhu, G.K.E. Scriba, *Chromatographia* 2016, **79**, 1403-1435.
15 J.M. Saz, M.L. Marina, *J. Chromatogr. A* 2016, **1467**, 79-94.
16 P. Rezanka, K. Navratilova, M. Rezanka, V. Kral, D. Sykora, *Electrophoresis* 2014, **35**, 2701-2721.
17 O. Trapp, *Electrophoresis* 2005, **26**, 487-493.
18 I. D'Acquarica, F. Gasparrini, M. Pierini, C. Villani, G. Zappia, *J. Sep. Sci*. 2006, **29**, 1508-1516.
19 R. Cirilli, R. Costi, R. Di Santo, F. La Torre, M. Pierini, G. Siani, *Anal. Chem*. 2009, **81**, 3560-3570.
20 R. Sabia, A. Ciogli, M. Pierini, F. Gasparrini, C. Villani, *J. Chromatogr A* 2014, **1362**, 144-149.
21 https://www.tga.gov.au/sites/default/files/auspar-daclatasvir-dihydrochloride-151214-cer.docx.
22 B. Chankvetadze, *Chem. Soc. Rev*. 2004, **33**, 337-347.
23 H. Dodziuk, W. Kozinsky, A. Ejchart, *Chirality* 2004, **16**, 90-105.
24 A. Salgado, B. Chankvetadze, *J. Chromatogr. A* 2016, **1467**, 95-114.
25 M. S. Silva, *Molecules* 2017, **22**, 247.

26 W. Chang, R. T. Mosley, S. Bansal, M. Keilman, A. M. Lam, P. A. Furman, M. J. Otte, M. J. Sofia, *Med. Chem. Lett*. 2012, **22**, 2928-2942.

27 K. H. Barakat, A. Anwar-Mohamed, J. A. Tuszynski, M. J. Robbins, D. L. Tyrrell, M. Houghton, *J. Chem. Inf. Model*. 2015, **55**, 362-373.

28 J. B. Cunniff, P. Vouros, *J. Am. Soc. Mass Spectrom*. 1995, **6**, 437-447.

29 V. Gabelica, N. Galic, De E. Pauw, *J. Am. Soc. Mass Spectrom*. 2002, **13**, 946-953.

30 H. Dodziuk, Cyclodextrins and Their Complexes: Chemistry, Analytical Methods and Applications, Wiley-VCH, Weinheim, 2006, pp. 1- 489.

31 K. A. Connors, *Chem. Rev*. 1997, **97**, 1325-1357.

32 M. V. Rekharsky, Y. Inoue, *Chem. Rev*. 1998, **98**, 1875-1917.

33 B. Pasquini, F. Melani, C. Caprini, M. Del Bubba, S. Pinzauti, S. Orlandini, S. Furlanetto, *J. Pharm. Biomed. Anal*. 2017, **144**, 220-229.

34 M. Greño, A. Salgado, M. Castro-Puyana, M. L. Marina, *Electrophoresis*. 2019, **40**, 1913-1920.

35 I. Terekhova, R. Kumeev, G. Alper, S. Chakraborty, H. Perez-Sanchez, E. Nunez-Delicado, *RSC Adv*. 2016, **6**, 49567-49577.

36 Y. Ikeda, F. Hirayama, H. Arima, K. Uekama, Y. Yoshitake, K. Harano, *J. Pharm. Sci*. 2004, **93**, 1659-1671.

37 L. A. Soares, A. F. Vasconcelos Borges Leal, L. F. Fraceto, E. R. Maia, I. S. Resck, M. R. Kkato, E. de Sousa Gil, A. Ribeiro de Sousa, L. C. da Cunha, K. R. Rezende, *J. Incl. Phenom. Macrocycl. Chem*. 2009, **64**, 23-35.

38 C. F. Dignam, L. A. Randall, R. D. Blacken, P. R. Cunningham, S.-K. G. Lester, M. J. Brown, S. C. French, S. E. Aniagyei, T. J. Wenzel, *Tetrahedron Asymmetry* 2006, **17**, 1199-1208.

39 A. Hazekamp, R. Verpoorte, *Eur. J. Pharm. Sci*. 2006, **29**, 340-347.

40 I. Correia, N. Bezzenine, N. Ronani, N. Platzer, J.-C. Beloeil, B.-T. Doan, *J. Phys. Org. Chem*. 2002, **15**, 647-659.

41 B. Chankvetadze, G. Schulte, D. Bergenthal, G. Blaschke, *J. Chromatogr. A* 1998, **798**, 315-323.

42 A. M. Rizzi, L. Kremser, *Electrophoresis* 1999, **20**, 2715-2722.

43 M. Hammitzsch-Wiedemann, G. K. E. Scriba, *Anal. Chem*. 2009, **81**, 8765-8773.

44 Y. Shi, J. S. Fritz, *J. Chromatogr*. 1994, **671**, 429-435.

45 J. Mähler, I. Persson, *Inorg. Chem*. 2012, **51**, 425-538.

46 L. T. Cherney, M. Kanoatov, S. N. Krylov, *Anal. Chem*. 2011, **83**, 8617-8622.

47 M. Kanoatov, V. A. Galievsky, S. M. Krylova, L. T. Cherney, H. K. Jankowski, S. N. Krylov, *Anal. Chem*. 2015, **87**, 3099-3106.

4. General discussion

This work includes three main themes. The main one is the determination of chiral purity of three drugs using experimental design approaches for method development (manuscripts 1,2,3). The second one is connected to the first one and comprises the elucidation of the chiral separation mechanism of two substances (manuscripts 2,4). The last theme involves clarifying an unusual complexation behavior of γ-CD and daclatasvir, which was observed in CE and studied with multiple analytical approaches (manuscript 5).

4.1. QbD-assisted development of CE methods for the chiral purity determination of drugs (manuscripts 1,2,3)

4.1.1. ATP, Initial method scouting and identification of chiral selectors

As mentioned in the introduction, cyclodextrins are the most widely applied selectors in chiral CE due to their versatility, stability, UV-transparency, commercial availability, and the affordability of most derivatives [60]. Many screening strategies were described in the literature for the enantiomeric separation methods in CE [110–114]. Native and neutral CDs are usually screened as possible chiral selectors for ionizable analytes in CZE mode and even for neutral compounds when using MEKC or MEEKC modes. Charged CDs proved high efficiency as chiral selectors, especially the sulfated CDs [115; 116]. The chiral separation with charged CDs has a higher opportunity when the electrophoretic mobility of the CD is opposite that of the analyte [115; 117]. The general rule would be using anionic CDs for basic and neutral analytes, and cationic CDs with acidic drugs, but this is also pH dependent since acidic analytes that are not ionized at low pH values, may also be separated with anionic CDs, especially the sulfated derivatives which were recently reported as the most commonly used chiral resolving agents in CE [61].

The first step in developing an analytical method following the QbD methodology is the and the definition of the analytical target profile. For the three drugs, the ATP was defined as a method allowing the precise determination of the enantiomeric impurity at a relative concentration of 0.1 % with acceptable precision and accuracy at the 0.1% level and within an analysis time of less than 10 minutes.

In order to identify the suitable chiral selectors, a phosphate buffer pH 2.5 was used as BGE for the initial screening of cyclodextrins in case of the basic compounds DXM and MDT. This insured both sample solubility and a slow EOF which would lead to a better enantioresolution in case of chiral bias. For the acidic compound ambrisentan Amb, cyclodextrins were screened in a basic borate buffer pH 9.0 and an acetate buffer pH 5.0, to ensure the solubility since the pK_a of Amb is approximately 4.0. However, the higher resolution was obtained in this case with lower pH due to the slower EOF.

Different native and neutral cyclodextrins and their derivatives were screened as possible chiral selectors in all three methods. In addition to the latter, the cationic 2-hydroxy-3-*N,N,N*-trimethylamino)propyl-β-CD was screened with Amb, while anionic CDs were screened with DXM and

MDT. The polarity of voltage was reversed when no peaks were detected after 60 minutes when evaluating ionic CDs.

γ-CD was chosen as chiral selector for Amb further method development because it yielded the highest resolution of the screened CDs.

The best enantiomeric resolution at pH 2.5 was obtained by applying the reversed polarity of voltage and sulfated β-cyclodextrin (S-β-CD) as a chiral selector in case of DXM and MDT.

4.1.1.1.   Improving the peak shape through adjustment of the experimental conditions

MDT. Despite the high chiral resolution obtained with S-β-CD, a severe tailing affected the peak shapes of D-MDT and L-MDT, which couldn't be improved by changing the counter ions of the phosphate buffer, or even trying other buffer substances at pH 2.5 or 4.8 with the same selector. Short end injection did not help either. Upon investigating a sodium phosphate buffer pH 7.0 at normal polarity of the applied voltage the peak shape was improved. A comparison of the initial and the improved peak shape is shown in Fig. 7.
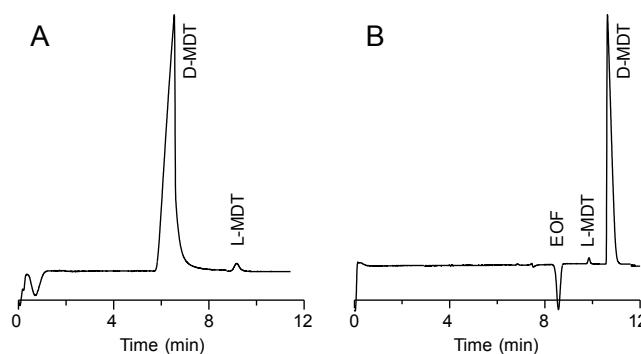
Figure 7 Electropherograms of the S-β-CD-mediated separation of D-MDT and L-MDT at **(A)** pH 2.5 and (B) pH 7.0. Experimental conditions: **(A)** 10.2/50.2 cm, 50 µm ID fused-silica capillary (short end injection); 50 mM sodium phosphate buffer, pH 2.5; 30 mg/mL S-β-CD; 20°C; −20 kV and **(B)** 21.3/31.5 cm, 50 µm ID fused-silica capillary; 50 mM sodium phosphate buffer, pH 7.0; 50 mg/mL S-β-CD; 20°C; 6 kV; UV detection at 200 nm. Sample concentration: 700 µg/mL D-MDT and 7 µg/mL L-MDT.

DXM. The chiral resolution of DXM and LVM using S-β-CD was associated with high baseline noise and peak fronting. Subsequently, 100 mM triethanolamine-phosphoric acid buffer, pH 2.5, 100 mM sodium acetate buffer, pH 5.0, and sodium citrate buffer, pH 6.0, were studied as alternative BGEs. However, none of these conditions improved the chiral separation, the peak shape of the analytes or baseline noise. Therefore, S-β-CD was further screened in sodium phosphate buffer, pH 7.0, and sodium borate buffer, pH 8.5, under normal polarity of the applied voltage. In the presence of 10 mM S-β-CD, high resolution was observed with R_S values of about 21 and 24, respectively. DXM migrated before LVM, but substantial peak tailing occurred. Because lower baseline noise was found for the phosphate-based

buffer, different buffer co-ions of phosphate including triethanolamine and lithium were studied but even worsened the peak shape. In 2-[4-(2-hydroxyethyl)-1-piperazinyl]-ethanesulfonic acid buffer, pH 7.0, piperazine-1,4-bis(2-ethanesulfonic acid) buffer, pH 7.0, or Tris-phosphoric acid buffer, pH 8.0, no peaks could be detected within 30 min. Addition of organic solvents up to a concentration of 20% v/v did not improve peak shape or baseline noise. Therefore, sodium phosphate buffer, pH 7.0, in combination with S-β-CD was selected for further evaluation.

Dual CD systems have been successfully applied to drug CE enantioseparations [118; 119] and were also employed to improve the peak shape of basic compounds [120]. Therefore, neutral and charged CDs were tested in combination with S-β-CD in 50 mM sodium phosphate buffer pH 7.0. The peak shape was substantially improved with an associated decrease of resolution upon using carboxymethyl-α-CD sodium salt (CM-α-CD) or methyl-α-CD sodium salt (M-α-CD) as a co-selector.

Being a neutral compound, M-α-CD was chosen for further method development because it will not increase the electric current of the BGE. Fig. 8 illustrates the effect of the combination of S-β-CD and M-α-CD on the resolution, peak shape, and baseline noise during the separation of the methorphan enantiomers.
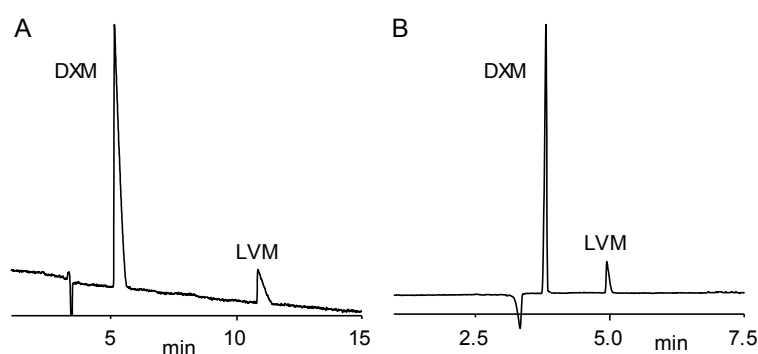
Figure 8 Electropherograms of the separation of DXM and LVM using **(A)** 20 mg/mL S-β-CD and **(B)** 20 mg/mL S-β-CD and 10 mg/mL M-α-CD in 50 mM sodium phosphate buffer, pH 7.0. Other experimental conditions: 30/40.2 cm, 50 μm ID fused-silica capillary; 20°C; 16 kV; detection at 200 nm.

4.1.1.2.   The role of the enantiomeric migration order (EMO) in the separation

It is favorable for the quantitative determination of impurities in CE/chromatographic methods that a minor impurity migrates/elutes before the main analyte when it is to be determined in the presence of a large excess of a drug, especially when they are detected close to each other. This was already the case with ambrisentan with γ-CD and the acetate buffer pH 5.0 used for the initial screening. In the case of D-MDT, changing the pH from 2.5 to 7.0 and reversing the polarity were necessary to reverse the EMO so that L-MDT migrated before D-MDT (Fig. 7). Nonetheless, a similar change of pH and polarity reversed the migration order of DXM and LVM so that the chiral impurity migrated afterwards, but the enantioresolution was large enough so this did not affect the subsequent quantification (Fig. 8).

4.1.2.   Knowledge space and initial screening of factors

The CPPs and the CQAs were identified considering the predefined ATP and the initial scouting experiments. For all three methods, similar factors were defined as CPPs for the initial screening using a fractional factorial design (table 2). Nevertheless, the enantioresolution, and the analytical run time were considered CQAs in all three methods, but the current was added as a third response in the case of MDT due to the relatively high amount of the charged cyclodextrin S-β-CD.

Table 2 Comparison of the QbD approaches used for screening of the three chiral purity methods for Amb, DXM, and D-MDT

		Identification of the knowledge space		
		Method		
		Amb	**DXM**	**D-MDT**
	Experimental design	fractional factorial resolution V+	fractional factorial resolution IV	fractional factorial resolution V+
	Selector(s) concentration	X	both	X
Screened factors	Buffer concentration	X	X	X
	Buffer pH	X	X	X
	Voltage	X	X	X
	Capillary Temperature	X	X	X
	Enantioresolution	X	X	X
Responses	Analytical run time	X	X	X
	Current	-	-	X

Amb. pH of the BGE exerted a major effect on peak resolution and a minor effect on the run time (Fig. 9). Thus, to obtain a high R_S value, the pH was fixed at pH 4.0 so that it was not directly set at the edge of the screening range. Also, because the CD concentration was insignificant for peak resolution and had only a minor effect on the run time, it was set at 30 mM, i.e., the medium value of the screening range. Voltage, temperature and BGE concentration, were considered CPPs for the RSM.

DXM. Although both CQAs were met for a large variety of experimental settings, the plot indicated that low electrolyte pH was favorable (Fig. 10). Consequently, BGE concentration was fixed at the lowest value of the screened range and pH was fixed at 6.5, and temperature was set at the center point 20°C. The concentration of the CDs and separation voltage were further optimized by RSM.
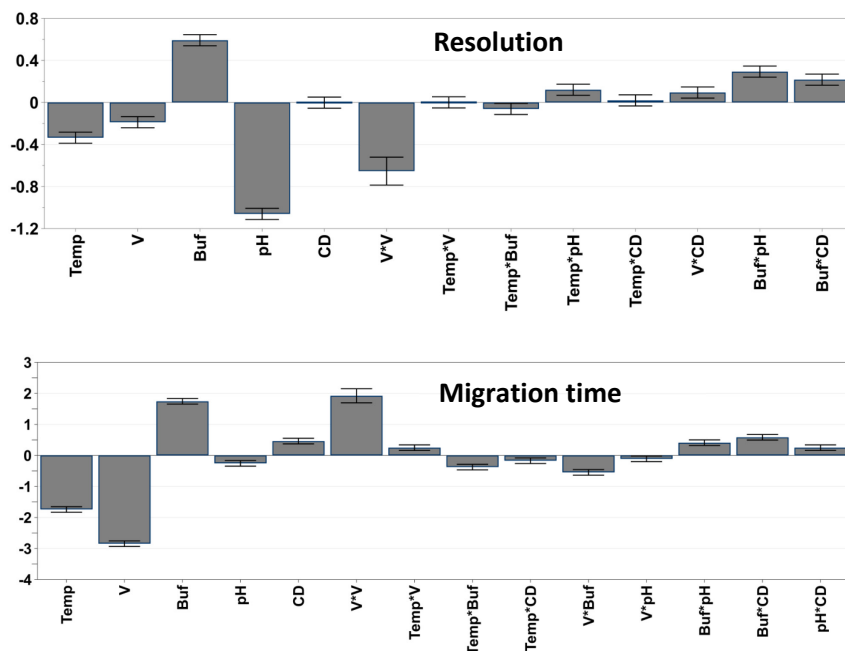
Figure 9 Regression coefficients plot of the screening design of Amb. *V* applied voltage, *Temp* capillary temperature, *Buf* acetate buffer concentration in the BGE, *CD* γ-CD concentration in the BGE, *pH* pH of the BGE
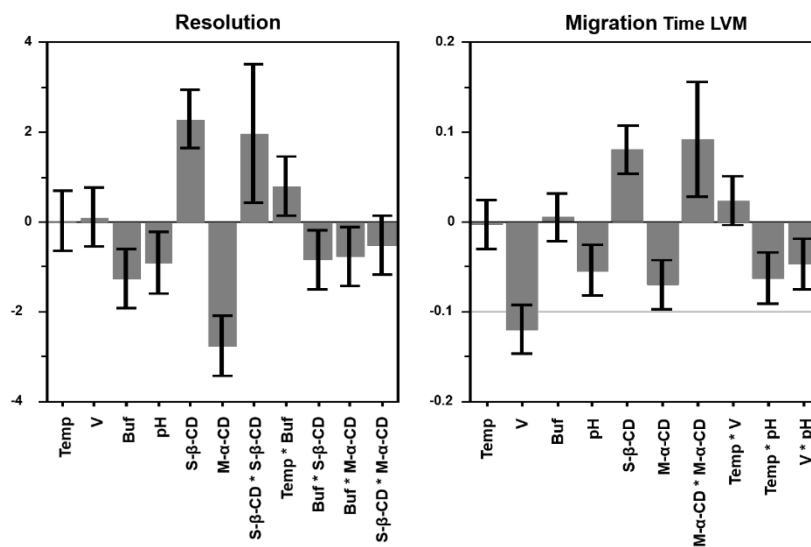
Figure 10 Coefficient plot (scaled and centered) of the screening design of DXM. **V,** applied voltage; **Temp**, capillary temperature; **pH**, pH of buffer solution; **Buf**, buffer concentration; **S-β-CD**, S-β-CD concentration; **M-α-CD**, M-α-CD concentration.

MDT. Significant effects were detected for all parameters and for most interaction terms (Fig. 11). Increasing the pH of the BGE negatively affected separation selectivity in addition to increasing the current. Thus, low pH seems favorable, although this leads to increased migration times. Similarly,

increasing phosphate buffer concentration results in lower enantioresolution and increased current but with a smaller effect on migration times. Voltage and temperature affected migration time and current more significantly than separation selectivity. Increasing S-β-CD concentrations increased all responses. Consequently, the concentration and pH of the phosphate buffer were fixed at 50 mM and pH 6.5 (i.e. lowest values), respectively, to achieve high separation selectivity and short migration times as well as low current. The concentration of S-β-CD, the capillary temperature and the separation voltage were considered CPPs and further optimized.
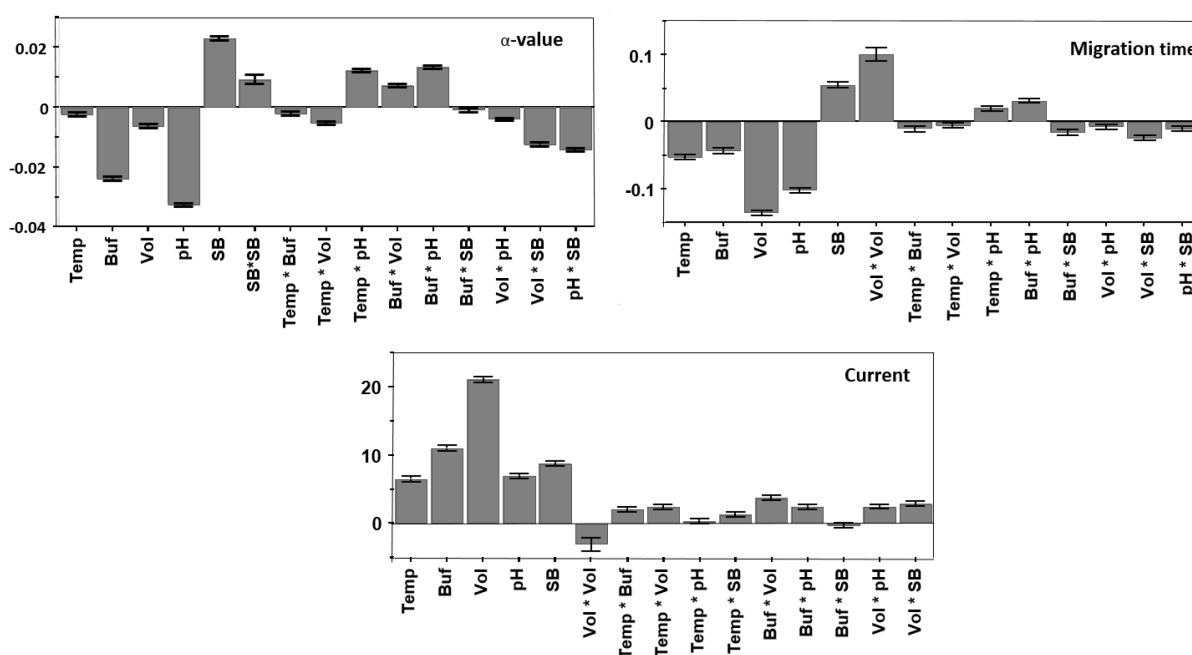
Figure 11 Coefficient plot of the screening design for D-MDT. *V*, Applied voltage; *Temp*, capillary temperature; *pH*, pH of BGE; *Buf*, BGE concentration; *SB*, S-β-CD concentration.

4.1.3.   Design space definition by RSM

Considering the screening results some experimental parameters were fixed in each method while the remaining parameters were considered CPPs and further optimized with response surface methodology. The same responses of the screening design were further considered CQAs in the optimization of Amb and D-MDT methods. Nevertheless, with DXM, the enantioresolution was above the initial threshold in all experiments, therefore, it was not considered a CQA. The optimization concentrated on analysis time and the peak performance criteria as responses, that is, the of the DXM peak (calculated according to the United States Pharmacopeia by the instrument software) as well as the number of theoretical plates and the peak height of the LVM peak. This was necessary to improve the peak shapes which leads to better quantification. A quick comparison of the CPPs and the CQAs for the RSM of the three methods is shown in Table 3.

Table 3 Comparison of the QbD approaches used for optimization of the three chiral purity methods for Amb, DXM, and D-MDT

		Design space definition by response surface methodology		
		Method		
		Amb	**DXM**	**D-MDT**
CQAs	Selector(s) concentration	-	S-β-CD (10–30 mg/mL) M-α-CD (5–15 mg/mL)	30–50 mg/mL
	Buffer concentration	50–200 mM	-	-
	Buffer pH	-	-	-
	Voltage	15–25 kV	10–20 kV	6–10 kV
	Capillary Temperature	15–25 °C	-	15–25°C
CPPs	Enantioresolution	$R_S \geq 1.5$	-	$\alpha > 1.05$
	Analytical run time*	≤10 min	≤ 8 min	≤10 min
	Current	-	-	< 100 µA
	Drug peak asymmetry (USP tailing factor)	-	0.5 to 3	-
	Impurity peak height	-	≥3000 µAU	-
	Theoretical plate count of impurity peak	-	≥3000	-
	* The analytical run time was marked by the migration time of the last peak of interest			

For the three compounds, a three-level central composite face-centered design of the assigned factors in their respective ranges was used for further investigation. Subsequently, Monte-Carlo simulations were carried out for defining the design space of each method. The design space represents a map for the risk of failure to meet the predefined CPPs. An example of a design space representing the probability map of DXM is shown in Fig. 12. In this case the migration time of LVM was set as measure of the analysis time at ≤ 8 min, the number of theoretical plates and the peak height of the LVM peak at ≥3000 and ≥3000 µAU, respectively, as well as the tailing factor of the DXM peak in the range of 0.5 to 3 with the target value of 1, the design space of the method was derived by Monte Carlo simulations.

In light of the results, an optimized working point was chosen for each method. The final working conditions of each method are summarized in Table 4. An internal standard was chosen for each method for the calibration of the impurity.
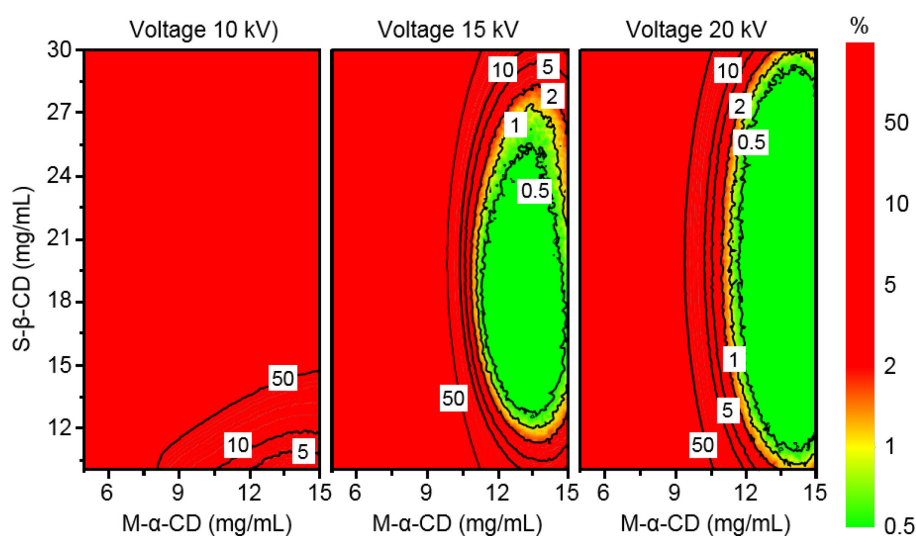
Figure 12 Probability plot of the design space. Notes: Threshold of responses (min/target/max): migration time of LVM (−/−/8 min), number of theoretical plates of LVM peak (3000/−/−), height of LVM peak (3000 µAU/−/−) and tailing factor of the DXM peak (0.5/1/3). The design space (green zone) is identified as the zone where the risk of failure is ≤ 1%.

Table 4 Overview of the final experimental conditions of the optimized chiral purity methods for Amb, DXM, and D-MDT

Experimental condition	Amb	DXM	D-MDT
Chiral selector	30 mM γ-CD	16 mg/mL S-β-CD + 14 mg/mL M-α-CD	40 mg. mL^{-1} S-β-CD
Buffer	50 mM sodium acetate buffer, pH 4.0	30 mM sodium phosphate buffer, pH 6.5	50 mM sodium phosphate buffer, pH 6.5
Voltage	+25 kV	+20 kV	+10 kV
Capillary Temperature	25° C	20° C	17° C
Capillary	fused-silica capillary 40/50.2 cm, 75 µm ID	fused-silica capillary 30/40.2 cm, 75 µm ID	fused-silica capillary 21.3/31.5 cm, 50 µm ID
UV detection wavelength	200 nm		
hydrodynamic injection	0.7 psi for 5 s	0.7 psi for 5 s	0.7 psi for 5 s

Fig. 13 shows the electropherograms of the optimized methods with the corresponding enantiomeric impurity spiked in each sample.
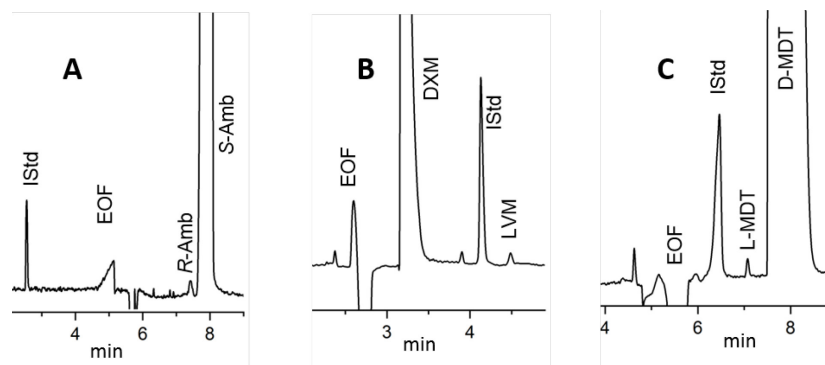
Figure 13 Electropherograms of the three compounds each spiked with the relevant enantiomeric impurity. (**A**) 700 µg/ mL (S)-ambrisentan and 0.7 µg/mL of the (R)-enantiomer (0.1%) with metformin hydrochloride 15 µg/mL as internal standard; (**B**) 1.5 mg/mL DXM spiked 1 µg/mL LVM (0.067%) with procainamide hydrochloride 30 µg/mL as internal standard; (**C**) 2 mg/mL D-MDT spiked with 2 µg/mL L-MDT (0.1%) 60 µg/mL L -Tryptophan as internal standard.

4.1.4. Robustness testing

The robustness of the three methods was also estimated with a QbD approach using a Plackett-Burman design with a variation of the experimental conditions around the center point of the optimized working conditions. The design matrices are summarized in the corresponding supplementary information appendix of each method.

Amb. Statistical analysis revealed no correlation with standard deviations including zero. Furthermore, the data were within the acceptance criteria, i.e., R_S > 1.5 and analysis time <10 min.

DXM. In addition to the factors initially screened as CPPs, the effect of different batches of different batches of S-β-CD and M-α-CD was investigated, since they are both randomly substituted. The variations of the parameters did not significantly affect the number of theoretical plates of the LVM peak or the tailing factor of the DXM peak. Except for buffer concentration on migration time and S-β-CD concentration on peak height, all variables were significant including variation of the CD batch. However, under all experimental conditions evaluated, the responses always met the predefined requirements and hence, the method can be considered robust. Nonetheless, care should be taken in the preparation of the BGE and instrumental parameters such as capillary temperature and voltage should be controlled carefully.

D-MDT. As with DXM, two batches of S-β-CD were included as additional factor to the screening CPPs. In addition to the three optimized responses, the quantitative robustness was assessed using the ratio of the corrected peak areas of L-MDT and the internal standard as a measure. The responses α-value, current and the ratio of corrected peak areas were not significantly affected by the small variations of

the experimental parameters. In contrast, in the case of migration time, a significant although minor effect of all variables on this response was detected. However, none of the conditions led to a migration time above 8.2 min, which is well below the threshold of ≤10 min set in the ATP. Therefore, the method can be considered robust. Nonetheless, the BGE should be prepared carefully and the instrumental parameters voltage and capillary temperature should be strictly controlled.

4.1.5.   Method validation

The developed methods were validated according to ICH guideline Q2(R1) [90]. Table 5. Represents a comparison of the developed methods in terms of validation parameters. The limit of quantitation (LOQ) of the chiral impurity corresponded to 0.1% relative concentration of the enantiomeric impurity in cases of both Amb and D-MDT, while it was possible to reach 0.07% in the case of DXM. This was mainly possible due to the higher enantioresolution in case of DXM (Fig. 13). The USP [36] and the Ph. Eur. [38] deploy chiral HPLC methods for the chiral purity of DXM with 0.1% as a specification limit of the impurity LVM. D-MDT has also a HPLC test for the enantiomeric purity in its USP monograph where the maximum limit of L-MDT is specified as 1.0%.

Table 5 Comparison of the validation parameters of the chiral purity methods for Amb, DXM, and D-MDT

Parameter	Amb		DXM		D-MDT	
	Level [1]	Recovery %	Level [1]	Recovery %	Level [1]	Recovery %
Accuracy [2] **(drug substance)**	1.4 µg/mL (0.2 %)	97.5 ± 6.9%	1.5 µg/mL (0.1%)	88.9 ± 3.6 %	4 µg/mL (0.2%)	92.0 ± 6.4 %
	3.85 µg/mL (0.55 %)	101.8 ± 7.0%	7.5 µg/mL (0.5 %)	96.1 ± 2.0 %	16 µg/mL (0.8 %)	96.8 ± 3.0 %
	6.3 µg/mL (0.9 %)	99.4 ± 2.9%	13.5 µg/mL (0.9 %)	99.2 ± 0.9 %	28 µg/mL (1.4 %)	98.9 ± 1.7 %
Migration time repeatability (RSD)	1.0 %		1.2 %		4.2 %	
Migration time intermediate precision (RSD)	5.9 %		5.8 %		9.3 %	
Content repeatability [3] (RSD)	4.9 %		5.3 %		4.7 %	
Content intermediate precision [4] (RSD)	6.6 %		5.7 %		5.4 %	
Range [1]	0.7 - 7 µg/mL (0.1 - 1.0 %)		1.0 - 15 µg/mL (0.1 - 1.0 %)		2.0 - 30 µg/mL (0.1 - 1.5 %)	
Coefficient of determination R²	0.9955		0.9989		0.9897	
LOD (S/N = 3)	0.2 µg/mL (0.03 %)		0.3 µg/mL (0.02 %)		0.6 µg/mL (0.03 %)	
LOQ (S/N = 10)	0.7 µg/mL (0.1 %)		1.0 µg/mL (0.07 %)		2.0 µg/mL (0.1 %)	

[1] The percentage represents the relative concentration of the spiked enantiomeric impurity in the sample solution

[2] Mean recovery ± confidence interval % (α/2 = 0.025). Amb and DXM samples were spiked with the indicated amount of the corresponding enantiomeric impurity, while D-MDT samples were spiked with the racemate.

[3] Nine runs, three samples at three concentrations on one day.

[4] Nine runs, mean of three samples at three concentrations on three consecutive days.

4.2. Elucidation of the chiral separation mechanism (manuscripts 2,4)

Mechanistic studies were performed in order to understand the migration interaction of the enantiomers with the selector(s). The study served in case of DXM to explain the effect of M-α-CD on peak tailing in the S-β-CD-mediated enantioseparation of methorphan (Fig. 8). In the case of MDT enantiomers, an opposite EMO was observed at pH 2.5 in the presence of the two native CDs β-CD and γ-CD, which differ in the cavity size (Fig. 14A and B). MDT enantiomers also exhibited an opposite EMO at pH 2.5 in the presence of sulfated CDs S-β-CD and HS-β-CD (Fig. 14C and D), which have the same cavity size but differ in the substitution pattern (Table. 1). Consequently, the apparent complexation parameters of MDT enantiomers with the four CDs were determined by CE, in order to understand the migration behavior. In addition to CE, the complexation of MDT enantiomers with β-CD, γ-CD , and HS-β-CD was also studied in detail by NMR spectroscopy and molecular modeling.
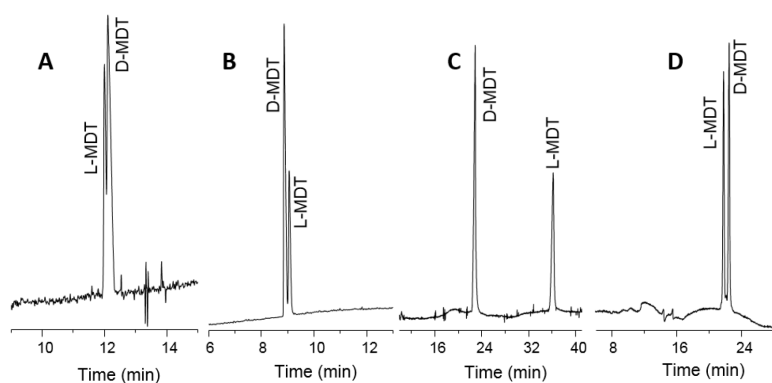
Figure 14 EMO reversal of MDT enantiomers using (A) β-CD, (B) γ-CD, (C) S-β-CD and (D) HS-β-CD. Experimental conditions: 40/50.2 cm, 50 μm I.D. fused silica capillary; 50 mM sodium phosphate buffer, pH 2.5; 20 °C; detection at 200 nm. Other conditions: (A) 20 mM β-CD, 2 M urea, 20 kV; (B) 20 mM γ-CD, 20 kV; (C) 20 mM S-β-CD, −20 kV; (D) 20 mM HS-β-CD, −20 kV.

4.2.1. Determination of the apparent complexation constants and complex mobilities by CE

The apparent complexation constants and complex mobilities of the diastereomeric CD–analyte complexes were determined by preparing a series of BGEs containing ascending concentrations of the relevant CDs and plotting the effective mobilities against the CD concentrations. The data were obtained as best fit parameters of the dependence of the effective mobility on the CD concentration assuming the formation of 1:1 CD–analyte complexes according to equation 6 [53].

CEVal is a helpful tool for the evaluation of experimental results obtained by CZE and affinity CE [121]. It was used for data fitting because this software allows correction of the migration times in case of strongly tailing peaks according to the Haarhoff−van der Linde function [122; 121].

Methorphan enantiomers. The mobilities were determined in 30 mM sodium phosphate buffer, pH 6.5 in the case of S-β-CD, i.e. the pH and buffer concentration of the optimized method. Meanwhile, in the presence of M-α-CD as selector because of the strong EOF at pH 6.5, an enantioseparation could not be observed. Therefore, the data for M-α-CD were determined in 100 mM sodium phosphate buffer, pH 2.1. DXM has a pK_a of 9.2 [123] which means it is fully protonated at both pH values so it can be assumed that the mobility of the free analytes, μ_f, the mobility of the complexes μ_c, and the complexation between the M-α-CD and the analyte enantiomers are not significantly altered at pH 6.5 versus pH 2.1 which are independent of the EOF. The obtained data are summarized in Table 6.

Table 6 Complexation constants, K, and mobilities of the free analytes, µf, and of the CD-analyte complexes, µc. The ranges in brackets represent the 95 % confidence intervals.

	S-β-CD		M-α-CD	
	DXM	**LVM**	**DXM**	**LVM**
µf (10^{-9} m^2 s^{-1} V^{-1})	14.8 (13.7, 15.8)		24.1 (23.6, 24.5)	
µc (10^{-9} m^2 s^{-1} V^{-1})	−38.0 (−42.2, −34.4)	−43.2 (−45.5, −41.2)	9.97 (9.42, 10.48)	9.91 (9.38, 10.40)
K (M^{-1})	260 (211, 319)	606 (516, 716)	354 (292, 429)	399 (330, 484)

LVM is complexed much stronger by S-β-CD compared to DXM, and the mobility of the S-β-CD–LVM complex is much higher than the mobility of the S-β-CD–DXM complex. This explains the enantiomer migration order, i.e. that DXM migrates faster than LVM (after the EOF), and the increasing peak deformation, especially of the LVM peak due to mismatch of the mobilities of the CD–analyte complexes and the buffer ions. In the case of M-α-CD, LVM is also bound stronger than DXM, but complex mobilities are not significantly different from each other for both enantiomers. The competing effects between both CDs, results in slowing down the overall mobility of LVM more effectively as compared to DXM resulting in a reduced peak resolution. However, the reduced mobility of the analytes also reduced the extent of the mobility mismatch between analytes and buffer ions, yielding lower peak deterioration and, consequently, sharper and higher peaks.

MDT enantiomers. The measurements were made in 50 mM sodium phosphate buffer, pH 2.5, where the EOF and was not considered because it could not be observed within 60 min. Due to the relatively poor enantioseparation in the case of β-CD in 50 mM sodium phosphate buffer, pH 2.5, the concentration of the phosphate buffer was increased to 150 mM and the pH lowered to pH 2.0 in order to obtain sharp peak allowing the determination of the mobilities of the enantiomers. The data are summarized in Table 7.

Table 7 Apparent complexation constants, K, and mobilities of the free analytes, μ_f, and of the CD-analyte complexes, μ_c. The numbers in brackets represent the confidence interval ($\alpha/2 = 0.025$).

	β-CD		γ-CD	
	D-MDT	**L-MDT**	**D-MDT**	**L-MDT**
μ_f (10^{-9} m^2 s^{-1} V^{-1})	19.54 (19.34, 19.74)		23.70 (23.33, 24.07)	
μ_c (10^{-9} m^2 s^{-1} V^{-1})	6.57 (4.98, 7.80)	6.70 (5.04, 7.99)	7.89 (4.6, 10.14)	8.28 (5.56, 10.23)
K (M^{-1})	48.2 (38.3, 59.8)	46.9 (36.9, 58.7)	42.3 (29.5, 58.3)	48.5 (34.9, 65.6)

	S-β-CD		HS-β-CD	
	D-MDT	**L-MDT**	**D-MDT**	**L-MDT**
μ_f (10^{-9} m^2 s^{-1} V^{-1})	25.03 (24.77, 25.29)		25.35 (25.13, 25.58)	
μ_c (10^{-9} m^2 s^{-1} V^{-1})	−15.20 (−15.67, −14.74)	−12.77 (−13.24, −12.30)	−16.92 (−17.51, −16.34)	−16.55 (−17.13, −15.98)
K (M^{-1})	557 (504, 620)	533 (480, 596)	204 (188, 221)	221 (204, 241)

The opposite EMO In the case of β-CD and γ-CD can be explained by opposite affinities of the analyte enantiomers toward the respective CDs. D-MDT bound stronger to β-CD compared to L-MDT, while the opposite was found for γ-CD (Table 6), and thus the stronger bound enantiomer migrates second. The lower resolution observed for β-CD versus γ-CD is due to the small difference between the complexation constants of MDT enantiomers with this CD. Interestingly, in both cases, the mobility of the (L-MDT)-CD complex exceeds the mobility of the diastereomeric complex of MDT. This counteracts the enantioseparation by γ-CD, but no significant deterioration of the resolution was observed with increasing CD concentrations. This can be attributed to the relatively small and insignificant differences between the complex mobilities and the relatively larger difference between the complexation constants of γ-CD so that the increasing mobility of the complex with increasing CD concentrations does not significantly affect the overall enantioseparation. Thus, in the case of β-CD as well as γ-CD the enantioseparation is governed by the complexation constants. Examples of EMO reversal based on opposite affinities of CDs toward the analyte enantiomers are summarized in [124].

Opposite recognition of the medetomidine enantiomers was also found for S-β-CD and HS-β-CD. D-MDT is complexed stronger than its enantiomer by S-β-CD, while L-MDT is complexed stronger than D-MDT by HS-β-CD. The limiting mobility of the stronger D-MDT–S-β-CD complex also significantly exceeded the mobility of the complex between the CD and L-MDT resulting in the large resolution between the enantiomers (Fig. 14C). However, higher complex mobility was observed for the weaker bound D-MDT in the case of HS-β-CD, which causes the deterioration of the enantioseparation at higher HS-β-CD concentrations. Thus, contrary to β-CD and γ-CD, the separation of the MDT enantiomers with

the negatively charged S-β-CD and HS-β-CD is governed by both, the complexation constants and the complex mobilities. For S-β-CD, both enantioselective principles in CE cooperate leading to a large enantioresolution while they counteract each other in the case of HS-β-CD resulting in a loss of enantioseparation at higher CD concentrations.

4.2.2. NMR and molecular dynamics studies

The complexation of MDT enantiomers (Fig. 15) with β-CD, γ-CD, and HS-β-CD was studied in detail by NMR spectroscopy and molecular modeling. S-β-CD was excluded from both the NMR studies molecular modeling because this randomly substituted CD is a mixture of positional and substitution isomers so that meaningful data could not be obtained by these techniques.

4.2.2.1. NMR studies

The ^{1}H NMR resonances of the MDT-CD complexes were recorded by measuring samples containing MDT (alone or spiked with D-MDT) mixed with each of β-CD, γ-CD or HS-β-CD in a deuterated sodium phosphate buffer pH 2.5. The samples also contained 2 mM urea in the case of β-CD.
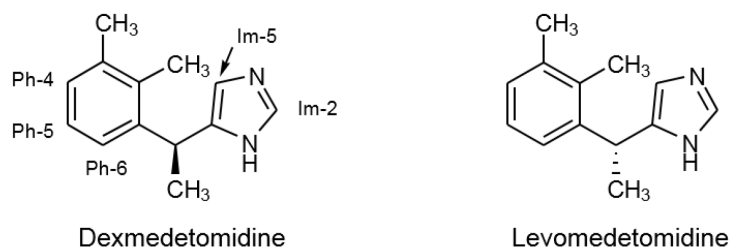
Figure 15 Structures of MDT enantiomers with the proton numbering on the imidazole and phenyl rings

1D ROESY experiments were performed and the intramolecular nuclear Overhauser effects (NOEs) were interpreted. Enantiomeric bias is indicated through the stronger NOE response of one enantiomer over the other. Racemic MDT was used for ROESY experiments, while non-racemic mixtures (MDT spiked with D-MDT) were applied in a second experiment in order to assign the signals of the respective enantiomer in case of signal splitting.

β-CD complex. The 1D ROESY experiments showed intermolecular NOE interactions between almost all medetomidine hydrogens with the internal H-3 and H-5 protons of β-CD. However, selective irradiation at the proton resonances of the MDT and β-CD indicated that the phenyl ring of MDT is inserted into the β-CD cavity through the larger rim, while the imidazole moiety remained outside the

cavity and is exposed to the solvent. A tentative representation of the complex structure is shown in (Fig. 16A).
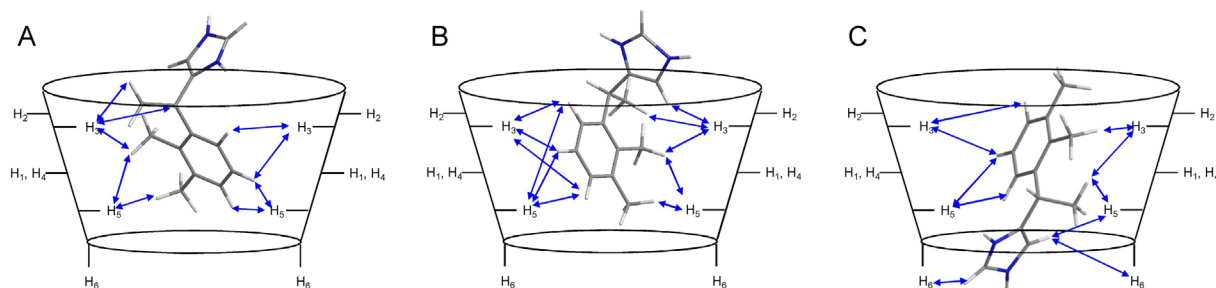
Figure 16 Schematic representation of the structures of the medetomidine-CD complexes derived from the NMR ROESY data. (A) complex with β-CD, (B) complex with γ-CD and (C) complex with HS-β-CD

A slight enantiomeric bias was observed in the NOEs with the aromatic Ph H-6 and Im H-5, as D-MDT seemed to give a slightly larger NOE response than the L-MDT. This is consistent with the CE experiments, where a stronger complexation of D-MDT by β-CD compared to L-MDT was found (Table 7).

γ-CD Complex. The NOE interaction pattern was similar to that observed for the MDT–β-CD complex, since all the observed intermolecular NOEs involved the internal hydrogen atoms of γ-CD. Once again, selective irradiation suggested the formation of an insertion complex, where the phenyl ring of MDT is positioned inside the γ-CD cavity and the imidazolium moiety is situated closer to the larger CD rim and exposed to the solvent. A tentative complex structure is shown in (Fig. 16B).

Enantiomeric bias was also found with γ-CD. Thus, irradiation at γ-CD H5 resulted in a stronger NOE response for the phenyl proton H-6 of L-MDT indicating it is complexed stronger by γ-CD as compared to D-MDT. This complexation pattern is opposite to that observed in the case of β-CD, yet consistent with the CE data as a larger complexation constant was derived between γ-CD and L-MDT compared to D-MDT (Table 7).

HS-β-CD complex. NOE interactions with all MDT hydrogens except the aliphatic CH were found. This implies proximity of MDT to the primary rim of HS-β-CD. Although those NOEs were not very strong, NOE responses of the imidazole protons were slightly larger than those of the phenyl hydrogens of MDT. This supports a structure of the HS-β-CD complex different from the structures of the respective β-CD and γ-CD complexes. With HS-β-CD, the protonated imidazolium moiety seems to be positioned inside the cavity close to the primary ring interacting probably through water-mediated hydrogen bonds with the negatively charged sulfate groups. The phenyl ring would therefore find itself inside the CD cavity as shown schematically in (Fig. 16C).

Irradiation at the HS-β-CD H-6 protons proved an enantiomeric bias as a larger response was noted for the protons of L-MDT. This suggests a tighter complexation of the L-MDT with HS-β-CD compared to D-MDT, which is consistent with the complexation data derived by CE (Table 7).

In conclusion, the results of the NMR studies were concordant with the CE data for the three CDs.

4.2.2.2. Molecular modeling

The structures of complexes formed between β-CD, γ-CD, and S-β-CD and MDT enantiomers as derived by molecular modeling are summarized in (Fig. 17). In both β-CD inclusion complexes (Fig. 17A), each MDT enantiomer is bound with the imidazolium moiety pointing towards the secondary rim and essentially exposed to the solvent, while the phenyl group is positioned in the hydrophobic CD cavity.

Essentially the same orientation is observed in the γ-CD-MDT complexes (Fig. 17B). The hydrophobic phenyl group is positioned inside the CD cavity.

In the HS-β-CD complexes, the imidazolium appears to be buried inside the cavity and surrounded by the sulfate groups attached to the O6 atom of each glucose unit (Fig. 17C). This favorable electrostatic interaction is quite strong but direct hydrogen bonds are permanently in competition with similar interactions with solvent water molecules. In this orientation, Ph-5 and Ph-6 protons of medetomidine face protons on H-3 and H-5 of the CD, hence the observed NOEs.
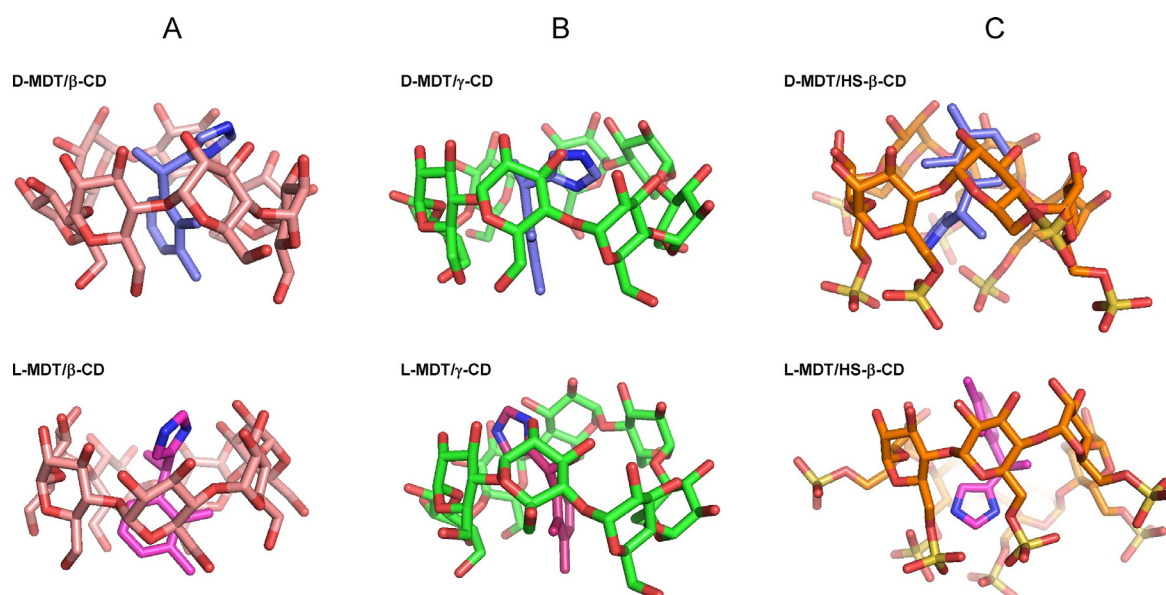
Figure 17 Molecular modeling structures of the medetomidine enantiomers with **(A)** β-CD, **(B)** γ-CD and **(C)** HS-β-CD. The complexes with dexmedetomidine (D-MDT) are presented in the top layer, while the complexes with levomedetomidine (L-MDT) are shown in the bottom layer.

This shows that the complex structures derived from molecular modeling (Fig. 17) are in good agreement with the tentative structures deduced from NMR experiments (Fig 16).

4.3. Unusual complexation behavior between daclatasvir and γ-CD (manuscript 5)

Daclatasvir (DCV) is an inhibitor of the hepatitis C nonstructural protein 5A replication complex [125]. DCV is a biphenyl with two identical halves each containing two stereogenic centers each. The compound possesses *S,S,S,S* configuration while the enantiomer (RRRR-DCV) is *R,R,R,R* configured. Due to the four stereogenic centers, there are also other diastereomers including meso forms of the compound (Fig. 18).
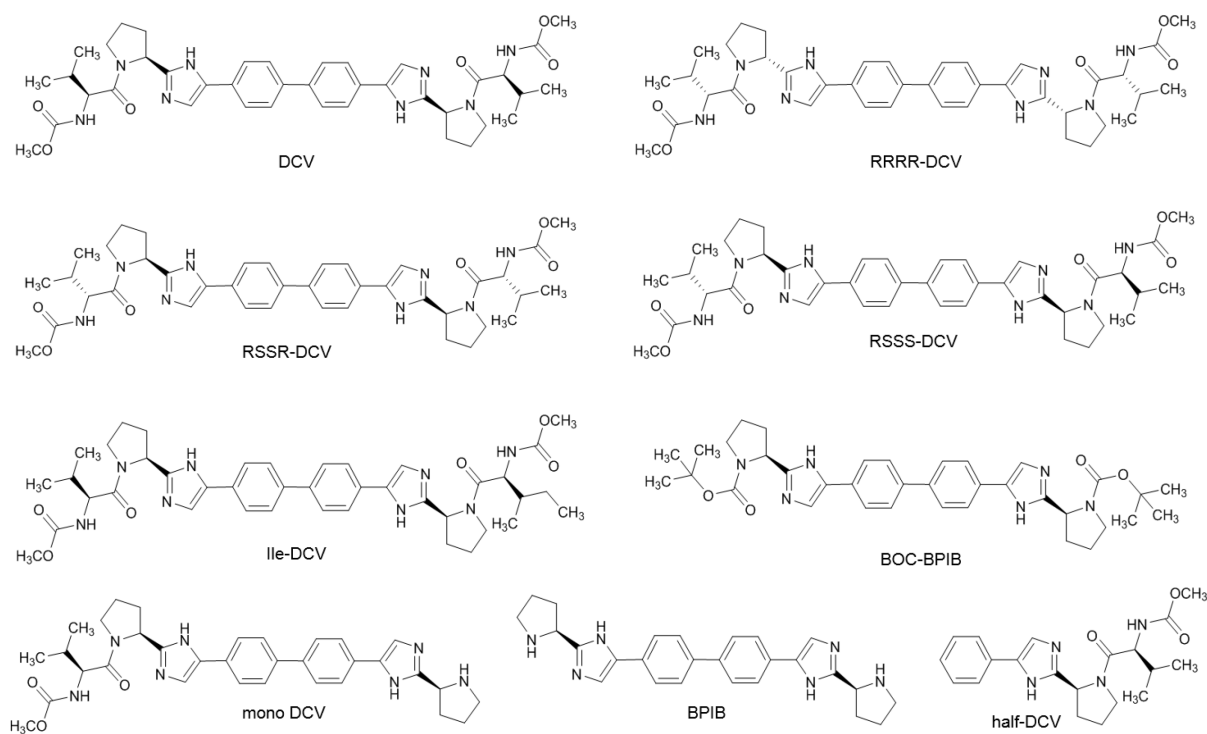
Figure 18 Structures of the DCV with 3 stereoisomers, the synthetic impurities BPIB, BOC-BPIB, Ile-DCV, mono DCV, and half-DCV

When screening CDs in sodium phosphate buffer, pH 2.5, as BGE for their ability to separate DCV and its enantiomer it was noted, that some CDs such as methyl-β-CD (M-β-CD) (Fig. 16A) or hydroxypropyl-β-CD yielded an enantioseparation, while two peaks with a plateau between them were observed in the case of other CDs such as γ-CD (Fig. 16B) or sulfated β-CD.

4.3.1. Unusual electrophoretic migration, dependence on solute structure and experimental conditions

4.3.1.1. Solute structure

The two peaks with a plateau in between, were also observed when enantiopure DCV or the enantiomer RRRR-DCV were analyzed in a γ-CD containing BGE at pH 2.5 (Fig. 19C and 19D), while a single peak

was detected for DCV or RRRR-DCV when M-β-CD was added to the BGE. Therefore, the plateau phenomenon is apparently not related to an enantiodifferentiation, and indicates an equilibrium, which is slow on the CE time scale since complexation equilibria between analytes and CDs in CE enantioseparations are very fast so that separate peaks are not detected for the free and complexed analyte.
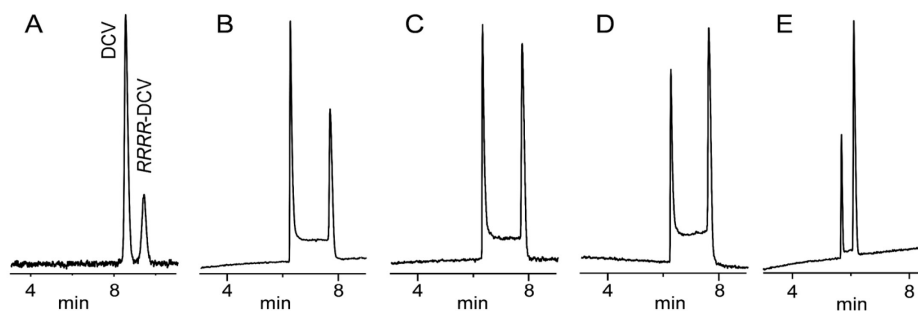
Figure 19 Electropherograms of **(A)** a nonracemic mixture of DCV and *RRRR*-DCV in the presence of 7 mg/mL M-β-CD in the BGE, **(B)** a nonracemic mixture of DCV and RRRR-DCV in the presence of 20 mM γ-CD in the BGE, **(C)** DCV in the presence of 20 mM γ-CD in the BGE, **(D)** RRRR-DCV in the presence of 20 mM

In addition, two diastereoisomers of DCV (RSSR-DCV and RSSS-DCV), a structural analogue containing Ile instead of Val as one of the amino acid moieties (Ile-DCV), a derivative that lacks one MOC-Val moiety (mono-DCV), two synthetic precursors, BPIB (lacking both MOC-Vals side chains) and the BOC-protected derivative BOC-BPIB, as well as the "monomeric" half-DCV were analyzed by CE (Fig. 18). Similarly to DCV, two peaks with a plateau in between were also observed for the R,S,S,R- and R,S,S,S-configured diastereomers as well as Ile-DCV (Fig 20), while only a single peak was observed for mono-DCV, half-DCV or the pyrrolidine derivatives BPIB and BOC-BPIB. Therefore, a structural prerequisite for the appearance of the plateau seems to be a "symmetrical" structure containing two MOC-amino acid moieties, which may, however, differ to some extent (as in Ile-DCV). The stereochemistry at the chiral centers did not play an important role as this behavior was seen with all available stereoisomers of DCV.
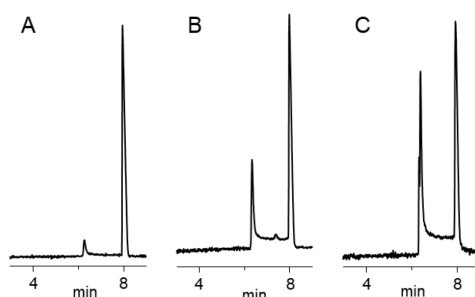
Figure 20 Electropherograms of the analysis of (A) RSSR-DCV, (B) RSSS-DCV, (C) Ile-DCV, using 50 mM sodium phosphate buffer, pH 2.5, containing 20 mM γ-CD as BGE.

4.3.1.2. Experimental CE conditions

The plateau was observed in the γ-CD concentration range up to 100 mM and could be detected at CD concentrations as low as 0.1 mM. The effects of the capillary temperature between 15°C and 45 °C (Fig. 21A) showed a dynamic behavior indicating in-capillary equilibria with two well separated peaks at slow exchange regimes at lower temperatures and progressive coalescence at higher temperatures. The plateau area between the resolved peaks became more pronounced under fast exchange regimes between 20 and 35 °C, eventually leading to complete coalescence at 45°C.
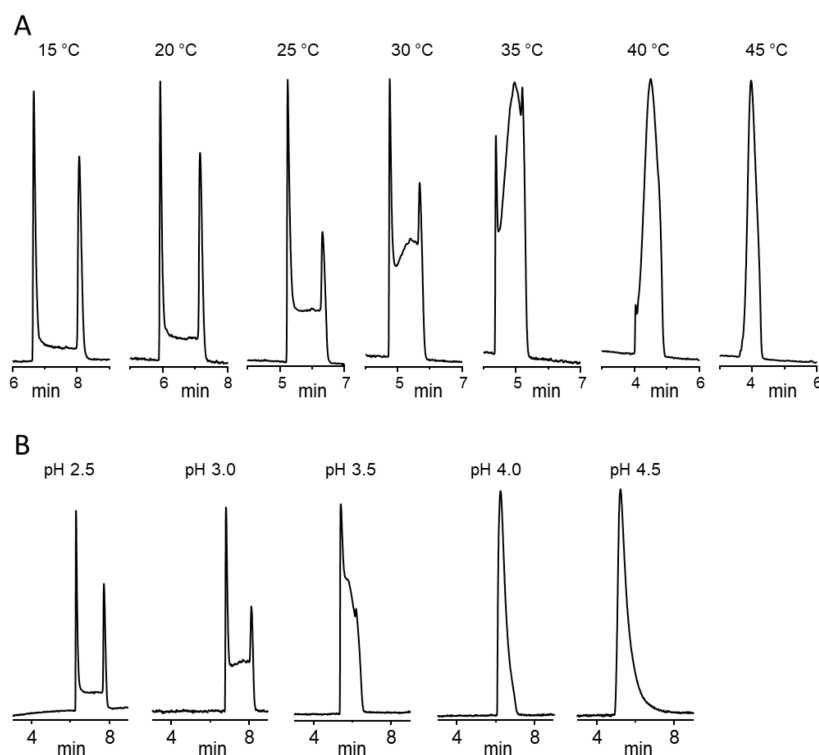
Figure 21 Electropherograms showing the effect of (A) temperature and (B) pH of the BGE using a 50 mM sodium phosphate buffer, pH 2.5, containing 20 mM γ-CD.

Upon increasing the pH of the BGE from 2.5 to 4.5 peak coalescence around pH 4 was observed (Fig. 21B). DCV possesses two basic imidazole nitrogen atoms with pKa values of 5.6 and 4.9 [126]. Thus, protonation of both imidazole nitrogen atoms appears to be a prerequisite for the observation of the slow equilibrium leading to the plateau in the CE experiments.

Surprisingly, when a sample of DCV mixed with γ-CD was analyzed by CE using a CD-free phosphate buffer-based BGE, pH 2.5, two peaks with a plateau in between were also observed (Fig. 19E). The plateau was independent of parameters for the preparation of the γ-CD-containing DCV sample solution. A temperature study revealed coalescence of the peaks also at about 45°C.

So far, such a phenomenon has not been described for CDs as chiral selectors. Therefore, a deep investigation was conducted to obtain some insight into the complexation between DCV and γ-CD. In addition to CE experiments, NMR, electrospray ionization mass spectrometry (ESI-MS) and CE-ESI-MS studies were conducted in order to obtain information on the structures involved in the equilibrium.

4.3.2. Structure of dynamic supramolecular complexes

The structures of the complexes of γ-CD with DCV, the RSSR diastereomer, mono-DCV as well as half-DCV were studied in deuterated sodium phosphate buffer pH 2.5 by ^{1}H-NMR experiments because nuclear Overhauser effect (NOE) based NMR methods, in particular ROESY techniques, allow the analysis of spatially close nuclei also in CD-based complexes [98; 100; 127; 128]. Signals were assigned based on COSY, TOCSY and HSQCED data. The following discussion is focused on the structures of DCV: γ-CD complexes.

The 1H-NMR spectrum of a sample containing DCV and γ-CD was compared with the spectra of γ-CD and DCV. The interpretation of the additional sets of 1H resonances and the chemical shifts together with a 2D ROESY experiment demonstrated the presence of two structurally different complexes in the solution. All observed intermolecular NOE responses involved the inner hydrogens of γ-CD (H-3 and H-5) and the aromatic protons of DCV, and indicated the presence of a 1:1 inclusion complex in addition to a 2:1 complex (DCV: γ-CD) in which two DCV molecules are inserted into the CD cavity. Further 2D and 1D ROESY experiments affirmed this assumption. Fig. 22. represents a schematic illustration of the tentative structures of both complexes.
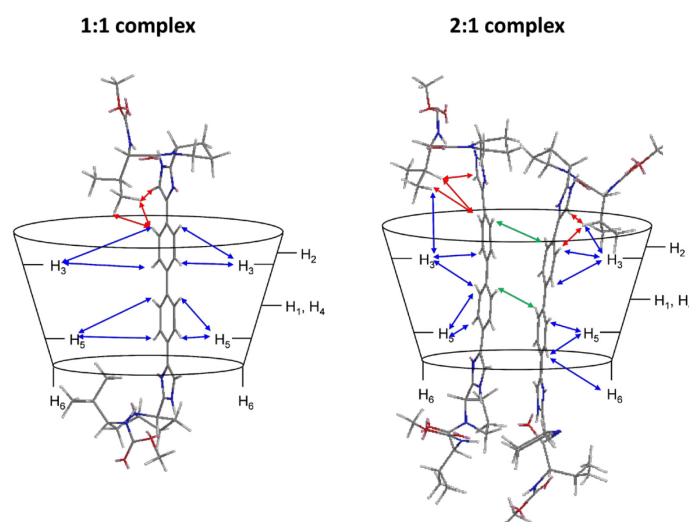
Figure 22 Schematic representation of the 1:1 and 2:1 complexes formed between DCV and γ-CD. The intermolecular NOEs derived from ROESY experiments are indicated by arrows; red: intramolecular NOEs, blue: intermolecular NOEs between DCV and γ-CD, green: intermolecular NOEs between DCV molecules in the 2:1 complex.

The ratio of the 1:1 versus the 2:1 complex was about 0.24:1.0 based on the integrals of NMR signal. Measuring the spectra at 40 °C, 60 °C and 80 °C resulted in ratio between the complexes of about 0.39:1.0, 0.9:1.0 and 2.3:1.0, respectively. Thus, the 2:1 complex is more abundant at lower temperatures, while the 1:1 complex is the major species at 80 °C with inversion of the ratio above 60 °C. Therefore, the peak coalescence at about 40 °C observed in the CE experiments is not based on the equilibrium between the complexes. Upon cooling the sample to 25 °C, the 1:1 versus 2:1 complex ratio returned to the original value of 0.24:1.0.

Because pH-dependent peak coalescence was observed in CE at pH 4.0, NMR experiments were also performed at this apparent pH. The ^{1}H-NMR spectra of DCV alone and mixed with γ-CD at pH 4.0 were essentially identical to the spectrum recorded at pH 2.5. Moreover, the data obtained from further NMR studies (as studied with the pH 2.5 buffer) also demonstrated the presence of identical 1:1 and 2:1 complexes at pH 4.0, with the molar ratio being 0.23:1.0 which is similar to pH 2.5. This proved that the plateau observed in CE is not due to an equilibrium between the two complexes.

The presence of both complexes in solution was confirmed by direct infusion ESI-TOF-MS of a solution containing DCV and γ-CD in ammonium formate buffer, pH 2.6, which confirms the NMR results on the concomitant formation of complexes with 1:1 and 2:1 stoichiometry between DCV and γ-CD in solution.

Several literature examples reported different stoichiometries of the cyclodextrins with guest molecules using different analytical approaches [105; 107; 106; 108], but the nature of the complexes (inclusion or "external" complex) cannot be concluded, unless NMR has been employed. Several reports demonstrated the formation of to 2:1 complexes involving CDs [129–132]. In most cases the stoichiometry of the complexes was derived from Job´s plots, while the orientation and stacking of both solutes within the CD cavity was derived from molecular modelling [129–131]. There are also reports of 2:1 complexes, in which one solute molecule was included in the CD cavity, while the second one was coordinated externally [39; 40; 133; 134]. Neither these studies nor the abovementioned publications on 2:1 aggregates provided evidence for the presence of two complexes with different stoichiometries in solution.

So far, only one publication could be found in the literature which reported the simultaneous presence of complexes with different stoichiometry (1:1 and 2:1) between dimetindene and carboxymethyl-β-CD [134], but the structures could not be unequivocally resolved in that study. In contrast, the presence of the two complexes between DCV and γ-CD including their stoichiometry was unequivocally demonstrated based on NMR and MS data.

In addition, the structures of the complexes of the diastereomeric RSSR-DCV as well as mono-DCV and half-DCV with γ-CD were determined by ^{1}H-NMR spectroscopy. Table 1 compares the CE behavior as well as complex stoichiometries, their ratios and structures of the guest molecules of DCV and the three analogues studied in more detail. Although the number of analytes is limited, a biphenyl structure appears to be required for the formation of a 2:1 complex. The stereochemistry of the amino acid moiety does not affect the simultaneous formation of two complexes but might change the ratio between them.

Table 8 CE behavior, stoichiometry and structure of γ-CD complexes with DCV and analogues

Compound	CE	Complex stoichiometry	Complex ratio	Structure of guest molecule(s) in complex(es)
DCV	Plateau	1:1 and 2:1	~ 0.24:1	Folded conformation of MOC-Val residues
RSSR-DCV	Plateau	1:1 and 2:1	~ 1:1	Extended conformation of MOC-Val residues in complexes
Mono-DCV	–	1:1 and 2:1*	~ 0.4:1	Folded conformation of MOC-Val residue in complexes
Half-DCV	–	1:1	–	Folded conformation of MOC-Val residue in complex

* no unequivocal proof of a 2:1 complex by NOEs but presence likely

4.3.3. Migration order

In order to confirm the role of interaction between DCV and γ-CD, the CE capillary was used as a microreactor. Individual plugs of DCV and γ-CD were injected in a capillary containing CD-free BGE, pH 2.5, which were separated by a short plug of buffer to prevent contact between the plugs due to diffusion. The results are shown in Fig. 23.
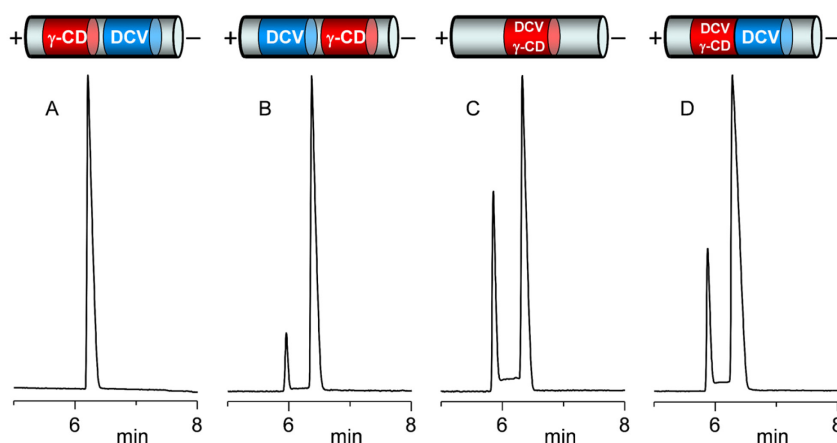
Figure 23 Plug-plug CE experiments. The order of the injected plugs is schematically shown above the electropherograms. Injection sequence: (A) DCV > γ-CD, (B) γ-CD > DCV, (C) DCV + γ-CD, (D) DCV > DCV + γ-CD. The BGE consisted of 50 mM sodium phosphate

When DCV was injected as the first plug so it did not migrate through the γ-CD plug only a single peak was detected (Fig. 23A), while two peaks with a plateau were found when DCV was injected as the second plug so that it had to migrate through the γ-CD plug on the way to the detector (Fig. 23B). Injecting a mixture of DCV and γ-CD also resulted in two peaks with a plateau (Fig. 23C). Moreover, the area of the second migrating peak increased significantly when a DCV-plug was injected before a plug

of a mixed DCV plus γ-CD sample (Fig. 23D), indicating that the first migrating peak represents the unresolved mixture of the 1:1 and 2:1 DCV-γ-CD complexes, while the second peak is due to free DCV.

This was confirmed by CE-MS experiments (Fig. 24). When analyzing pure DCV in a CD-free BGE, only a single peak with *m/z* 739.4 at the migration time of DCV is observed (Fig. 24A). In contrast, two peaks with the plateau were detected in the analysis of a sample containing DCV and γ-CD using a CD-free BGE (Fig. 24B). The trace of m/z 739.4 proved that DCV is present in the peaks as well as the plateau, while the mass traces m/z 925.4 and m/z 1018.4 representing the 2:1 and 1:1 complex, respectively, were only detected in the first migrating peak. When γ-CD is present in the BGE (Fig. 24C), the mass traces of the 1:1 and 2:1 complexes at m/z 925.4 and m/z 1018.4 as well as free DCV (m/z 739.4) were detected, while in the second migrating peak free DCV dominated. In contrast to the analysis of the DCV plus γ-CD sample analyzed in a CD-free BGE (Fig. 24B), the plateau is also formed by the complexes in addition to non-complexed DCV. This difference can be explained by the presence of γ-CD in the BGE. Free DCV resulting from the dissociation of the complexes can be complexed again if the CD is present in the BGE, while this is not possible in the absence of γ-CD in the BGE because in the latter case γ-CD and DCV are electrophoretically separated.
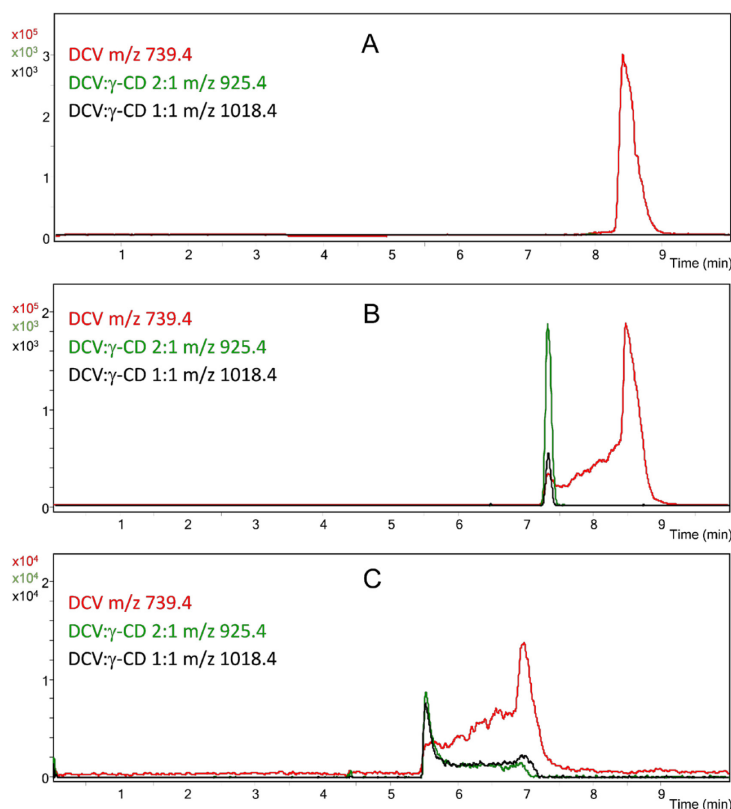
Figure 24 CE-MS experiments of **(A)** pure DCV and **(B)** a sample containing DCV and γ-CD using 50 mM ammonium formate buffer pH 2.6 as BGE. **(C)** CE-MS analysis of DCV using 50 mM ammonium formate buffer pH 2.6, containing 50 mM γ-CD as BGE.

The CE-MS data show that both complexes exhibit the same mobility so that they are not separated independent of the presence or absence of γ-CD in the BGE. This is also unexpected considering the theoretical difference in the mass-to-charge ratios of both complexes. Taking into account the low abundance of the ion representing the 1:1 complex in the experiments obtained in the absence of γCD in the BGE (Fig. 24B) it could be hypothesized that the 2:1 complex possesses a higher stability, which results in the fact that the complex can still be observed in a CD-free BGE injecting a sample containing DCV and γ-CD. Upon dissociation of one DCV molecule, the resulting 1:1 complex is considerably less stable and quickly liberates DCV, which cannot form a complex again because γ-CD and DCV are electrophoretically separated. In contrast, when γ-CD is present in the BGE, the complexes can be reestablished upon dissociation into γ-CD and DCV so that the plateau between the peaks is composed of all three species, i.e. both complexes as well as free DCV (Fig. 24C).

The faster migration of the complexes compared to free DCV as demonstrated by the plug-plug as well as CE-MS data is unexpected, because non-complexed DCV should have a higher charge density (charge-to-mass ratio) than the complex based on the molecular weight of the species and, consequently, migrate first. A speculative explanation could be based on differences in the solvation shell of the molecules/complexes assuming a larger shell in the case of free DCV. It is known that small inorganic ions such as Li^+ migrate slower than larger ions in CE [135] because of a much larger solvation shell [136].

5. Summary

The stereochemistry of the drugs plays in important in their pharmacological effects since the enantiomers of chiral drugs interact in a stereoselective way with the targets, which may lead to different activity or even undesirable effects. An increased awareness of the importance of the chiral purity of single isomer drugs led the development of separation methods for the quantitative determination of the chiral purity.

CE is a microanalytical technique that has been increasingly used in pharmaceutical analysis due to its advantages such as small sample volume, high resolution, low cost, and reduced use of organic solvents. In addition, chiral CE proved its efficiency as an established method analytical enantioseparations of drugs in the last decades with many examples in the literature. The development of chiral CE methods is particularly flexible due to the large number of available chiral selectors especially cyclodextrins, which have many neutral and charged derivatives in addition to the native α-CD, β-CD and γ-CD.

QbD methodology approach is the state-of-the-art strategy for method development in analytical separations including CE, due to the systematic approach which allows the understanding of the relative effects of the experimental factors and their interaction within a lower number of experiments compared to testing one factor each time. QbD employs multivariate DoE and risk-assessment tools for the identification of CPPs, which are the experimental factors that influence the CQAs of the method. Subsequently the knowledge space is identified by screening designs which provides an initial understanding of quantitative effects of the CQAs on the analytical process. This leads to fixing some experimental factors and the selection of other factors as CPPs to be further optimized using response surface designs. This allows the definition of the design space and selecting a working point. The robustness of the working point is tested by assessing the effects of deliberate small variations of the experimental parameters on the method. The assessment is made within QbD approach using a fractional factorial design (e.g. Plackett-Burman design). Considering this all, the risk based QbD framework was followed in analytical method development, optimization, and validation.

Consequently, three methods were developed for the determination of the enantiomeric purity of three drug substances Amb, DXM, and D-MDT using cyclodextrin-mediated capillary electrophoresis. All methods were validated according to the requirements of the ICH Q2(R1) guideline and proved robust with acceptable precision and accuracy for the determination of the chiral impurities. The methods were simple, cost effective, and had short run times which enables using them for routine analysis.

The working point conditions of chiral purity determination of Amb included a BGE of 50-mM sodium acetate buffer, pH 4.0, containing 30 mM γ-CD, in a 40/50.2 cm, 75 µm ID fused-silica capillary at an applied voltage of 25 kV and a capillary temperature of 25 °C. The method allowed the determination of a relative concentration of the (R)-enantiomer of 0.1 % within less than 10 minutes of run time and was subsequently applied to the analysis of an Amb sample obtained from a chemical supplier

The chiral purity method of DXM employed a 30/40.2 cm, 50 µm ID fused-silica capillary with a BGE consisting of 30 mM sodium phosphate buffer, pH 6.5, 16 mg/mL S-β-CD, and 14 mg/mL M-α-CD at 20°C and 20 kV. The method allowed the determination of LVM with acceptable precision and accuracy at the 0.1 % level within ca. 5 minutes of run time and was applied to the analysis of a capsule dosage form of DXM.

Furthermore, the apparent complexation constants and mobilities of the diastereomeric CD-enantiomer complexes were determined, in order to explain the chiral separation mechanisms for DXM, which led to the improvement of the peak shape by addition of M-α-CD to the S-β-CD-containing BGE. The stronger tailing of the LVM peak compared to the DXM peak especially at higher S-β-CD concentrations could be explained by the high mobility of the CD-LVM complex. Both enantiomers displayed essentially identical complex mobilities in the case of M-α-CD, which were also considerably lower than the mobilities of the corresponding S-β-CD complexes. This reduced the overall mobility of LVM and DXM, thereby improving the peak shape.

S-β-CD was chosen as chiral selector for the determination of the stereochemical purity of D-MDT. Separation after the EOF in a BGE pH 6.5 resulted in the desired migration order so that the minor impurity L-MDT migrated before the large peak of D-MDT. The working conditions were a 21.3/31.5 cm, 50 µm ID fused-silica capillary, a BGE composed of 50 mM sodium phosphate buffer, pH 6.5, containing 40 mg/mL sulfated β-CD, with a capillary temperature of 17°C and an applied voltage of 10 kV. The analysis time was less than 10 min, and this was the first CE method for the determination of the enantiomeric purity of D-MDT with acceptable precision and accuracy at the 0.1% level.

Moreover, the role of the cavity size and the substitution pattern of the cyclodextrins in the migration order of medetomidine enantiomers in the presence of CDs was investigated. This involved the opposite migration order in the presence of β-CD and γ-CD as well as S-β-CD and HS-β-CD, which was observed during the screening of various CDs as possible chiral selectors. The apparent complexation constants and complex mobilities of the diastereomeric CD–analyte complexes were determined by CE. Additionally, the complexation was studied in detail by NMR spectroscopy and molecular modeling.

S-β-CD was not included in NMR and molecular modeling because it is a mixture of positional and substitution isomers so that meaningful data could not be obtained by these techniques.

The enantioseparation in the case of β-CD as well as γ-CD was governed by the complexation constants. The opposite EMO In the case of β-CD and γ-CD could be explained by opposite affinities of the analyte enantiomers toward the respective CDs. D-MDT bound stronger to β-CD compared to L-MDT, while the opposite was found for γ-CD, and thus the stronger bound enantiomer migrates second.

Opposite recognition of the medetomidine enantiomers was also found for S-β-CD and HS-β-CD. D-MDT is complexed stronger than its enantiomer by S-β-CD, while L-MDT is complexed stronger than D-MDT by HS-β-CD. Contrary to β-CD and γ-CD, the separation of the MDT enantiomers with the negatively charged S-β-CD and HS-β-CD is governed by both, the complexation constants and the

complex mobilities. For S-β-CD, both enantioselective principles in CE cooperate leading to a large enantioresolution while they counteract each other in the case of HS-β-CD resulting in a loss of enantioseparation at higher CD concentrations.

NMR data supported the results of mechanistic CE studies. Thus, D-MDT was bound stronger by β-CD than L-MDT, which was also reflected in an enantioselective NOE of the resonance of the imidazole H-5 and H-6 of the phenyl moiety of the drug in ROESY experiments. In contrast, levomedetomidine was complexed stronger by γ-CD and HS-β-CD and a stronger NOE was observed for the phenyl H-6 in the presence of both CDs as well as the imidazole protons when complexed with HS-β-CD.

Molecular modeling also agreed with the structures derived from NMR experiments. In the case of β-CD and γ-CD, the phenyl ring of medetomidine entered the cavity through the wider secondary rim of the CDs, whereas the protonated imidazole ring was positioned inside the CD cavity interacting with the sulfate groups of HS-β-CD. Compared to CE and NMR data, enantioselective recognition of the medetomidine enantiomers by the CDs was also suggested by MD simulations and reflected the observed reversal of the enantiomer migration order in the case of β-CD and γ-CD.

Lastly, during a screening of CDs as chiral selectors for the separation of DCV and its enantiomer by CE, an unprecedented phenomenon for CDs was observed, that is two peaks with a plateau in between using γ-CD as chiral selector. The same result was encountered when enantiopure DCV was injected or when analyzing a sample containing enantiopure DCV and γ-CD in a CD-free background electrolyte. Coalescence of peaks was observed at 45 °C and at a pH above 3.5. Two peaks with a plateau were also observed for DCV stereoisomers as well as a structural analog. However, only a single peak was detected if one or both amino acid moieties of DCV were lacking. NMR experiments including NOE-based methods showed that in solution DCV adopted a folded conformation in which the isopropyl side chain of the valine residues pointed toward the aromatic rings of DCV. Moreover, NMR unequivocally demonstrated the simultaneous formation of DCV-γ-CD inclusion complexes with 1:1 and 2:1 stoichiometry, which was corroborated by mass spectrometry. In both complexes, DCV also adopted a folded structure. The RSSR-diastereomer of DCV as well as an analog lacking one of the amino acid moieties also formed 1:1 and 2:1 complexes with γ-CD although a plateau was only observed in the case of the RSSR-diastereomer. As shown by CE-MS, both DCV-γ-CD complexes surprisingly comigrated as the first peak, while the second migrating peak represents non-complexed DCV.

6. Zusammenfassung

Die Stereochemie der Arzneimittel spielt für ihre pharmakologischen Wirkungen eine wichtige Rolle, da die Enantiomere chiraler Arzneimittel stereoselektiv mit den molekularen Targets interagieren, was zu unterschiedlichen Aktivitäten oder sogar unerwünschten Wirkungen führen kann. Die Bedeutung der Stereochemie von Arzneistoffen führte zur Entwicklung von Trennmethoden zur Bestimmung der chiralen Reinheit.

CE ist eine mikroanalytische Technik, die aufgrund ihrer Vorteile wie kleinem Probenvolumen, hoher Auflösung, geringen Kosten und reduziertem Einsatz organischer Lösungsmittel zunehmend in der pharmazeutischen Analyse eingesetzt wird. Darüber hinaus ist die chirale CE eine etablierte Methode zur analytischen Enantiomerentrennung von Arzneimitteln, was durch zahlreiche Literaturbeispiele belegt ist. Die Entwicklung chiraler CE-Methoden ist besonders flexibel aufgrund der großen Anzahl verfügbarer chiraler Selektoren, insbesondere Cyclodextrinen, die neben nativen α-CD, β-CD und γ-CD viele neutrale und geladene Derivate beinhalten.

Die QbD-Methodik ist die aktuelle Strategie für die Methodenentwicklung bei analytischen Trennungen einschließlich der CE. Dies beruht auf dem systematischen Ansatz, der es ermöglicht, die relativen Auswirkungen der experimentellen Faktoren und ihre Wechselwirkung untereinander mit einer geringeren Anzahl von Experimenten zu verstehen, anstatt nur jeweils einen Faktor zu variieren. QbD verwendet statistische Versuchsplanung und Risikobewertungsinstrumente zur Identifizierung von CPPs, welche die experimentellen Faktoren sind, die die CQAs der Methode beeinflussen. Anschließend wird der sogenannte Knowlege Space durch ein Screening-Design identifiziert, das ein erstes Verständnis der quantitativen Auswirkungen der CQAs auf den Analyseprozess liefert. Dies führt dazu, dass einige experimentelle Faktoren festgelegt und andere Faktoren als CPPs ausgewählt werden, die mithilfe von Response Surface-Methodik weiter optimiert werden sollen. Dies ermöglicht die Definition des Design Space und die Auswahl eines Arbeitspunkts. Die Robustheit des Arbeitspunkts wird getestet, indem die Auswirkungen absichtlicher kleiner Variationen der experimentellen Parameter auf die Methode bewertet werden. Dies erfolgt im Rahmen der QbD-Methodik unter Verwendung eines fraktionalen faktoriellen Designs (z. B. Plackett-Burman-Design). In Anbetracht aller bisherigen Aspekte wurde das risikobasierte QbD-Methodik bei der Entwicklung, Optimierung und Validierung von Analysemethoden befolgt.

Folglich wurden drei Methoden zur Bestimmung der Enantiomerenreinheit von drei Wirkstoffen Ambrisentan (Amb), Dextromethorphan (DMX) und Dexmedetomidin (D-DMT) mittels Kapillarelektrophorese unter Verwendung von CDs als chiralen Selektoren entwickelt. Alle Methoden wurden gemäß den Anforderungen der ICH Q2 (R1) -Richtlinie validiert und erwiesen sich als robust mit akzeptabler Präzision und Genauigkeit für die Bestimmung der chiralen Verunreinigungen. Die Methoden waren unkompliziert, kostengünstig und hatten kurze Laufzeiten, so dass sie für Routineanalysen verwendet werden können.

Die Arbeitspunktbedingungen der chiralen Reinheitsbestimmung von Amb umfassten eine BGE von 50 mM Natriumacetatpuffer, pH 4,0, mit 30 mM γ-CD, in einer 40/50,2 cm, 75 µm ID Quarzglaskapillare bei einer angelegten Spannung von 25 kV und einer Kapillartemperatur von 25° C. Die Methode ermöglichte die Bestimmung einer relativen Konzentration des (R)-Enantiomers von 0,1% innerhalb von weniger als 10 Minuten Laufzeit und wurde anschließend auf die Analyse einer Ambrisentan Probe angewendet.

Bei der chiralen Reinheitsmethode von DXM wurde eine Quarzglaskapillare mit 30/40,2 cm und 50 µm ID und einer BGE verwendet, der aus 30 mM Natriumphosphatpuffer, pH 6,5, 16 mg/ml S-β-CD und 14 mg/ml M-α-CD bestand. Die Kapillartemperatur beträgt 20° C bei einer angelegten Spannung von 20 kV. Die Methode ermöglichte die Bestimmung von LVM mit akzeptabler Präzision und Genauigkeit bei 0,1% innerhalb von ca. 5 Minuten Laufzeit und wurde zur Analyse einer Dextromethorphankapsel angewendet.

Darüber hinaus wurden die scheinbaren Komplexierungskonstanten und Mobilitäten der diastereomeren CD-Enantiomerkomplexe bestimmt, um die chiralen Trennungsmechanismen für DXM zu erklären, die zur Verbesserung der Peakform durch Zugabe von M-α-CD zum S-β-CD-haltiges BGE führten. Das stärkere Tailing des LVM-Peaks im Vergleich zum DXM-Peak, insbesondere bei höheren S-β-CD-Konzentrationen, könnte durch die hohe Mobilität des CD-LVM-Komplexes erklärt werden. Beide Enantiomere zeigten im Fall von M-α-CD ähnliche komplexe Mobilitäten, die ebenfalls erheblich niedriger waren als die Mobilitäten der entsprechenden S-β-CD-Komplexe. Dies verringerte die Gesamtmobilität von LVM und DXM, wodurch die Peakform verbessert wurde.

S-β-CD wurde als chiraler Selektor zur Bestimmung der stereochemischen Reinheit von D-MDT ausgewählt. Die Trennung nach dem EOF in einem BGE pH 6,5 führte zu der gewünschten Migrationsreihenfolge, so dass die Verunreinigung L-MDT vor dem großen Peak von D-MDT wanderte. Für die Trennung wurde eine Quarzglaskapillare mit 21,3/31,5 cm und 50 µm ID verwandt, mit einem BGE aus 50 mM Natriumphosphatpuffer, pH 6,5, enthaltend 40 mg/ml sulfatiertes β-Cyclodextrin und eine Kapillartemperatur von 17° C und eine angelegte Spannung von 10 kV. Die Analysezeit betrug weniger als 10 Minuten, und dies war die erste CE-Methode zur Bestimmung der Enantiomerenreinheit von D-MDT mit akzeptabler Präzision und Richtigkeit bei 0,1%.

Darüber hinaus wurde die Rolle der Größe der Kavität und des Substitutionsmusters der CDs in der Migrationsreihenfolge der Medetomidin-Enantiomere untersucht. Dies beinhaltete die entgegengesetzte Migrationsreihenfolge in Gegenwart von β-CD und γ-CD sowie S-β-CD und HS-β-CD, die während des Screenings verschiedener CDs als mögliche chirale Selektoren beobachtet wurde. Die scheinbaren Komplexierungskonstanten und Komplexmobilitäten der diastereomeren CD-Analyt-Komplexe wurden durch CE bestimmt. Zusätzlich wurde die Struktur der Komplexe durch Kernspinresonanzspektroskopie und molekulare Modellierung detailliert untersucht. S-β-CD wurde nicht in die Kernspinresonanzspektroskopie und Molekülmodellierung einbezogen, da es eine Mischung aus Positions- und Substitutionsisomeren ist, so dass mit diesen Techniken keine aussagekräftigen Daten erhalten werden konnten.

Die Enantiomerentrennung sowohl mit β-CD als auch mit γ-CD wurde durch die Komplexierungskonstanten beeinflusst. Die entgegengesetzte Migrationsreihenfolge im Fall von β-CD und γ-CD könnte durch entgegengesetzte Affinitäten der Enantiomere zu den jeweiligen CDs erklärt werden. D-MDT wurde im Vergleich zu L-MDT stärker an β-CD gebunden, während für γ-CD das Gegenteil gefunden wurde und somit das stärker gebundene Enantiomer an zweiter Stelle wandert.

Eine entgegengesetzte Erkennung der MDT-Enantiomere wurde auch für S-β-CD und HS-β-CD gefunden. Dexmedetomidin wird mit S-β-CD stärker als sein Enantiomer komplexiert, während Levomedetomidin mit HS-β-CD stärker als Dexmedetomidin komplexiert wird. Im Gegensatz zu β-CD und γ-CD wird die Trennung der MDT-Enantiomere mit dem negativ geladenen S-β-CD und HS-β-CD sowohl von den Komplexierungskonstanten als auch von den komplexen Mobilitäten beeinflusst. Bei S-β-CD wirken beide enantioselektiven Mechanismen in CE zusammen, was zu einer großen Enantioresolution führt, während sie sich im Fall von HS-β-CD gegenseitig entgegenwirken, was bei höheren CD-Konzentrationen zu einem Verlust der Enantioseparation führt.

NMR-Daten bestätigten die Ergebnisse mechanistischer CE-Studien. D-MDT wurde durch β-CD stärker gebunden als L-MDT, was sich auch in einem enantioselektiven Kern-Overhauser-Effekt der Resonanz des Imidazols H-5 und H-6 der Phenyleinheit des Arzneimittels in ROESY-Experimenten zeigte. Im Gegensatz dazu wurde L-MDT mit γ-CD und HS-β-CD stärker komplexiert, und ein stärkeres Kern-Overhauser-Effekt wurde für das Phenyl H-6 in Gegenwart beider CDs sowie der Imidazolprotonen beobachtet, wenn es mit HS-β-CD komplexiert wurde.

Die molekulare Modellierung stimmte auch mit den aus NMR-Experimenten abgeleiteten Strukturen überein. Im Fall von β-CD und γ-CD trat der Phenylring von Medetomidin durch den breiteren Sekundärrand der CDs in den Hohlraum ein, während der protonierte Imidazolring innerhalb des CD-Hohlraums positioniert war und mit den Sulfatgruppen von HS-β-CD interagierte. Wie aus CE- und NMR-Daten hervorgeht, wurde die enantioselektive Erkennung der MDT-Enantiomere durch die CDs auch durch Moleküldynamik-Simulationen vorgeschlagen und spiegelte die beobachtete Umkehrung der Enantiomeren-Migrationsreihenfolge im Fall von β-CD und γ-CD wider.

Schließlich, Während eines Screenings von CDs als chirale Selektoren für die Trennung von DCV und seinem Enantiomer durch Kapillarelektrophorese wurde ein bislang beispielloses Phänomen für CDs beobachtet. In Gegenwart von γ-CD wurden zwei Peaks mit einem Plateau beobachtet. Das gleiche Ergebnis wurde erzielt, wenn enantiomerenreines DCV injiziert wurde oder wenn eine Probe, die enantiomerenreines DCV und γ-CD enthielt, in einem CD-freien BGE analysiert wurde. Koaleszenz der Peaks wurde bei 45 ° C und einem pH-Wert über 3,5 beobachtet. Zwei Peaks mit einem Plateau wurden auch für DCV-Stereoisomere sowie ein Strukturanalogon beobachtet. Es wurde jedoch nur ein einziger Peak nachgewiesen, wenn eine oder beide Aminosäureeinheiten von DCV fehlten. NMR-Experimente, einschließlich auf dem Kern-Overhauser-Effekt basierender Methoden, zeigten, dass DCV in Lösung eine gefaltete Konformation annahm, bei der die Isopropylseitenkette der Valinreste auf die aromatischen Ringe von DCV zeigte. Darüber hinaus zeigte NMR eindeutig die gleichzeitige Bildung

von DCV-γ-CD-Einschlusskomplexen mit 1:1- und 2:1-Stöchiometrie, was durch Massenspektrometrie bestätigt wurde. In beiden Komplexen nahm DCV auch eine gefaltete Struktur an. Das RSSR-Diastereomer von DCV sowie ein Analogon ohne eine der Aminosäureeinheiten bildeten ebenfalls 1:1- und 2:1-Komplexe mit γ-CD, obwohl nur im Fall des RSSR-Diastereomers ein Plateau beobachtet wurde. Wie durch CE-MS gezeigt, wanderten beide DCV-γ-CD-Komplexe überraschenderweise als erster Peak zusammen, während der zweite wandernde Peak nicht komplexiertes DCV darstellt.

References

[1]   EMA, Investigation of chiral active substances, https://www.ema.europa.eu/documents/scientific-guideline/investigation-chiral-active-substances_en.pdf, 1993.

[2]   Morris, D.G., "Stereochemistry", in: Abel, E.W., ed., *Stereochemistry,* The Royal Society of Chemistry, Cambridge, pp. 19–59, 2001.

[3]   Cushny, A.R., *JAMA*, Vol. 87, 962, 1926.

[4]   Nguyen, L.A., He, H., and Pham-Huy, C., *Int J Biomed Sci*, Vol. 2, 85–100, 2006.

[5]   Guo-Qiang Lin, Jian-Ge Zhang, and Jie-Fei Cheng, "Overview of Chirality and Chiral Drugs", in: *Chiral Drugs,* John Wiley & Sons, Ltd, pp. 3–28, 2011.

[6]   Gross, M., "Chapter 34. Significance of Drug Stereochemistry in Modern Pharmaceutical Research and Development", in: Bristol, J.A., ed., *Annual Reports in Medicinal Chemistry,* Academic Press, pp. 323–331, 1990.

[7]   Ariëns, E.J., *Eur J Clin Pharmacol*, Vol. 26, 663–668, 1984.

[8]   Chhabra, N., Aseri, M.L., and Padmanabhan, D., *Int. J. Appl. Basic Med. Res.*, Vol. 3, 16, 2013.

[9]   McConathy, J., and Owens, M.J., *Prim Care Companion J Clin Psychiatry*, Vol. 5, 70–73, 2003.

[10]   Cormack, J.R., Orme, R.M., and Costello, T.G., *J Clin Neurosci*, Vol. 12, 375–378, 2005.

[11]   Jones, C.R., *Int Anesthesiol Clin*, Vol. 51, 81–96, 2013.

[12]   Savola, J.-M., and Virtanen, R., *Eur. J. Pharmacol.*, Vol. 195, 193–199, 1991.

[13]   Vickery, R.G., Sheridan, B.C., Segal, I.S., and Maze, M., *Anesth Analg*, Vol. 67, 611–615, 1988.

[14]   Lauterbach, E.C., Shillcutt, S.D., and Phillips, D.E., "Chapter 71 - Dextromethorphan and Dextrorphan as Heuristic Rapid-Acting, Conventional, and Treatment-Resistant Antidepressants, with Substance Abuse Considerations", in: Preedy, V.R., ed., *Neuropathology of drug addictions and substance misuse,* Academic Press, London, pp. 707–717, 2016.

[15]   INCB, List of narcotic drugs under international control, http://www.incb.org/documents/Narcotic-Drugs/Yellow_List/55th_Edition/YL_-55th_edition_2016.pdf.

[16]   Shimazawa, R., Nagai, N., Toyoshima, S., and Okuda, H., *J. Health Sci.*, Vol. 54, 23–29, 2008.

[17]   Stinson, S.C., *Chem. Eng. News*, Vol. 75, 38–70, 1997.

[18]   Agranat, I., Caner, H., and Caldwell, J., *Nat Rev Drug Discov*, Vol. 1, 753–768, 2002.

[19]   Tucker, G.T., *Lancet*, Vol. 355, 1085–1087, 2000.

[20]   Agranat, I., and Wainschtein, S.R., *Drug Discov. Today*, Vol. 15, 163–170, 2010.

[21]   Baglai, I., Leeman, M., Kaptein, B., Kellogg, R.M., and Noorduin, W.L., *Chem. Commun. (Camb.)*, Vol. 55, 6910–6913, 2019.

[22]   Pypendop, B.H., "Chapter 10 - α2-Agonists*", in: Gaynor, J.S., and Muir, W.W., eds., *Handbook of veterinary pain management,* Elsevier/Mosby, St. Louis, Missouri, pp. 196–215, 2015.

[23]   https://www.accessdata.fda.gov/drugsatfda_docs/label/2013/021038s021lbl.pdf.

[24]   Murakami, H., "From Racemates to Single Enantiomers – Chiral Synthetic Drugs over the last20 Years", in: Sakai, K., Hirayama, N., and Tamura, R., eds., *Novel Optical Resolution Technologies,* Springer-Verlag, Berlin, Heidelberg, pp. 273–299, 2007.

[25]   Calcaterra, A., and D'Acquarica, I., *J Pharm Biomed Anal*, Vol. 147, 323–340, 2018.

[26]   Gellad, W.F., Choi, P., Mizah, M., Good, C.B., and Kesselheim, A.S., *Am J Manag Care*, Vol. 20, e90-7, 2014.

[27]   Agranat, I., and Caner, H., *Drug Discov. Today*, Vol. 4, 313–321, 1999.

[28]   FDA, Development of New Stereoisomeric Drugs, https://www.fda.gov/regulatory-information/search-fda-guidance-documents/development-new-stereoisomeric-drugs, 1992.

[29]   Williams, R.C., Riley, C.M., Sigvardson, K.W., Fortunak, J., Ma, P., Nicolas, E.C., Unger, S.E., Krahn, D.F., and Bremner, S.L., *J Pharm Biomed Anal*, Vol. 17, 917–924, 1998.

[30]   Camp, W.H. de, *J Pharm Biomed Anal*, Vol. 11, 1167–1172, 1993.

[31]   ICH, Specifications: New Chemical Drug Substances and Products Q6A, https://database.ich.org/sites/default/files/Q6A%20Guideline.pdf, 1999.

[32]   ICH, Impurities in New Drug Products Q3B (R2), https://database.ich.org/sites/default/files/Q3B%28R2%29%20Guideline.pdf, 2006.

[33]   ICH, Impurities in New Drug Substances Q3A (R2), https://database.ich.org/sites/default/files/Q3A%28R2%29%20Guideline.pdf, 2006.

[34]   WHO Drug Alert No. 126, http://www.who.int/medicines/publications/drugalerts/Final_Alert_126_Information_on_Dextromethorphan.pdf, 2013.

[35]   WHO Drug Alert No. 129, http://www.who.int/medicines/publications/drugalerts/App_Drug_Alert_No_129_Paraguay_Dextro.pdf, 2013.

[36]   *The United States pharmacopeia,* United States Pharmacopeial Convention, Rockville, Maryland, 4 volumes, 2016.

[37]   *The international pharmacopoeia,* 6th ed., World Health Organization, Geneva, 2016.

[38]   *European Pharmacopoeia, 9th edition 2016, English,* 1st ed., Deutscher Apotheker Verlag, Stuttgart, 2016.

[39]   Landers, J.P., *Handbook of capillary and microchip electrophoresis and associated microtechniques,* 3rd ed., Taylor & Francis Group, Boca Raton, FL, 2008.

[40]   Kenndler, E., *J Chromatogr A*, Vol. 1335, 16–30, 2014.

[41]   de Jong, G., "Detection in Capillary Electrophoresis - An Introduction", in: de Jong, G., ed., *Capillary electrophoresis - mass spectrometry (CE-MS),* Wiley-VCH, Weinheim, pp. 1–5, 2016.

[42]   Altria, K.D., *Capillary electrophoresis guidebook,* Humana, Totowa, N.J., 1996.

[43]   Chagas, C.L.S., Moreira, R.C., Bressan, L.P., de Jesus, D.P., da Silva, J.A.F., and Coltro, W.K.T., "Instrumental Platforms for Capillary and Microchip Electromigration Separation Techniques", in: Poole, C.F., ed., *Capillary electromigration separation methods,* Elsevier, Amsterdam, pp. 269–292, 2018.

[44]   Thormann, W., "Theoretical Principles of Capillary Electromigration Methods", in: Poole, C.F., ed., *Capillary electromigration separation methods,* Elsevier, Amsterdam, pp. 21–44, 2018.

[45]   Shallan, A., Guijt, R., and Breadmore, M., "Capillary Electrophoresis: Basic Principles", in: Siegel, J.A., and Saukko, P.J., eds., *Encyclopedia of Forensic Sciences,* Academic, Oxford, pp. 549–559, 2013.

[46]   Buszewski, B., Dziubakiewicz, E., and Szumski, M., *Electromigration techniques,* Springer, Heidelberg, 2013.

[47]   Doherty, E.A.S., Meagher, R.J., Albarghouthi, M.N., and Barron, A.E., *Electrophoresis*, Vol. 24, 34–54, 2003.

[48]   Wehr, T., "Capillary Zone Electrophoresis", in: Meyers, R.A., ed., *Encyclopedia of Physical Science and Technology,* Academic, San Diego, London, pp. 355–368, 2002.

[49]   Rabel, S.R., and Stobaugh, J.F., *Pharm Res*, Vol. 10, 171–186, 1993.

[50]   Holzgrabe, U., Schmitt, S., and Wienen, F., "Micellar Electrokinetic Chromatography of Aminoglycosides", in: Schmitt-Kopplin, P., ed., *Capillary electrophoresis,* Humana Press, New York, pp. 77–90, 2016.

[51]   Wren, S.A., *Electrophoresis*, Vol. 16, 2127–2131, 1995.

[52]   Scriba, G.K.E., Harnisch, H., and Zhu, Q., "Enantiomer Separations by Capillary Electrophoresis", in: Schmitt-Kopplin, P., ed., *Capillary electrophoresis,* Humana Press, New York, pp. 277–299, 2016.

[53]   Wren, S.A.C., *J. Chromatogr. A*, Vol. 636, 57–62, 1993.

[54]   Rizzi, A., *Electrophoresis*, Vol. 22, 3079–3106, 2001.

[55]   Hammitzsch-Wiedemann, M., and Scriba, G.K.E., *Anal Chem*, Vol. 81, 8765–8773, 2009.

[56]   Chankvetadze, B., Lindner, W., and Scriba, G.K.E., *Anal Chem*, Vol. 76, 4256–4260, 2004.

[57]   Gübitz, G., and Schmid, M.G., *J Chromatogr A*, Vol. 1204, 140–156, 2008.

[58]   Scriba, G.K.E., "Recognition Mechanisms of Chiral Selectors: An Overview", in: Scriba, G.K.E., ed., *Chiral separations,* Humana Press, New York, NY, pp. 1–33, 2019.

[59]   Scriba, G.K.E., and Jáč, P., "Cyclodextrins as Chiral Selectors in Capillary Electrophoresis Enantioseparations", in: Scriba, G.K.E., ed., *Chiral separations,* Humana Press, New York, NY, pp. 339–356, 2019.

[60]   Wren, S., Berger, T.A., Boos, K.-S., Engelhardt, H., Adlard, E.R., Davies, I.W., Altria, K.D., and Stock, R., "The Use of Cyclodextrins as Chiral Selectors", in: Berger, T.A., Boos, K.-S., Engelhardt, H., and Wren, S., eds., *The Separation of Enantiomers by Capillary Electrophoresis,* Springer Vieweg, Wiesbaden, pp. 59–77, 2001.

[61]   Evans, C.E., and Stalcup, A.M., *CHIRALITY*, Vol. 15, 709–723, 2003.

[62]   Chankvetadze, B., *Capillary electrophoresis in chiral analysis,* Wiley, Chichester, 1997.

[63]   Schurig, V., *Ann Pharm Fr*, Vol. 68, 82–98, 2010.

[64]   Xiao, Y., Ng, S.-C., Tan, T.T.Y., and Wang, Y., *J Chromatogr A*, Vol. 1269, 52–68, 2012.

[65]   Kemp, G., *Biotechnol. Appl. Biochem.*, Vol. 27, 9–17, 1998.

[66]   Sánchez-Hernández, L., Guijarro-Diez, M., Marina, M.L., and Crego, A.L., *Electrophoresis*, Vol. 35, 12–27, 2014.

[67]   Zhu, Q., and Scriba, G.K.E., *J Pharm Biomed Anal*, Vol. 147, 425–438, 2018.

[68]   El Deeb, S., Wätzig, H., Abd El-Hady, D., Sänger-van de Griend, C., and Scriba, G.K.E., *Electrophoresis*, Vol. 37, 1591–1608, 2016.

[69]   Deeb, S.E., Wätzig, H., El-Hady, D.A., Albishri, H.M., Sänger-van de Griend, C., and Scriba, G.K.E., *Electrophoresis*, Vol. 35, 170–189, 2014.

[70]   Altria, K., Marsh, A., and Sänger-van de Griend, C., *Electrophoresis*, Vol. 27, 2263–2282, 2006.

[71]   Suntornsuk, L., *Anal. Bioanal. Chem.*, Vol. 398, 29–52, 2010.

[72]   Scriba, G.K.E., *Electrophoresis*, Vol. 24, 2409–2421, 2003.

[73]   Ha, P.T.T., Hoogmartens, J., and van Schepdael, A., *J. Pharm. Biomed. Anal.*, Vol. 41, 1–11, 2006.

[74]   Preinerstorfer, B., Lämmerhofer, M., and Lindner, W., *Electrophoresis*, Vol. 30, 100–132, 2009.

[75]   Scriba, G.K.E., *J Pharm Biomed Anal*, Vol. 55, 688–701, 2011.

[76]   Lu, H., and Chen, G., *Anal. Methods*, Vol. 3, 488, 2011.

[77]   Ját, P., and Scriba, G.K.E., *J. Sep. Sci.*, Vol. 36, 52–74, 2013.

[78]   Holzgrabe, U., Brinz, D., Kopec, S., Weber, C., and Bitar, Y., *Electrophoresis*, Vol. 27, 2283–2292, 2006.

[79]   Rozet, E., Lebrun, P., Hubert, P., Debrus, B., and Boulanger, B., *Trends Anal Chem*, Vol. 42, 157–167, 2013.

[80]   Orlandini, S., Gotti, R., and Furlanetto, S., *J Pharm Biomed Anal*, Vol. 87, 290–307, 2014.

[81]   Hanrahan, G., and Gomez, F.A., *Chemometric methods in capillary electrophoresis,* Wiley, Hoboken, N.J., 1 online resource (xxi, 431, 2009.

[82]   Hubert, C., Houari, S., Rozet, E., Lebrun, P., and Hubert, P., *J Chromatogr A*, Vol. 1395, 88–98, 2015.

[83]   Sänger-van de Griend, C.E., and van Schepdael, A., "Method Development and Validation of Capillary Electromigration Methods", in: Poole, C.F., ed., *Capillary electromigration separation methods,* Elsevier, Amsterdam, pp. 235–267, 2018.

[84]   Orlandini, S., Pinzauti, S., and Furlanetto, S., *Anal Bioanal Chem*, Vol. 405, 443–450, 2013.

[85]   ICH, Pharmaceutical development Q8 (R2), https://database.ich.org/sites/default/files/Q8%28R2%29%20Guideline.pdf, 2009.

[86]   ICH, Quality risk management Q9, https://database.ich.org/sites/default/files/Q9%20Guideline.pdf, 2005.

[87]   Vogt, F.G., and Kord, A.S., *J Pharm Sci*, Vol. 100, 797–812, 2011.

[88]   Bezerra, M.A., Santelli, R.E., Oliveira, E.P., Villar, L.S., and Escaleira, L.A., *Talanta*, Vol. 76, 965–977, 2008.

[89]   Ferreira, S.L.C., Bruns, R.E., da Silva, E.G.P., Dos Santos, W.N.L., Quintella, C.M., David, J.M., Andrade, J.B. de, Breitkreitz, M.C., Jardim, I.C.S.F., and Neto, B.B., *J Chromatogr A*, Vol. 1158, 2–14, 2007.

[90]   ICH, Validation of Analytical Procedures: Text And Methodology Q2(R1), https://database.ich.org/sites/default/files/Q2%28R1%29%20Guideline.pdf, 2005.

[91]   Lämmerhofer, M., *J Chromatogr A*, Vol. 1217, 814–856, 2010.

[92]   Scriba, G.K.E., *Chromatographia*, Vol. 75, 815–838, 2012.

[93]   Scriba, G.K.E., *J Chromatogr A*, Vol. 1467, 56–78, 2016.

[94]   Chankvetadze, B., Schulte, G., Bergenthal, D., and Blaschke, G., *J Chromatogr A*, Vol. 798, 315–323, 1998.

[95]   Chankvetadze, L., Servais, A.-C., Fillet, M., Salgado, A., Crommen, J., and Chankvetadze, B., *J Chromatogr A*, Vol. 1267, 206–216, 2012.

[96]   Gogolashvili, A., Tatunashvili, E., Chankvetadze, L., Sohajda, T., Szeman, J., Salgado, A., and Chankvetadze, B., *Electrophoresis*, Vol. 38, 1851–1859, 2017.

[97]   Chankvetadze, B., *Chem Soc Rev*, Vol. 33, 337–347, 2004.

[98]   Dodziuk, H., Koźmiński, W., and Ejchart, A., *CHIRALITY*, Vol. 16, 90–105, 2004.

[99]   Mura, P., *J Pharm Biomed Anal*, Vol. 101, 238–250, 2014.

[100]   Salgado, A., and Chankvetadze, B., *J Chromatogr A*, Vol. 1467, 95–144, 2016.

[101]   Zhang, C., Woolfork, A.G., Suh, K., Ovbude, S., Bi, C., Elzoeiry, M., and Hage, D.S., *J Pharm Biomed Anal*, Vol. 177, 112882, 2020.

[102]   Nevídalová, H., Michalcová, L., and Glatz, Z., *Electrophoresis*, Vol. 40, 625–642, 2019.

[103]   Yu, F., Zhao, Q., Zhang, D., Yuan, Z., and Wang, H., *Anal Chem*, Vol. 91, 372–387, 2019.

[104]   Galievsky, V.A., Stasheuski, A.S., and Krylov, S.N., *Anal Chem*, Vol. 87, 157–171, 2015.

[105]   Dodziuk, H., *Cyclodextrins and their complexes,* Wiley-VCH, Weinheim, 489 p., 2006.

[106]   Rekharsky, M.V., and Inoue, Y., *Chem Rev*, Vol. 98, 1875–1918, 1998.

[107]   Connors, K.A., *Chem Rev.*, Vol. 97, 1325–1358, 1997.

[108]   Pasquini, B., Melani, F., Caprini, C., Del Bubba, M., Pinzauti, S., Orlandini, S., and Furlanetto, S., *J Pharm Biomed Anal*, Vol. 144, 220–229, 2017.

[109]   Greño, M., Salgado, A., Castro-Puyana, M., and Marina, M.L., *Electrophoresis*, Vol. 40, 1913–1920, 2019.

[110]   Fillet, M., Hubert, P., and Crommen, J., *Electrophoresis*, Vol. 19, 2834–2840, 1998.

[111]   Wätzig, H., Degenhardt, M., and Kunkel, A., *Electrophoresis*, Vol. 19, 2695–2752, 1998.

[112]   Jimidar, M.I., van Ael, W., van Nyen, P., Peeters, M., Redlich, D., and Smet, M. de, *Electrophoresis*, Vol. 25, 2772–2785, 2004.

[113]   Rocheleau, M.-J., *Electrophoresis*, Vol. 26, 2320–2329, 2005.

[114]   Ates, H., Mangelings, D., and Vander Heyden, Y., *J Pharm Biomed Anal*, Vol. 48, 288–294, 2008.

[115]   Tait, R.J., Thompson, D.O., Stella, V.J., and Stobaugh, J.F., *Anal Chem*, Vol. 66, 4013–4018, 1994.

[116]   Stalcup, A.M., and Gahm, K.H., *Anal Che.*, Vol. 68, 1360–1368, 1996.

[117]   Morin, P., Dreux, M., Usse, S., Viaud, M.C., and Guillaumet, G., *Electrophoresis*, Vol. 20, 2630–2637, 1999.

[118]   Fillet, M., Chankvetadze, B., Crommen, J., and Blaschke, G., *Electrophoresis*, Vol. 20, 2691–2697, 1999.

[119]   Fillet, M., Hubert, P., and Crommen, J., *J. Chromatogr. A*, Vol. 875, 123–134, 2000.

[120] Grard, S., Morin, P., Dreux, M., and Ribet, J.-P., *Electrophoresis*, Vol. 21, 3028–3034, 2000.

[121] Dubský, P., Ördögová, M., Malý, M., and Riesová, M., *J Chromatogr A*, Vol. 1445, 158–165, 2016.

[122] Erny, G.L., Bergström, E.T., Goodall, D.M., and Grieb, S., *Anal Chem*, Vol. 73, 4862–4872, 2001.

[123] Kumar, A., Mann, H.J., and Remmel, R.P., *J Chromatogr B, Biomed Appl*, Vol. 853, 287–293, 2007.

[124] Chankvetadze, B., *Electrophoresis*, Vol. 23, 4022–4035, 2002.

[125] Belema, M., van Nguyen, N., Bachand, C., Deon, D.H., Goodrich, J.T., James, C.A., Lavoie, R., Lopez, O.D., Martel, A., Romine, J.L., Ruediger, E.H., Snyder, L.B., St Laurent, D.R., Yang, F., Zhu, J., Wong, H.S., Langley, D.R., Adams, S.P., Cantor, G.H., Chimalakonda, A., Fura, A., Johnson, B.M., Knipe, J.O., Parker, D.D., Santone, K.S., Fridell, R.A., Lemm, J.A., O'Boyle, D.R., Colonno, R.J., Gao, M., Meanwell, N.A., and Hamann, L.G., *J Med Chem*, Vol. 57, 2013–2032, 2014.

[126] https://www.tga.gov.au/sites/default/files/auspar-daclatasvir-dihydrochloride-151214-cer.docx.

[127] Chankvetadze, B., *Chem. Soc. Rev.*, Vol. 33, 337–347, 2004.

[128] Silva, M.S., *Molecules*, Vol. 22, 2017.

[129] Terekhova, I., Kumeev, R., Alper, G., Chakraborty, S., Pérez-Sánchez, H., and Núñez-Delicado, E., *RSC Adv*, Vol. 6, 49567–49577, 2016.

[130] Ikeda, Y., Hirayama, F., Arima, H., Uekama, K., Yoshitake, Y., and Harano, K., *J Pharm Sci*, Vol. 93, 1659–1671, 2004.

[131] Soares, L.A., Leal, A.F.V.B., Fraceto, L.F., Maia, E.R., Resck, I.S., Kato, M.J., Sousa Gil, E., Sousa, A.R., Cunha, L.C., and Rezende, K.R., *J Incl Phenom Macrocycl Chem*, Vol. 64, 23–35, 2009.

[132] Dignam, C.F., Randall, L.A., Blacken, R.D., Cunningham, P.R., Lester, S.-K.G., Brown, M.J., French, S.C., Aniagyei, S.E., and Wenzel, T.J., *Tetrahedron Asymmetry*, Vol. 17, 1199–1208, 2006.

[133] Hazekamp, A., and Verpoorte, R., *Eur J Pharm Sci*, Vol. 29, 340–347, 2006.

[134] Correia, I., Bezzenine, N., Ronzani, N., Platzer, N., Beloeil, J.-C., and Doan, B.-T., *J Phys Org Chem*, Vol. 15, 647–659, 2002.

[135] Shi, Y., and Fritz, J.S., *J Chromatogr A*, Vol. 671, 429–435, 1994.

[136] Mähler, J., and Persson, I., *Inorg Chem*, Vol. 51, 425–438, 2012.

7. Supplementary material appendices

7.1. Annex I: Supplementary material of manuscript 1

Quality by Design-Guided Development of a Capillary Electrophoresis Method for the Chiral Purity Determination of Ambrisentan

Sulaiman Krait[1], Michal Douša[2], Gerhard K.E. Scriba[1] *

[1] Department of Pharmaceutical Chemistry, Friedrich Schiller University Jena, Philosophenweg 14,07743 Jena, Germany.

[2] Zentiva, a.s., U Kabelovny 130, 10237 Praha 10, Czech Republic.

Table S1. Matrix of the fractional factorial Res V+ design used for critical process parameter screening and experimental responses peak resolution (R_S) and (*S*)-ambrisentan migration time (MT).

Exp. No.	Temp [°C]	V [kV]	Buf [mM]	pH	CD [mM]	R_S	MT [min]
1	25	15	200	5.5	10	1.81	12.31
2	20	20	125	4.65	30	2.92	8.48
3	25	25	50	5.5	10	0	4.51
4	25	25	50	3.8	50	2.29	5.36
5	25	15	50	5.5	50	0	8.74
6	15	25	50	5.5	50	0	6.88
7	25	15	50	3.8	10	3.02	10.32
8	25	25	200	3.8	10	2.53	6.09
9	15	15	200	5.5	50	2.55	19.51
10	20	20	125	4.65	30	2.81	8.38
11	25	25	200	5.5	50	1.86	8.06
12	15	15	50	5.5	10	0.99	11.60
13	25	15	200	3.8	50	3.35	13.40
14	15	25	200	5.5	10	1.85	9.07
15	15	15	200	3.8	10	4.09	16.68
16	15	25	200	3.8	50	4.24	11.55
17	15	15	50	3.8	50	3.24	12.92
18	15	25	50	3.8	10	3.27	8.45
19	20	20	125	4.65	30	2.81	8.40

V: applied voltage; Temp: capillary temperature; Buf: acetate buffer concentration; CD: γ-CD concentration; pH: pH of the BGE.

Table S2. Response surface design matrix of the three level central composite face-centered design used for method optimization and experimental responses peak resolution (R_S) and (*S*)-ambrisentan migration time (MT).

Exp. No.	Temp [°C]	V [kV]	Buf [mM]	R_S	MT [min]
1	20	20	125	4.35	11.06
2	25	25	200	4.01	9.08
3	15	25	50	3.44	8.31
4	15	15	50	3.61	14.49
5	25	15	50	2.96	11.58
6	15	20	125	4.23	13.92
7	20	20	50	3.18	9.51
8	15	15	200	4.19	20.68
9	20	25	125	3.82	9.49
10	25	20	125	3.75	11.35
11	15	25	200	4.76	13.80
12	20	20	200	4.59	16.02
13	20	15	125	3.88	17.90
14	20	20	125	3.77	13.06
15	25	25	50	2.66	6.53
16	20	20	125	3.68	13.11
17	25	15	200	4.11	18.95

V: applied voltage; Temp: capillary temperature; Buf: acetate buffer concentration.

Table S3. Matrix of the Plackett-Burman design for robustness testing experimental responses peak resolution (R_S) and (*S*)-ambrisentan migration time (MT).

Exp. No.	Temp [°C]	V [kV]	Buf [mM]	pH	CD [mM]	R_S	MT [min]
1	26	24	48	4.1	27.5	1.72	8.38
2	26	26	48	3.9	32.5	1.77	7.65
3	26	26	52	3.9	27.5	1.79	7.16
4	24	26	52	4.1	27.5	1.77	9.41
5	26	24	52	4.1	32.5	1.71	9.02
6	24	26	48	4.1	32.5	1.73	8.05
7	24	24	52	3.9	32.5	1.73	8.55
8	24	24	48	3.9	27.5	1.73	7.91
9	25	25	50	4.0	30	1.78	8.90
10	25	25	50	4.0	30	1.79	8.22
11	25	25	50	4.0	30	1.80	7.90

V: applied voltage; Temp: capillary temperature; Buf: acetate buffer concentration; CD: γ-CD concentration; pH: pH of the BGE.

7.2.   Annex II: Supplementary material of manuscript 2

Development of a Capillary Electrophoresis Method for the Determination of the Chiral Purity of Dextromethorphan by a Dual Selector System using Quality by Design Methodology

Sulaiman Krait[1], Matthias Heuermann[2], Gerhard K. E. Scriba[1*]

[1] Friedrich Schiller University, Department of Pharmaceutical Chemistry, Philosophenweg 14, 07743 Jena, Germany

[2] Centre For Health (LZG.NRW), Gesundheitscampus-Süd 9, 44801 Bochum, Germany

Table S1. Matrix of the fractional factorial resolution IV design used for evaluation of CCPs in the investigation of the knowledge space. Resolution (RS) and migration time of the LVM peak (MT_{LVM}) were used as responses.

#	Parameters						Responses	
	Temperature (°C)	Voltage (kV)	Buffer conc. (mM)	pH	S-β-CD (mg/mL)	M-α-CD (mg/mL)	R_S	MT_{LVM} (min)
1	15	10	30	6.6	10	6	9.12	7.66
2	25	10	30	6.5	24	6	13.86	10.28
3	15	20	30	6.5	24	20	12.06	4.34
4	25	20	30	6.5	10	20	4.99	4.45
5	15	10	100	6.4	24	20	3.96	8.4
6	25	10	100	6.4	10	20	5.28	5.64
7	15	20	100	6.5	10	6	8.43	3.97
8	25	20	100	6.4	24	6	14.02	10.16
9	15	10	30	8.2	10	20	3.68	6.07
10	25	10	30	8.0	24	20	8.8	6.35
11	15	20	30	8.0	24	6	15.86	5.43
12	25	20	30	8.0	10	6	6.86	2.7
13	15	10	100	8.0	24	6	11.41	11.51
14	25	10	100	8.0	10	6	8.03	6.28
15	15	20	100	8.2	10	20	0	2.78
16	25	20	100	8.0	24	20	3.79	3.16
17	20	15	65	7.2	17	13	5.97	4.4
18	20	15	65	7.2	17	13	6.19	4.53
19	20	15	65	7.2	17	13	6.45	4.58

Table S2. Design matrix for the central composite face centered design for method optimization. Responses were migration time (TM_{LVM}), number of theoretical plates (N_{LVM}) and height (H_{LVM}) of the LVM peak and the tailing factor of the DXM peak (TF_{DXM}). Peak resolution, R_S, was not included in the responses used for method optimization.

#	Parameters			R_S	Responses			
	Voltage (kV)	S-β-CD (mg/mL)	M-α-CD (mg/mL)		TM_{LVM}	N_{LVM}	H_{LVM}	TF_{DXM}
N01	10	10	5	11.8	10.12	30835	2370	8.3
N02	20	10	5	11.8	5.23	29408	2052	4.89
N03	10	30	5	21.3	22.98	26698	2505	8.09
N04	20	30	5	19.3	10.5	25162	2077	5.48
N05	10	10	15	13.3	7.82	73057	3535	0.69
N06	20	10	15	10.1	3.45	53058	3099	0.9
N07	10	30	15	22.1	12	79843	3559	0.63
N08	20	30	15	22.3	5.63	65006	3120	0.85
N09	10	20	10	11.5	18.6	51786	3355	3.99
N10	20	20	10	15.8	5.25	42992	3100	2.79
N11	15	10	10	13.0	5.33	47218	2946	2.48
N12	15	30	10	24.9	9.67	52091	2758	2.66
N13	15	20	5	19.5	14.86	23991	1997	7.97
N14	15	20	15	20.4	6.27	78643	3294	0.95
N15	15	20	10	17.4	7.26	51371	3150	3.23
N16	15	20	10	19.0	8.22	49950	2908	3.17
N17	15	20	10	17.8	7.23	54385	3098	3.13

Table S3. Design matrix of the Plackett-Burman design used for robustness testing. Responses were migration time (TM$_{LVM}$), number of theoretical plates (N$_{LVM}$) and height (H$_{LVM}$) of the LVM peak and the tailing factor of the DXM peak (TF$_{DXM}$).

| #	Parameters								Responses			
	Temp (°C)	V (kV)	Conc. (mM)	pH	S-β-CD (mg/mL)	M-α-CD (mg/mL)	S-β-CD Batch	M-α-CD Batch	MT$_{LVM}$	N$_{LVM}$	H$_{LVM}$	TF$_{DXM}$
N01	21	19	31	6.4	15	13	S2	M2	5.14	21170	4941	4.6
N02	21	21	29	6.6	15	13	S1	M2	4.40	22859	5119	4.2
N03	19	21	31	6.4	17	13	S1	M1	4.42	30803	5540	1.9
N04	21	19	31	6.6	15	15	S1	M1	4.18	45965	6760	1.3
N05	21	21	29	6.6	17	13	S2	M1	4.11	33379	5904	2.3
N06	21	21	31	6.4	17	15	S1	M2	4.52	26188	5099	3.8
N07	19	21	31	6.6	15	15	S2	M1	3.89	39647	5986	1.1
N08	19	19	31	6.6	17	13	S2	M2	5.54	25193	5344	4.4
N09	19	19	29	6.6	17	15	S1	M2	5.33	29129	5396	4.6
N10	21	19	29	6.4	17	15	S2	M1	4.55	33695	5974	1.7
N11	19	21	29	6.4	15	15	S2	M2	4.56	23432	4604	4.3
N12	19	19	29	6.5	15	13	S1	M1	4.69	32758	5659	1.9
N13	20	20	30	6.5	16	14	S1	M1	4.29	38234	6050	1.5
N14	20	20	30	6.5	16	14	S1	M1	4.25	38152	6113	1.5
N15	20	20	30	6.5	16	14	S1	M1	4.27	37972	6092	1.5
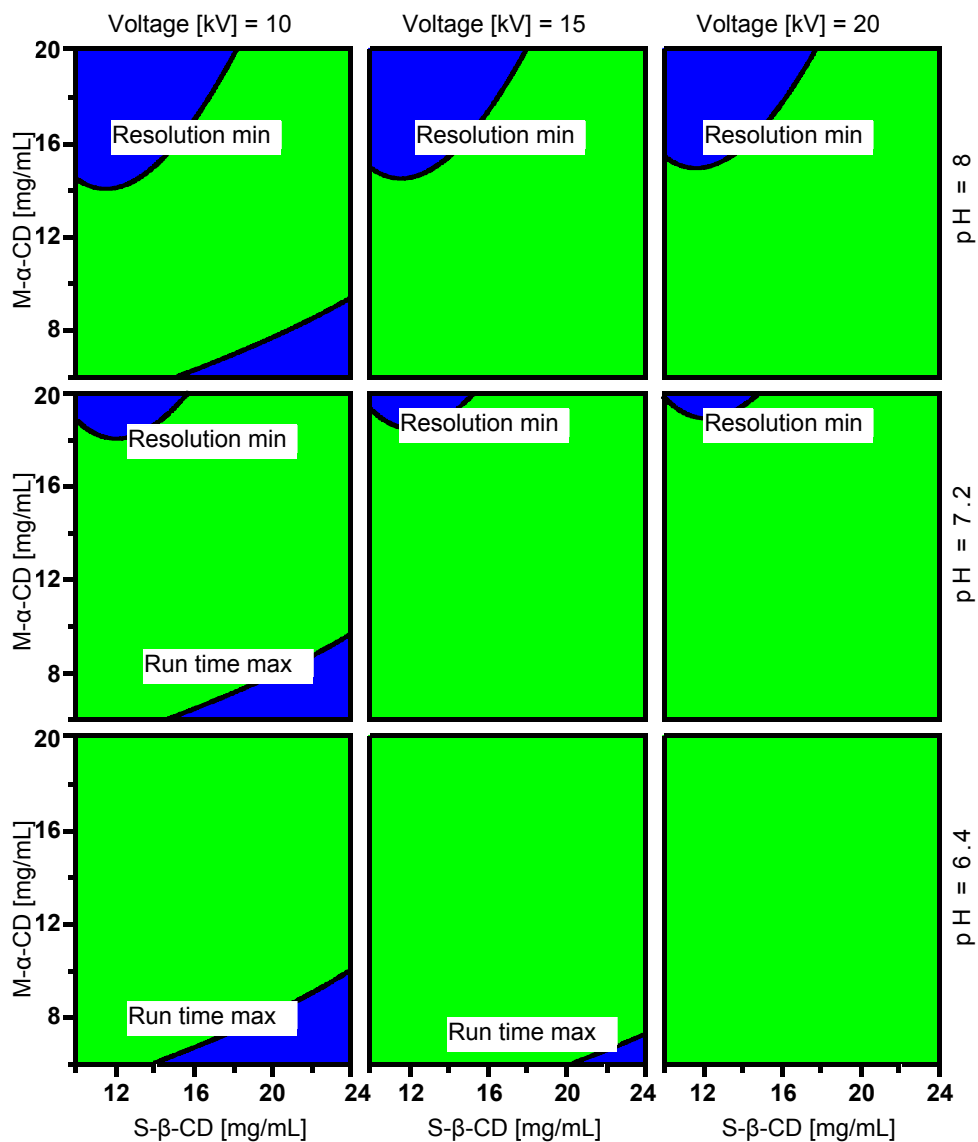
Figure S1. Sweet spot plots with buffer concentration set at 30 mM and temperature at 20° C.

Green: sweet spot (all criteria met), blue: 1 criterion met. Threshold of the responses:

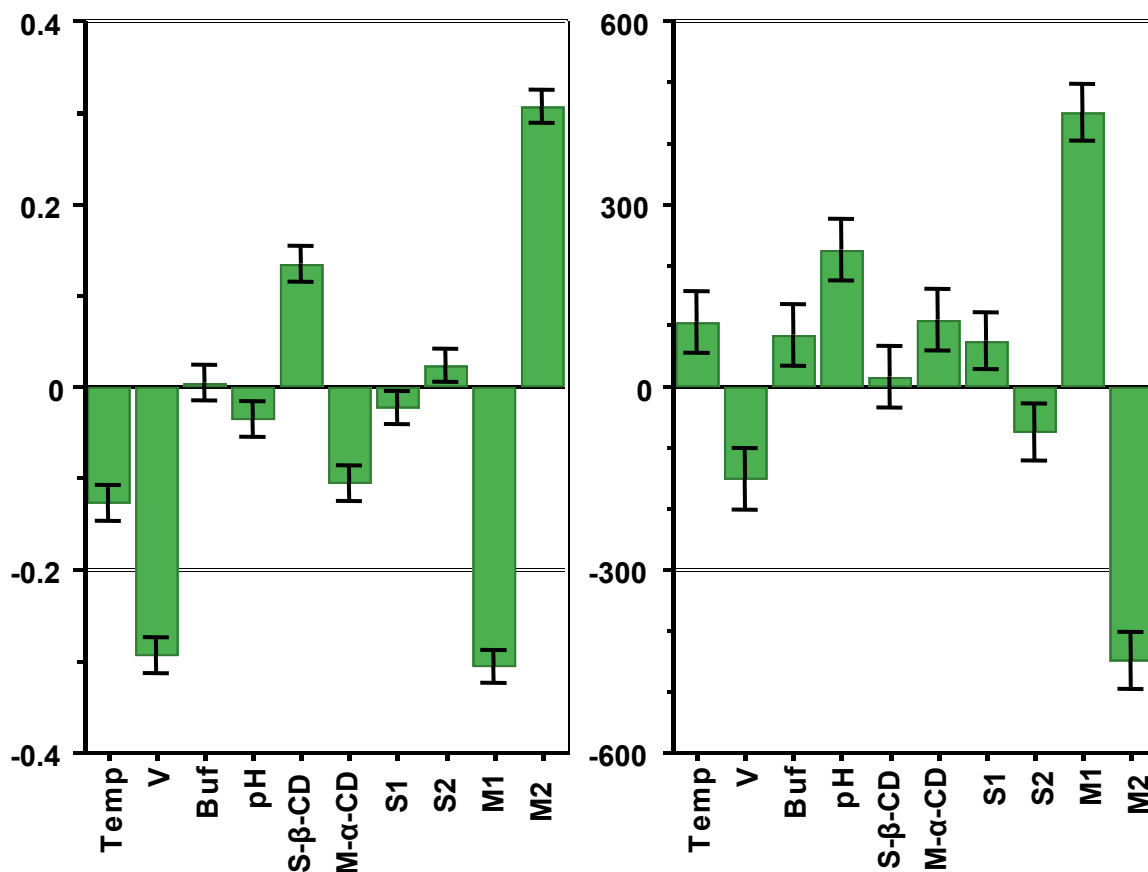Resolution ($R_S \geq 5$) and migration time LVM ($t \leq 8$ min).

Figure S2   Coefficient plot (scaled and centered) of the screening design showing the relative effect

of the factors on the responses; x*x represents the quadratic terms for the respective

parameters and x*y the interaction terms between two parameters. Temp, capillary

temperature; V, Applied voltage; Buf, buffer concentration; pH, buffer pH; S-β-CD, S-β-

CD concentration; M-α-CD, M-α-CD concentration; S1 and S2, S-β-CD batches; M1 and

M2, M-α-CD batches.

7.3.   Annex III: Supplementary material of manuscript 3

Quality by Design-Assisted Development of a Capillary Electrophoresis Method for the Chiral Purity Determination of Dexmedetomidine

Sulaiman Krait, Gerhard K. E. Scriba

Friedrich Schiller University, Department of Pharmaceutical Chemistry, Philosophenweg 14, 07743

  Jena, Germany

Correspondence

Prof. Dr. Gerhard K. E. Scriba

Friedrich Schiller University

Department of Pharmaceutical Chemistry

Philosophenweg 14

07743 Jena, Germany

Phone: +49-3641-949830

Fax: +49-3641-949802

Email: gerhard.scriba@uni-jena.de

Table S1. Matrix of the fractional factorial resolution V+ design used for evaluation of CPPs in the investigation of the knowledge space. The responses were α-value, migration time of the D-MDT peak (MT $_{D-MDT}$) and the resulting current (Cur).

#	Temperature (°C)	Voltage (kV)	Buffer conc. (mM)	pH	S-β-CD (mg/mL)	α-value	MT $_{D-MDT}$ (min)	Cur (µA)
1	15	6	50	6.4	50	1.181	22.5	46
2	25	6	50	6.4	30	1.068	10.7	37.5
3	15	6	100	6.4	30	1.000	11.1	42.7
4	25	6	100	6.4	50	1.074	10.9	65.2
5	15	10	50	6.4	30	1.101	8.8	55.6
6	25	10	50	6.4	50	1.114	8.3	92.4
7	15	10	100	6.4	50	1.093	8.0	96.5
8	25	10	100	6.3	30	1.000	4.8	94
9	15	6	50	8.1	30	1.000	7.3	39.8
10	25	6	50	8.5	50	1.000	6.2	61.4
11	15	6	100	8.3	50	1.000	9.5	66.6
12	25	6	100	8.1	30	1.000	6.7	66.4
13	15	10	50	8.0	50	1.000	5.3	90
14	25	10	50	8.5	30	1.000	3.3	85.2
15	15	10	100	8.1	30	1.000	4.6	101
16	25	10	100	8.0	50	1.000	3.9	144
17	20	8	75	7.2	40	1.039	6.2	76.4
18	20	8	75	7.2	40	1.037	6.1	76
19	20	8	75	7.2	40	1.037	6.1	76.6

Table S2. Design matrix for the central composite face centered design for method optimization. The responses were α-value, migration time of the D-MDT peak (MT $_{D-MDT}$) and the resulting current (Cur).

#	Parameters			Responses		
	Temperature (°C)	Voltage (kV)	S-β-CD (mg/mL)	α-value	MT $_{D-MDT}$ (min)	Cur (µA)
N01	15	6	30	1.110	17.7	32.4
N02	25	6	30	1.054	10.6	39.9
N03	15	10	30	1.098	9.6	56
N04	25	10	30	1.053	5.9	68.8
N05	15	6	50	1.162	22.5	48
N06	25	6	50	1.114	15.0	54.7
N07	15	10	50	1.188	13.4	79.7
N08	25	10	50	1.084	7.8	99.5
N09	15	8	40	1.086	8.7	50.5
N10	25	8	40	1.049	6.2	61.6
N11	20	6	40	1.059	10.0	41
N12	20	10	40	1.058	5.8	72.3
N13	20	8	30	1.076	10.1	48.4
N14	20	8	50	1.117	11.9	68.8
N15	20	8	40	1.060	7.4	56.2
N16	20	8	40	1.080	7.7	56.3
N17	20	8	40	1.061	7.5	55.9

Table S3. Design matrix of the Plackett-Burman design used for robustness testing. The responses were α-value, migration time of the D-MDT peak (MT $_{D-MDT}$) resulting current (Cur) and the corrected area ratio of D-MDT to that of the internal standard (A_D/A_{ISt}).

#	Parameters						Responses			
	Temp. (°C)	Buffer conc. (mM)	Voltage (kV)	pH	S-β-CD (mg/mL)	S-β-CD Batch	α-value	MT $_{D-MDT}$ (min)	Cur (µA)	$A_D/A_{I.St}$
N1	18	47.5	9.5	6.6	38	S-2	1.090	7.5	73.5	0.839
N2	18	52.5	9.5	6.4	42	S-1	1.110	8.1	69.5	0.743
N3	18	52.5	10.5	6.4	38	S-2	1.090	7.1	73.5	0.804
N4	16	52.5	10.5	6.6	38	S-1	1.086	6.7	65.5	0.763
N5	18	47.5	10.5	6.6	42	S-1	1.089	6.9	78.0	0.861
N6	16	52.5	9.5	6.6	42	S-2	1.090	8.0	68.0	0.862
N7	16	47.5	10.5	6.5	42	S-2	1.117	8.2	75.0	0.863
N8	16	47.5	9.5	6.4	38	S-1	1.104	8.1	59.3	0.792
N9	17	50	10	6.5	40	S-1	1.096	7.4	74.5	0.824
N10	17	50	10	6.5	40	S-1	1.091	7.7	74.0	0.870
N11	17	50	10	6.5	40	S-1	1.102	7.5	74.6	0.821
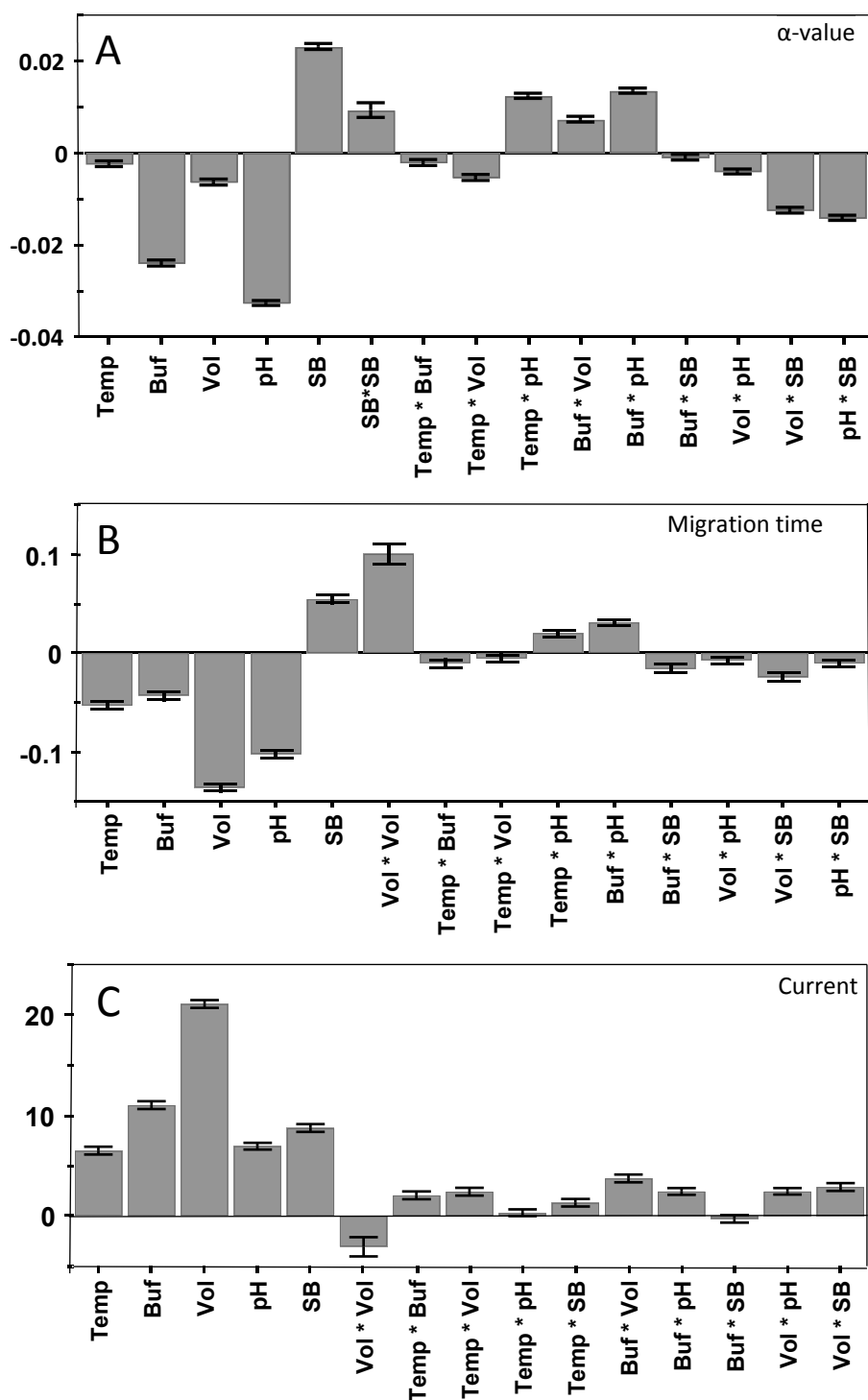
Figure S1. Coefficient plot (scaled and centered) of the screening design showing the relative effect of the factors on the responses (A) α-value, (B) migration time of D-MDT and (C) current. x*y represent the interaction terms between two parameters. V, Applied voltage; Temp, capillary temperature; pH, pH of BGE; Buf, BGE concentration; SB, S-β-CD concentration. The error bars represent the 95 % confidence interval.
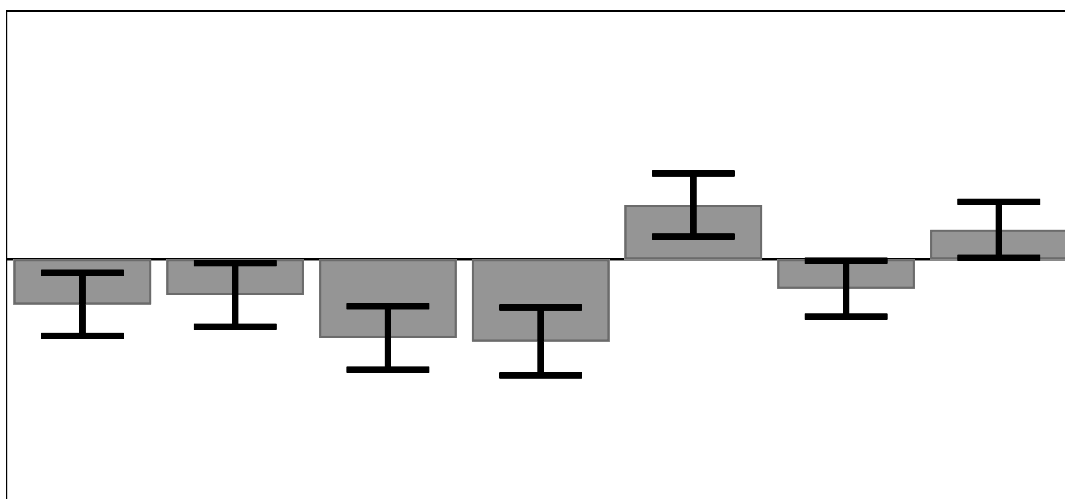
Figure S2. Coefficient plot (scaled and centered) of the Plackett-Burman design showing the relative effect of the factors on the migration time of D-MDT. Temp, capillary temperature; V, Applied voltage; pH, pH of BGE; Buf, BGE concentration; CD-C, S-β-CD concentration; CD-B, batches of S-β-CD. The error bars represent the 95 % confidence interval.

7.4.   Annex IV: Supplementary material of manuscript 4

Investigation of the Complexation between Cyclodextrins and Medetomidine Enantiomers by Capillary Electrophoresis, NMR Spectroscopy and Molecular Modeling

Sulaiman Krait[a], Antonio Salgado[b], Bezhan Chankvetadze[c], Federico Gago[d], Gerhard K. E Scriba[a]

[a]   Friedrich-Schiller-University Jena, Department of Pharmaceutical/Medicinal Chemistry, Philosophenweg 14, 07743 Jena, Germany

[b]   University of Alcalá, NMR Spectroscopy Centre (CERMN), CAI Químicas, Faculty of Pharmacy, 28805 Alcalá de Henares, Madrid, Spain

[c]   Tbilisi State University, Institute of Physical and Analytical Chemistry, School of Exact and Natural Sciences, 0179 Tbilisi, Georgia

[d]   University of Alcalá, Department of Biomedical Sciences (Unidad Asociada IQM-CSIC) and Instituto de Investigación Química "Andrés M. del Río" (IQAR), 28805 Alcalá de Henares, Madrid, Spain

Reference spectrum medetomidine

Fig. S1.   Expanded ^{1}H NMR (top) and 1D ROESY (bottom) spectra of the complex between β-CD and medetomidine spiked with dexmedetomidine upon irradiation of β-CD H-3 and H-6. The enantioselective ROESY response is indicated with a frame.
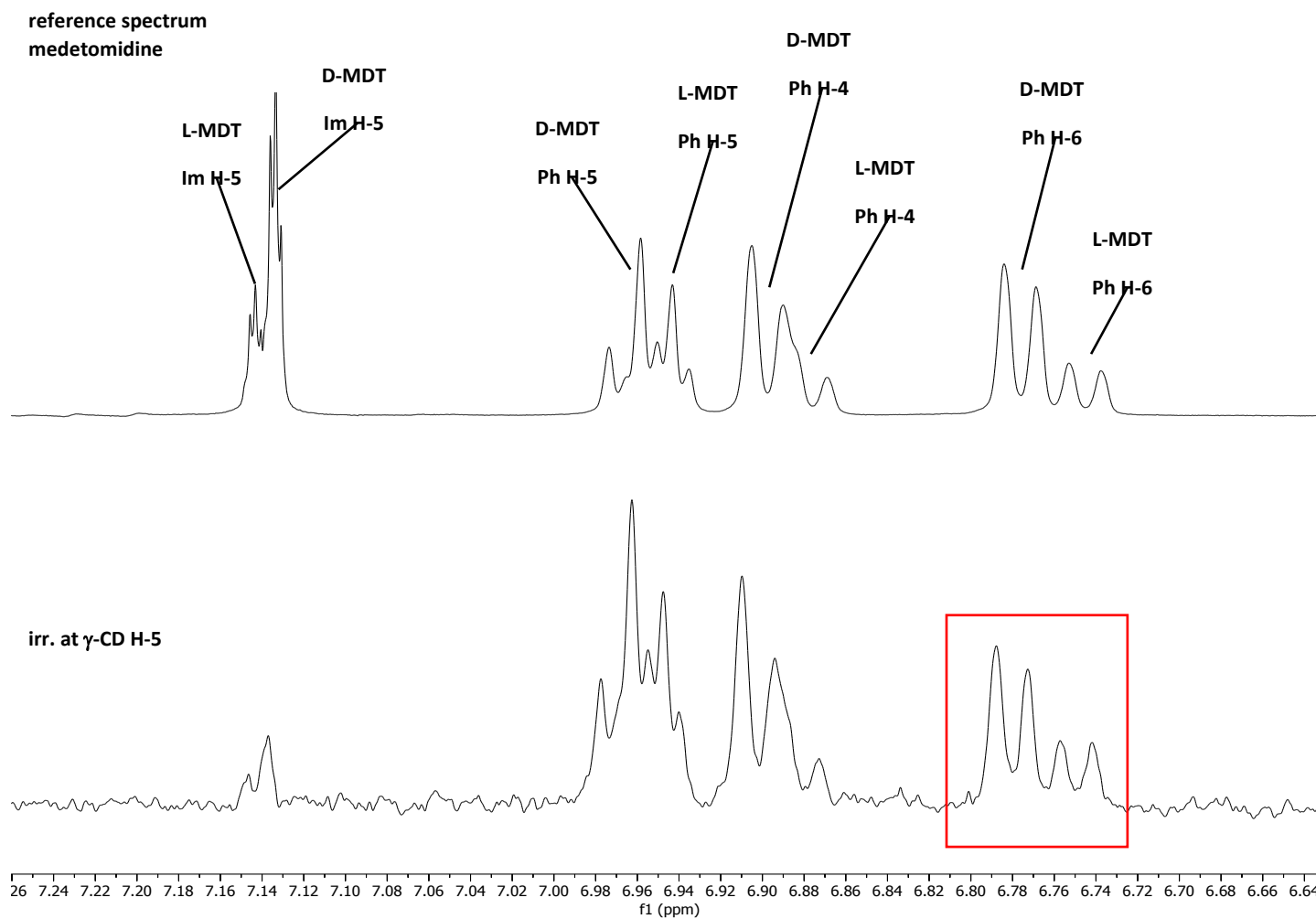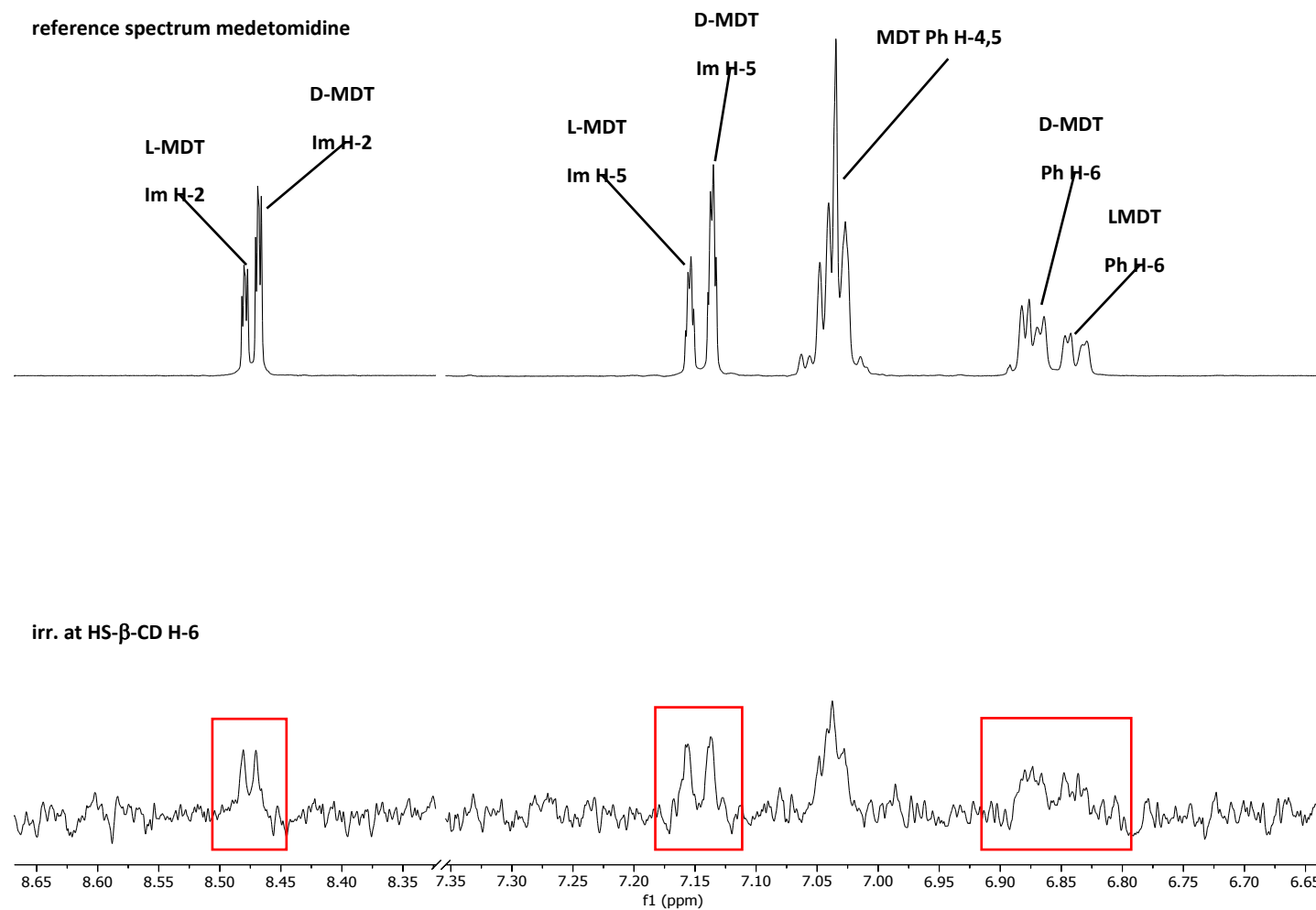
Fig. S2. Expanded ¹H NMR (top) and 1D ROESY (bottom) spectra of the complex between γ-CD and medetomidine spiked with dexmedetomidine upon irradiation of γ-CD H-5. The enantioselective ROESY response is indicated with a frame.

Fig. S3. Expanded ^{1}H NMR (top) and 1D ROESY (bottom) spectra of the complex between HS-β-CD and medetomidine spiked with dexmedetomidine upon irradiation of HS-β-CD H-6. The enantioselective ROESY responses are indicated with frames.

7.5.   Annex V: Supplementary material of manuscript 5

Unusual Complexation between Daclatasvir and γ-Cyclodextrin. A Multiplatform Study

Sulaiman Krait,[+] [a] Antonio Salgado,[+] [b] Claudio Villani,[c] Lukas Naumann,[d] Christian Neusüß,[d] Bezhan Chankvetadze,[e] and Gerhard K. E. Scriba*[a]

Department of Medicinal/Pharmaceutical Chemistry, Friedrich Schiller University Jena, Philosophenweg 14, 07743 Jena, Germany. E-mail: gerhard.scriba@uni-jena.de
NMR Spectroscopy Centre (CERMN), CAI Químicas, Faculty of Pharmacy, University of Alcalá, 28805 Alcalá de Henares, Madrid, Spain.
Department of Chemistry and Technology of Drugs, Sapienza University of Rome, Piazzale Aldo Moro 5, 00185 Rome, Italy
Aalen University, Department of Chemistry, Beethovenstrasse 1, 73430 Aalen, Germany
Tbilisi State University, Institute of Physical and Analytical Chemistry, School of Exact and Natural Sciences, 0179 Tbilisi, Georgia
† These authors contributed equally to the work.

SYNTHESIS OF HALF-DCV

The synthesis followed literature procedures[1,2] and is outlined in the scheme shown below.
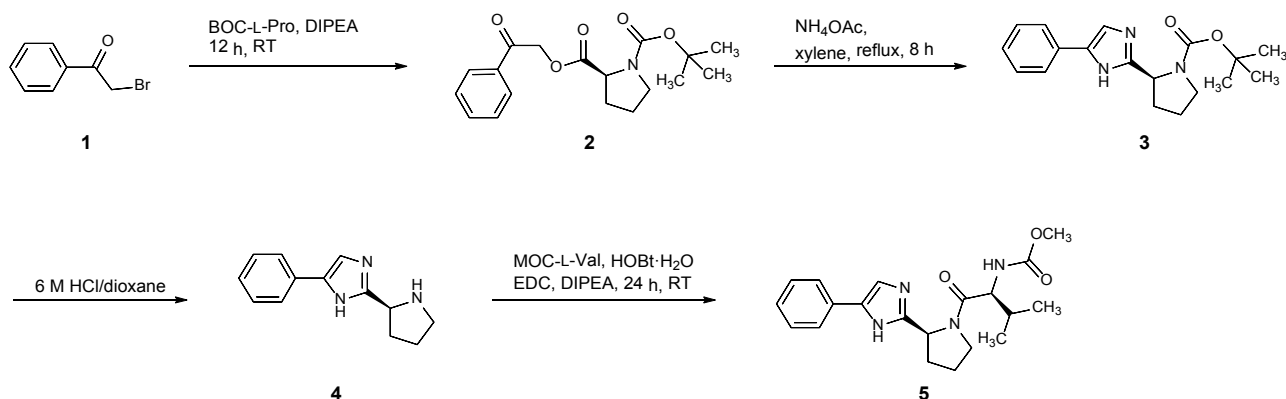
(S)-tert-butyl 2-(2-oxo-2-phenylethylcarbamoyl)pyrrolidine-1-carboxylate (**2**)

12 g (55.8 mmol) BOC-L-Pro and 17.6 mL *N,N*-diisopropylethylamine in 120 mL dry dichloromethane were stirred under nitrogen at 0 °C for 10 min. 11 g (55 mmol) of 2-bromoacetophenone (**1**) were added, the solution was warmed to room temperature and stirred overnight. Subsequently the solution was washed with 100 mL water and 100 mL brine and dried over sodium sulfate. Removal of the organic solvent under reduced pressure yielded an off-white solid (16 g, 85 %), which was used in the next step without further purification.

(*S*)-tert-butyl 2-(5-phenyl-1H-imidazol-2-yl)pyrrolidine-1-carboxylate (**3**)

14 g (42 mmol) of **2** and 30 g ammonium acetate in 120 mL toluene were refluxed for 8 h. The solution was cooled to room temperature, diluted with 100 mL ethyl acetate and washed with 100 mL water and 100 mL brine and dried over sodium sulfate. Evaporation of the solvent under reduces pressure yielded an oil, which was further purified by column chromatography (hexane/ethyl acetate 2:1, followed by methanol) to yield an off-white solid. Yield 6 g (45 %); m.p. 63-64 °C (ref. 2, 63-65 °C); MS: m/z = 314 [M+H]$^+$, 313 M$^+$, 257, 240, 213, 212, 185, 171, 170, 158, 57; ^{1}H-NMR (250 MHz, CDCl$_3$) δ (ppm) = 1.51 (s, 9H), 1.98-2.18 (m, 4H), 2.90 (br s, 1H), 3.43-3.48 (m, 1H), 5.03 (br s, 1H), 7.23-7.28 (m, 3H), 7.35-7.38 (m, 2H), 7.60 (s, 1H).

(*S*)-5-phenyl-2-(pyrrolidin-2-yl)-1H-imidazole (**4**)

1.5 g (4.8 mmol) of **3** were stirred in 15 mL dry dioxane and 15 mL 6 M HCl in dioxane at 0 °C for 1 h. Removal of the solvent under reduced pressure yielded a white solid. Yield 0.9 g (66 % as hydrochloride); m.p. 243-244 °C; MS: m/z = 214 [M+H]$^+$, 213 M$^+$, 185, 184, 171, 170, 158; ^{1}H-NMR (250 MHz, D$_3$COD) δ (ppm) = 2.24-2.78 (m, 4H), 3.61-3.78 (m, 2H), 5.26 (t, J = 8.2 Hz, 1H), 7.52-7.60 (m, 3H), (d, J = 6.5 Hz, 2H), 8.07 (s, 1H).

N-[(1*S*)-2-methyl-1-[[(2*S*)-2-(5-phenyl-1*H*-imidazol-2-yl)-1-pyrrolidinyl]carbonyl]propyl]-carbamic acid methyl ester (**5**, half-DCV)

1.52 g (8.6 mmol) *N*-MOC-L-Val, 1.46 g (10.8 mmol) HOBt and 1.82 g (11.7 mmol) 1-ethyl-3-(3-dimethylaminopropyl)carbodiimide were stirred under nitrogen in 50 mL dry acetonitrile for 1 h at room temperature. Upon cooling to 0 °C, 1.68 g (5.9 mmol) of **4** (as hydrochloride) were added followed by dropwise addition of 5 mL *N,N*-diisopropylethylamine. The mixture was warmed to room temperature and stirring was continued for 24 h. 120 mL brine were added, the mixture was stirred at 50 °C for 1 h and after cooling to room temperature extracted with 100 mL ethyl acetate. The organic phase was washed with 0.5 M NaOH (2 times 50 mL) and brine (50 mL). Evaporation of the solvent under reduced pressure yielded 2 g of a brown oil. Column chromatography (ethyl acetate:hexane, 40:60 followed by ethyl acetate) yielded 450 mg of a yellowish oil, which were dissolved in the minimum amount of methanol. Upon addition of 5 drops toluene, the solvents were removed under reduced pressure yielding an off-white solid. Yield 400 mg (13 %); m.p. 133-134 °C; MS: m/z = 371 [M+H]⁺, 370 M⁺, 282, 240, 212, 130, 98, 43. For ^{1}H-NMR data see Fig. S11A and Table S8. Purity: 97.6 % by CE (40/50.2 cm, 50 µm ID fused-silica capillary, 50 mM sodium phosphate, pH 2.5, 20 °C, detection at 215 nm).

References

(1)   Amblard, F.; Zhang, H.; Zhou, L.; Shi, J.; Bobeck, D. R.; Nettles, J. H.; Chavre, S.; McBrayer, T. R.; Tharnish, P.; Whitaker, T.; Coats, S. J.; Schinazi, R. F. Synthesis and evaluation of non-dimeric HCV NS5A inhibitors. *Bioorg. Med. Chem. Lett.* **2013**, *23*, 2031-3034.

(2)   Kang, I.-J.; Hsu, S.-J.; Yang, H.-Y.; Yeh, T.-K.; Lee, C.-C.; Lee, Y.-C.; Tian, Y.-W.; Song, J.-S.; Hsu, T.-A.; Chao, Y.-S.; Yueh, A.; Chern, J.-H. A potent, selective and orally bioavailable HCV NS5A inhibitor for treatment of hepatitis C virus: (S)-1-((R)-2-(cyclopropanecarboxamido)-2-phenylacetyl)-*N*-(4-phenylthiazol-2-yl)Pyrrolidine-2-carboxamide. *J. Med. Chem*. **2017**, *60*, 228-247.
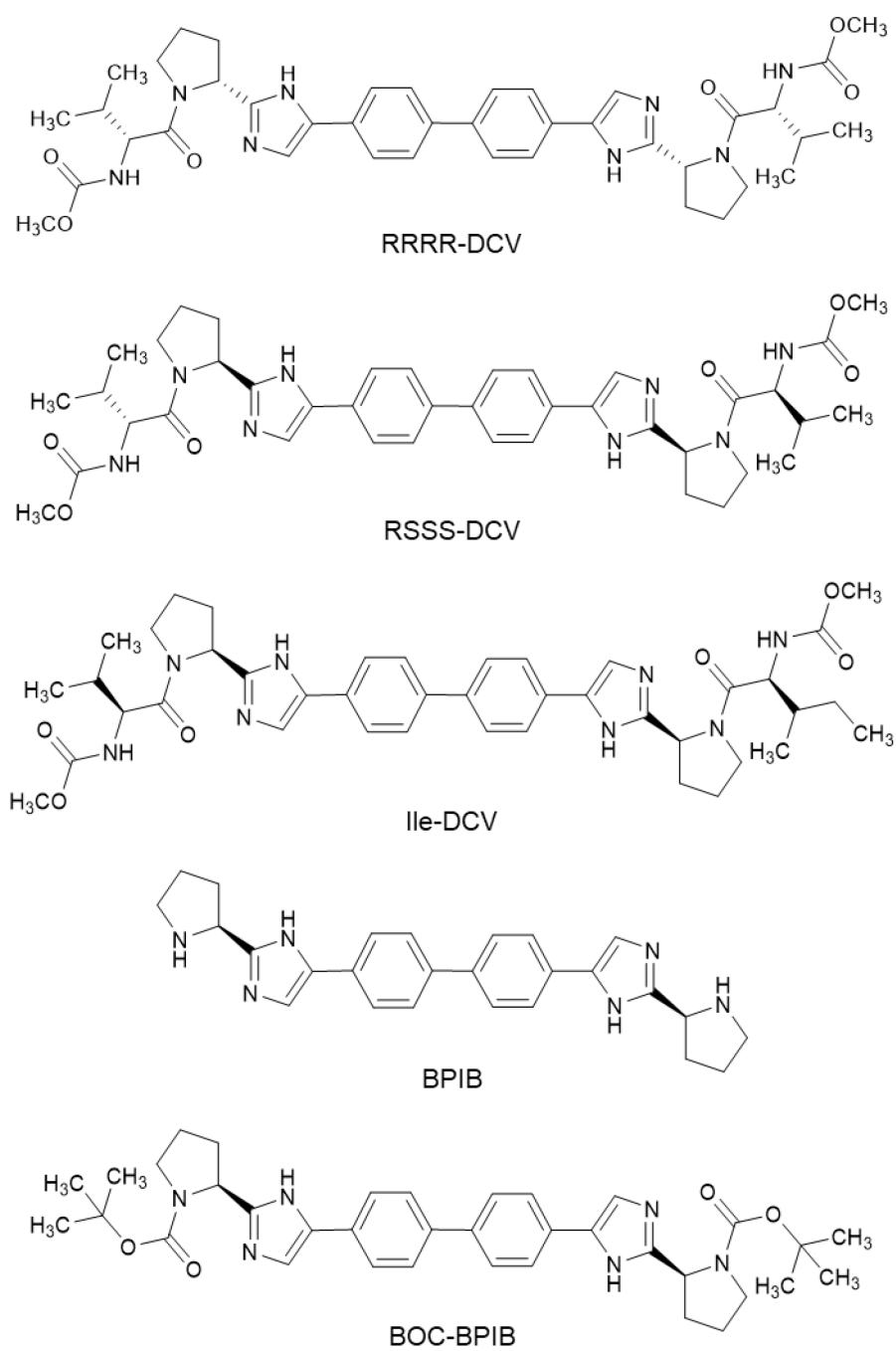
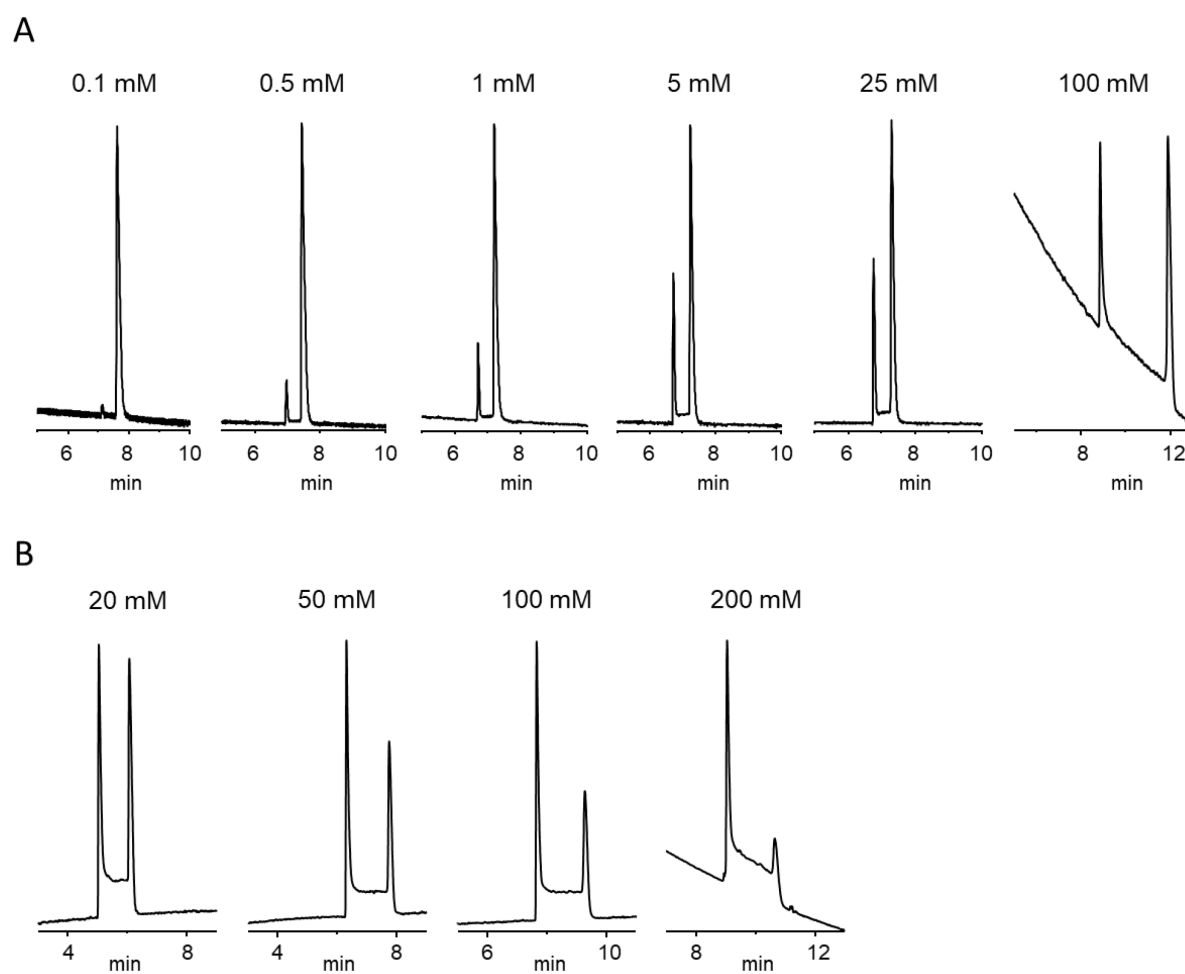**Figure S1** Structures of the RRRR-DCV, RSSS-DCV, Ile-DCV, BPIB and BOC-BPIB.

Figure S2 Electropherograms of the analysis of DCV using sodium phosphate buffer, pH 2.5, as BGE. (A) Effect of γ-CD concentration in 50 mM sodium phosphate buffer, (B) effect of buffer concentration in the presence of 20 mM γ-CD. For other experimental conditions see experimental procedures section.
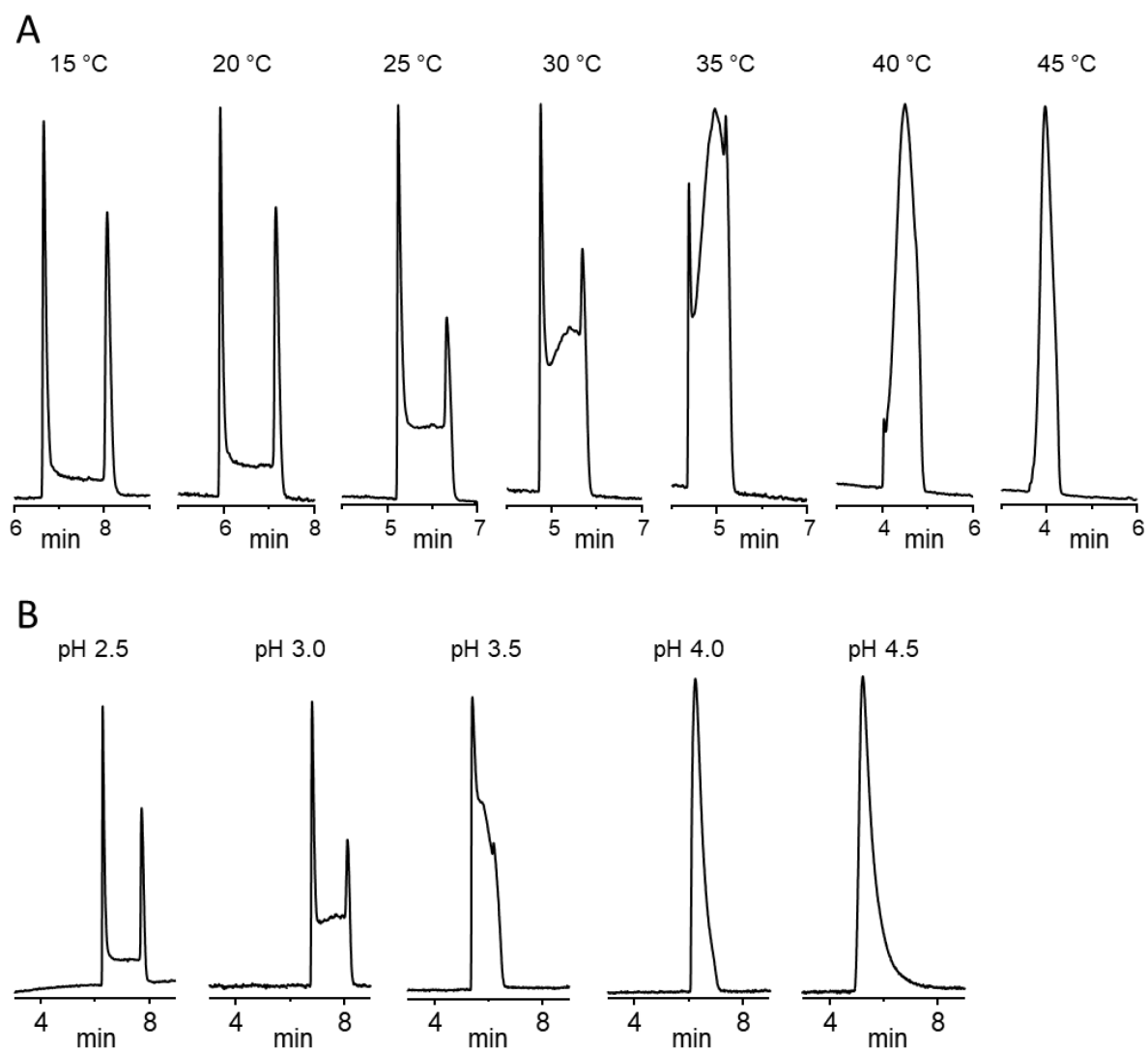
Figure S4   Electropherograms showing the effect of (A) temperature and (B) pH of the BGE using a 50 mM sodium phosphate buffer, pH 2.5, containing 20 mM γ-CD. For other experimental conditions see experimental procedures section.

T (°C)	T (K)	k12 (s^{-1})	ΔG12‡ (kcal·mol^{-1})	ΔH‡ (kcal·mol^{-1})	ΔS‡ (cal·mol^{-1}·K^{-1})
15.0	288.15	0.0007	21.02	20.80	- 0.56
20.0	293.15	0.0015	20.95		
25.0	298.15	0.0030	20.89		
30.0	303.15	0.0048	20.97		
35.0	308.15	0.0089	20.95		
40.0	313.15	0.0138	21.03		

Figure S4   Experimental (red) and simulated (blue) electropherograms of DCV using a 50 mM sodium phosphate buffer, pH 2.5, containing 20 mM γ-CD as BGE at variable temperature. Experimental plots have been baseline corrected for comparison with simulated plots. ΔG12‡ values are within 0.01 kcal/mol, k12 constant of interconversion of peak 1 to peak 2.
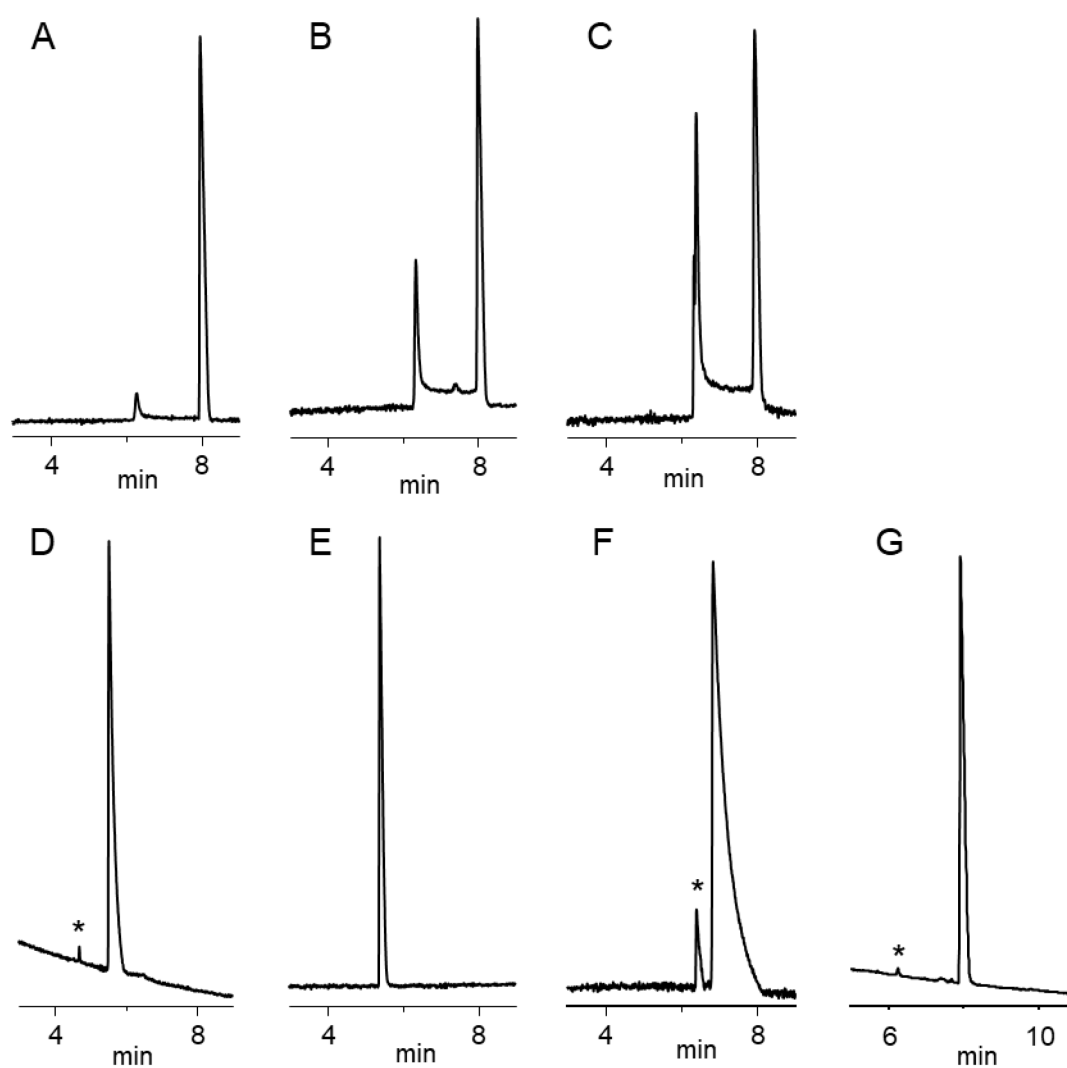
Figure S5 Electropherograms of the analysis of (A) RSSR-DCV, (B) RSSS-DCV, (C) Ile-DCV, (D) mono-DCV, (E) BPIB, (F) BOC-BPIB and (G) half-DCV using 50 mM sodium phosphate buffer, pH 2.5, containing 20 mM γ-CD as BGE. For other experimental conditions see experimental procedures section. * synthetic impurity.
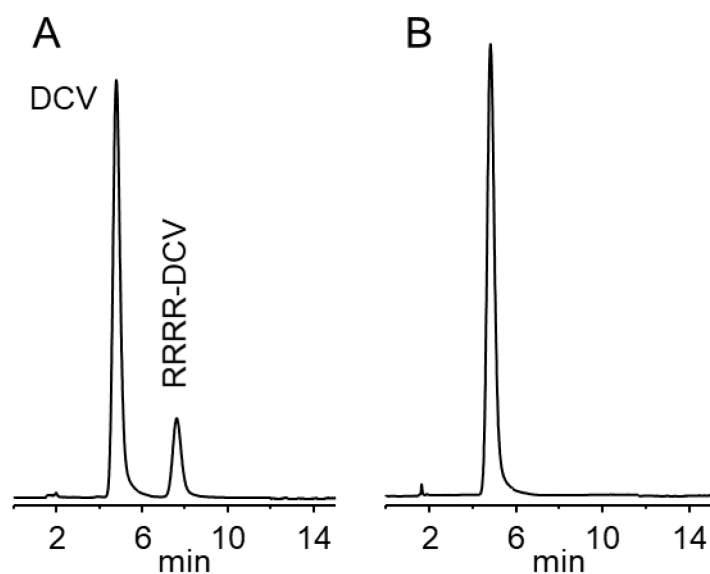
Figure S6   Chromatograms of the analysis of (A) a non-racemic mixture of DCV and RRRR-DCV
and (B) a sample containing DCV and γ-CD on a Lux i-Cellulose 5 column (150 x 4.6 mm,
5 µm), mobile phase: 1.58 g/L NH_4HCO_3 in water/acetonitrile (30:70, v/v), 1.0 mL/min,
40 °C, detection wavelength 305 nm. The sample was prepared by dissolving DCV.2HCl
at a concentration of 200 µg/mL in 50 mM sodium phosphate buffer, pH 2.5, containing
20 mM γ-CD and keeping it at room temperature for 30 min before injection.
Measurements were performed on a Shimadzu HPLC system from (Shimadzu, Kyoto,
Japan) consisting of two LC-10AS pumps, a SPD-10 A UV-vis detector, a SIL-10 A auto
injector, a CTO-20AC column oven and a SCL-10AVP system control unit using the
Shimadzu Class-VP Ver 4.03 software for system control and data acquisition.
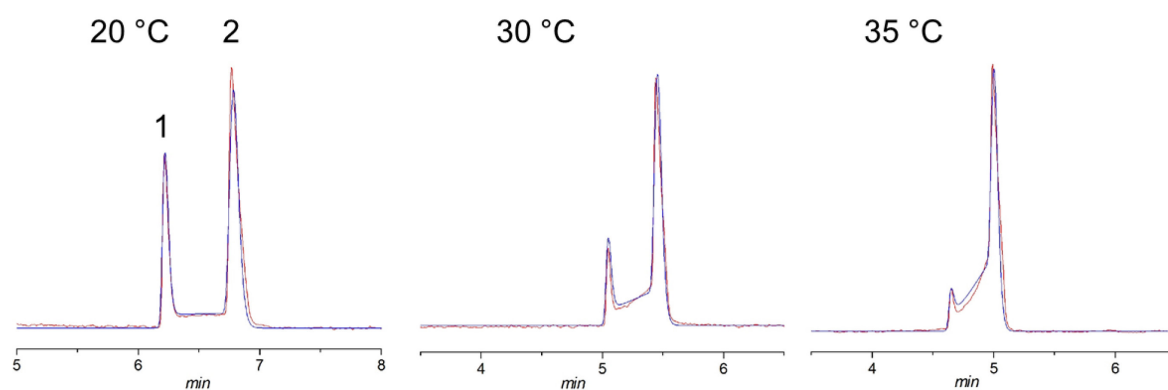
T (°C)	T (K)	k12 (s^{-1})	ΔG12‡ (kcal·mol^{-1})
20.0	293.15	0.00057	21.51
30.0	303.15	0.00295	21.26
35.0	308.15	0.0057	21.22

Figure S7   Experimental (red) and simulated (blue) electropherograms of a sample containing DCV (sample concentration 200 µg/mL as 2HCl salt) and 20 mM γ-CD analyzed in 50 mM CD-free sodium phosphate buffer, pH 2.5, at variable temperature. Experimental plots have been baseline corrected for comparison with simulated plots. ΔG12‡ values are within 0.01 kcal/mol
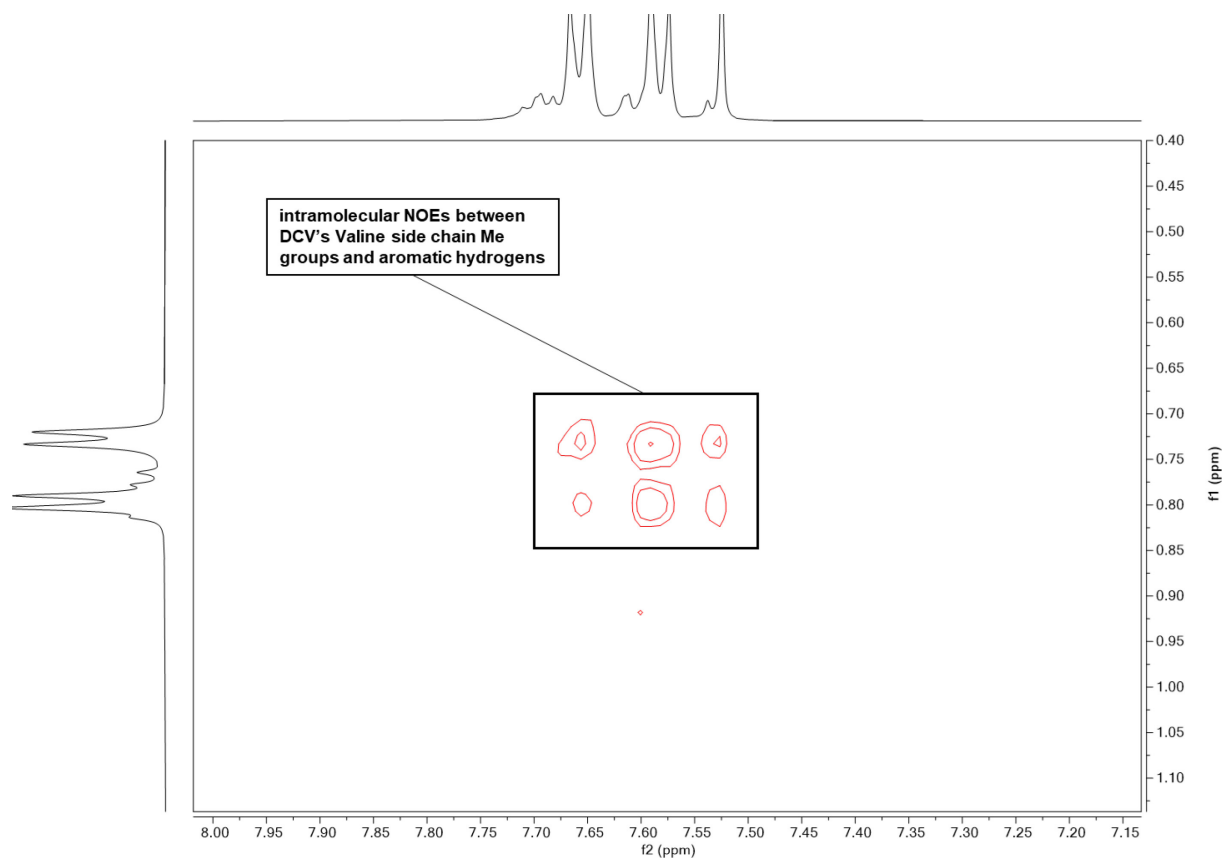
Figure S8 Expanded 2D ROESY spectrum of DCV in 50 mM deuterated sodium phosphate buffer in D_2O, apparent pH 2.5, showing intramolecular NOEs. Experimental conditions: 3.6 mg DCV·2HCl in 0.7 mL 50 mM D_3PO_4 in D_2O, pH 2.5, 25 °C.
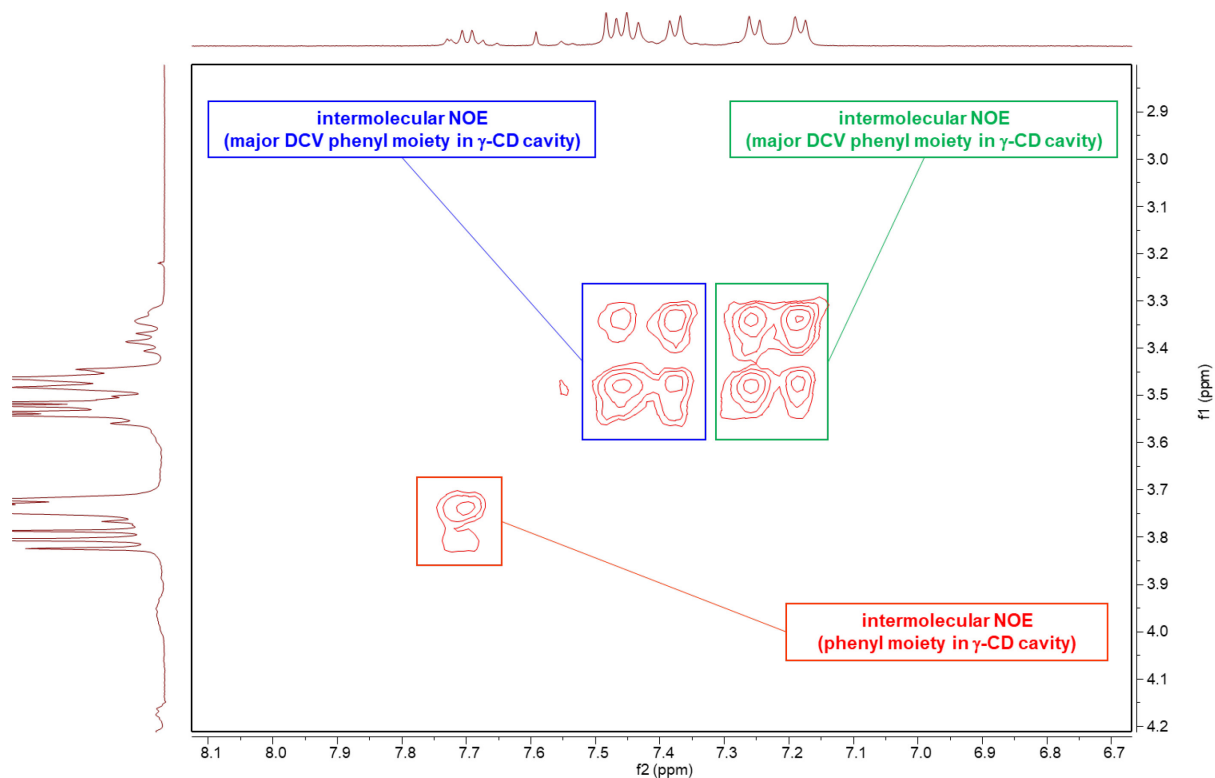
Figure S9 Expanded 2D ROESY spectrum of DCV in the presence of γ-CD in 50 mM deuterated sodium phosphate buffer in D_2O, apparent pH 2.5, showing intermolecular NOEs between aromatic DCV protons and γ-CD protons. Experimental conditions: 3.0 mg DCV·2HCl and 13.0 mg γ-CD in 0.7 mL 50 mM D_3PO_4 in D_2O, pH 2.5, 25 °C.
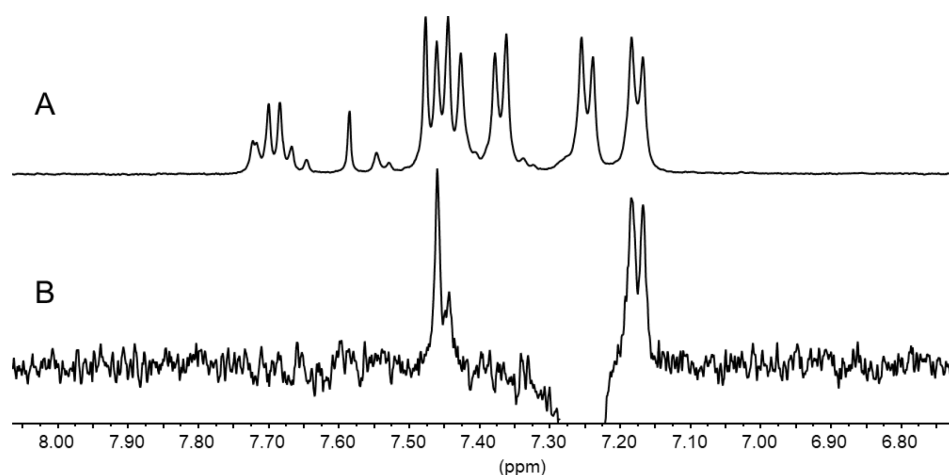
Figure S10 Expanded ^{1}H-NMR spectrum (aromatic region) of (A) DCV plus γ-CD in 0.05 M
deuterated phosphate buffer in D_2O, apparent pH 2.5, and (B) 1D ROESY spectrum
irradiating at Ph H-2,6 of DCV-(III) (7.25 ppm), showing the intermolecular interaction with
Ph H-2,6 of DCV-(II) (7.18 ppm) within the 2:1 complex. Experimental conditions: 3.0 mg
DCV·2HCl and 13.0 mg γ-CD in 0.7 mL 50 mM D_3PO_4 in D_2O, pH 2.5, 25 °C.
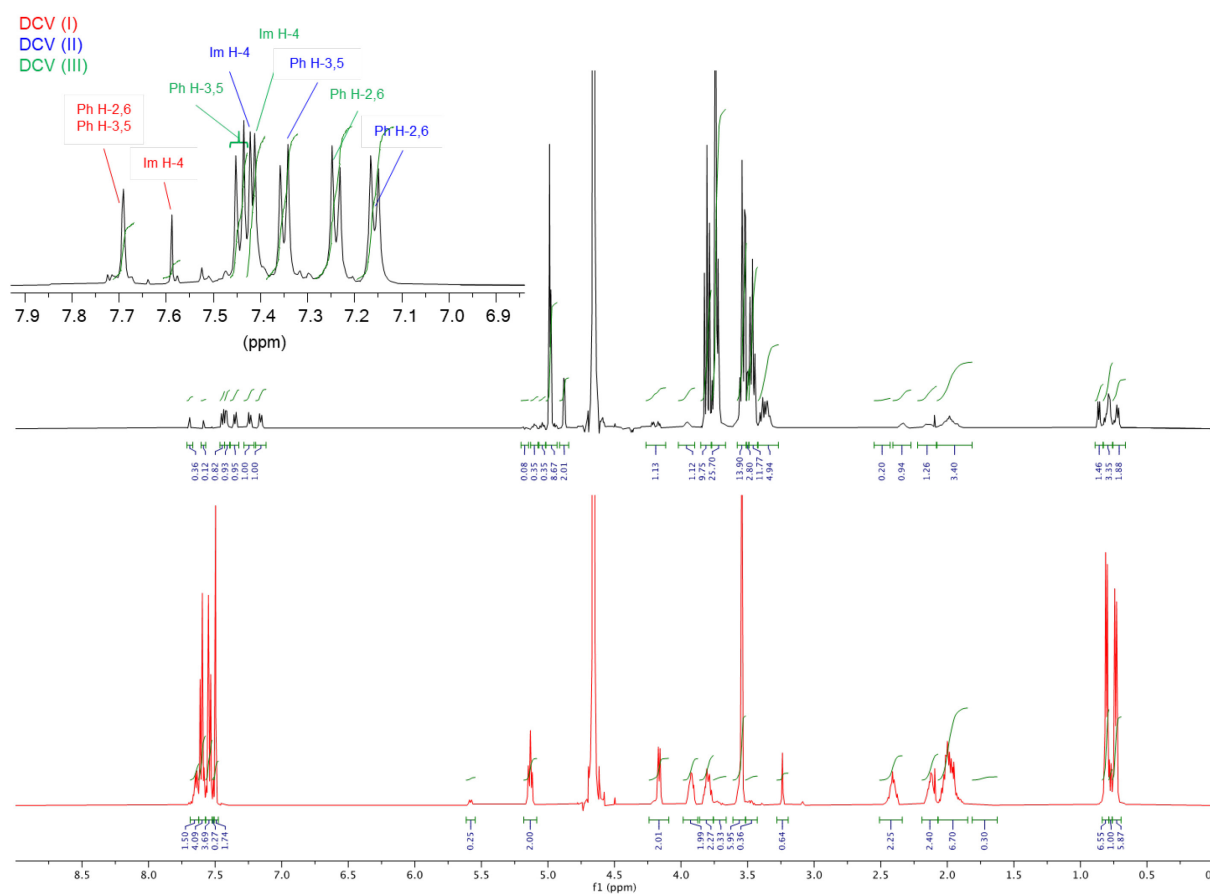
Figure S11 ^{1}H-NMR spectrum (A) DCV and (B) of a mixture of DCV and γ-CD in 50 mM deuterated sodium phosphate buffer in D$_2$O, apparent pH 4.0. The insert shows the expanded region of the aromatic protons. Experimental conditions: 3.4 mg DCV·2HCl and 14.1 mg γ-CD in 0.8 mL 50 mM D$_3$PO$_4$ in D$_2$O (5.2 mM, 13.6 mM), pH 4.0, 25 °C.
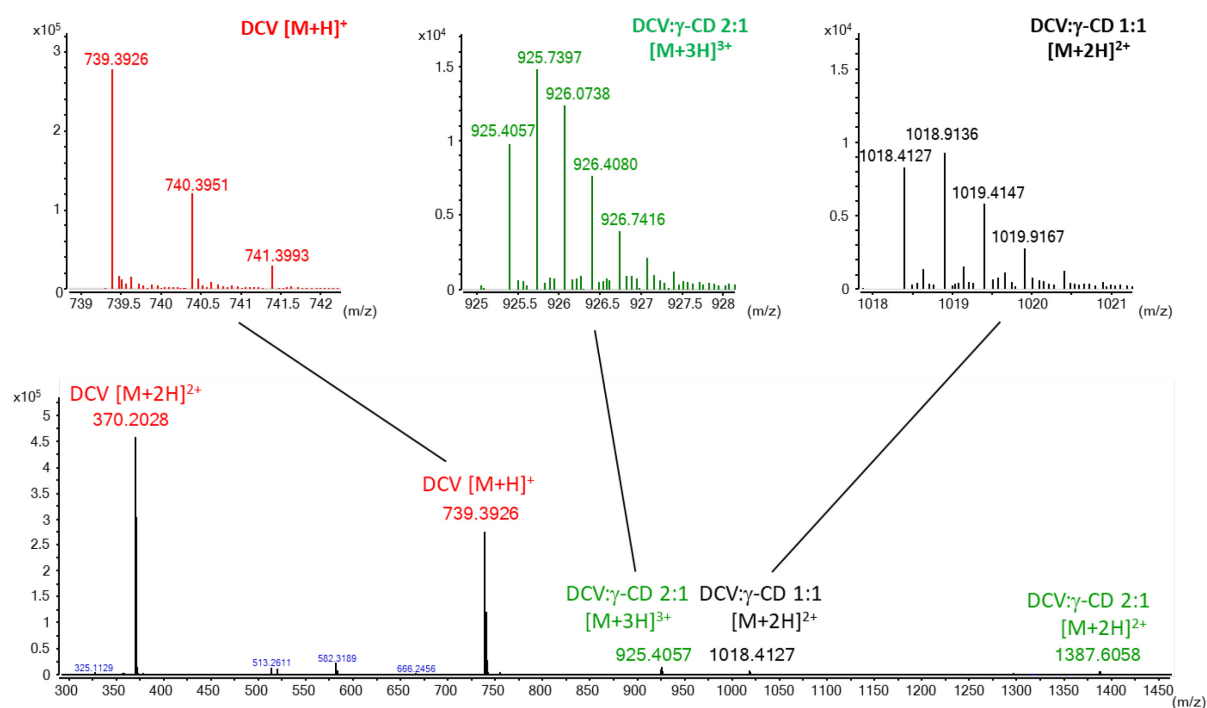
Figure S12 ESI-mass spectra of a sample of DCV and γ-CD. The sample contained 0.1 mg/mL DCV and 2.5 mM γ-CD dissolved in 50 mM ammonium formate buffer pH 2.6. Experimental conditions: Agilent 6520 QTOF with a Dual-ESI Source (G6510A, G3251B; Agilent, Santa Clara, CA, U.S.A.). The sample was delivered by a syringe pump Model 100 Series (KD Scientific, Holliston MA, U.S.A.) with a 500 µL syringe (Trajan Scientific, Victoria, Australia). The MS instrument settings were as follows: sample delivery rate of 4 µL/min, spray voltage (VCap) of 4,5 kV, nebulizer and dry gas flow of 15 psig and 4 L/min, gas temperature of 275 °C, fragmentor, skimmer and OCT 1RF voltage of 200 V/65 V/600 V. Measurements were performed in a range of m/z 150-3000 and with an acquisition rate of 5 spectra per second.

Table S1   Results of screening of CDs as selectors for the separation of DCV and RRRR-DCV.

Cyclodextrin[1]	Concentration	Separation factor α	Migration order	Comments
α-CD	5 mM	1.000	–	–
	20 mM	1.000	–	–
M-α-CD	5 mM	1.000	–	–
	20 mM	1.000	–	–
HP-α-CD	5 mM	1.000	–	–
	20 mM	1.000	–	–
CM-α-CD	5 mM	1.013	RRRR[2] > DCV	Partial separation
	20 mM	1.049	RRRR > DCV	Partial separation
S-α-CD	5 mM	1.000	–	–
	20 mM	1.000	–	–
β-CD	5 mM	1.000	–	–
	20 mM	1.000	–	–
M-β-CD	5 mM	1.070	DCV > RRRR	Baseline separation
	20 mM	1.053	DCV > RRRR	Baseline separation
HP-β-CD	5 mM	1.000	–	–
	20 mM	1.036	DCV > RRRR	Partial separation
CM-β-CD	5 mM	1.000	–	–
	20 mM	1.000	–	–
S-β-CD	5 mM	–	–	Plateau between peaks
	20 mM	–	–	Plateau between peaks
γ-CD	5 mM	–	–	Plateau between peaks
	20 mM	–	–	Plateau between peaks
M-γ-CD	5 mM	1.000	–	Shoulder
	20 mM	1.000	–	–
HP-γ-CD	5 mM	1.000	–	–
	20 mM	1.000	–	–
CM-γ-CD	5 mM	1.080	DCV > RRRR	Baseline separation
	20 mM	1.066	DCV > RRRR	Baseline separation
S-γ-CD	5 mM	1.038	DCV > RRRR	Baseline separation
	20 mM	1.060	DCV > RRRR	Baseline separation

[1] M-α-CD, methyl-α-CD; HP-α-CD, 2-hydroxypropyl-α-CD; CM-α-CD, carboxymethyl-α-CD; S-α-CD sulfated α-CD; M-β-CD, methyl-β-CD; HP-β-CD, 2-hydroxypropyl-β-CD; CM-β-CD, carboxymethyl-β-CD; S-β-CD sulfated β-CD; M-γ-CD, methyl-γ-CD; HP-γ-CD, 2-hydroxypropyl-γ-CD; CM-γ-CD, carboxymethyl-γ-CD; S-γ-CD sulfated γ-CD.

[2] RRRR-DCV (enantiomer)

Experimental conditions: 40/50.2 cm, 50 µm ID fused-silica capillary, 50 mM sodium phosphate buffer, pH 2.5, 20 °C and 20 kV. Detection was carried out at 200 nm at the cathodic end of the capillary. In the case of sulfated CDs the applied voltage was –20 kV and detection was performed at the anodic end. The sample consisted of 100 µg/mL DCV and 50 µg/mL DCV enantiomer dissolved in 0.01 mM HCl.

Table S2 ^{1}H-NMR resonances of DCV in buffered D_2O at pH 2.5 in ppm. For assignments see structure.
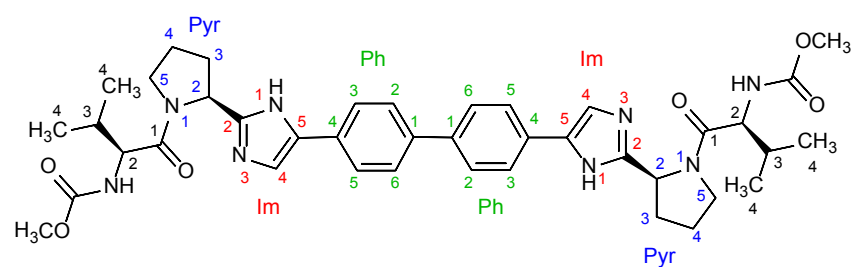
Proton(s)	DCV (major isomer)	DCV (minor isomer)
H-2	4.15	4.15
H-3	1.95	1.95
H-4 (Me)	0.73, 0.80	0.73, 0.80
OMe	3.53	3.22
Pyr-2	5.14 (t, J = 7.6 Hz)	5.61 (dd, J = 7.6, 1.5 Hz)
Pyr-3	2.01, 2.43	2.18, 2.46
Pyr-4	2.02, 2.12	1.74, 1.99
Pyr-5	3.79, 3.92	3.48, 3.74
Im-4	7.52	7.52
Ph-2,6	7.66	7.66
Ph-3,5	7.59	7.58

Experimental conditions: 3.6 mg DCV·2HCl in 0.7 mL 50 mM D_3PO_4 in D_2O, pH 2.5, 25 °C.

Table S3   ^{1}H-NMR resonances of DCV–γ-CD complexes in buffered D_2O at pH 2.5 in ppm. For assignments see structures.
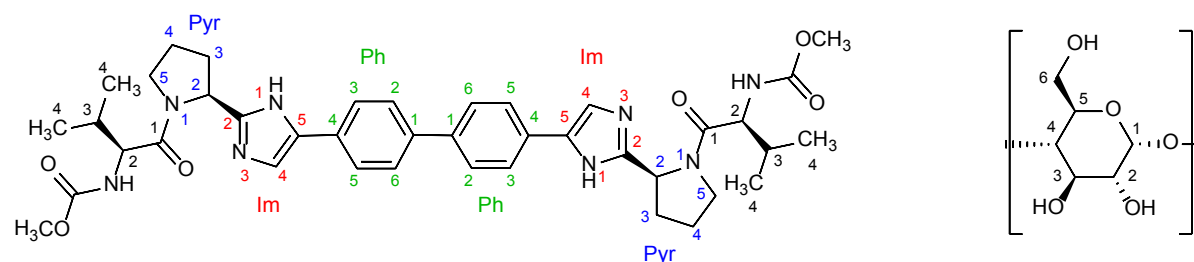
	1:1 Complex				2:1 Complex			
Proton(s)	DCV (I)	Proton(s)	γ-CD (I)	Proton(s)	DCV (II)	DCV (III)	Proton(s)	γ-CD (II)
H-2	4.18	H-1	4.98	H-2	4.17	4.21	H-1	4.87
H-3	1.98	H-2	3.52	H-3	1.94	2.04	H-2	3.46
H-4 (Me)	0.74, 0.80	H-3	3.80	H-4 (Me)	0.73, 0.80	0.80, 0.87	H-3	3.47
OMe	3.55	H-4	3.46	OMe	3.55	3.55	H-4	3.38
Pyr-2	5.18	H-5	3.74	Pyr-2	5.07	5.10	H-5	3.33
Pyr-3	2.06, 2.47	H-6	3.73	Pyr-3	1.98, 2.36	1.98, 2.36	H-6	3.48, 3.53
Pyr-4	2.06, 2.16			Pyr-4	2.01, 2.16	2.01, 2.16		
Pyr-5	3.82, 3.94			Pyr-5	3.80, 3.97	3.80, 3.97		
Im-4	7.59			Im-4	7.48	7.42		
Ph-2,6	7.72			Ph-2,6	7.18	7.25		
Ph-3,5	7.70			Ph-3,5	7.37	7.45		

Experimental conditions: 3.0 mg DCV·2HCl and 13.0 mg γ-CD in 0.7 mL 50 mM D_3PO_4 in D_2O, pH 2.5, 25 °C.

Table S4   Observed and calculated masses in ESI-TOF-MS

	Molecular formula	Ion	m/z observed	m/z calculated	delta (ppm)
DCV	$C_{40}H_{50}N_8O_6$	$[M+H]^+$	739.3926	739.3926	0.0
		$[M+2H]^{2+}$	370.2028	370.1999	−7.8
DCV:γCD (1:1)	$C_{88}H_{130}N_8O_{46}$	$[M+2H]^{2+}$	1018.4127	1018.4112	−1.4
DCV:γCD (2:1)	$C_{128}H_{180}N_{16}O_{52}$	$[M+2H]^{2+}$	1387.6058	1387.6039	−1.4
		$[M+3H]^{3+}$	925.4057	925.4050	−0.7

ELUCIDATION OF THE SOLUTION STRUCTURE AS WELL AS THE STRUCTURES OF THE COMPLEXES WITH γ-CD BY ¹H-NMR SPECTROSCOPY

RSSR-DCV

The spectrum RSSR-DCV is shown in Figure SA 1A, for signal assignments see Table SA 1. A minor signal for the pyrrolidine H-2 at 5.78 ppm (dd, J = 8.3, 1.5 Hz) and a major signal at 5.26 ppm (dd, J = 8.3 Hz, 3.5 Hz) were observed indicating the presence of two conformers with a ratio of about 0.05:1.0, which is lower than that found for DCV. The coupling constants point to equatorial configurations of the proton at pyrrolidine C-2 in both conformers in contrast to DCV. Another difference is the large upfield shift of the methyl protons of the valine side chain to 0.45 and 0.68 ppm. This might be explained by the anisotropic ring current of the aromatic moieties in case of a folded structure with the methyl groups in the proximity to the phenyl rings. However, this tentative structure could not be corroborated from ROESY experiments because no significant NOEs were observed (data not shown). The major RSSR-DCV conformer displayed NOEs between the phenyl hydrogens at 7.58 and 7.64 ppm and the methoxy function at 3.47 ppm. Thus, RSSR-DCV also adopts a folded structure but unlike DCV, the methoxy groups of the MOC residues were folded back toward the aromatic structures, while the valine side chains pointed away from the molecule.

The ¹H-NMR spectrum of the mixture of RSSR-DCV and γ-CD in deuterated phosphate buffer in comparison to RSSR-DCV is displayed in Figure SA 1B, for signal assignment see Table SA 2. As in the case of DCV, three sets of signals were observed for RSSR-DCV, while two other sets of signals were consistent with γ-CD. The minor γ-CD component is best evidenced by the upfield shift of the anomeric H-1 proton at 4.87 ppm and of the internal H-3 and H-5 protons at 3.51 and 3.35 ppm, respectively. The presence of three sets of signals for RSSR-DCV in the aromatic region (Figure SA 1B, insert). The ratio of the integrals was about the same, so that no "minor" and "major" RSSR-DCV species could be assigned. The simultaneous presence of 1:1 and 2:1 inclusion complexes was concluded based on intermolecular NOE responses between the aromatic protons of all RSSR-DCV species and the inner H-3 and H-5 hydrogens of γ-CD in a 2D ROESY experiment (Figure SA 2). In addition, an intermolecular NOE cross peak was observed between the aromatic signals of the phenyl H-3,5 protons at 7.13 and 7.22 ppm of two of the RSSR-DCV species. This substantiates a 2:1 complex in addition to the 1:1 complex. Based on the integrals of the signals of aromatic protons and the anomeric proton of the minor "minor" γ-CD at 4.87 ppm a molar ratio of 1:1:1 was derived further supporting a 2:1 complex, while the NOE interactions found for the aromatic RSSR-DCV protons at lower field with the "major" γ-CD protons were consistent with a 1:1 complex. An approximate ratio of 1:1 for the complexes at 25 °C was estimated from the integrals of the aromatic protons. Thus, the ratio is different from DCV

No NOEs were detected between protons of the Val side chain and aromatic protons, while NOEs indicated spatial vicinity between Val-Hα and pyrrolidine H-5 of all three RSSR-DCV species. In the case of the 1:1 complex a NOE of pyrrolidine H-5 (3.75 ppm) with valine H-α (4.15 ppm) was also observed. These results indicated that RSSR-DCV adopted an extended conformation in both types of complexes, which is in contrast to the folded structure of DCV in the complexes. Thus, the stereochemistry of the MOC-valine side chain does not affect the formation of a 2:1 complex with γ-CD

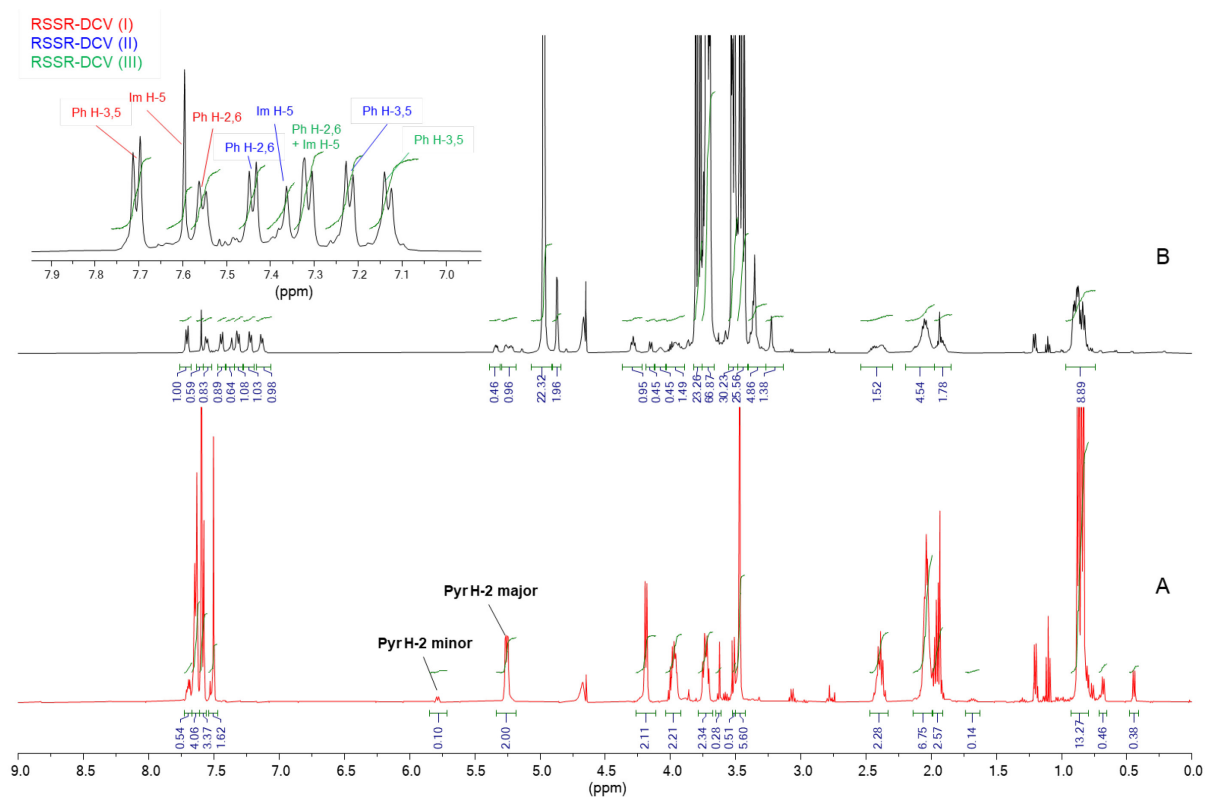although it may affect the general structure of the complex as well as the ratio between the 1:1 and 2:1 complexes.

Figure SA 1 ^{1}H-NMR spectra of (A) RSSR-DCV and (B) RSSR-DCV plus γ-CD in 0.05 M deuterated phosphate buffer in D$_2$O, apparent pH 2.5. For signal assignments see Tables S4 and S5 (supplementary electronic material). Experimental conditions: (A) 2.3 mg RSSR-DCV in 0.6 mL 50 mM D$_3$PO$_4$ in D$_2$O (5.2 mM), pH 2.5, 25 °C; (B) 2.0 mg RSSR-DCV and 12.4 mg γ-CD in 0.7 mL 50 mM D$_3$PO$_4$ in D$_2$O (3.9 mM, 13.7 mM), pH 2.5, 25 °C.
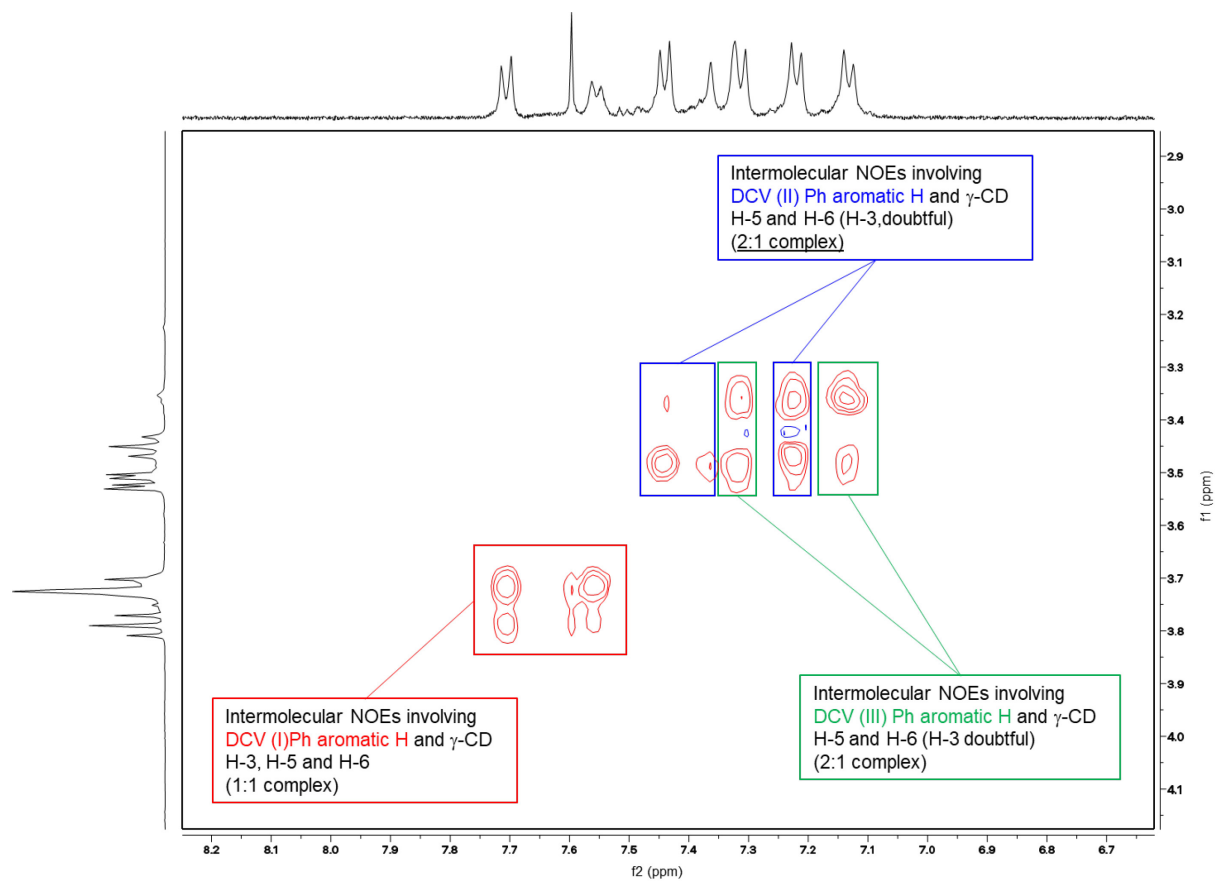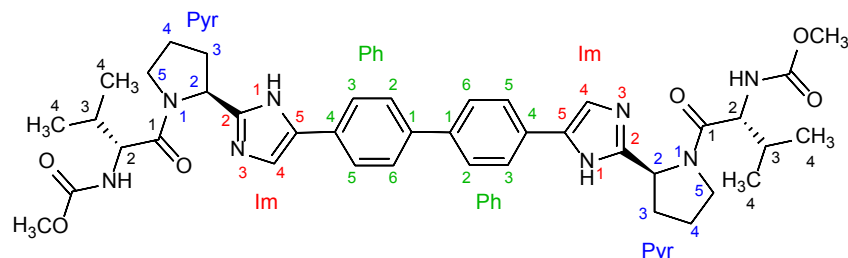
Figure SA 2   Expanded 2D ROESY spectrum of a mixture of RSSR-DCV and γ-CD in 50 mM deuterated sodium phosphate buffer in D_2O, apparent pH 2.5, showing intermolecular NOEs. Experimental conditions: 2.0 mg RSSR-DCV and 12.4 mg γ-CD in 0.7 mL 50 mM D_3PO_4 in D_2O (3.9 mM, 13.7 mM), pH 2.5, 25 °C.

Table SA 1   ^{1}H-NMR resonances of RSSR-DCV in buffered D_2O at pH 2.5. For assignments see structure.

Proton(s)	RSSR-DCV (major isomer)	RSSR-DCV (minor isomer)
H-2	4.19	3.63
H-3	1.95	1.68
H-4 (Me)	0.84, 0.87	0.45, 0.68
OMe	3.47	3.51
Pyr-2	5.26 (dd, J = 8.3, 3.5 Hz)	5.78 (dd, J = 8.3, 1.5 Hz)
Pyr-3	2.04, 2.39	2.11, 2.40
Pyr-4	2.04	1.86, 1.99
Pyr-5	3.73, 3.97	3.49, 3.72
Im-4	7.50	7.53
Ph-2,6	7.64	n.d.
Ph-3,5	7.58	n.d.

Experimental conditions: 2.3 mg RSSR-DCV in 0.6 mL 50 mM D_3PO_4 in D_2O, pH 2.5, 25 °C.

Table SA 2   ^{1}H-NMR resonances of RSSR-DCV–γ-CD complexes in buffered D_2O at pH 2.5 in ppm. For assignments see structures.
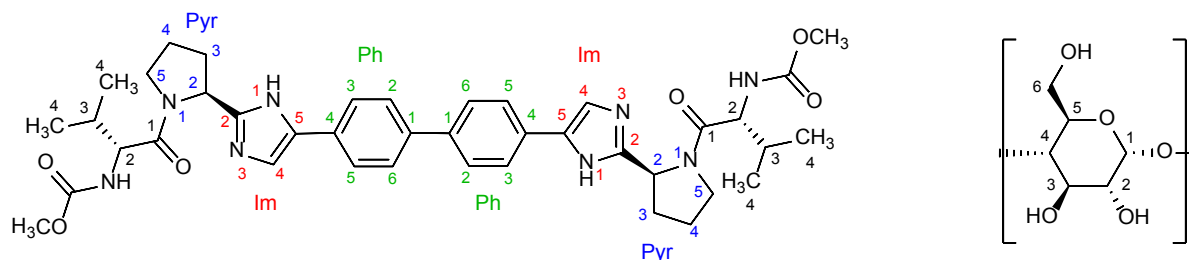
	1:1 Complex				2:1 Complex			
Proton(s)	RSSR-DCV (I)	Proton(s)	γ-CD (I)	Proton(s)	RSSR-DCV (II)	RSSR-DCV (III)	Proton(s)	γ-CD (II)
H-2	4.15	H-1	4.97	H-2	4.28 or 4.29	4.28 or 4.29	H-1	4.87
H-3	1.91	H-2	3.52	H-3	2.03	2.03	H-2	3.49
H-4 (Me)	0.86	H-3	3.79	H-4 (Me)	0.82 or 0.84, 0.90	0.82 or 0.84, 0.90	H-3	3.51
OMe	approx. 3.50	H-4	3.45	OMe	approx. 3.50	approx. 3.50	H-4	3.36
Pyr-2	5.33 (dd, J = 8, 4 Hz)	H-5	3.71	Pyr-2	5.22 (dd, J = 8, 4 Hz)	5.25 (dd, J = 8, 4 Hz)	H-5	3.35
Pyr-3	2.11, 2.43	H-6	3.72 (x 2)	Pyr-3	1.90, 2.37	1.93, 2.39	H-6	3.50 (x 2)
Pyr-4	2.07 (x 2)			Pyr-4	2.04 (x 2)	2.03 (x 2)		
Pyr-5	3.75, 4.07			Pyr-5	3.74, 3.94	3.73, 3.97		
Im-4	7.60			Im-4	7.36	7.32		
Ph-2,6	7.55			Ph-2,6	7.44	7.31		
Ph-3,5	7.70			Ph-3,5	7.22	7.13		

Experimental conditions: 2.0 mg RSSR-DCV and 12.4 mg γ-CD in 0.7 mL 50 mM D_3PO_4 in D_2O, pH 2.5, 25 °C

Mono-DCV

The ^{1}H-NMR spectrum of mono-DCV in phosphate buffer also revealed the presence of a major and a minor isomer (Figure SA 3A, Table SA 3). In the pyrrolidine ring substituted with MOC-valine, H-2 is equatorial in the minor isomer (5.61 ppm, dd, J = 8, 1.5 Hz) and axial in the major species (5.15 ppm, t, J = 8 Hz), i.e. very similar to DCV. In the unsubstituted pyrrolidine ring, only the axial configuration was derived for H-2 (5.01 ppm, dd, J = 10, 8 Hz). The molar ratio of major-to-minor isomer at 25 °C was about 1.0:0.13, i.e. in the same range as seen for DCV. The MOC-valine moiety is also "folded back" toward the aromatic rings as concluded from NOEs between the methyl protons of the side chain and the aromatic protons. As in the case of DCV, a NOE was also seen between the valine methyl groups and H-2 of the minor isomer. Thus, the conformation of the substituted pyrrolidine moiety of mono-DCV has the same folded structure as DCV.

The ^{1}H-NMR spectrum of mono-DCV in the presence of γ-CD (Figure SA 3B, Table SA 4) was less resolved compared to the spectrum of DCV and γ-CD as considerable signal overlap was encountered. Like DCV and the RSSR-diastereomer, five sets of signals were identified, two referring to γ-CD and three to mono-DCV. The γ-CD signals were divided into a minor and a major abundant species with signals of the minor species displaying an upfield shift of almost all resonances. The three sets of resonances due to mono-DCV could not be clearly assigned to higher and lower abundant species due to signal overlap (Figure SA 3B insert). However, six partially overlapping doublets between 0.7 and 0.8 ppm were observed for the methyl groups of the valine side chain indicating three different species of mono-DCV. A 2D ROESY experiment (Figure SA 4) showed intermolecular NOE interactions between all mono-DCV aromatic hydrogens with the H-3, H-5 and H-6 protons of both, the "major" and the "minor" γ-CD, indicating the presence of two different complexes, presumably with 1:1 and 2:1 stoichiometry. Due to the signal overlap in the aromatic region of the spectrum, no clear intermolecular NOEs between the aromatic protons of different mono-DCV species were detected so that no unequivocal proof of a 2:1 complex could be derived. Nonetheless, based on the integrals of the (overlapping) aromatic protons the molar ratio between the minor and the major complexes was about 0.4:1.0. Therefore, it can be assumed, that both complexes with 1:1 and 2:1 stoichiometries are also formed between mono-DCV and γ-CD. The exact orientation of the mono-DCV molecules inside the CD cavity, i.e. the orientation of the MOC-valine group versus the wider or narrower rim of γ-CD, could not be derived either because no sufficient NOE evidence was obtained.
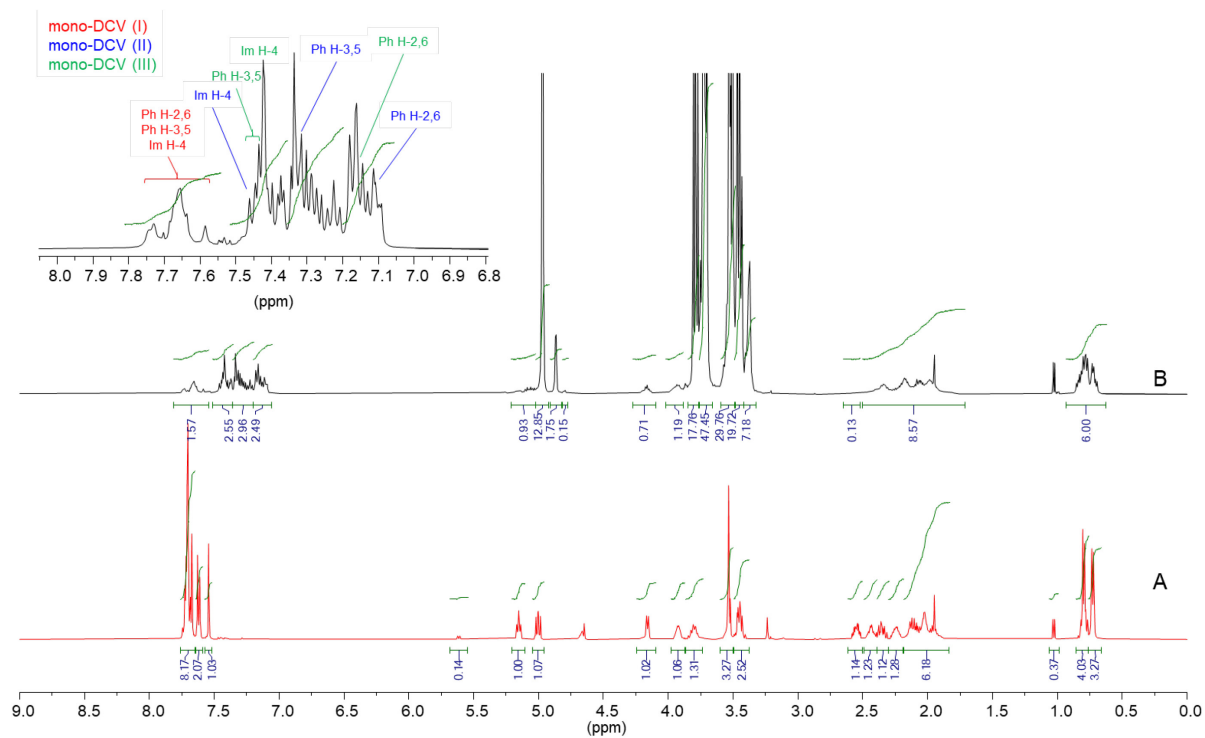
Figure SA 3 ^{1}H-NMR spectra of (A) mono-DCV and (B) mono-DCV plus γ-CD in 0.05 M deuterated phosphate buffer in D_2O, apparent pH 2.5. For signal assignments see Tables S6 and S7 (supplementary electronic material). Experimental conditions: (A) 2.7 mg mono-DCV in 0.7 mL 50 mM D_3PO_4 in D_2O (6.6. mM), pH 2.5, 25 °C; (B) 2.7 mg mono-DCV and 13.0 mg γ-CD in 0.7 mL 50 mM D_3PO_4 in D_2O (6.6 mM, 14.3 mM), pH 2.5, 25 °C.
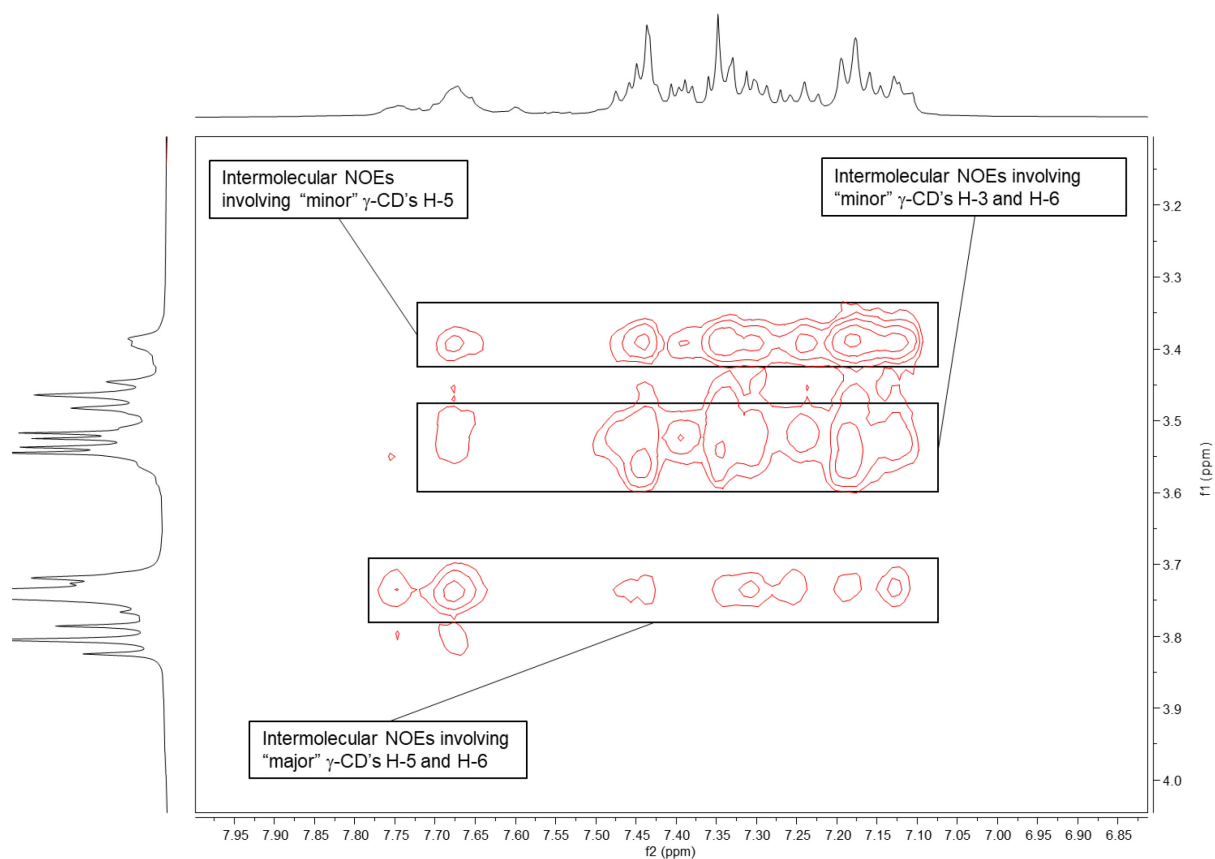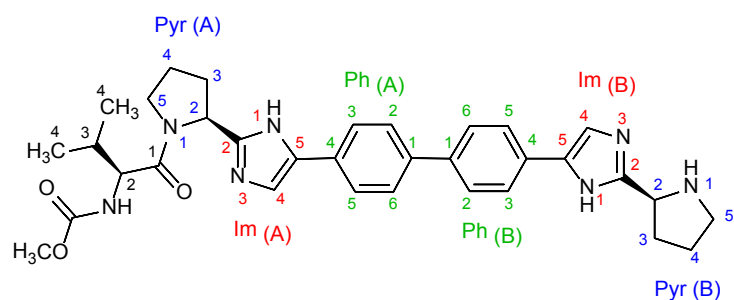
Figure SA 4 Expanded 2D ROESY spectrum of a mixture of mono-DCV and γ-CD in 50 mM deuterated sodium phosphate buffer in D_2O, apparent pH 2.5, showing intermolecular NOEs. Experimental conditions: 2.7 mg mono-DCV and 13.0 mg γ-CD in 0.7 mL 50 mM D_3PO_4 in D_2O (6.6 mM, 14.3 mM), pH 2.5, 25 °C.

Table SA 3   ^{1}H-NMR resonances of mono-DCV in buffered D_2O at pH 2.5. For assignments see structure.

Proton(s)	mono-DCV (major isomer)	mono-DCV (minor isomer)
(A)		
H-2	4.14	n.d.
H-3	1.94	n.d.
H-4 (Me)	0.72, 0.79	0.80*
OMe	3.53	n.d.
Pyr-2	5.15 (t, J = 8 Hz)	5.61 (dd, J = 8, 1.5 Hz)
Pyr-3	2.01, 2.43	2.19, 2.45*
Pyr-4	2.01, 2.12	1.78, 1.99*
Pyr-5	3.79, 3.92	3.50, 3.76*
Im-4	7.54	n.d.
Ph-2,6	7.71	n.d.
Ph-3,5	7.62	n.d.
(B)		
Pyr-2	5.01 (dd, J = 10.1, 8 Hz)	n.d.
Pyr-3	2.36, 2.54	n.d.
Pyr-4	2.08, 2.25	n.d.
Pyr-5	3.43	n.d.
Im-4	7.67	n.d.
Ph-2,6	7.69-7.74	n.d.
Ph-3,5	7.69-7.74	n.d.

* doubtful

Experimental conditions: 2.7 mg mono-DCV in 0.7 mL 50 mM D_3PO_4 in D_2O, pH 2.5, 25 °C.

Table SA 4   ^{1}H-NMR resonances of mono-DCV–γ-CD complexes in buffered D_2O at pH 2.5 in ppm.
For assignments see structures.
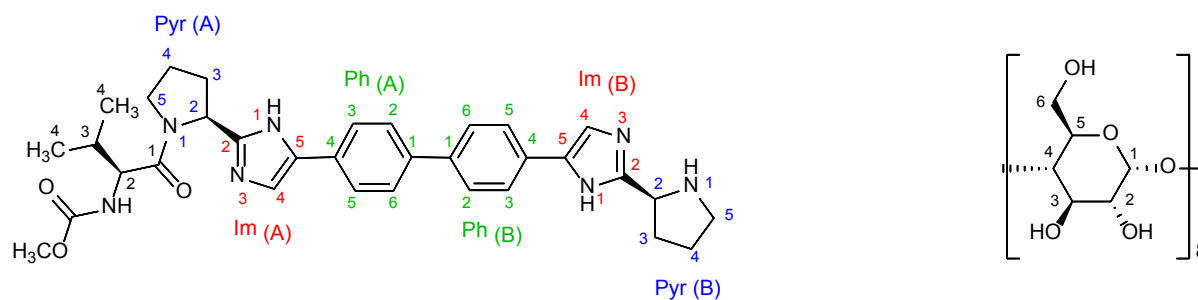
2:1 and 1:1 complexes			1:1 complexes	2:1 complexes
Proton(s)	**Mono-DCV**	**Proton(s)**	**γ-CD (II)**	**γ-CD (I)**
(A)				
H-2	4.16	**H-1**	4.97	4.87
H-3	1.97	**H-2**	3.51	3.49
H-4 (Me)	0.70 - 0.88**	**H-3**	3.79	3.49
OMe	3.55	**H-4**	3.45	3.38
Pyrr-2	5.08	**H-5**	3.71	3.38
Pyrr-3	2.15, 2.33	**H-6**	3.73 (x 2)	3.50, 3.54
Pyrr-4	approx. 2.00 (x 2)			
Pyrr-5	3.79, 3.95			
Im-4				
Ph-2,6	7.09-7.78**			
Ph-3,5				
(B)				
Pyr-2	4.81			
Pyr-3	2.15*, 2.33*			
Pyr-4	2.06, 2.17			
Pyr-5	3.41 (x 2)			
Im-4				
Ph-2,6	7.09 - 7.78**			
Ph-3,5				

* doubtful

** poorly resolved due to overlapping

Experimental conditions: 2.7 mg mono-DCV and 13.0 mg γ-CD in 0.7 mL 50 mM D_3PO_4 in D_2O, pH 2.5, 25 °C.

Half-DCV

The ^{1}H-NMR spectra of half-DCV in the absence and presence of γ-CD are shown in Figure SA 5, for peak assignment see Tables SA 5 and SA 6). As seen for DCV and analogs, two conformers with regard to the conformation of the pyrrolidine ring could be detected at a ratio of about 1.0:0.12, which is similar to the one found for DCV. The triplet of the major conformer at 5.15 ppm refers to the axially oriented H-2, while the double doublet at 5.62 ppm indicated that the pyrrolidine H-2 is in the equatorial position in the minor conformer. From 2D ROESY spectra a folded structure of half-DCV was concluded in analogy to DCV. NOEs were observed between the aromatic protons and the methyl protons of the isopropyl side chain of the major conformer. In case of the minor conformer, a NOE response was seen between the methoxy protons and pyrrolidine H-2. Moreover, the resonances of H-2 as well as the methoxy group appear at a higher filed compared to the major conformer (3.84 and 3.23 ppm versus 4.16 and 3.54 ppm). This can be explained by a ring current anisotropy when the Val side chain is close to the aromatic rings in agreement with a folded structure of the minor conformer.

In the presence of γ-CD, the resonances of half-DCV did not shift significantly compared to the spectrum in the absence of the CD (Figure SA 5B). All resonances were approximately identical. A 2D ROESY experiment also indicated a folded conformation of the compound. Moreover, for the major conformer intermolecular NOEs between H-5 and to a minor extent H-3 of γ-CD with the aromatic hydrogens of the phenyl and imidazole rings indicated that half-CDV enters the cavity via the narrower primary rim of the CD as schematically shown in Figure SA 6. In case of the minor conformer, no significant NOEs could be detected probably due to low signal intensity. No indication of a 2:1 complex could be derived. Thus, a dimeric biphenyl structure appears to be required for the formation of a 2:1 complex.
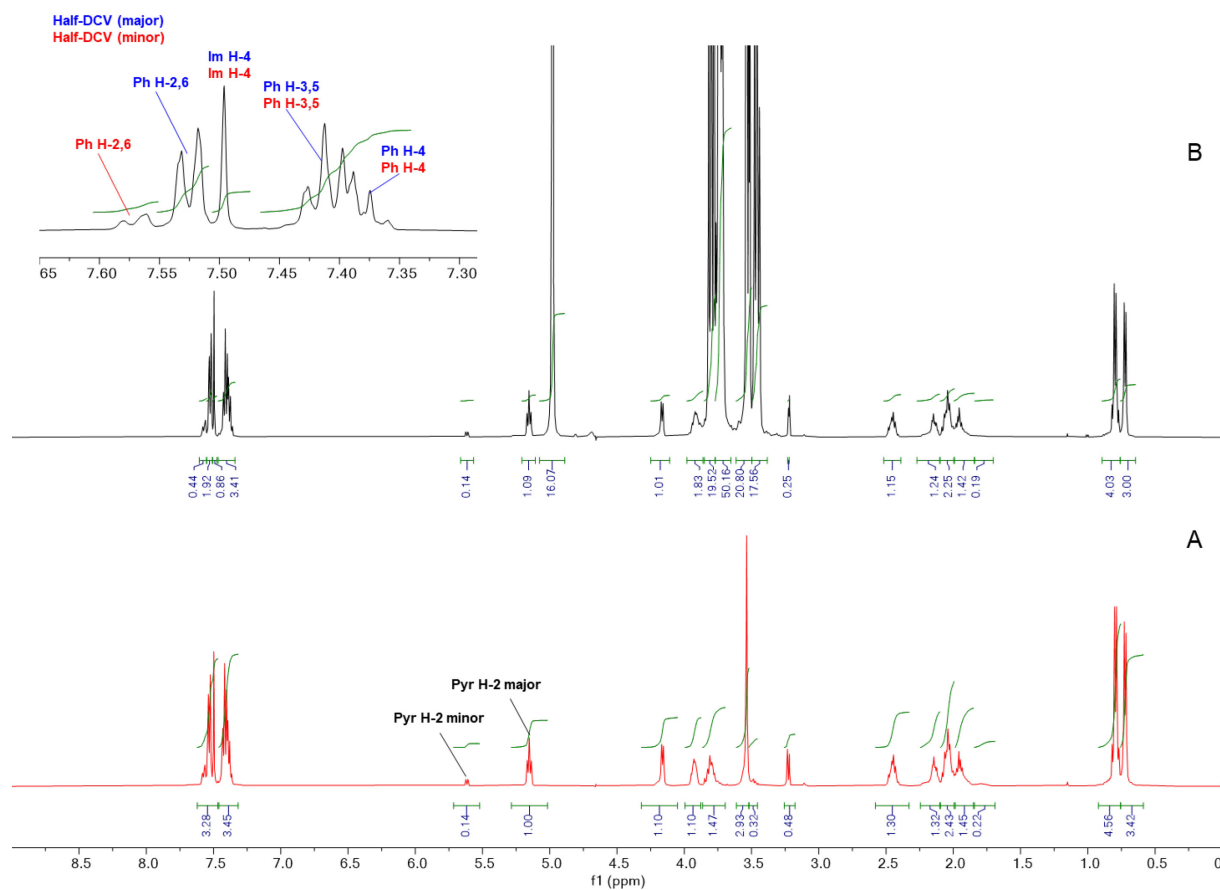
Figure SA 5 ¹H-NMR spectra of (A) half-DCV and (B) half-DCV plus γ-CD in 0.05 M deuterated phosphate buffer in D₂O, apparent pH 2.5. For signal assignments see Tables S8 and S9. Experimental conditions: (A) 3.0 mg half-DCV in 0.7 mL 50 mM D₃PO₄ in D₂O (11.6 mM), pH 2.5, 25 °C; (B) 3.0 mg half-DCV and 16.0 mg γ-CD in 0.7 mL 50 mM D₃PO₄ in D₂O (11.6 mM, 17.6 mM), pH 2.5, 25 °C.
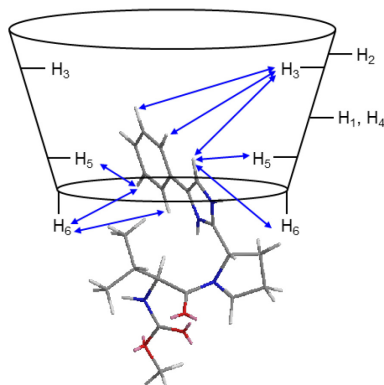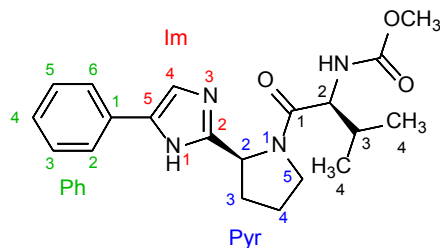
Figure SA 6 Schematic representation of the complex formed between half-DCV and γ-CD. The
intermolecular NOEs derived from ROESY experiments are indicated by blue arrows.

Table SA 5 ^{1}H-NMR resonances of half-DCV in buffered D_2O at pH 2.5 in ppm. For assignments
see structure.

Proton(s)	Half-DCV (major isomer)	Half-DCV (minor isomer)
H-2	4.16	3.84
H-3	1.95	1.90
H-4 (Me)	0.72, 0.79	0.77, 0.81
OMe	3.54	3.23
Pyr-2	5.15	5.62
Pyr-3	2.03, 2.45	2.21, 2.47
Pyr-4	2.02, 2.14	1.77, 1.99
Pyr-5	3.81, 3.93	3.49, 3.76
Im-4	7.50	7.50
Ph-2,6	7.53	7.57
Ph-3,5	7.42	7.42
Ph-4	7.39	7.39

Experimental conditions: 3.0 mg half-DCV in 0.7 mL 50 mM D_3PO_4 in D_2O, pH 2.5, 25 °C.

Table SA 6 ^{1}H-NMR resonances of half-DCV–γ-CD complexes in buffered D_2O at pH 2.5 in ppm. For assignments see structures.
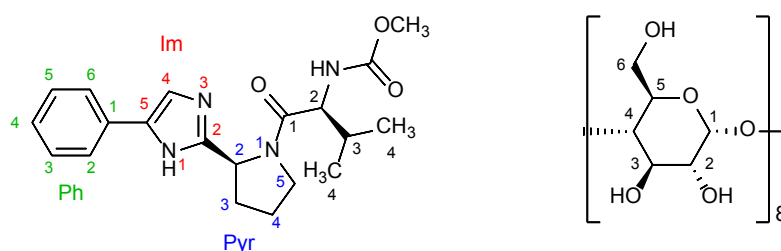
| | **Half-DCV** | | | |
Proton(s)	**(major isomer)**	**(minor isomer)**	**Proton(s)**	**γ-CD**
H-2	4.17	3.83	**H-1**	4.98
H-3	1.96	1.95*	**H-2**	3.53
H-4 (Me)	0.72, 0.80	0.78, 0.81	**H-3**	3.80
OMe	3.55	3.23	**H-4**	3.46
Pyr-2	5.15	5.62	**H-5**	3.72
Pyr-3	2.04, 2.45	2.22, 2.47	**H-6**	3.74 (x2)
Pyr-4	2.04, 2.15	1.78, 1.99		
Pyr-5	3.81, 3.92	3.48, 3.75		
Im-4	7.50	7.50		
Ph-2,6	7.53	7.57		
Ph-3,5	7.41	7.42		
Ph-4	7.39	7.39		

* doubtful

Experimental conditions: 3.0 mg half-DCV and 16.0 mg γ-CD in 0.7 mL 50 mM D_3PO_4 in D_2O, pH 2.5, 25 °C.

Selbstständigkeitserklärung

Hiermit erkläre ich, dass mir die Promotionsordnung der Fakultät für Biowissenschaften der Friedrich-Schiller-Universität Jena bekannt ist, ich die Dissertation selbst angefertigt habe und alle von mir benutzten Hilfsmittel, persönlichen Mitteilungen und Quellen in meiner Arbeit angegeben sind.

Ich versichere, dass ich die Hilfe eines Promotionsberaters nicht in Anspruch genommen habe und dass Dritte weder unmittelbar noch mittelbar geldwerte Leistungen von mir für Arbeiten erhalten haben, die im Zusammenhang mit dem Inhalt der vorgelegten Dissertation stehen.

Die vorliegende Dissertation wurde von mir bei keiner bisherigen Prüfungsarbeit für eine staatliche oder andere wissenschaftliche Prüfung eingereicht. Weiterhin versichere ich, dass ich die gleiche, eine in wesentlichen Teilen ähnliche oder eine andere Abhandlung nicht bei einer anderen Universität als Dissertation eingereicht habe.

Jena, den 05.06.2020

Sulaiman Krait